Submillimeter, Millimeter and Microwave Frequency Selective Surfaces, Design and Development

by

Muaad Naser Hussein

Submitted in accordance with the requirements for the award of the degree of Doctor of Philosophy of the University of Liverpool

February 2018

Copyright

To my Family and friends: Thank you for your support.

Table of Contents

Copyright ..... **i**

Table of Contents ..... **iii**

Acknowledgements ..... **vii**

List of Publications ..... **viii**

Abstract ..... **xi**

Chapter 1: Introduction **1**

1.1 Background 1

1.2 Motivations 4

1.3 Shaping a periodic structure 6

1.4 Dielectric effect on FSS 7

1.4.1 FSS mesh type 8

1.4.2 FSS patch type 11

1.5 Experimental setup 14

1.6 Outline of the thesis 16

1.7 References 17

Chapter 2: Basics and Literature Review **22**

2.1 Introduction 22

2.2 A brief FSSs history 22

2.3 Practical design problems 23

2.3.1 Wave incident angle 23

2.3.2 Curved FSS 24

2.3.3 Grating lobe 24

2.4 Strip equivalent circuit 26

2.4.1 Wide bandpass FSS 27

2.4.2 Wide bandstop FSS 30

2.4.3 Dual-band bandstop FSS 31

2.5 Shape and size of FSS array elements 32

2.5.1 Miniaturised FSS 33

2.5.2 High order FSS 38
2.6 Examples for designing FSS 43
2.6.1 Using stepped-impedance element 43
2.6.2 Using vias 47
2.7 Conclusion 50
2.8 References 50
Chapter 3: Asymmetrical Array Elements 54
3.1 Introduction 54
3.2 Single-layer element 55
3.2.1 Experimental results 56
3.3 Interconnected adjacent elements on orthogonal layers 58
3.3.1 Miniaturisation approaches 58
3.3.2 Circuit design 67
3.3.3 Experimental results 74
3.4 Conclusion 77
3.5 References 78
Chapter 4: Multi-Layer FSS 80
4.1 Introduction 80
4.2 Single polarised FSS element 81
4.3 Dual polarised FSS element 88
4.3.1 Surrounding dielectric materials 91
4.3.2 Experimental results 96
4.4 Conclusion 100
4.5 Reference 100
Chapter 5: Multi-Band FSS 102
5.1 Introduction 102
5.2 Dual-band bandstop FSS 103
5.2.1 Experimental results 108
5.3 High selectivity FSS 109

5.3.1 Experimental results 113
5.4 Conclusion 114
5.5 References 115
Chapter 6: High Order FSS 117
6.1 Introduction 117
6.2 Miniaturised second order FSS 117
6.2.1 Circuit design 118
6.2.2 Experimental results 124
6.3 Low profile second order FSS 126
6.3.1 Circuit design 126
6.3.2 Experimental results 132
6.4 Conclusion 134
6.5 References 135
Chapter 7: THz FSS 137
7.1 Introduction 137
7.2 Sharp transition edge FSS 138
7.2.1 Circuit design 138
7.3 Low loses high order bandpass FSS 143
7.3.1 Fabrication and measurements 144
7.4 Conclusion 146
7.5 References 147
Chapter 8: FSS for HIS and Antenna Applications 150
8.1 Introduction 150
8.2 A low profile miniaturised HIS 150
8.2.1 The structure 151
8.3 FSS for antennas 155
8.3.1 Dielectric effect on patch-mesh FSS 155
8.3.2 Circuit design 157
8.3.3 A dipole antenna loaded with the proposed FSS 162

8.3.4 Experimental results 165
8.4 Conclusion 169
8.5 References 169
Chapter 9: Summary and Future Works 172
9.1 Summary 172
9.2 Future work 174
9.2.1 Lower frequency band 174
9.2.2 A mobile phone 175
9.2.3 THz frequency band 175
9.3 References 175

Acknowledgements

I would like to express my deepest gratitude to my supervisor Dr Jiafeng Zhou for the continuous support of my PhD research, for his patience, motivation, enthusiasm, and immense knowledge. His guidance has helped me throughout the research and writing up this thesis. I would like to thank Prof. Yi Huang for his motivation and insightful comments. Thanks also go to Prof. Shen Yaochen and Dr. Saqib Khursheed for their beneficial feedback during the annual review at our department.

I should also thank my home sponsor The Higher Committee for Education Development in Iraq (HCED) for the financial fund to pursue my study. It was a great support to improve my occupation and get introduced to new cultures abroad.

Thanks must also be paid to my colleagues at the Wireless Engineering Research Group; in particular to and for the stimulating discussions in a work related context.

I would like to thank my research lab colleagues and my friends: Abed Pour Sohrab, Dr. Muayad Kod, Manoj Stanley, Sumin David Joseph, Ahmed Aliedani, Baha Aljoubori, Dr Chaoyun Song, Yuan Zhuang, Dr Sheng Yuan, Saidatul Izyanie, Zhouxiang Fei, Umniyyah Ulfa, Anqi Chen, Dr Rula Alrawashdeh, Wenzhang Zhang, Zhihao Tian, Tianyuan Jia, Dr Saqer Alja'afreh, Dr Qian Xu and Dr Lei Xing. I have enjoyed working with you all and I appreciate the ideas, help and good humour.

Last but not the least; I would like to offer my special thanks to my parents and family for their support, encouragement and help. I am eternally grateful for everything they have done, your prayers have been answered. I would also like to express my gratitude to my lovely wife Muntaha, your love, patient and encouragement helped me to be succeeded. My lovely Kids, your curious and love have extremely motivated me to do the best.

List of Publications

[1] **M. Hussein**, J. Zhou, Y. Huang, Muayad Kod, and A. Sohrab, "Dual-band bandstop frequency selective surface by using half rings and slots," *Microwave and Optical Technology Letters,* vol. 58, pp. 1136-1139, 2016.

[2] **M. N. Hussein**, J. Zhou, Y. Huang, M. Kod, and A. P. Sohrab, "Frequency Selective Surface Structure Miniaturization Using Interconnected Array Elements on Orthogonal Layers," *IEEE Transactions on Antennas and Propagation,* vol. 65, pp. 2376-2385, 2017.

[3] **M. N. Hussein**, J. Zhou, Y. Huang, M. Kod, and A. P. Sohrab, "A Miniaturized Low-Profile Multilayer Frequency-Selective Surface Insensitive to Surrounding Dielectric Materials," *IEEE Transactions on Microwave Theory and Techniques,* 10.1109/TMTT.2017.2709317, 2017.

[4] **M. N. Hussein**, J. Zhou, Y. Huang, B. Al-Juboori, "A Low-profile Miniaturized Second-Order Bandpass Frequency Selective Surface," *IEEE Antennas and Wireless Propagation Letters,* Vol. 16, pp. 2791 – 2794, 2017.

[5] J. Zhou, **M. Hussein**, Y. Huang and G Yang, "A Novel Frequency Selective Surface Insensitive to Surrounding Environment", *Patent*, Application No: 201710349144.1, 2017.

[6] **M. Hussein**, Y. Huang, B. Al-Juboori, and J. Zhou, "A multi-band high selectivity FSS for Ka-band applications," *FERMAT,* Volume 22, Communication 19, Jul-Aug., 2017.

[7] **M. Hussein**, J. Zhou, Y. Huang, Muayad Kod, and A. P. Sohrab, "A novel array element for wideband frequency selective surface," *Active and Passive RF Devices Seminar*, London, Feb., 2016.

[8] **M. Hussein**, J. Zhou, Y. Huang, A. P. Sohrab, and Muayad Kod, "Frequency selective surface with simple configuration stepped-impedance elements," in *2016 10th European Conference on Antennas and Propagation (EuCAP)*, pp. 1-4, Davos, 2016.

[9] **M. Hussein**, Y. Huang, B. Al-Juboori, and J. Zhou, "A multi-band high selectivity frequency selective surface for Ka-band applications," *Millimeter-*

Waves,Global Symposium on, 2017, pp. 63-65. (Invited talk).

[10] **M. Hussein**, J. Zhou, Y. Huang, M. Kod, "High Directivity THz Log Periodic antenna with Luneburg Lenses", *(Proceeding) UCMMT 7th,* China, Sep. 2014.

[11] **M. Hussein**, J. Zhou, and Y. Huang, "A miniaturized frequency selective surface by using vias to connect spiral lines and square patches." *Antennas and Propagation & USNC/URSI National Radio Science Meeting, 2017 IEEE International Symposium on* pp. 269-270.

[12] **M. N. Hussein**, J. Zhou, Y. Huang, J. Jin, C. Balocco, R. A. Habeeb, " Low-profile second-order terahertz bandpass frequency selective surface with sharp transitions," *UCMMT 10th,* UK, Sep., 2017.

[13] **M. Hussein**, J. Zhou, Y. Huang, J. Jin, C. Balocco, A. Valavanis, B. Yang, "Second-order terahertz bandpass frequency selective surface with stable angular responses", *IET Colloquium on Millimetre-wave and Terahertz Engineering & Technology,* London, 2017.

[14] Muayad Kod, J. Zhou, Y. Huang, M. Stanley, **M. Hussein**, A. P. Sohrab, R. Alrawashdeh and G. Wang, " Feasibility Study of Using the Housing Cases of Implantable Devices as Antennas," *IEEE Access*, vol. 4, pp. 6939-6949, 2016.

[15] Muayad Kod, J. Zhou, Y. Huang, R. Alrawashdeh, and **M. Hussein**, "A dual broadband butterfly loop antenna for body wearable applications," *Antennas & Propagation Conference (LAPC), Loughborough*, pp. 1-3, 2015.

[16] A. P. Sohrab, Y. Huang, **M. Hussein**, Muayad Kod, P. Carter, "A UHF RFID Tag With Improved Performance on Liquid Bottles," *IEEE Antennas and Wireless Propagation Letters,* vol. 15, pp. 1673-1676, 2016.

[17] A. P. Sohrab, Y. Huang, M. Kod, **M. Hussein**, and P. Carter, "Label-type 3D RFID tag mountable on metallic and non-metallic objects," *Antennas & Propagation Conference (LAPC), Loughborough*, 2016, pp. 1-3.

[18] B. Aljuboori, Y. Huang, D. Klugmann, **M. Hussein**, Jiafeng Zhou, "Millimeter wave cross-coupled bandpass filter based on Groove gap waveguide technology", *UCMMT 10th,* UK, Sep., 2017.

[19] A. P. Sohrab, Y. Huang, **M. Hussein**, P. Carter, "A hybrid UHF RFID tag

robust to host material", *IEEE Radio Frequency Identification,* vol. 1, pp. 163-169, Oct., 2017.

Abstract

This dissertation presents new approaches to design and development of submillimeter, millimeter, and microwave frequency-selective surfaces (FSSs) having extensive applications in wireless communications and radar systems.

The theory of the surfaces is introduced in Chapter 3 where a new approach to miniaturise the size of an FSS array element is presented by interconnecting array elements in one direction in a two-layer FSS structure. The top layer acts as an enhanced inductor while the bottom layer acts as a capacitor. The interconnection between adjacent array elements changes the equivalent circuit and produces a strong cross-layer capacitance, which lowers the resonant frequency significantly. The dimensions of the miniaturised FSS element are much smaller than the wavelength at the resonant frequency (periodicity << λ). Chapter 4 introduces a new methodology to design the FSS by maximizing the value of the capacitance between adjacent layers. The proposed structure offers three distinctive advantages: Firstly, the strong cross-layer capacitance makes the FSS element very compact. Secondly, for the proposed structure, the lower the profile, the stronger the cross-layer capacitance, and the lower the resonant frequency. This is unique to the proposed structure since the resonant frequency is usually higher for a lower profile than for traditional structures. Thirdly and most importantly, any external dielectric material attached to the FSS will not significantly affect the performance of the FSS due to this strong cross-layer capacitance. Chapter 5 introduces novel methodologies to design dual band spatial filters by using FSS periodic arrays composed of a bandpass and a bandstop element. The fabrication of the dual band filters is significantly simplified by using a single metal layer on a dielectric substrate. Chapter 6 introduces a new schematic to design a miniaturised high order bandpass FSSs ($N \geq 1$), where N is the order of the FSS filter, with high performance with a flat in-band frequency response and fast roll-off is introduced. Two miniaturised resonant surfaces coupled by a non-resonant inductive layer are used to build the proposed FSSs. An FSS operating at around 3.8 GHz is designed to verify the method. The element size is smaller than $0.076\lambda \times 0.076\lambda$ for the proposed structure. This is significantly smaller than the element size of second-order FSSs designed using conventional approaches. The overall thickness is less than $\lambda/24$. The method could be particularly useful for the

design of FSSs at lower frequencies with longer wavelengths. Thus, a novel approach for designing extreme low profile high-order bandpass frequency selective surfaces is introduced in this chapter. The structure is built in such way to obtain bandpass response by the coupling between the third harmonic responses of the resonators instead of the fundamentals. By parametric study of the proposed structure, one can make the coupling between the third harmonics weak with a thinner substrate, and then a flat in-band response can be achieved. The overall thickness can be reduced to λ/75. Chapter 7 demonstrates FSSs with sharp transition edges and almost flat bandpass for submillimetre wave and terahertz applications. The proposed structure exhibits a low insertion loss in the desired band. The structure is realised by combining bandstop and bandpass FSS structures on the same plane. By cascading more than one layer of surfaces, separated by dielectric slabs, the response with the desired flat passband characteristics can be achieved. The structure is polarisation independent and exhibits low insertion loss at the passband around 170 GHz. Finally, Chapter 8 demonstrates an extremely small-size high impedance surface (HIS) array element. A trade-off between a miniaturised element size and a lowered thickness of the grounded substrate is made to design an extremely low profile HIS. Additionally, we propose a way to modify existing classical RFID tag designs to enable them to operate well when they are attached to dielectric materials. Compared with using an HIS, the antenna bandwidth after being loaded with the proposed FSS is increased by approximately 100%.

Chapter 1: Introduction

1.1 Background

A frequency selective surface (FSS) is formed by periodic arrays of usually metallic elements on a dielectric substrate. The geometry of the surface in one period (array element) determines the frequency response of an FSS. Various responses can be achieved by using different traditional FSS element shapes. The FSS often displays selectivity not only on the frequency, but also on the angle and polarisation of the incident wave. FSS can be constructed by using identical elements arranged in a one or two-dimensional infinite array. If an aperture type FSS is created from a patch type FSS in such a way that the metal portions of the former are replaced by aperture portions of the latter, then the two FSS are said to be duals of one another. The FSSs can be classified as the bandstop patch type and the bandpass mesh type. If the metal plates are not connected, it is called a capacitive surface, and it reflects high frequencies whilst transmitting low frequencies. On the other hand, its complementary structure is called an 'inductive surface', which reflects low frequencies whilst transmitting high frequencies. Babinet's principle can be applied to prove that the transmission coefficient for the complementary structure of one array is equal to the reflection coefficient for the array [1, 2]. The frequency response of the transmitted signal of the complementary FSS is not exactly the dual of the reflected signal of the FSS due to the loss in the dielectric substrate. A perfectly dual behaviour for the complementary screen of the proposed filter is expected if the loss of the dielectric substrate, as well as the effects of the metal thickness, are neglected [2]. Hence, Babinet's principle can be employed to produce bandpass FSS from bandstop FSS, low pass FSS from high pass and vice versa. Different characteristics can also be obtained by cascading or combining individual filters. For instance, a bandstop filter could be formed by combining a number of bandpass filters.

The equivalent circuits for a bandstop FSS or a bandpass FSS are the combination of *LC* in series or in parallel, respectively [1, 3]. Traditionally, many different shapes have been used to construct an FSS. However, the equivalent FSS circuit is directly related to the array element size, shape and the polarisation. Equivalent circuits and analysis of some of the traditional structures are provided in [3, 4].

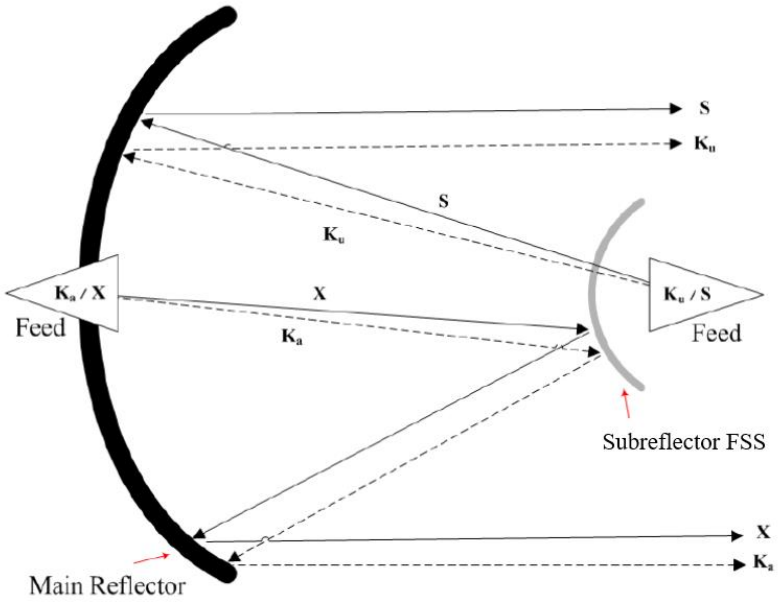

Fig. 1.1. Cassini high-gain antenna (HGA) with a four-frequency FSS [5].

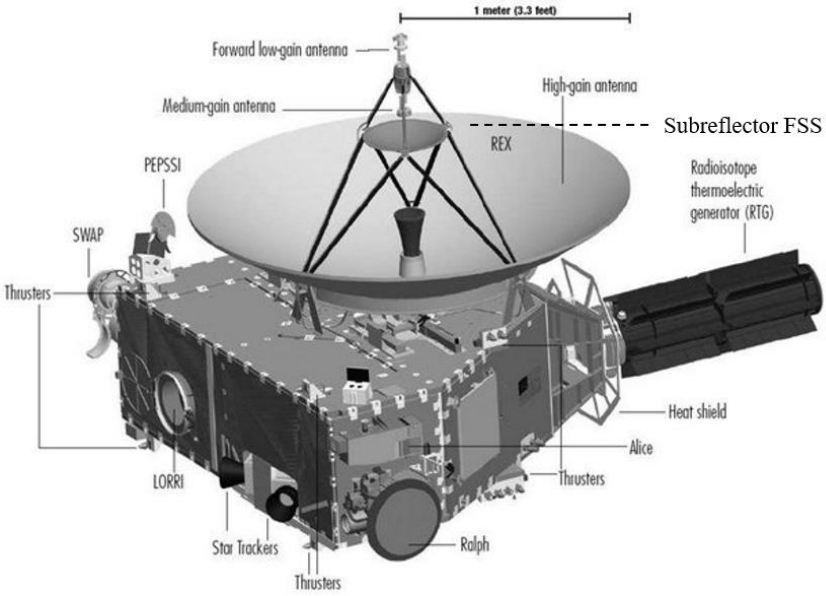

Fig. 1.2. The high-gain dish has a Cassegrain reflector [6].

FSSs have been most commonly used in microwave and optical frequency regions of the electromagnetic spectrum and for applications such as antennas, radomes, radio frequency absorbers, wireless securities to electromagnetic (EM) shielding applications and metamaterials [3, 7-13]. Decreasing loss in antennas and improving the radiated power are successfully realised by using these structures [13, 14]. They are designed to reflect, transmit or absorb electromagnetic radiation at different frequencies [1, 15, 16]. The use of dual-reflector antennas in space missions such as Galileo, Cassini, Cassegrain and Voyager, sharing the main reflector among different

Fig. 1.3. FSS in different military and civil applications [17].

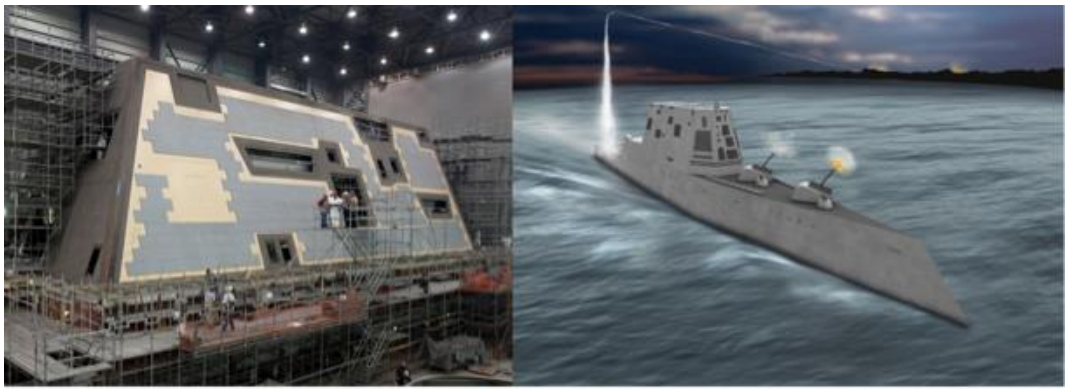

Fig. 1.4. The Zumwalt, the largest destroyer ever built for the US Navy [18].

frequency bands, has been made possible by using an FSS, [19-22]. Fig. 1.1 shows Cassini high-gain antenna (HGA) with a four-frequency FSS [5]. Fig. 1.2 shows a Cassegrain reflector in the high-gain dish [6]. FSSs are used in modern military platforms such as aircraft, ships and missiles, as can be seen from Fig. 1.3 [17]. FSSs can be used in many applications in the civil sector as well, such as the isolation of unwanted and harmful radiation in L-band and S-band in hospitals, schools and domestic environments. FSSs are widely used for antennas and radar cross section (RCS) reduction or components in radar absorbing material (RAM) [23-25]. The concept of stealth and operating without the knowledge of the enemy has always been a key driver in the development of military technology. As example, Fig. 1.4 shows the Zumwalt, the largest destroyer ever built for US Navy [18].

1.2 Motivations

FSSs have been the subject of intense investigations on a large scale, as microwave and optical filters, for decades [3, 7-13]. The use of FSSs has contributed to the increase in the communication capabilities of satellite platforms [20-22, 26]. FSS suffers from practical design problems that can be categorised as the bandwidth, size of FSS element, sensitivity to the incident angle and sensitivity to the polarisation. The reflection and transmission coefficients of the FSS are mainly dependent on the shape and size of array elements. Thus, the bandwidth can be influenced by the gaps between element's parts and the gap between adjacent elements. The close grating lobe is the main drawback of a passband FSS which characteristically damages the stopband behaviour [27, 28]. To position the grating lobe far from the passband, the inter-element spacing of single free standing FSS must be set less than $\lambda/2$, where λ is wavelength at the resonant frequency[1]. It is important that the shape, dimensions and spacing of the array elements are designed all together to reach the desired resonant frequency and bandwidth, as well as to avoid grating lobes.

Recently, many approaches have been proposed to miniaturise FSS array element dimensions. For example, a parallel lumped inductor and a lumped capacitor can be used to reduce the size of the FSS array element [29, 30]. Adding meander-slots to the circular ring structure can produce FSS array element dimensions much smaller than the wavelength [31]. A study in [32] demonstrated a miniature FSS by printing micro wire on a dielectric. Printing four symmetrical spiral patterns of metallic meander lines can increase the electrical length of the array element and increase the value of the resonant components [33]. However, increasing the electrical length of an array element with the same physical dimensions has limitations, and could increase the complexity of the FSS structure. Thus, a parallel lumped inductor and lumped capacitor can be used to design a dually polarised FSS array element in [29]. Two metallic layers of an asymmetrical pattern are placed on the top and bottom side of a dielectric substrate to display a dually polarised frequency response in [34]. FSS structures are composed of arbitrary shapes comprised of metallic patches or apertures which are supported by a dielectric substrate. FSSs have been the subject of intense investigations in a great number of applications, such as spatial microwave and optical filters for decades [1, 7, 8, 35].

Traditionally, the element of a FSS is rotationally symmetrical and the element arrays in a multi-layer FSS are aligned with each other. Different techniques have been used to achieve stable frequency responses in different polarisations for single and multi-layer FSSs under various angles of incident waves. Accomplishing a symmetrical FSS array element can contribute to achieving a stable resonance with respect to the polarisation and the angle of incidence [29-33, 36]. However, using symmetrical array element shapes to avoid polarisation sensitivity can restrict FSS design options.

In most applications, an FSS needs to be attached to a wide variety of dielectric materials. In conventional FSSs, the performance of an FSS is greatly influenced by the dielectric material it is attached to.

FSSs have been used in radar absorbing materials (RAM) [24, 25], but it is still a challenge to select a wideband FSS for this application. Classical RAM is composed of several layers of dielectric or magnetic media. For instance, the two most common absorbing screens are the Salisbury and the Dallenbach screens. The first consists of a thin resistive film deposited on a perfect metal-backed dielectric, while the second is a short-circuited lossy dielectric or magnetic layer. Those absorbing screens are described in [37]. An FSS can be deposited on the outer surface of the Dallenbach screen to modify and improve the absorption performance of Dallenbach screens. In the last few decades, many methods have been adopted to improve the FSS performance. The effects of dielectric loading on FSSs were studied in [38].

FSSs are also used to build up an artificial magnetic conductor (AMC) or high impedance surface (HIS) where the FSSs are placed above a perfect electric conductor (PEC) ground plane, with a dielectric material in between [39]. It does not support propagating surface waves. It displays a 0^{o} reflection coefficient phase at a given frequency [13]. While using a conventional conductor as a ground plane for a planar antenna, the power transferred into the surface waves does not contribute to the main radiation of the antenna, but is scattered off the edges of the finite ground plane and leads to ripples in radiation patterns, increased back radiation, and lower polarisation purity. In a traditional HIS, the grounded substrate (the substrate between the periodic element and the ground plane) tends to be thick to achieve a small HIS array element size.

1.3 Shaping a periodic structure

The choice of selecting the proper element may be of most importance when designing either a bandpass or band-stop FSS. Some elements are inherently more narrow-band or more broadband than others, while some can be varied considerably by design. Different FSS types can be chosen based on the application requirements. These requirements usually include a level of dependence on the polarisation and incidence angle of the incoming wave and bandwidth. However, it is worth mentioning that in general, at least for mechanical and miniaturisation reasons, all FSS must eventually be supported by a substantial assembly of dielectric slabs. This has a strong effect on the bandwidth variation with angle of incidence and the element size.

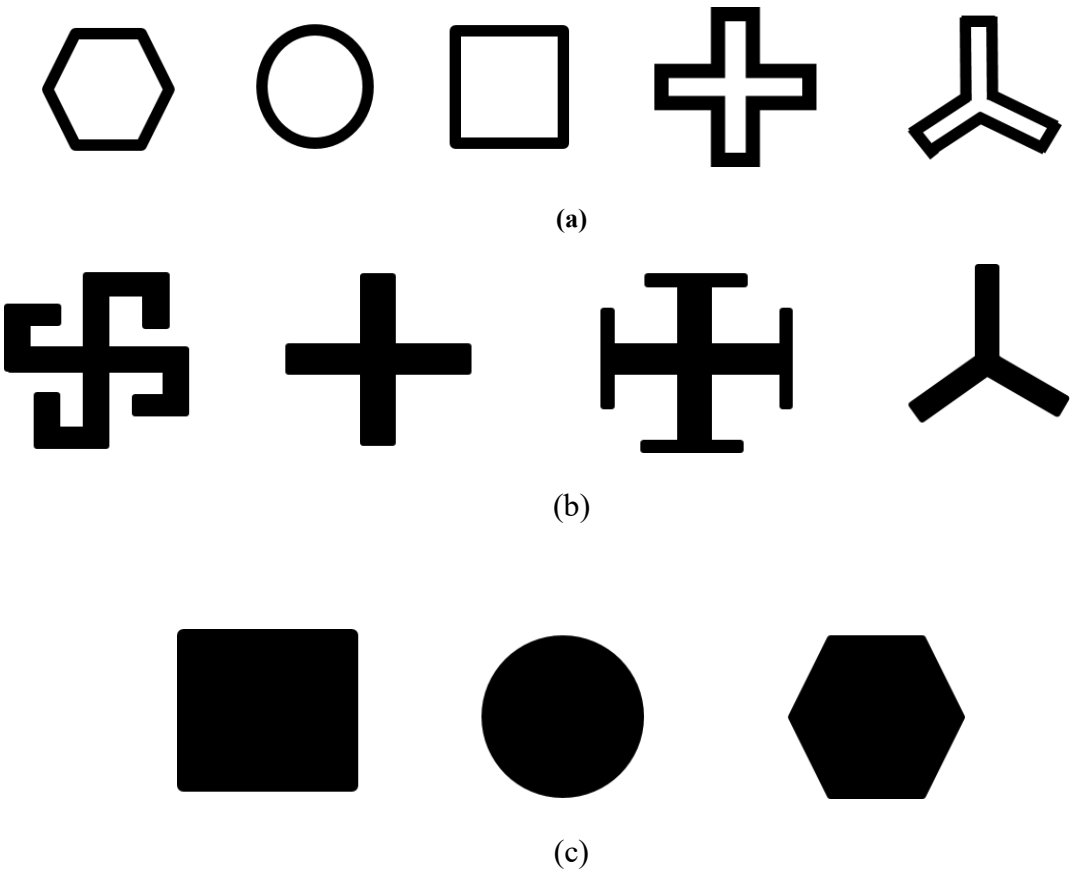

Fig. 1.5. (a) Loop elements, (b) centre connected elements, (c) patch elements [1]**.**

In this chapter we present the most common element types available to FSS designers. The elements can be arranged into three groups, Chapter 2, Section 2.1 of [1], as shown in Fig. 1.5: The first group is the loop FSSs, such as the hexagonal rings, the circular ring, the square rings, the three and four-legged loaded elements.

The second group is the centre connected FSSs, such as the square spiral elements, the four-legged elements, the Jerusalem cross and the three-legged elements. The third one is patch FSSs, such as square, circular paths and hexagonal patches. The mechanism of operation in traditional FSSs is based on the resonant elements. The idea is that a plane-wave illuminates an array element. This will excite electric current on the element. The amplitude of the generated electric current depends on the strength of the coupling of energy between the element and the incident wave. At the fundamental frequency where the length of the element is λ/2, the coupling reaches its highest. As a result, the elements are formed so that they are resonant near the frequency of operation. The current itself can act as an electromagnetic source depending on its distribution. It produces a scattered field. The scattered field added to the incident field forms the total field in the space surrounding the FSS. The scattered field can be controlled through the design of the elements.

The plane of incidence and polarisation of incidence are defined in Fig. 1.6. The FSS is excited by an electromagnetic wave with the propagation vector (**k**) towards the *z* axis, a magnetic field vector (**H**) towards the *x* axis and an electric field vector (**E**) towards the *y* axis direction. ɵ represents the incident angle, while ϕ represents the polarisation angle.

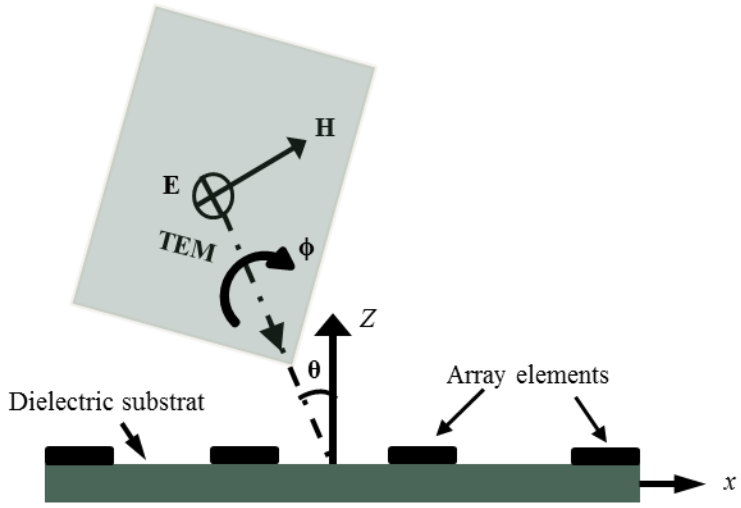

Fig. 1.6. The plane of incident wave, ɵ is the angle of incidence, ϕ is the polarisation angle.

1.4 Dielectric effect on FSS

What happens if the periodic structure has been completely surrounded by an infinite dielectric material with relative dielectric constant ε_r? The answer to this

equation can be drawn from Maxwell's equations that the resonant frequency would reduce by the factor $\sqrt{\varepsilon_r}$, Chapter 1, Section 1.6.3 of [1]. The second equation, what happens when the infinite dielectric material extent reduced to be finite thickness? To answer this question - we need to classify the FSS as the two types based on the equivalent circuit; the capacitive surface, or the patch type, and the inductive surface, or the mesh type. In this way, the study of the effects of dielectric materials on the FSS will be easier.

1.4.1 FSS mesh type

The dielectric slabs can have a profound effect on the reflection or transmission responses. With a finite thickness, the dielectric material's effect on the FSS structures can be explained by using the equivalent circuit analysis and structure simulation. The square ring with a strip width (w), as shown in Fig. 1.7, is used here as an example for the inductive FSS. Fig. 1.8 shows the equivalent circuit of the inductive FSS with both sides attached to dielectric slabs. L represents the intrinsic inductance value of the inductive surface. The approximate value of the intrinsic inductance L at normal incident wave can be calculated from the strip inductance using equations, Chapter 5, Section 5.19 of [40],[41]:

$$L = \mu_o \mu_e \frac{P}{2\pi} [\ln \operatorname{cosec}(\frac{\pi w}{2P})] \tag{1.1}$$

where L is the strip inductance, which is determined by the strip length P, the strip width w, and the effective magnetic permeability μ_e of the structure and it is assumed to be 1.

The dielectric slabs can be represented by two short pieces of transmission lines h_1 and h_2. The characteristic impedance of the transmission lines is $Z_{d1} = Z_o/\sqrt{\varepsilon_{r1}}$ and $Z_{d2} = Z_o/\sqrt{\varepsilon_{r2}}$, where Z_o is the free space impedance. The transmission lines can be replaced with their equivalent circuit model composed of a series inductor and shunt capacitor, as shown in Fig. 1.8(b). Using the Telegrapher's model for TEM transmission lines, the series inductance L_{t1}, L_{t2} are simply equal to [42]:

$$L_{t1} = \mu_o \mu_{r1} h_1 \tag{1.2}$$

$$L_{t2} = \mu_o \mu_{r2} h_1 \tag{1.3}$$

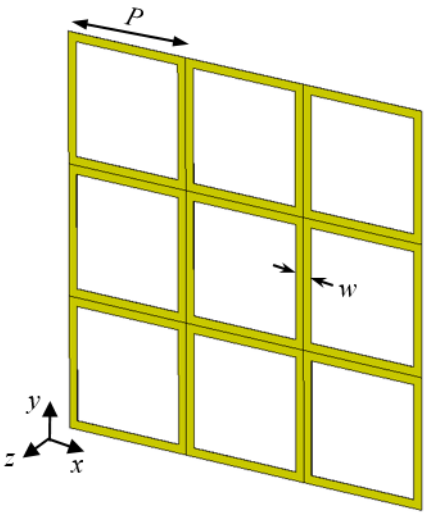

Fig. 1.7. An inductive FSS with 3×3 elements, *P* = 6.8mm.

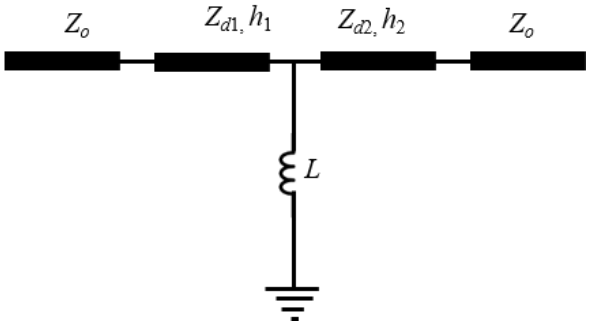

(a)

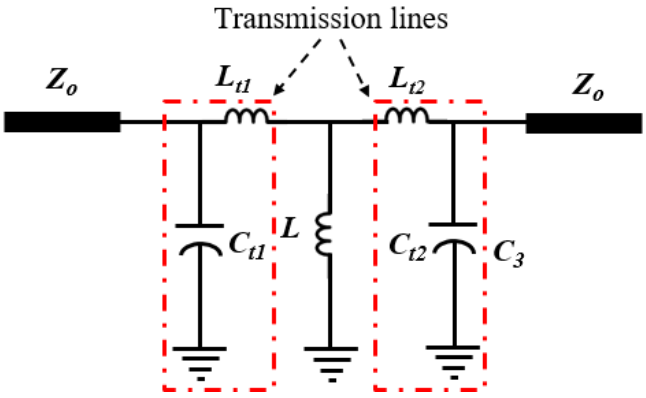

(b)

Fig. 1.8. The equivalent circuit of the inductive FSS type surrounded with dielectric substrates. (a) With transmission lines. (b) Using shunt capacitor and series inductor instead of transmission lines.

where μ_o is the permeability of free space, μ_r is the relative permeability of the dielectric substrate used and h is the length of the transmission line (equal to the thickness of the dielectric substrate). Using a procedure similar to the one used to

obtain the values of C_{t1}, and C_{t2}, the values of these shunt capacitances are equal to:

$$C_{t1} = \varepsilon_o \varepsilon_{r1} h_1/2 \quad (1.4)$$

$$C_{t2} = \varepsilon_o \varepsilon_{r2} h_2/2 \quad (1.5)$$

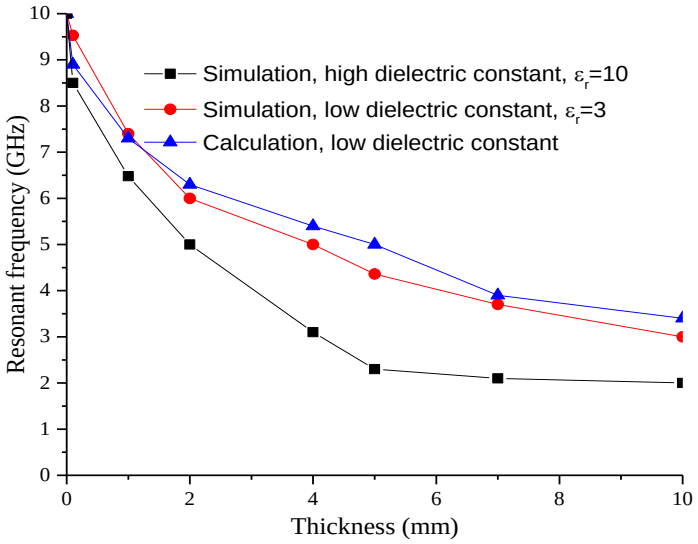

Fig. 1.9. Inductive FSS's resonant frequency shift when attached directly to a variety of dielectric materials of arbitrary thicknesses.

To find the shift in frequency response of the inductive structure due to the surrounding dielectric materials, the periodic inductive structure is firstly simulated with no dielectric materials nearby. Then the achieved frequency response is compared with ones that are achieved when the structure is attached to dielectric materials on both sides with varied dielectric constant and arbitrary thickness. Lower and higher dielectric constant materials (ε_r = 3 and 10) are used in these simulations. Fig. 1.9 shows the resonant frequency shifts of the inductive FSS structure due to the presence of dielectric materials with variable thicknesses. It can be observed that the resonant frequency shift is around $f_o/\sqrt{\varepsilon_r}$ when the low constant dielectric material is 3 mm thick and the high dielectric material is 4.2 mm thick.

If the periodic inductive structure is loaded with single side dielectric materials of arbitrary thickness, the resonance shift is smaller than when attached to both sides. Fig. 1.10, shows the equivalent circuit of the inductive FSS which attached to one side. Fig. 1.11 shows the resonant frequency shifts of the structure when it is attached to low and high constant dielectric materials of arbitrary thickness on a side. It can be seen that the resonant frequency shift is about $f_o/\sqrt{(\varepsilon_r+1)/2}$ at 3 mm and 5 mm thick for the low and high dielectric constant materials, respectively. However, the

calculated frequency shifts in case the structure attached to the low dielectric constant material shows a good agreement with the simulated ones, as shown in Fig. 1.9 and 1.11.

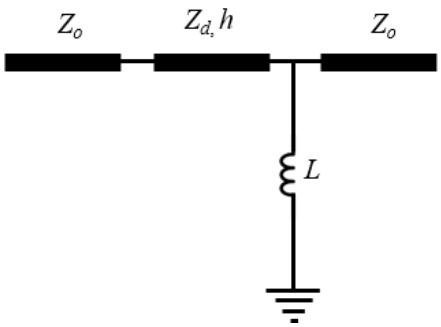

Fig. 1.10. The equivalent circuit of the inductive FSS type when one side attached to a dielectric slab.

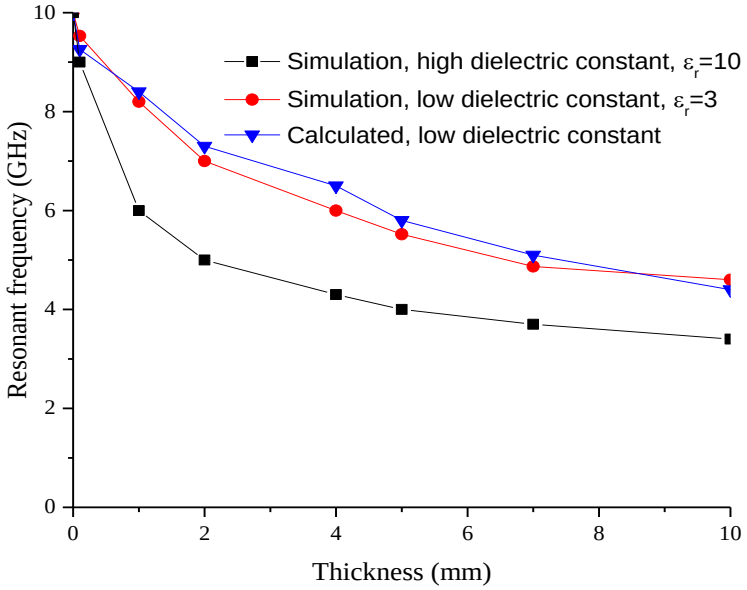

Fig. 1.11. Inductive FSS's resonant frequency shift when attached directly to a variety of dielectric materials of arbitrary thicknesses.

1.4.2 FSS patch type

If the periodic structure is capacitive, and has been completely surrounded by a finite dielectric material with relative dielectric constant ε_r and finite extent, the resonant frequency would reduce further compared to the periodic inductive structure. This is because the value of the intrinsic capacitor in the periodic structure

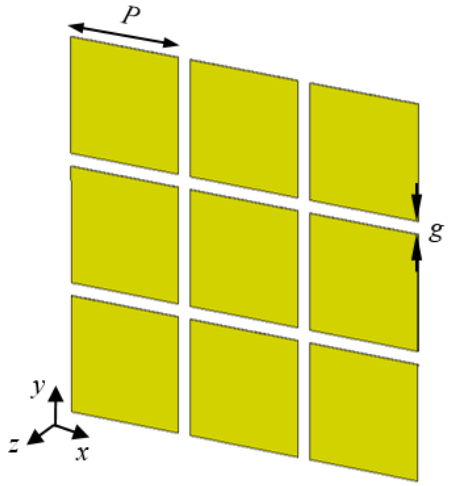

Fig.1.12. 3×3 of the capacitive FSS type, *P* = 5.8mm.

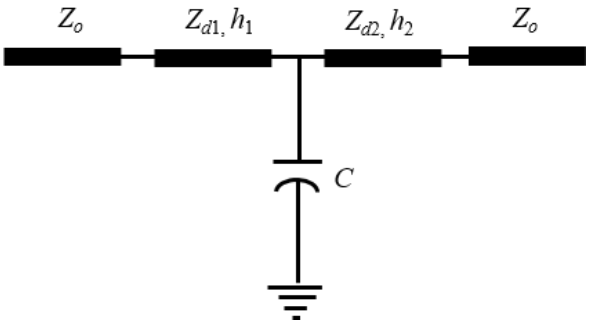

Fig. 1.13. The equivalent circuit of the capacitive FSS type surrounded with dielectric materials.

is increased. In the following paragraphs in this section, more details about the intrinsic capacitor will be described.

A periodic patch is used to represent the capacitive FSS, as shown in Fig. 1.12. Fig. 1.13 shows the equivalent circuit of the capacitive FSS with dielectric slabs attached to both sides. *C* represents the intrinsic capacitance value of the capacitive surface. The approximate values of the intrinsic capacitance at a normal incident wave can be calculated from the path capacitance using equations, Chapter 5, Section 5.18 of [40], [41]:

$$C = \varepsilon_o \varepsilon_e \frac{2P}{\pi} [\ln \operatorname{cosec}(\frac{\pi g}{2P})] \tag{1.6}$$

where *C* is the intrinsic capacitance between the two adjacent patches in each layer, which is determined by the patch length *P*, the gap *g* between adjacent patches and the effective dielectric constant ε_e of the structure. Observe that ε_e is $(1+\varepsilon_r)/2$ if the dielectric attached to one side of the FSS, while it is ε_r when attached for both sides,

Appendix E of [1].

The shift in resonant frequency of the periodic structure can be calculated by using the equivalent circuit shown in Fig. 1.13 with a procedure similar to the one used to obtain the values of C, L_{t1}, L_{t2}, C_{t1} and C_{t2}.

Thus, the periodic capacitive structure is firstly simulated with no dielectric materials nearby. Then the achieved frequency response is compared with ones that are achieved when the structure is attached to dielectric materials on both sides with varied dielectric constant and arbitrary thickness. Lower and higher dielectric constant materials (ε_r = 3 and 10) are used in these simulations. Fig. 1.14 shows the resonant frequency shifts of the patch FSS when attached directly to a variety of dielectric materials of different thicknesses, with g is 0.4 mm.

It can be observed that the frequency is shifted to around $f_o/\sqrt{\varepsilon_r}$ when the dielectric slabs on both sides are 0.3 mm thick or thicker for the low dielectric constant material, and 0.1 mm for the high dielectric constant material.

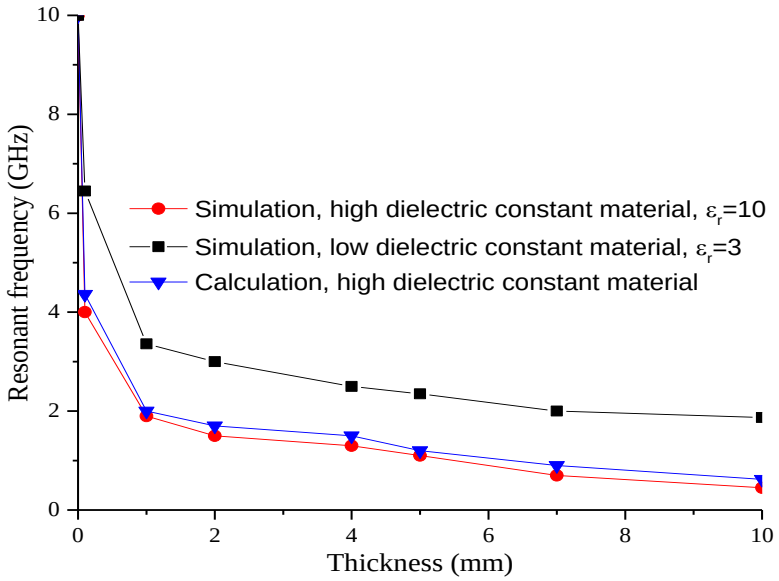

Fig. 1.14. Patch FSS's resonant frequency shift when attached directly to a variety of dielectric materials of arbitrary thicknesses.

Fig. 1.15 shows the equivalent circuit of the capacitive FSS attached to dielectric materials on one side only. Fig. 1.16 shows the simulation and calculation results of the resonant frequency shift of the capacitive FSS. It can be seen that the resonant frequency is shifted to about $f_o/\sqrt{(\varepsilon_r+1)/2}$ at 0.3 mm thick and 0.1 mm thick for the low and high dielectric constant materials, respectively.

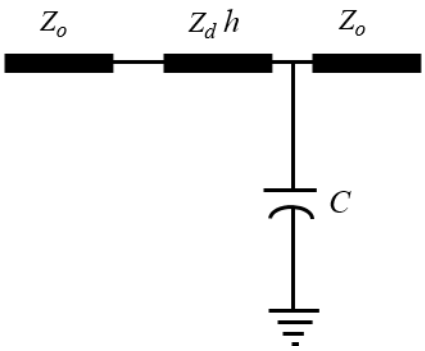

Fig. 1.15. The equivalent circuit of the capacitive FSS type when one side is attached to a dielectric slab.

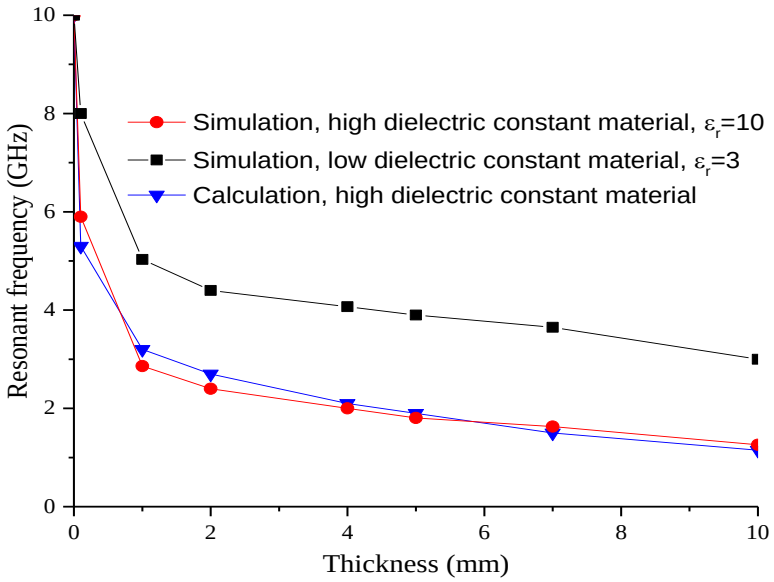

Fig. 1.16. Capacitive FSS's resonant frequency shift when attached directly to a variety of dielectric materials of arbitrary thicknesses.

The shift of the resonant frequency of a capacitive structure is bigger than an inductive one when attached to dielectric materials. It can be clearly explained from (1.6), where the intrinsic capacitance depends on the effective dielectric constant ε_e. The surrounding dielectric directly changes the effective dielectric constant value and thus the capacitance.

1.5 Experimental setup

Transmission characteristics of FSS devices can be measured via several methods [43, 44]. The measurement setup for an FSS is shown in Fig. 1.17. Two horn

antennas and a vector network analyser are used. The experiment setup is composed of two antennas which are pointing toward each other. The FSS under test is placed between the antennas. The distance should be large enough to satisfy the far field condition (meeting > $2A^2/\lambda$ criteria) [45], where A is the antenna size and λ is the free space wavelength at the resonant frequency. Thus, the wave arriving at the FSS can be considered as a plane wave.

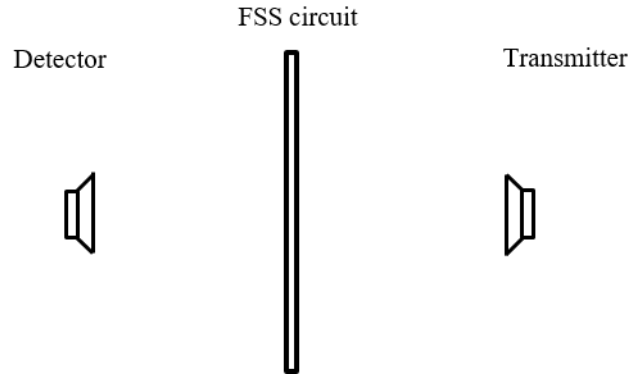

Fig. 1.17. Experiment setup to measure the transmission coefficient.

To avoid spillover or diffraction at the edge of the FSS, RF absorbing materials are used around the edges. In order to ensure the measurement accuracy, a calibration can be carried out. Without the FSS, the transmission coefficient could first be measured as the reference for 100% transmission (S_{21} = 1 or 0 dB). When the FSS is under test, the measured transmission coefficient will be normalised to the reference. In order to measure the transmission at different incident angles, the FSS holder fixture can be rotated to the angle of interest. In this case, the measurement accuracy is not as good as the normal incident angle due to the limited size of the FSS.

The line of sight between the two antennas passes through the centre of the FSS prototype. The antennas are aligned to ensure the formation of uniform plane wave impinging upon the FSS structure. The phase error can be calculated using the path length difference between the centre and the edge. The formula to calculate the phase difference across the aperture is the distance difference•$2\pi/\lambda$. Typically, it should be smaller than 90 degrees.

Ideally the array size should be as large as possible. Since the measurement is a comparative one (compared with the response without the FSS), the array size of $1.45\lambda \times 1.45\lambda$ appears to be large enough to give reliable results.

To measure the reflection, the two antennas are used as the transmitter and receiver, respectively, at the same side of the FSS, as shown in Fig. 1.18. They are separated by an absorber screen to eliminate the direct coupling between them. A calibration can be carried out in order to ensure the measurement accuracy. The reflection coefficient will be first measured with a plane sheet of metal instead of the FSS as the reference for 100% reflection (S_{11} = 1 or 0 dB). When the FSS is under test, the measured reflection coefficient can be normalised to the reference.

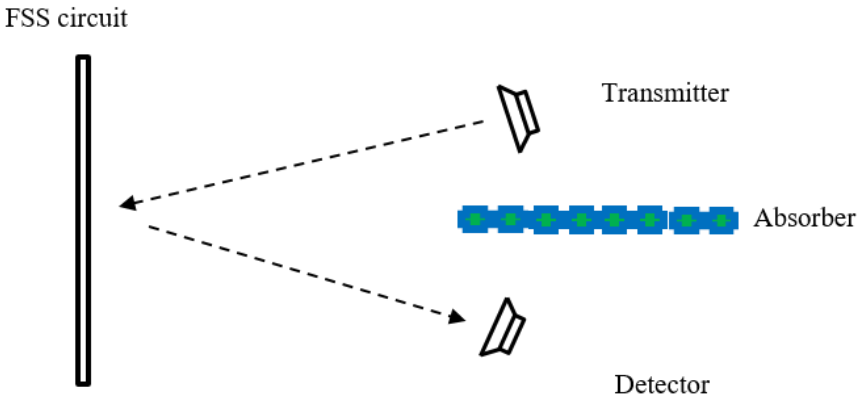

Fig. 1.18. Experiment setup to measure the reflection coefficient with oblique incidence orientation.

1.6 Outline of the thesis

In this article, Chapter 1 presents the background about the FSSs and an overview of technologies researched and developed with the aim of solving them. It also shows the dielectric effects on the periodic structures.

Chapter 2 introduces the theory and background of FSS operation. A brief history of the development and research of FSS design is presented. It also presents typical different designs of FSS array elements.

Chapter 3 introduces a new technique to miniaturise FSS array elements by interconnecting adjacent elements in one direction, and deals with the problem of the sensitivity of polarisation angles when using asymmetrical array elements.

In Chapter 4, a novel multi-layer structure is proposed to construct an FSS. The performance of the proposed structure is very stable when it is attached directly to a wide variety of dielectric materials of varied thicknesses.

Chapter 5 presents design examples of FSS array elements with multiple bands for

millimeter and microwave applications.

In Chapter 6, design methods of high order bandpass FSSs with desired features, such as lower-profile, compact size and sharp transition edges, are proposed and verified.

Chapter 7 focuses on THz FSSs and proposes new approaches to design FSSs with low loss and sharp edges. The structure is also easy to fabricate.

Chapter 8 focuses on the application of FSS, such as an extreme small size artificial magnetic conductor (AMC) array element, and the use of an FSS for robust antenna mounted on a plurality of dielectric surfaces.

Chapter 9 concludes with the summary and outlines potential future work resultant from the dissertation.

1.7 References

[1] B. A. Munk, "Frequency selective surfaces theory and design", New York: Wiley-Interscience, 2000.

[2] R. Ulrich, “Far-infrared properties of metallic mesh and its complementary structure,” *Infrared Physics,* vol. 7, no. 1, pp. 37-55, 1967.

[4] F. Costa, A. Monorchio, and G. Manara, “Efficient analysis of frequency-selective surfaces by a simple equivalent-circuit model,” *IEEE Antennas and Propagation Magazine,* vol. 54, no. 4, pp. 35-48, 2012.

[5] T.-K. Wu, "Double-square-loop FSS for multiplexing four (S/X/Ku/Ka) bands." *Antennas and Propagation Society International Symposium, 1991. AP-S. Digest* pp. 1885-1888.

[6] "Cassergrain reflector," https://www.quora.com/How-is-NASA-communicating-with-New-Horizons.

[7] R. Ott, R. Kouyoumjian, and L. Peters, “Scattering by a two-dimensional periodic array of narrow plate,” *Radio Science,* vol. 2, no. 11, pp. 1347-1359, 1967.

[8] B. Munk, and R. Luebbers, “Reflection properties of two-layer dipole arrays,” *IEEE Transactions on Antennas and Propagation,* vol. 22, no. 6, pp.

766-773, 1974.

[9] C. Winnewisser, F. Lewen, and H. Helm, “Transmission characteristics of dichroic filters measured by THz time-domain spectroscopy,” *Applied Physics A-Materials Science & Processing,* vol. 66, no. 6, pp. 593-598, 1998.

[10] S. Govindaswamy, J. East, F. Terry, E. Topsakal, J. L. Volakis, and G. I. Haddad, “Frequency-selective surface based bandpass filters in the near-infrared region,” *Microwave and Optical Technology Letters,* vol. 41, no. 4, pp. 266-269, 2004.

[11] F. Bayatpur, and K. Sarabandi, “Single-layer high-order miniaturized-element frequency-selective surfaces,” *IEEE Transactions on Microwave Theory and Techniques,* vol. 56, no. 4, pp. 774-781, 2008.

[12] B. Schoenlinner, A. Abbaspour-Tamijani, L. C. Kempel, and G. M. Rebeiz, “Switchable low-loss RF MEMS Ka-band frequency-selective surface,” *IEEE Transactions on Microwave Theory and Techniques,* vol. 52, no. 11, pp. 2474-2481, 2004.

[13] D. Sievenpiper, L. J. Zhang, R. F. J. Broas, N. G. Alexopolous, and E. Yablonovitch, “High-impedance electromagnetic surfaces with a forbidden frequency band,” *IEEE Transactions on Microwave Theory and Techniques,* vol. 47, no. 11, pp. 2059-2074, 1999.

[14] K. Kumar, D. Sievenpiper, L. Zhang, R. Broas, N. Alexopolous, and E. Yablonovitch, “Comments on" High-impedance electromagnetic surfaces with a forbidden frequency band"[with reply],” *IEEE Transactions on Microwave Theory and Techniques,* vol. 49, no. 1, pp. 228, 2001.

[15] T.-K. Wu, *Frequency selective surface and grid array*: Wiley-Interscience, 1995.

[16] H. T. Liu, H. F. Cheng, Z. Y. Chu, and D. Y. Zhang, “Absorbing properties of frequency selective surface absorbers with cross-shaped resistive patches,” *Materials & Design,* vol. 28, no. 7, pp. 2166-2171, 2007.

[17] https://www.slideshare.net/altairhtcus/cj-reddy-radomes-altairatc-final

[18] http://www.ccm.udel.edu/research_summaries/design-and-testing-of-structural-composite-rf-metamaterials-for-use-in-radomes-and-frequency-

selective-surfaces-2/.

[19] T.-K. Wu, "Cassini frequency selective surface development," *Journal of Electromagnetic Waves and Applications,* vol. 8, no. 12, pp. 1547-1561, 1994.

[20] Y. Rahmat-Samii, and A. N. Tulintseff, "Diffraction analysis of frequency selective reflector antennas," *IEEE Transactions on Antennas and Propagation,* vol. 41, no. 4, pp. 476-487, 1993.

[21] Y. Rahmat-Samii, and M. Gatti, "Far-field patterns of spaceborne antennas from plane-polar near-field measurements," *IEEE Transactions on Antennas and Propagation,* vol. 33, no. 6, pp. 638-648, 1985.

[22] G. Schennum, "Frequency-selective surfaces for multiple-frequency antennas," *Microwave Journal,* vol. 16, pp. 55-57, 1973.

[23] S.-W. Lee, "Scattering by dielectric-loaded screen," *IEEE Transactions on Antennas and Propagation,* vol. 19, no. 5, pp. 656-665, 1971.

[24] F. Sakran, Y. Neve-Oz, A. Ron, M. Golosovsky, D. Davidov, and A. Frenkel, "Absorbing frequency-selective-surface for the mm-wave range," *IEEE Transactions on Antennas and Propagation,* vol. 56, no. 8, pp. 2649-2655, 2008.

[25] S. Chakravarty, R. Mittra, and N. R. Williams, "On the application of the microgenetic algorithm to the design of broad-band microwave absorbers comprising frequency-selective surfaces embedded in multilayered dielectric media," *IEEE Transactions on Microwave Theory and Techniques,* vol. 49, no. 6, pp. 1050-1059, 2001.

[26] T. K. Wu, "Cassini Frequency-Selective Surface Development," *Journal of Electromagnetic Waves and Applications,* vol. 8, no. 12, pp. 1547-1561, 1994.

[27] F. Costa, and A. Monorchio, "A frequency selective radome with wideband absorbing properties," *IEEE Transactions on Antennas and Propagation,* vol. 60, no. 6, pp. 2740-2747, 2012.

[28] M. Yan, S. Qu, J. Wang, J. Zhang, A. Zhang, S. Xia, and W. Wang, "A novel miniaturized frequency selective surface with stable resonance," *IEEE Antennas and Wireless Propagation Letters,* vol. 13, pp. 639-641, 2014.

[29] K. Sarabandi, and N. Behdad, “A frequency selective surface with miniaturized elements,” *IEEE Transactions on Antennas and Propagation,* vol. 55, no. 5, pp. 1239-1245, 2007.

[30] C. N. Chiu, and K. P. Chang, “A novel miniaturized-element frequency selective surface having a stable resonance,” *IEEE Antennas and Wireless Propagation Letters,* vol. 8, pp. 1175-1177, 2009.

[31] F. C. Huang, C. N. Chiu, T. L. Wu, and Y. P. Chiou, “A circular-ring miniaturized-element metasurface with many good features for frequency selective shielding applications,” *IEEE Transactions on Electromagnetic Compatibility,* vol. 57, no. 3, pp. 365-374, 2015.

[32] S. N. Azemi, K. Ghorbani, and W. S. T. Rowe, “Angularly stable frequency selective surface with miniaturized unit cell,” *IEEE Microwave and Wireless Components Letters,* vol. 25, no. 7, pp. 454-456, 2015.

[33] G. H. Yang, T. Zhang, W. L. Li, and Q. Wu, “A novel stable miniaturized frequency selective surface,” *IEEE Antennas and Wireless Propagation Letters,* vol. 9, pp. 1018-1021, 2010.

[34] W.-l. Li, G.-h. Yang, T. Zhang, and Q. Wu, "A novel frequency selective surface with ultra-wideband polarization selective response." *Communication Technology (ICCT), 2010 IEEE International Conference on* pp. 1315-1318.

[35] J. C. Vardaxoglou, *Frequency selective surfaces: analysis and design*: Research Studies Press, 1997.

[36] M. B. Yan, S. B. Qu, J. F. Wang, J. Q. Zhang, A. X. Zhang, S. Xia, and W. J. Wang, “A novel miniaturized frequency selective surface with stable resonance,” *IEEE Antennas and Wireless Propagation Letters,* vol. 13, pp. 639-641, 2014.

[37] F. K. Eugene, F. John, and T. Michael, "Radar cross section," SciTech Publishing, Inc., Raleigh, NC, 2004.

[38] R. Luebbers, and B. Munk, “Some effects of dielectric loading on periodic slot arrays,” *IEEE Transactions on Antennas and Propagation,* vol. 26, no. 4, pp. 536-542, 1978.

[39] D. J. Kern, D. H. Werner, A. Monorchio, L. Lanuzza, and M. J. Wilhelm,

"The design synthesis of multiband artificial magnetic conductors using high impedance frequency selective surfaces," *IEEE Transactions on Antennas and Propagation,* vol. 53, no. 1, pp. 8-17, Jan, 2005.

[40] N. Marcuvitz, *Waveguide handbook*: IET, 1951.

[41] I. Anderson, "On the theory of self-resonant grids," *The Bell system technical journal,* vol. 54, no. 10, pp. 1725-1731, 1975.

[42] M. Al-Joumayly, and N. Behdad, "A new technique for design of low-profile, second-order, bandpass frequency selective surfaces," *IEEE Transactions on Antennas and Propagation,* vol. 57, no. 2, pp. 452-459, 2009.

[43] T. Cwik, R. Mittra, K. Lang, and T. Wu, "Frequency selective screens," *IEEE Antennas and Propagation Society Newsletter,* vol. 29, no. 2, pp. 5-10, 1987.

[44] D. K. Ghodgaonkar, V. V. Varadan, and V. K. Varadan, "A free-space method for measurement of dielectric constants and loss tangents at microwave frequencies," *IEEE Transactions on Instrumentation and Measurement,* vol. 38, no. 3, pp. 789-793, 1989.

[45] R. C. Johnson, H. A. Ecker, and J. S. Hollis, "Determination of far-field antenna patterns from near-field measurements," *Proceedings of the IEEE,* vol. 61, no. 12, pp. 1668-1694, 1973.

Chapter 2: Basics and Literature Review

2.1 Introduction

This chapter provides a summary of the relevant theoretical basics for FSS designs. It also provides a revision of the research areas of this work and aims to: summarise all the basic required knowledge for the design of FSSs; review the subject to understand the current challenges and the contributions of this work and build a solid base for the analysis in the following chapters.

2.2 A brief FSSs history

The defining feature of an FSS is its ability to act as a surface with bandpass or bandstop filtering properties to incident waves. This is accomplished through a periodic array of conductive elements that capacitively and inductively couple when excited by incident electromagnetic waves (e.g., a plane wave). A parabolic reflector grid using an array of resonant dipoles was one of the earliest forms of an FSS which was designed and patented by Marconi and Franklin in 1919 [1]. Much of the research into what are now referred to as FSSs did not gain momentum until the 1960s and 1970s. During this time, the Air Force Avionics Laboratory was involved in FSS development for radar and stealth applications [1], [2]. This research included new FSS element designs such as crossed dipoles which had greater versatility than the single resonant dipoles investigated previously. They provided better performance, including insensitivity to angle of incidence (the angle between the direction normal to the plane of the FSS and a plane wave's direction of propagation), which also made FSSs useful for certain applications such as stealth radomes and multi-band Cassegrain reflector dishes in antenna systems, [1], [3]. A few decades ago, a new trend for related research began. It focused on new methods of FSS design and development for general use. More recently, improvements in computing technology led to the use of numerical solvers, leading to many different FSS designs and applications including active FSSs [4], fractal element [5], and three-dimensional (3D) FSS structures [6].

2.3 Practical design problems

In addition to the shape, the response of an FSS is affected by other factors, such as the incident angle of an impinging plane wave which can cause the resonant frequency to draft or be dampened. Curvature of the FSS can greatly alter the frequency response. The inter-element spacing of the FSS must be set less than λ/2 to avoid grating lobes. Thus, the frequency response of an FSS is influenced by the presence of the dielectric material (see Chapter 1, Section 1.4). As, a result, the practical issues of the FSS structure must be evaluated to understand how an FSS will behave in a real system.

2.3.1 Wave incident angle

An FSS will be excited by normal incident waves. The resonant frequency and the bandwidth of an FSS will be affected by the incident angle. These effects are mainly due to the fact that the values of the inductance and capacitance of an FSS depend not only on the polarisation angle but also on the angle of incidence and on whether the polarisation is TE or TM. The resonant frequency of an FSS changes mainly because values of reactances (capacitance and inductance) are changed as the angle of incidence (Θ) changes and also on whether the polarisation is TE or TM. More details will be provided in Section 2.4.

The variations in the bandwidth of the structure as the angle of incidence varies can be attributed to the change of wave impedance, which will change the loaded quality factor of a resonator in an FSS structure. For the TE mode, the wave impedance changes to $Z_o/\cos(\Theta)$ [7], where Θ is the incident angle. Therefore, in the case of a large incident angle, the wave impedance increases, and the bandwidth decreases for parallel resonators because the loaded equality factor Q_L increases, while the bandwidth increases for a series resonator. For TM mode, the wave impedance changes to $Z_o \cos(\Theta)$ [7], as the incident angle changes. For this reason, Q_L decreases for large incident angles, and consequently the bandwidth increases for the parallel resonator, while it decreases for the series resonator.

However, in a practical demonstration, an FSS may need to be designed to operate under different angles of incidence. For most cases, the effects of incident angle on the frequency response of an FSS can be mitigated by three design techniques. Firstly, the effects can be reduced when the FSS is embedded in dielectric materials

[3, 8]. Secondly, miniaturisation of the FSS element size can enable the FSS to have sufficient number of elements, which can contribute to reduce the effects of the changes in the incident angle [9].

The third method, is to be reducing the inter-element spacing [1]. By doing this, whilst the space between elements is minimised, the effect of phase difference between elements caused by incident angle can be also reduced.

2.3.2 Curved FSS

Another practical issue for the implantation of an FSS structure is that the FSS structure may need to be a curved. Examples of applications for a curved FSS are stealth radome structure and sub-reflector antenna [10]. When an FSS is curved, changes in the frequency response of the FSS can occur depending on the nature of the curvature. It is worth considering two particular types of curvature [11]; the single curved FSS and the doubly curved FSS. The single curved FSS conforms to the shape of a cylinder, whilst the double curved FSS conforms to a conically rounded or spherical shape. In fact, the effect of the single curvature FSS on frequency response is less severe than that of the double curvature. Compared to an equivalent planar FSS, a curved FSS will have altered resonant response. This is mainly because curvature can cause changes in coupling between FSS elements. Thus, the curvature causes a different incident angle amongst FSS elements, causing differences in both magnitude and phase for each element in FSS structure [11, 12]. In addition for that, the curvature can cause a variation in phase difference over the FSS[12], and coupling between non-adjacent elements [11].

2.3.3 Grating lobe

The grating lobe can be explained by using a plane wave incident upon a one-dimensional periodic structure with inter-element space D_x, Chapter 1, Section 1.9 of [1], as shown in Fig. 2.1. It can observed from Fig. 2.1(a) that each element will have phase delay ($\beta\ D_x \sin\ \eta$) with respect to its neighbour to the left, where η is the incident angle. The same element will be ahead in phase for both the forward and the specular directions, and plane waves can always propagate in these directions.

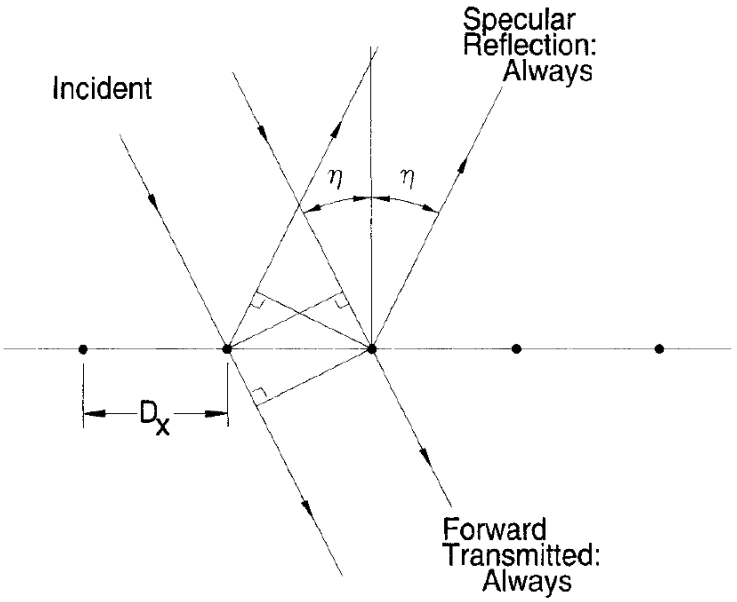

(a)

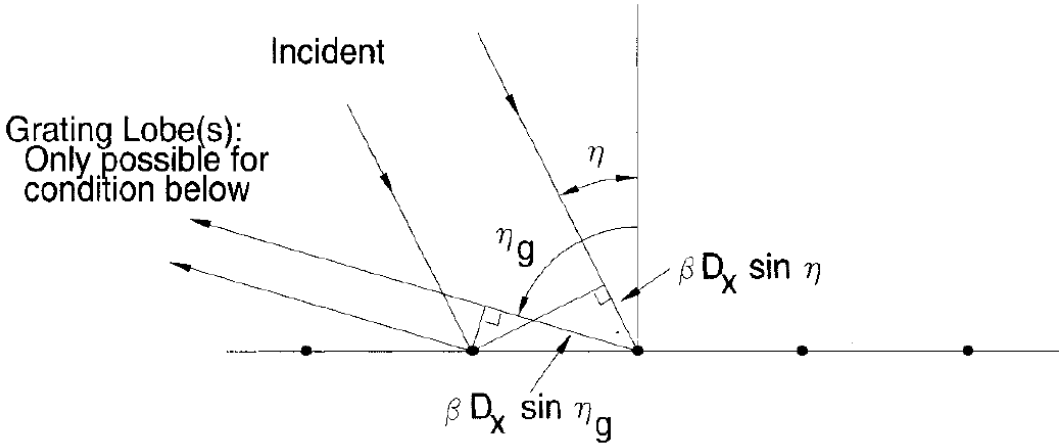

(b)

Fig. 2.1. Plane wave incident upon a periodic structure [1].

However, the incident wave can propagate in other directions as can be seen in Fig. 2.1(b), where, η_g is a possible grating lobe direction. It can be observed from Fig. 2.1(b) that the total phase delay of an element is $\beta\ D_x\ (\sin\ \eta\ +\ \sin\ \eta_g)$. Propagation is possible only if the delay equals a multiple of 2π, or

$$\beta\ D_x\,(\sin\,\eta + \sin\,\eta_g) = 2\pi n \qquad (2.1)$$

where $\beta = 2\pi/\lambda_g$, n is integer number, D_x is the interelement spacing along x axis, and λ_g is the wavelength at grating lobe frequency.

2.4 Strip equivalent circuit

Transmission and reflection coefficients of periodic arrays of conducting strips are frequency dependent and also dependent upon the orientation of the incident electric field relative to the strips [3]. The reactance of the strips is inductive when the tangential of the incident electric field is parallel to the strips, as shown in Fig. 2.2, causing high reflection (or very little transmission) at low frequencies. The transmission declines further, as a consequence of decreasing the inductance when the periodicity P decreases, or when their width w increases. The values of reactances depends not only on P and w but also on the incident angle (Θ) and also on whether the incidence is TE or TM. The approximation value of inductance, Chapter 5 of [13] is:

$$L = \mu \frac{P}{2\pi} \cos\theta \cdot [\ln \operatorname{cosec}(\frac{\pi w}{2P})] \tag{2.2}$$

where L is the strip inductance, which is determined by the strip length P, the strip width w, and the permeability μ of the structure.

When the E field is perpendicular to the strips, the approximation value of the capacitance, Chapter 5 of [13] is:

$$C = \varepsilon \frac{2P}{\pi} \cos\theta \cdot [\ln \operatorname{cosec}(\frac{\pi g}{2P})] \tag{2.3}$$

where C is the intrinsic capacitance between the two adjacent patches, which is determined by the strip length P, the gap g between adjacent strips and the dielectric permittivity (ε).

Based on the equivalent circuit, a different response can be achieved. Designing an FSS by using conducting strip can be performed in three simple steps. The first step is to obtain the appropriate element values for an equivalent circuit model for a desired response. This can be accomplished using circuit simulation software such as the Agilent Advanced Design System (ADS). In the second step, the FSS element can be formed to have structures to realise the components in the equivalent circuit which were obtained in the first step. The final step of the design procedure is to map the desired capacitors and inductors values obtained from above formula to geometrical parameters of the periodic structures.

Numerical analysis is performed on the complete array element of the proposed FSS consisting of the metallic structures and the dielectric substrates by using CST Microwave Studio. Unit cell boundary condition is applied to provide periodicity along the x and y axes. The FSS is excited by an electromagnetic wave with the propagation vector (**k**) parallel to the z axis, magnetic field vector (**H**) parallel to the x axis and electric field vector parallel to the y axis direction (see Fig. 1.6). Based on the results achieved from the full-wave simulation, the dimensions of the wires are fine-tuned to obtain the desired frequency response.

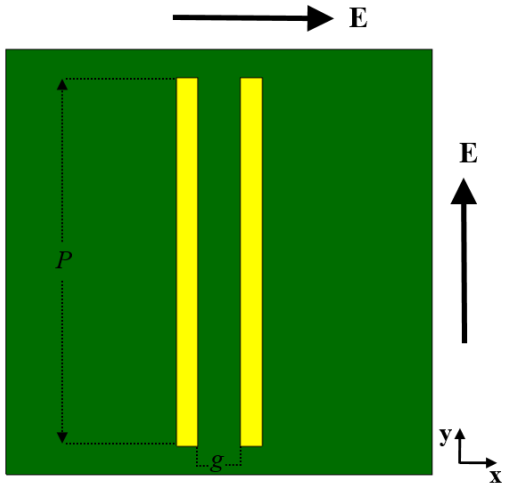

Fig. 2.2. Parallel wires used as the inductor or capacitor based on the electric field direction.

A bandpass, a bandstop and a dual-stopband FSS will be designed as examples of the proposed procedure. In all cases, the array element dimensions are 6×6 mm^2, the wire width is 0.2 mm and the thickness of the FR4 substrate is 1.6 mm. FR4 is a dielectric materials (glass epoxy), with 4.4 dielectric constant and 0.025 tangent loss at 10 GHz.

2.4.1 Wide bandpass FSS

As mentioned in the design procedure, the first step to design an FSS is by obtaining the equivalent circuit of a frequency response. As an example, Fig. 2.3 shows the response of the FSS; such a response can be obtained by using the equivalent circuit, as shown in Fig. 2.4. It is designed by combining L with series LC in parallel, where Z_o is the free space impedance and is equal to 377 Ω. The equivalent circuit exhibiting the wideband response, is shown in Fig. 2.5, with the components of: C_1= 0.3 pF, L_1= 2.73 nH, L_s = 2.36 nH. In the next step, the initial

dimensions of these *LC* components can be approximated using (1.1) and (1.6).

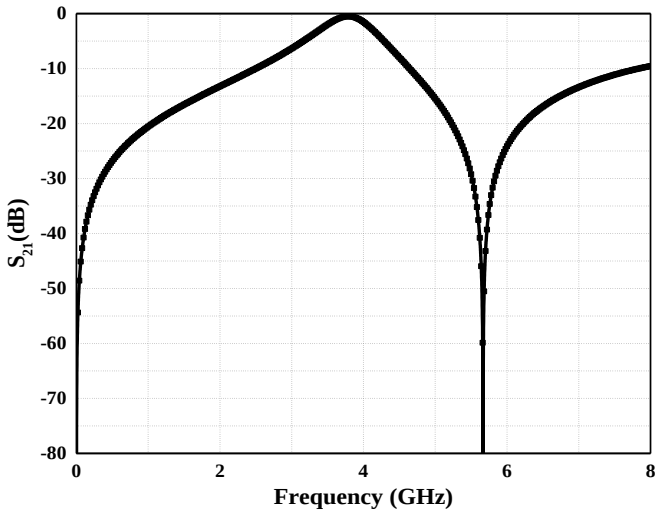

Fig. 2.3. Transmission coefficient of the bandpass response.

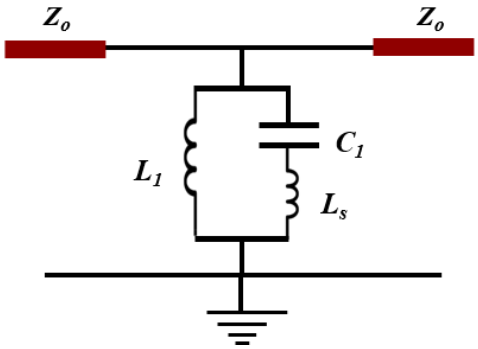

Fig. 2.4. The equivalent circuit of the desired bandpass response.

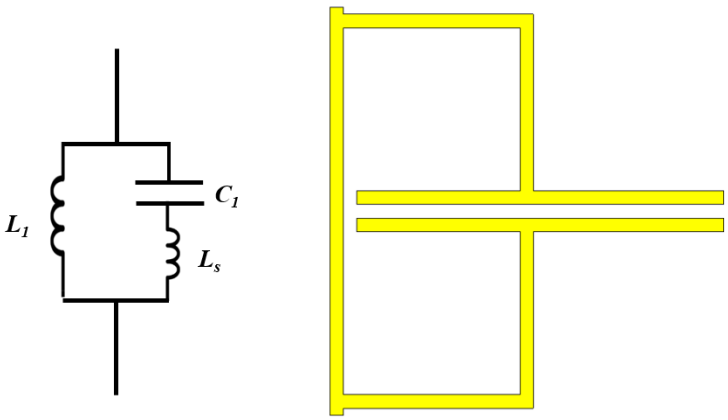

Fig. 2.5. The equivalent circuit of the proposed FSS structure (bandpass FSS), and the equivalent surface shape.

Finally, based on the results obtained from full-wave simulation (CST Microwave Studio) on the array element of the proposed FSS, the dimensions of the inductive

and resonant surfaces of the structure are tuned to achieve the desired frequency response. The theoretical values for the final geometry dimensions are: C_1= 0.195 pF, L_1= 3.05 nH, L_s = 2.64 nH.

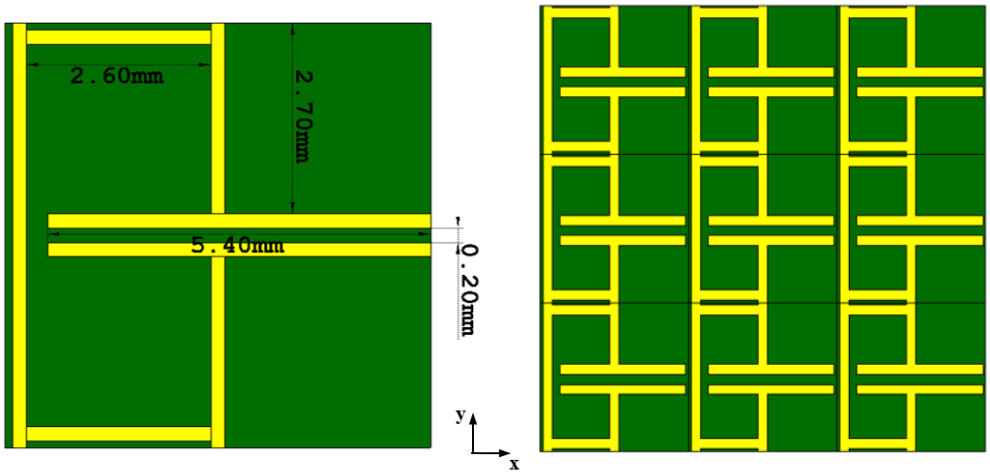

(a) **(b)**

Fig. 2.6. (a) Geometry dimensions of the proposed bandpass FSS, (b) 3×3 array elements of the proposed FSS structure.

Fig. 2.6(a) shows the geometry dimensions of the array element of the proposed bandpass FSS. Fig. 2.6(b) shows the 3×3 array element of the FSS. Fig. 2.7 shows the simulated transmission coefficient. The resonant frequency is about 3.8 GHz. The insertion loss is 0.13 dB at the resonant frequency. The size of the array element is 0.08λ × 0.08λ.

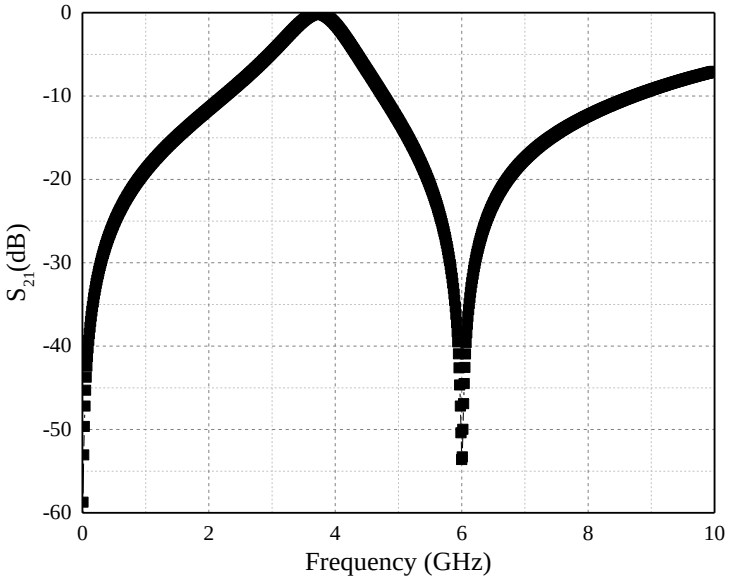

Fig. 2.7. Simulation result of the transmission coefficient of the designed bandpass FSS.

2.4.2 Wide bandstop FSS

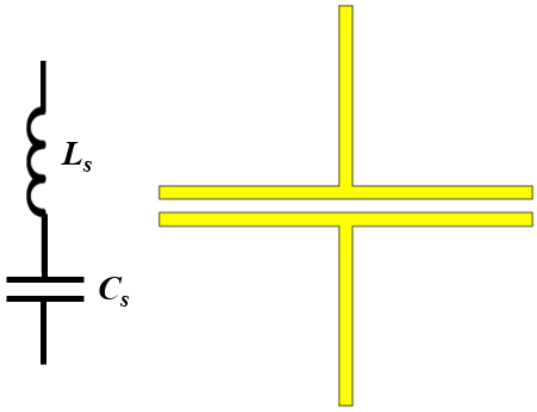

Fig. 2.8. The equivalent circuit of the desired response (wide stopband), and the equivalent surface shape.

In this section, the proposed design procedure will be used for designing an FSS with a wideband bandstop response. The response can be obtained by using a series *LC*, as shown in Fig. 2.8. The geometry dimensions of the array element of the bandstop FSS are shown in Fig. 2.9(a). Fig. 2.9(b) shows the 3×3 array elements of the structure.

The simulated result of the transmission coefficient is shown in Fig. 2.10. The structure exhibits bandstop response at 5.1 GHz, with the array element size of 0.102λ. It also has a wideband bandstop bandwidth. The fractional bandwidth (BW/f_o) is 120%, where BW is 3 dB bandwidth and f_o is the resonant frequency.

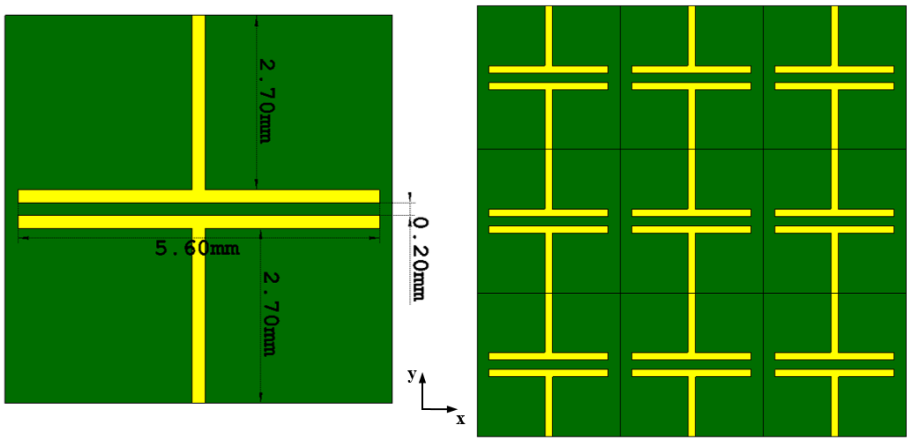

(a) **(b)**

Fig. 2.9. (a) Geometry dimensions of the proposed wide stopband FSS, (b) 3×3 array elements of the proposed wide stopband FSS structure.

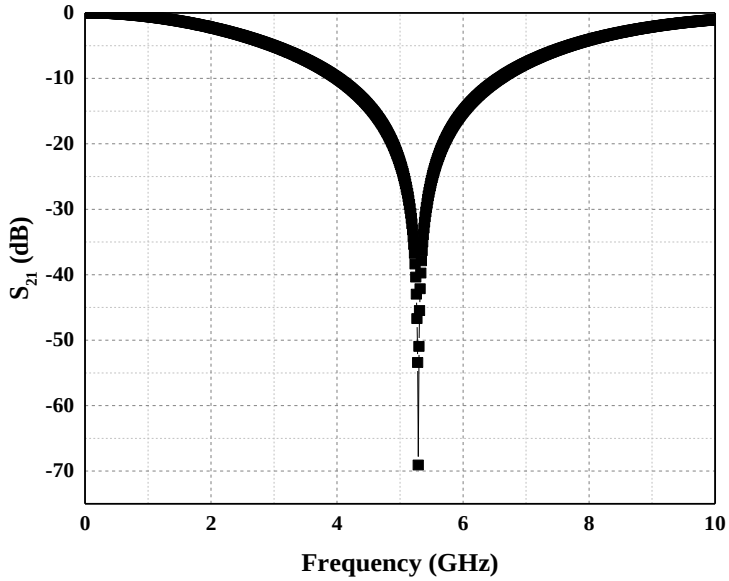

Fig. 2.10. Simulation result of the transmission coefficient of the designed bandpass.

2.4.3 Dual-band bandstop FSS

Fig. 2.11 shows an equivalent circuit model which is proposed to characterise a dual-stopband FSS. The equivalent circuit of the proposed dual-band bandstop is based on connecting a parallel *LC* with a series *LC* in series. The resonant frequencies of the parallel *LC* circuit and the series *LC* circuits are very close to each other. Such equivalent circuit can be formed by using the wires in the shape shown in Fig. 2.11. The geometry dimensions of the array element of the dual-band bandstop FSS are shown in Fig. 2.12(a), while the 3×3 array elements of the proposed structure are shown in Fig. 2.12(b).

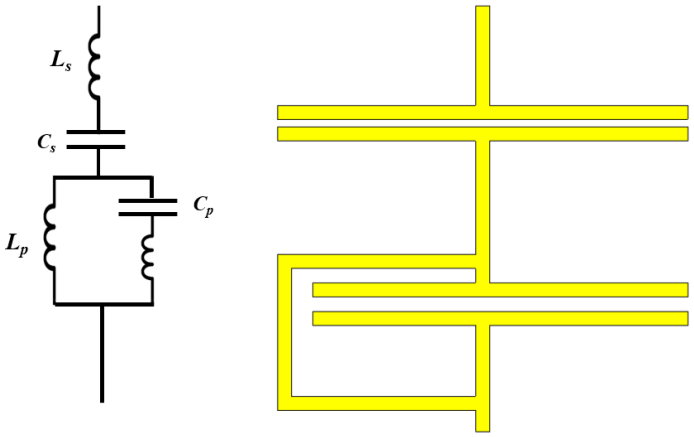

Fig. 2.11. The equivalent circuit of the desired response (dual stopband), and the equivalent surface shape.

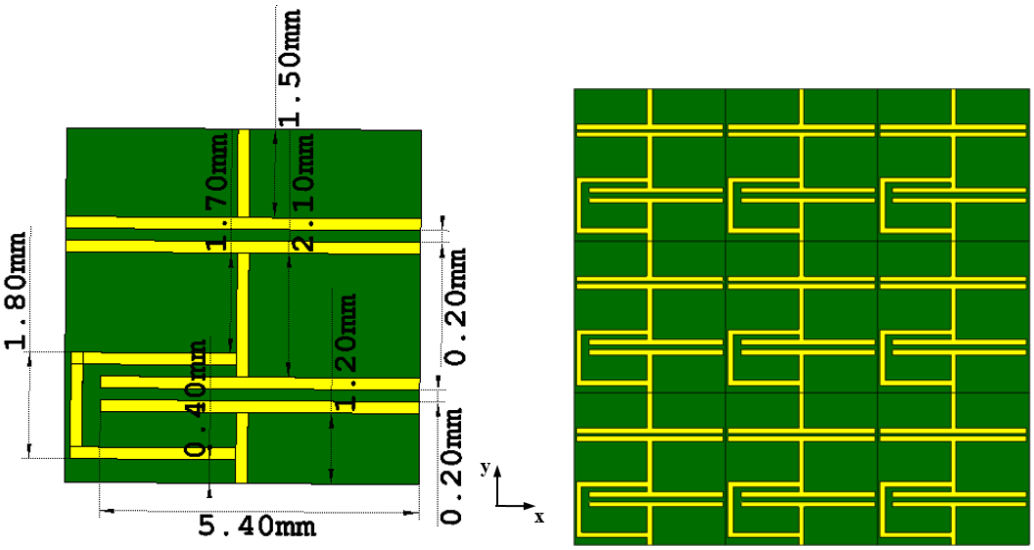

(a) (b)

Fig. 2.12. Geometry dimensions of the proposed dual-band bandstop FSS, (b) 3×3 array elements of the proposed FSS structure.

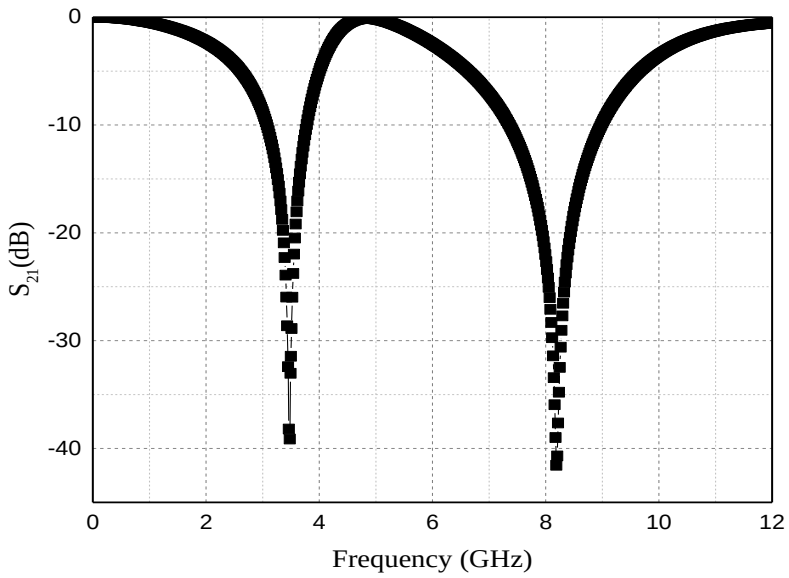

Fig. 2.13. Simulation result of the transmission coefficient of the designed dual stopband.

2.5 Shape and size of FSS array elements

The shape and size of the array element contributes to the response of an FSS for waves with various incident angles. Designing an FSS with array elements that have a specific response and compact size is difficult because it requires very good analytical skills to achieve a desired response. Many approaches have been proposed to miniaturise FSS array element dimensions. The miniaturisation is mainly achieved

by increasing the equivalent lumped-element values of resonant structures and it requires increasing the electrical length of an array element, where the electrical length is the length of an element in terms of the wavelength. The increasing of electrical length can be obtained by using lumped components (capacitor and inductor) in an array element. Additionally, it can be achieved by using a complex and sophisticated structure. Thus, the electrical length of an array element can be increased by increasing the effective dielectric constant or embedding the entire FSS in a material that has a higher dielectric constant than air. Unfortunately, high dielectric constant materials tend to have high loss tangents.

The most significant work that was conducted in the subject areas of the thesis is reviewed in the following sections.

2.5.1 Miniaturised FSS

Different approaches have been used to design miniaturised FSS and to obtain stable frequency responses in different polarisations under various angles of incident waves for single and multi-layer FSSs [9, 14-18].

Metallic patches and wire meshes are separated by a dielectric substrate which were used to miniaturise the array elements in [9, 14]. An FSS element miniaturised by using lumped components has been presented in [19]. Another approach was adopted in [20] by cascading interdigitated capacitors on a thin substrate layer. By cascading a square-loop slot with a periodic array of metallic patches, a compact FSS is implemented on an ultra-thin dielectric layer in [21].

In [9], the cascading of traditional structures, patch and grid, are separated by a dielectric layer which together act a bandpass FSS. The structure is shown in Fig. 2.14. The corresponding equivalent circuit of this resonator is a parallel *LC,* where *L* acts the grid layer, while *C* acts the patch layer. The structure shows a relatively stable resonant frequency for a range of incident wave angles. The dimensions of the array element of this structure are $0.2\lambda \times 0.2\lambda$, where λ is the wavelength at resonant frequency. This structure is large, especially for lower band applications.

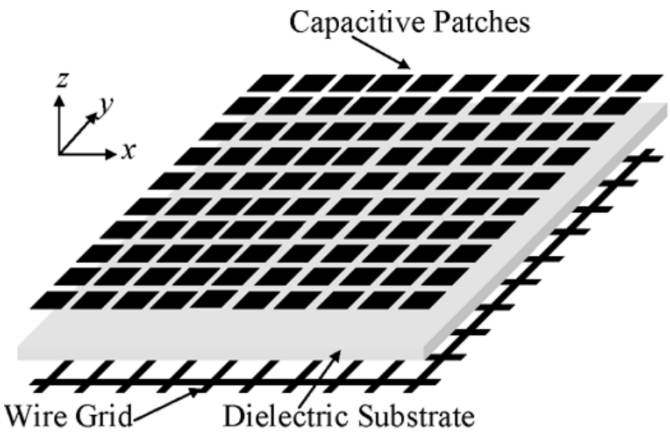

Fig. 2.14. bandpass by printing patches and grids on both sides as proposed in [9].

In [22], a bandpass FSS is constructed by using patch and inductive layers. This structure is built by using four symmetrical metallic patches and patterned-wires as shown in Fig. 2.15, separated by dielectric slab. The inductive layer is constructed by using meander lines to increase the inductance. Fig. 2.16(a) and (b) shows the structure frequency response with respect to different incident angles for TE and TM modes, respectively. It can be observed from Fig. 2.16 that the structure demonstrates a relatively stable resonant frequency with respect to different polarisations and incidence angles. The structure has a compact element, moreover the element dimensions are 0.104λ×0.104λ.

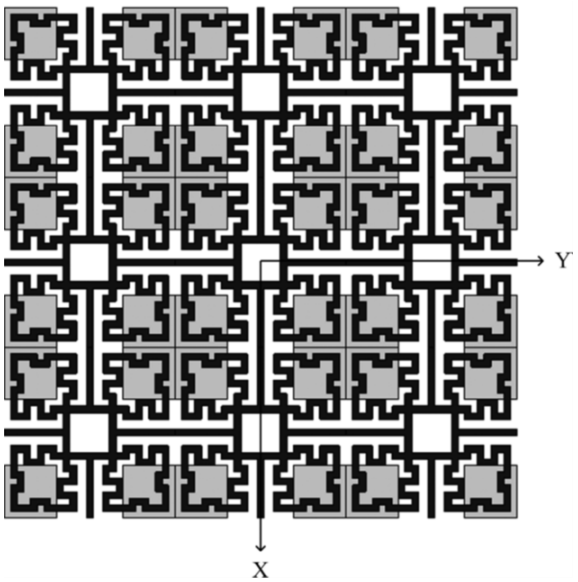

Fig. 2.15. The bandpass by printing patches and grids on both sides of a dielectric slab as proposed in [22].

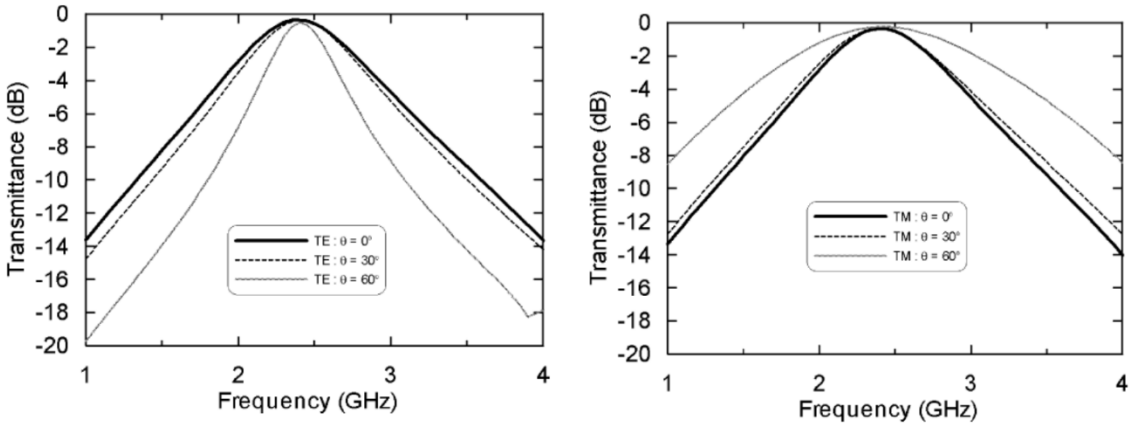

(a) **(b)**

Fig. 2.16. Transmission coefficients under various incident angles [22], (a) TE mode, (b) TM mode.

In [15], adding meander-slots to the circular ring structure can make FSS array element dimensions much smaller. Fig. 2.17 shows two unit elements of this structure. This structure is a single-layer (metal-dielectric). By adding meander-slots to the circular ring element, the values of capacitor and inductor can be increased. The dimensions of the array element can be reduced to 0.088λ×0.088λ.

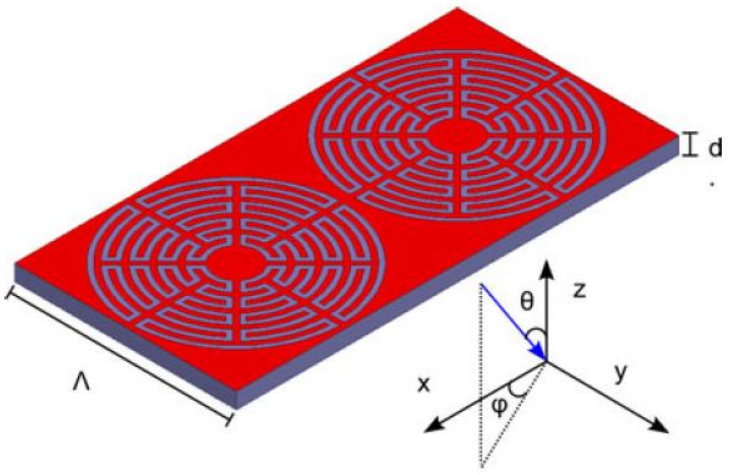

Fig. 2.17. Two elements of the proposed structure in [15].

In [16], a miniature low-profile FSS by printing wire (200 μm width) on both sides of a thin dielectric slab has been demonstrated. This structure, as shown in Fig. 2.18, exhibits a bandstop response at 3.33 GHz, with stable resonant frequency until 88º for TE and TM modes, as can be observed from Fig. 2.19. The dimensions of the element are 0.067λ×0.067λ, with a 0.127 mm thick Rogers RT/duroid 5880 substrate with a dielectric constant of 2.2.

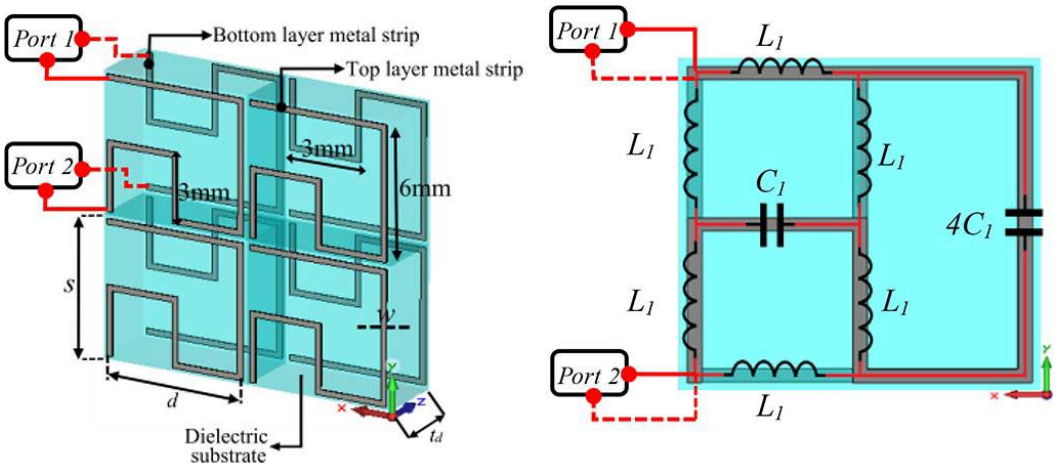

Fig. 2.18. The proposed FSS in[16], (a) 2×2 array elements , (b) equivalent circuit model for the element.

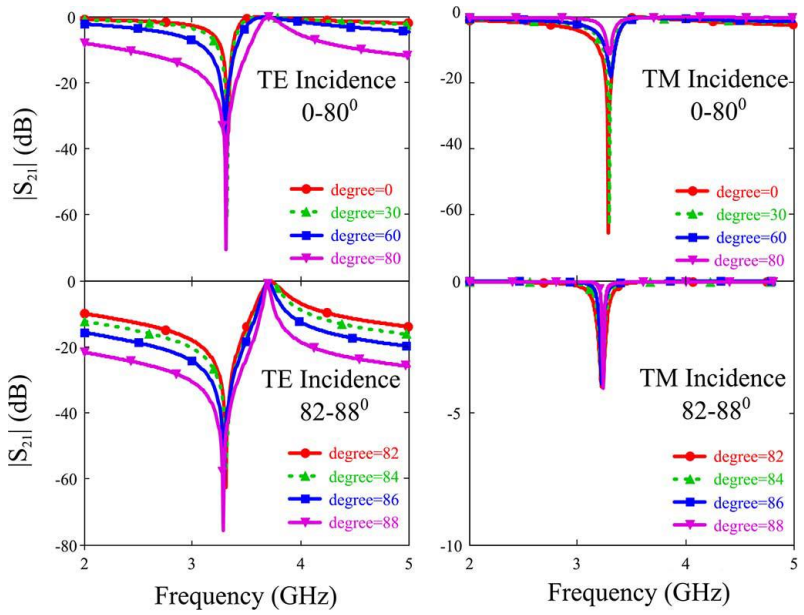

(a) **(b)**

Fig. 2.19. The frequency response of the proposed structure in [16], under a wide range of incident angles, (a) for TE mode (b) for TM mode.

In [17], using four symmetrical spiral patterns of metallic meander lines can increase the electrical length of the array element and increase the value of the resonant components. The array element of this structure is miniaturised based on increasing the inductance value by using the spiral shape, as shown in Fig. 2.20. While, by decreasing the space between the spiral turns, the capacitor value will be increased. The array element size for this structure is 0.061λ×0.061λ. The structure shows a stable resonant frequency under different incident angles, especially for TE mode.

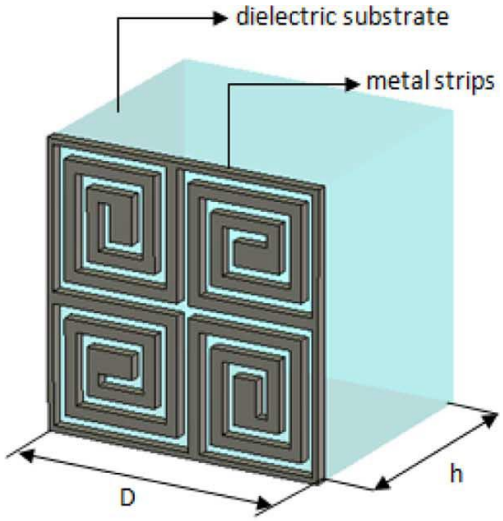

Fig. 2.20. The four symmetrical spiral element proposed in [17].

One way to make a compact element is by using vias. They are employed in the 2.5-Dimensional (2.5-D) FSS to increase the capacitive coupling between proximal elements and for connecting the various substrate layers within the element to increase its inductance [23, 24].

In [25], two pairs of split rectangle rings (one pair on the top and the other pair on the bottom of the substrate) are connected in series by vias to miniaturise the element. The proposed FSS element has a longer perimeter due to the connection between the top and bottom layers by using vias, as shown in Fig. 2.21. The dimensions of the element for this structure are 0.048λ × 0.048λ, and provides favourable resonant stability at various polarisations and incident angles.

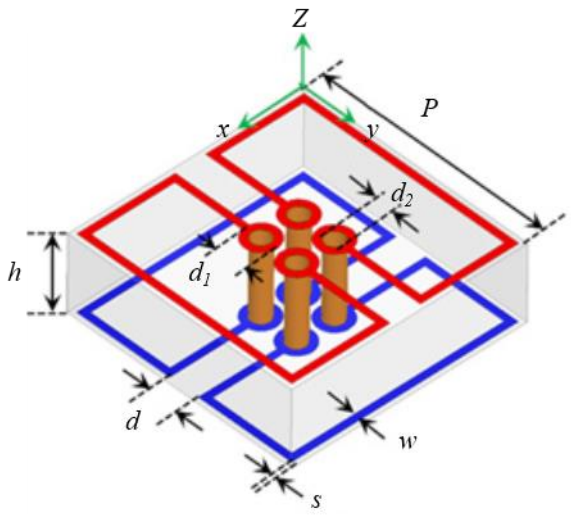

Fig. 2.21. The two pairs of split rectangle rings proposed in [25].

However, all references mentioned in the literature review are sensitive to the nearby dielectric materials. This is because the intrinsic capacitor in an FSS is sensitive to dielectric materials. Thus, the corresponding equivalent circuit of an element will be changed when the element is attached to dielectric materials, as mentioned in Chapter 1.

2.5.2 High order FSS

Although theoretically similar to a classical microwave filter, a spatial filter is more complicated. A classical filter has a pair of terminals (input and output). The response is recorded at the output when a signal is fed to the input terminal. A spatial filter has a wave arriving at variable incident angles as well as polarisations. This fact has major impact on the transmission responses. Moreover, FSSs have finite dimensions. The desired frequency selective response can only be observed when the finite surface includes a sufficient number of constituting elements and is illuminated by a planar phase front, Chapter 1, Section 1.1 [1]. For some applications, such as low-frequency antenna radomes, FSSs with array elements of relatively small electrical dimensions are highly desirable because they are less sensitive to the angle of incidence and can operate for non-planar phase fronts [26]. A bandpass FSS can be built by cascading two or more surfaces isolated by dielectric slabs. The thickness of the dielectric slabs is usually around a quarter of wavelength in order to obtain flat frequency response and fast roll-off, Chapter 1, Section 7.1 [1]. As a result, the structure will be bulky, and sensitive to the wave incident angle, especially for low frequency applications.

Many different techniques have been used to design miniaturised and low profile high order FSSs.

In [27], using non-resonant traditional patch and grid to design a low profile second-order bandpass FSS was given. Fig. 2.22 shows the array element of the second-order FSS. The simulated transmission coefficient for this structure is shown in Fig. 2.23. For the TE mode, the bandwidth decreases and the bandpass ripple level increases when the angle of incidence increases, as can be observed from Fig. 2.23(a). Fig. 2.23(b) shows the simulated frequency response of the same structure under various angles of incidence for TM mode. There are also variations in bandwidth as can be observed from Fig. 2.23(b).

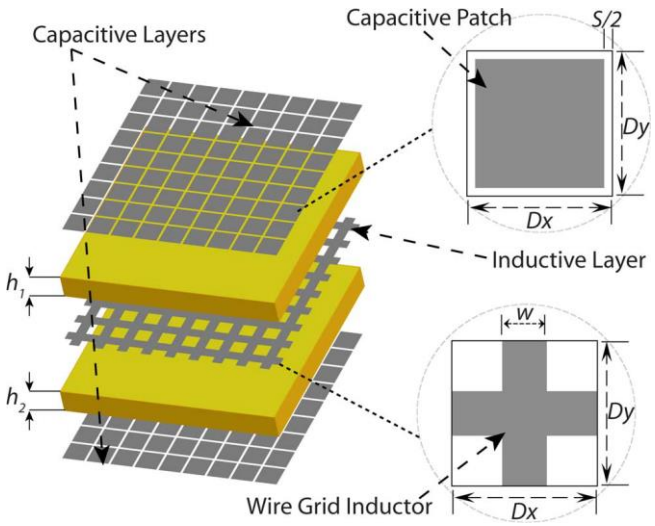

Fig. 2.22. The low profile, second-order bandpass FSS presented in [27].

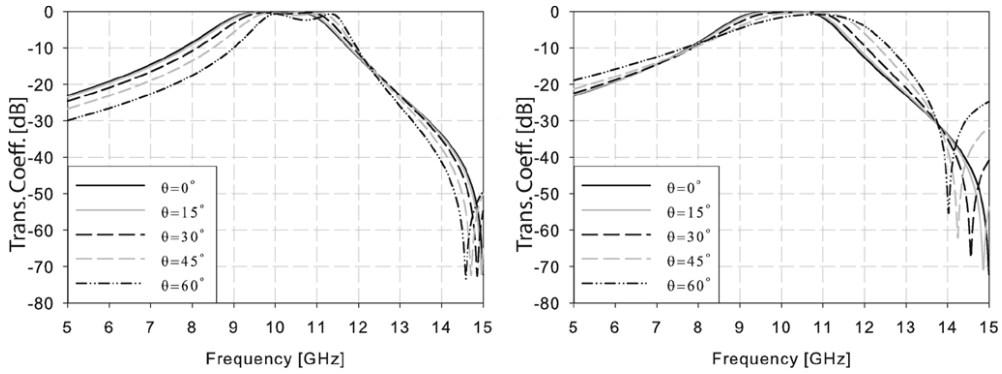

(a) **(b)**

Fig. 2.23. The simulation result of the prosed structure in [27]) TE mode, (b) TM mode.

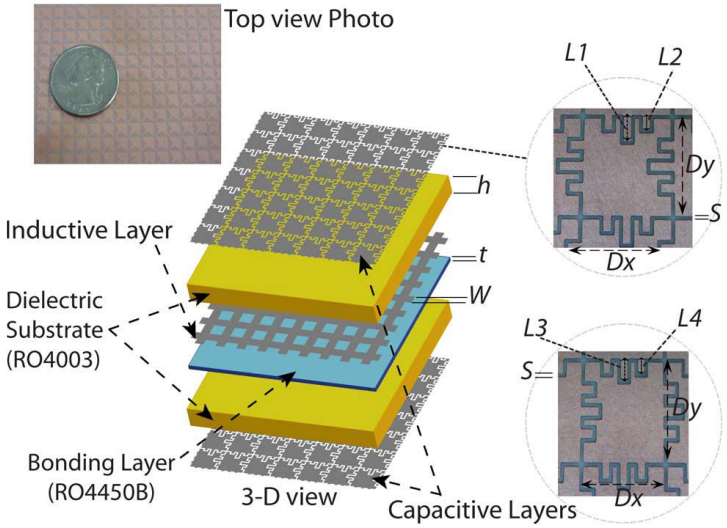

Fig. 2.24. The miniaturised second-order bandpass FSS utilising interdigital capacitors, as proposed in [27].

The variations observed in the bandwidth of the structure as the angle of incidence changes, can be attributed to the change of wave impedance, which in turn will change the loaded quality factor of the resonators of the coupled resonator FSS (see Chapter 2, Section 2.3.1).

The size of the array element of this structure is miniaturised further by increasing the capacitor value. This is done by using interdigital capacitive patches for the first and third layers, as shown in Fig. 2.24. The element size of this structure when using patches is 0.19λ×0.19λ, while it is to 0.15λ×0.15λ after using the interdigital capacitive patches, with λ/30 overall thickness.

In [28], a high order bandpass FSS with narrowband responses by using inductively coupled miniaturized element is reported. In these structures, two resonators or more are coupled together using impedance inverters to obtain the desired frequency response. The resonators in this FSS filter are formed by using dielectric spacers (substrate), and they are coupled by using shunt inductors, as shown in Fig. 2.25.

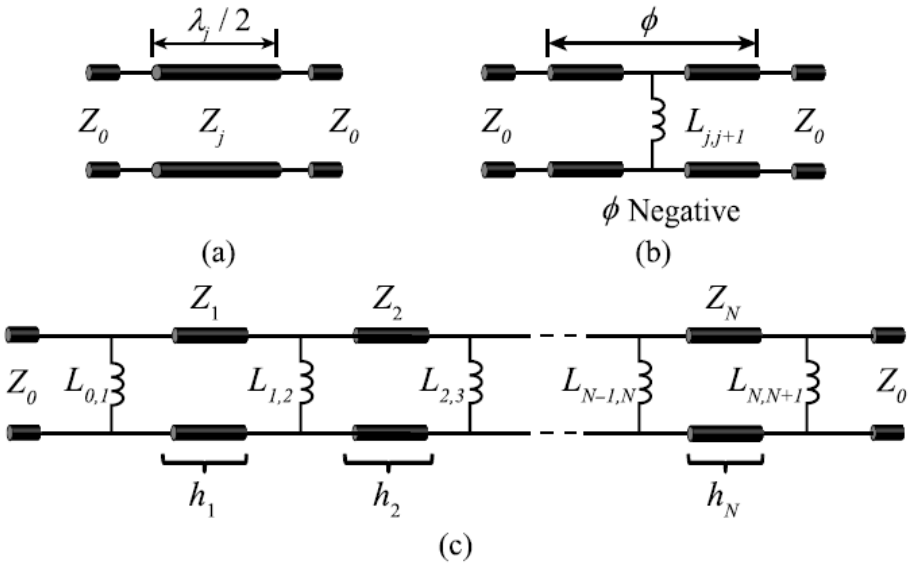

Fig. 2.25. Equivalent circuit of the high order FSS proposed in [28], (a) the transmission-line resonators (dielectric spacers), (b) circuit model of the admittance inverters used to couple the resonators, (c) equivalent circuit of the high order FSS when the resonators and the admittance inverters of (a) and (b) are put together in a ladder network.

The resonators in this structure are half-wavelength spacers. The spacers are modelled with transmission lines with characteristics impedance $Z_j = Z_o/\sqrt{\varepsilon_{r,j}}$, where Z_o is the free space impedance (377Ω). Fig. 2.26 shows a second-order

bandpass is designed based on using inductively coupled element. The two inductive wire grids placed in the centre are separated from one another by a thin prepreg layer. These two inductive layers constitute a single hybrid inductive layer, in order to maintain the symmetry of the structure.

The structures exhibit a narrow bandpass with element size is 0.21λ×0.21λ, and the overall thickness is λ/3.7.

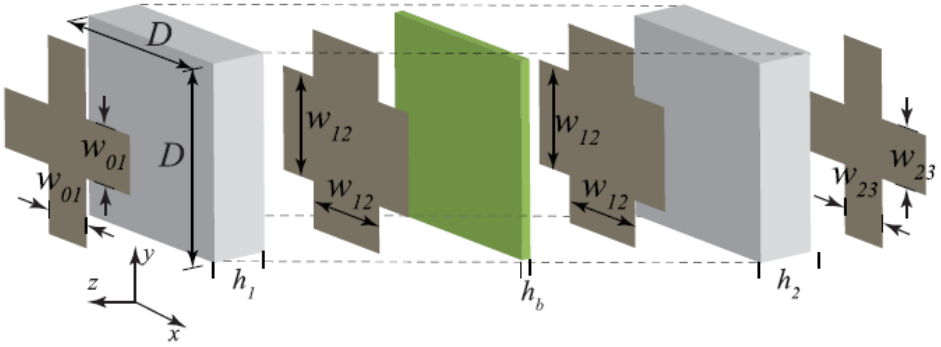

Fig. 2.26. Element of the second-order bandpass proposed in [28].

FSSs capable of providing transparency windows at two or more frequency bands are highly desired. Multilayer structures composed of a combination of resonant and non-resonant elements have been used to obtain dual-band operations with closely spaced [29] or arbitrary bands of operation [30]. A composite element consisting of four compact U-shaped slot resonators rotated by 90° was used to achieve a closely spaced dual-band operation [31].

In [32], a miniaturised dual-band FSS high order bandpass response at each operation band is designed by cascading a two-dimensional periodic array of grids, and capacitive patches separated by dielectric slabs. This structure, as shown in Fig. 2.27, is built based on combining inductively coupled resonators with using the capacitively loaded dielectric spacers as main resonators. As an example, for the second-order bandpass FSS, the array element size at first band is 0.1λ×0.1λ with the overall thickness being λ/4.5.

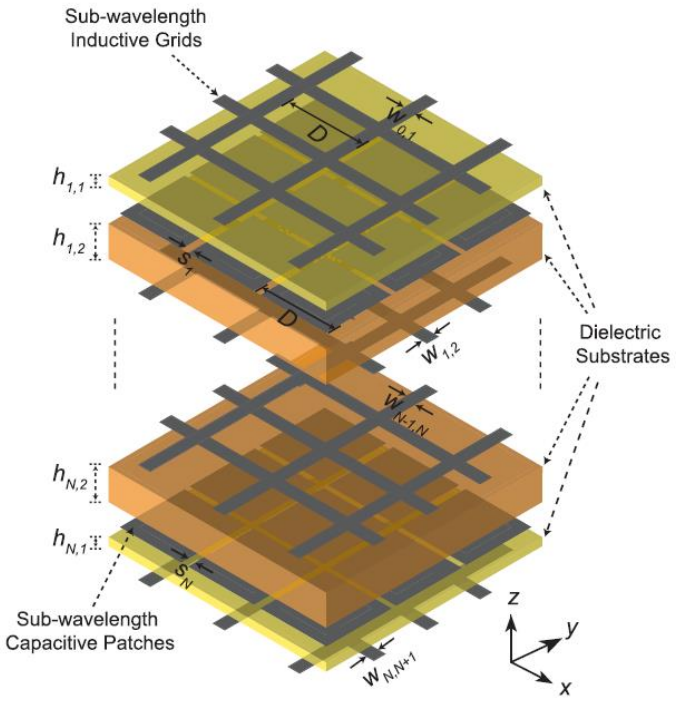

Fig. 2.27. The dual-band N[th]-order bandpass FSS. The structure has *N* sets of composite resonators. Each composite resonator is composed of two dielectric substrates with thicknesses of *h j*,1 and *h j*,2, having a capacitive patch layer in between [32].

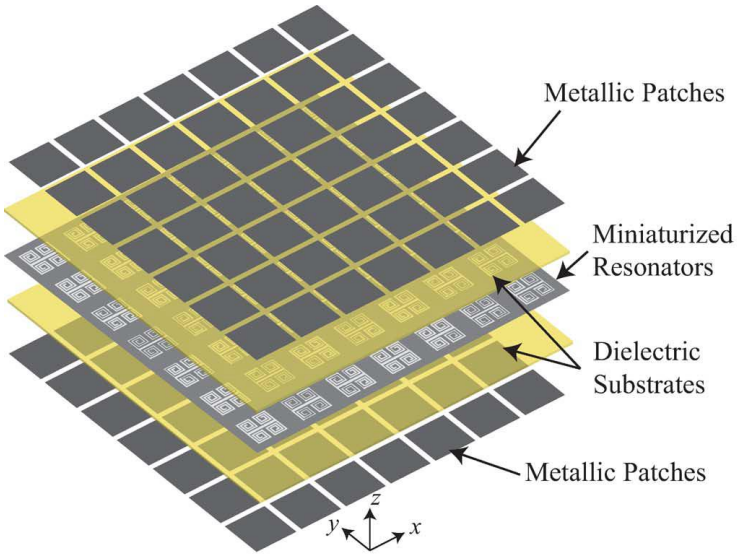

Fig. 2.28. Topology of the third-order bandpass FSS presented in [26].

In [26], a third order bandpass FSS by using a combination of resonant and non-resonant elements is presented. This structure is built up using two arrays of sub-wavelength patches which separated from a periodic array of miniaturised slot antennas by two very thin dielectric slabs, as shown in Fig. 2.28. The dimensions of the array element are 0.16λ×0.16λ, with an overall thickness of λ/24.

The high order FSSs discussed in the literature would be unsuitable for lower band application due to the relatively large element size. Thus, most of the structures which presented in these references have thick substrates (around λ/4).

2.6 Examples for designing FSS

Designing an FSS with different response characteristics and compact size will be described in this section. The use of stepped-impedance structures to design a stable FSS structure for various angles of incident wave will be introduced in Section 2.6.1. In Section 2.6.2, the design of a miniaturised FSS by using vias will be explained.

2.6.1 Using stepped-impedance element

In this section, a novel approach to design a miniaturised FSS is proposed. The miniaturisation is achieved by enhancing the inductance of the proposed stepped-impedance array element. This enhancement is done by using a wire and controlling the path of the current which passes through the metallic surface of the element. As a result, the dimensions of the miniaturised element are much smaller than the wavelength at the resonant frequency. The periodicity is 0.09λ. The structure consists of single metal layer array elements with a simple configuration shape. It can be presented for the both single and dual polarisations. For dual polarisation, through an example with a pass-band at 3GHz, it exhibits insensitive frequency responses of different angles of incident wave. It is demonstrated that a stable resonant frequency under various angles of incidence (up to 88^{o}) can be achieved, which is the most attractive feature of this design. The miniaturised element is much smaller than the wavelength (up to 0.09 λ).

2.6.1.1 Circuit design

The proposed approach is based on modifying the current path of a square patch FSS array element to enhance the inductance. Increasing the length of the current path can be an alternative technique to increase the inductance while keeping the shape of array element simple.

The frequency response of the resonator elements can be determined by evaluating the capacitance and inductance of the array element. An approximate value of the inductance of an FSS element can be given by (1.1). The value of the

inductance L is

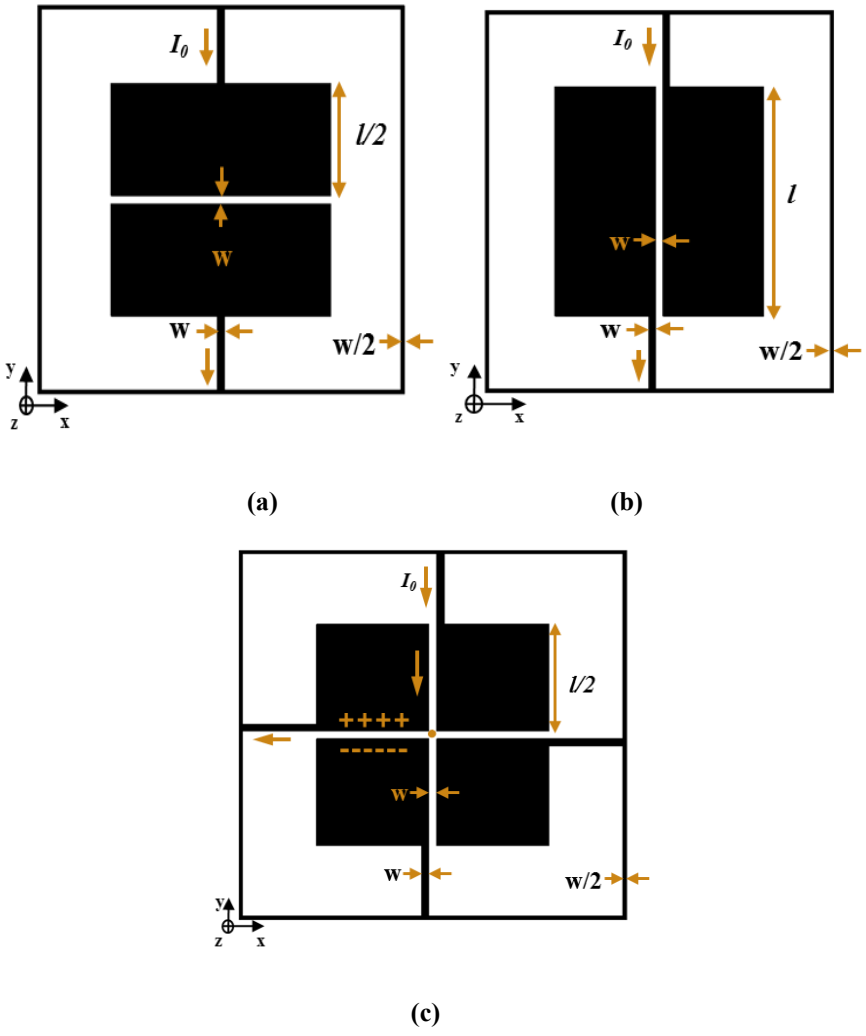

Fig. 2.29. Array element of the proposed FSS structures, (a) the single polarised element with the slot toward x axis, (b) the single polarised element with the slot toward y axis, (c) the dual polarised array element.

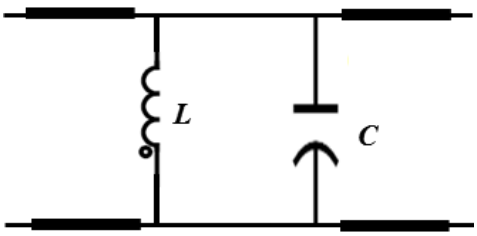

Fig. 2.30. The equivalent circuit of the proposed FSS structure.

determined by the strip length P, the width of strip w and permeability of the substrate μ. Fig. 2.29 shows three cases of array element configuration. Fig. 2.29(a) shows the structure with a slot parallel to the x axis, while Fig. 2.29(b) illustrates the structure with a slot parallel to the y axis. The wire has an inductive effect and the

slot has a capacitive effect. However, these two structures (Fig. 2.29 (a) and (b)) are single polarised structures. A modification of the structure in Fig. 2.29 (b) by adding a slot and micro-wires parallel to the *x* axis is shown in Fig. 2.29(c). This makes the structure dual polarised. The equivalent circuit is a parallel *LC* circuit, as shown in Fig. 2.30.

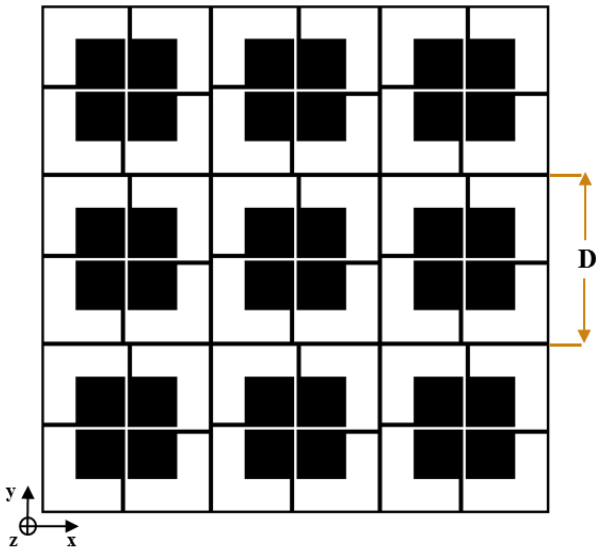

Fig. 2.31. 3×3 array elements of the proposed FSS structure.

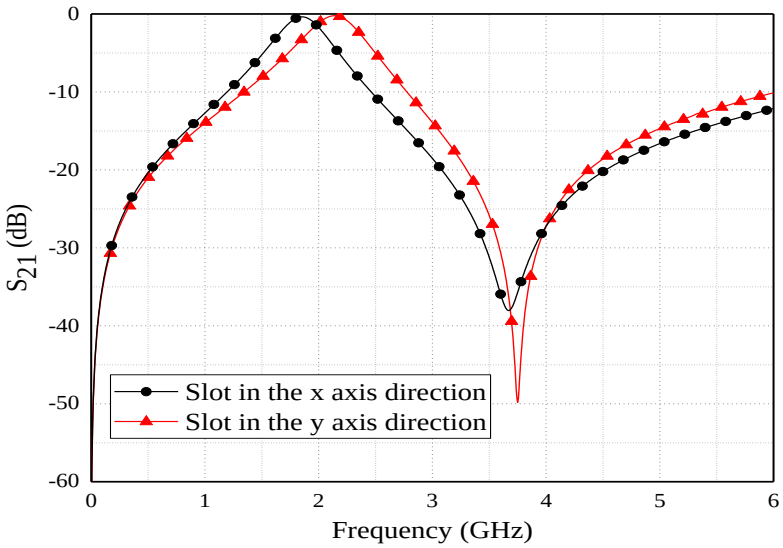

Fig. 2.32. The transmission coefficients of the single polarised proposed FSSs.

The resonator is designed on a 1.5 mm thick FR4 substrate with a relative dielectric constant of 4.3. The length of the square patch *l* is 6 mm. The slot width and wire width *w* are 0.2 mm. The periodic constant *P* of the array is 9 mm. Fig. 2.31 shows the 3×3 array elements of the proposed structure. The simulated transmission

coefficient of the single polarised FSS structure is shown in Fig 2.32. When the slot is parallel to the *x* axis, the resonant frequency is 2.14 GHz with up to 24% fractional bandwidth, while the resonant frequency is 1.85 GHz with up to 27% fractional bandwidth when the slot is parallel to the *y* axis. The difference of the resonant frequencies and bandwidths of the single polarised structures are expected because the structures have different values of resonant elements.

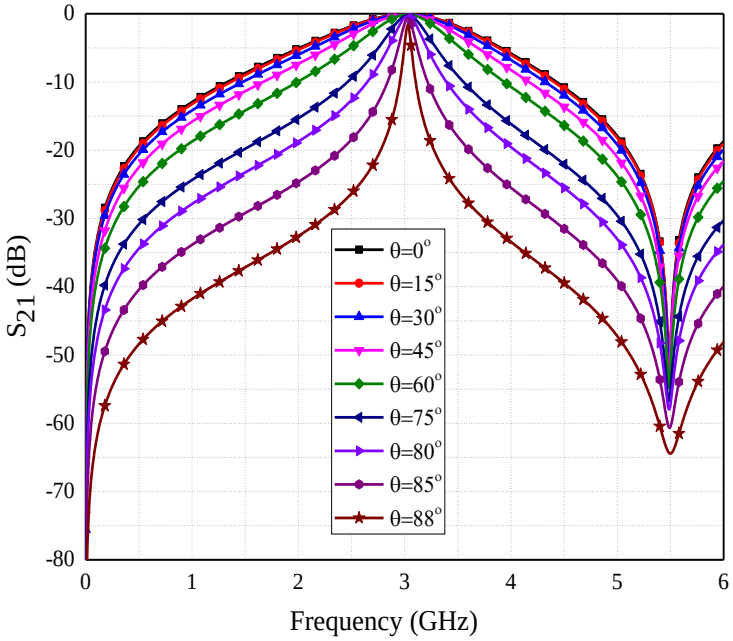

Fig. 2.33. The transmission coefficient of the proposed FSS as a function of incident angles.

Table 2.1: Comparison of the element with other references

FSS structure	Substrate Thickness (mm)	ε_r	Element size
[9]	1.6	4.3	0.22λ
[22]	1.6	4.3	0.104λ
[15]	0.5	3.55	0.088λ
[16]	0.127	2.2	0.067λ
[17]	1.6	5	0.061λ
The proposed dual polarised FSS	1.6	4.3	0.09λ
The proposed single polarised FSS	1.6	4.3	0.055λ

In the same way, it is shown that the resonant frequency of the proposed dual

polarised FSS structure, as shown in Fig. 2.29(c), is 3 GHz with up to 41% fractional bandwidth. The resonant frequency of the proposed structure is insensitive to the angle of incidence (θ) and valid up to 88°, although the bandwidth is decreased, as shown in Fig 2.33.

A comparison of the FSS array element between the proposed structure and other reported miniaturised FSS elements is illustrated in Table 2.1. It can be observed that the stepped-impedance FSS is the smallest compared with the listed references. In addition, it can exhibit very stable resonant frequency for non-zero incident angles.

2.6.2 Using vias

In this section, vias are used to miniaturise the element of a bandstop FSS by connecting a spiral layer (inductive) in series with a patch layer (capacitive). Compared with previous FSSs, the proposed structure has promising miniaturisation features. Stable performance against oblique incidence angles can be realised by the miniaturized unit structure and using vias between top and bottom surfaces. The dimensions of the proposed array element are only 0.035λ×0.035λ. The top layer is constructed by four spiral-shaped structures; the bottom is made of four square-shaped patches. They are connected in series by vias. In so doing, the values of the resonant component values are increased, thus the resonant frequency is shifted downwards. The frequency response is insensitive to the oblique incidence angle. Also, the proposed design is symmetric around the *z* axis and can be applied for circular polarisation applications.

2.6.2.1 Circuit design

A miniaturised FSS is proposed based on connecting two different layers using vias to increase the electrical length. In the FSS array element, four spiral lines are connected to the centre point as a unit on the top layer. Four square patch surfaces are printed on the bottom of the dielectric substrate. The four spiral lines are connected with the four patches by four metal vias. Compared with the traditional FSS element, the proposed FSS element has a much lower resonant frequency due to its longer electrical length (the length of an element in terms of the wavelength). The performance of the FSS using the proposed structure is polarisation independent because the structure symmetrical around *z* axis. The resonant frequency is also stable at various polarisations and incident angles. The main design variables and the

layout of the proposed element are shown in Fig. 2.34. The proposed FSS with 2×2 array elements is shown in Fig. 2.35. To verify the proposed structure, numerical analysis of the proposed element was performed by using CST Microwave Studio, using array element boundary conditions to provide periodicity along the *x* and *y* axes. The FSS is excited by an EM wave with the propagation vector (**K**) in the direction of the *z*-axis, magnetic field vector (**H**) in the direction of the *x*–axis and electric field vector (**E**) in the direction of the **y**-axis direction.

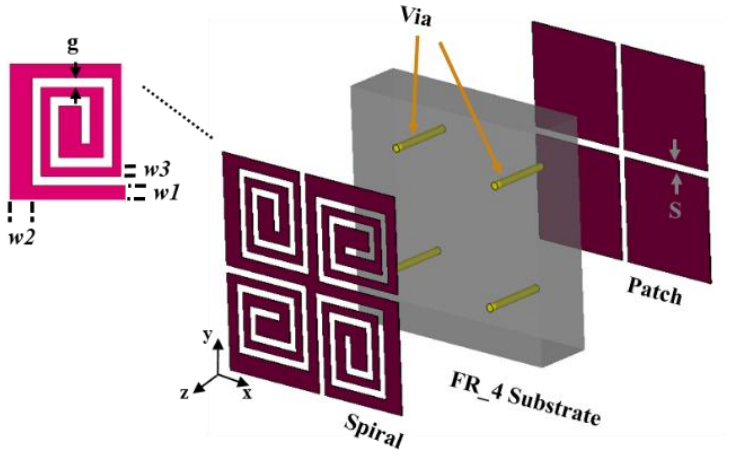

Fig. 2.34. An array element of the proposed FSS.

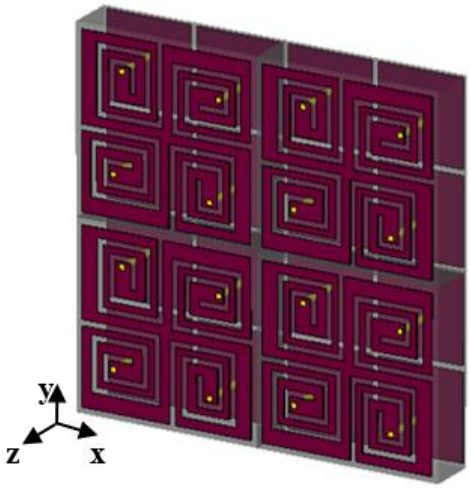

Fig. 2.35. An FSS using 2×2 array element of the proposed structure.

The resonator is designed on a 1.6 mm thick FR4 substrate with a relative dielectric constant of 4.3. The periodic constant of the array is 6 mm. The area of the square patch is 2.8 × 2.8 mm^2. The slot width between patches, *S*, is 0.2 mm. The spiral strip widths are: w_1 = 0.3 mm, w_2 = 0.5 mm and w_3 = 0.2 mm. The space between these strips, *g*, is 0.2 mm. Vias with a radius of 0.2 mm were used to connect

the spiral lines and patches between the two layers. Fig. 2.36 shows the simulated transmission characteristics of the FSS for the TE and TM modes, with variable incident angles of 0º, 15º, 30º, 45º, and 60°. The resonant frequency is 1.746 GHz with an up to 45 % fractional bandwidth. The size of the proposed element was substantially reduced to 0.035λ × 0.035λ, where λ is the wavelength in free space at the resonant frequency. The resonant frequency remains stable for both polarisations, even though the incident angle is up to 60º.

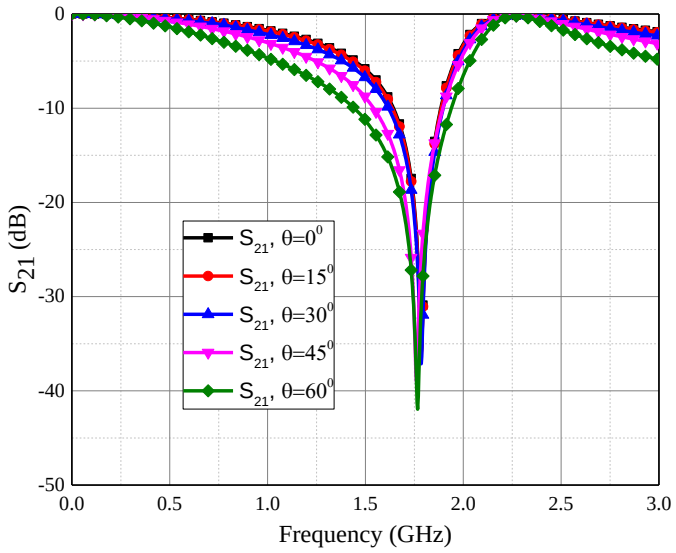

(a)

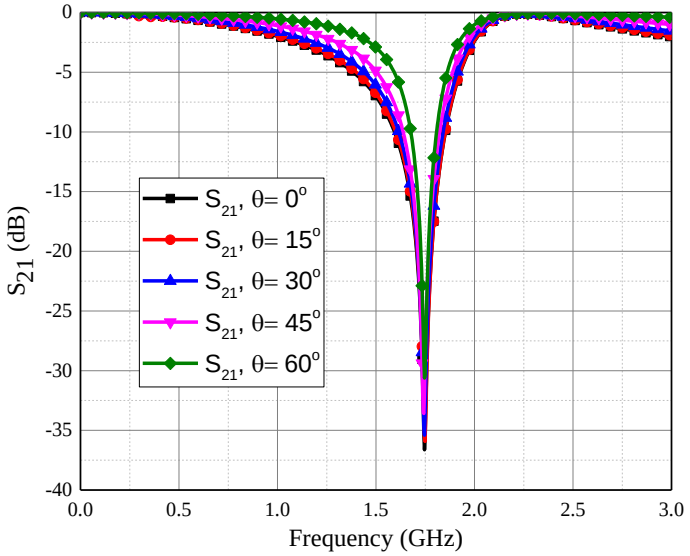

(b)

Fig. 2.36. The transmission coefficient of the proposed FSS as a function of incident angles (a) for the TE Mode, (b) for the TM mode.

2.7 Conclusion

In this chapter, FSS history, theory and operation were presented. A number of issues for practical implementation of FSS were considered, such as the effects of incident angle(s), FSS curvature, and the grating lobe. Examples to design FSS with different characterstics and to highlight the geometrical dependence of the FSS's resonant filtering behaviour are descibed. Strips and their eqiuvalent models have been discussed. Additionally, different FSS structures and responses were discussed, including first and high order FSS. However, they are all sensitive to the dielectric materials nearby. The majority of the dimensions of array elements are relatively large and supported by thick dielectric substrates, especially for high order FSSs.

In summary, for any given FSS, an incident wave is either reflected or transmitted over certain frequencies because of capacitances and inductances generated. The transmission and reflection coefficients of an FSS are affected not only by the geometry of the conductors of the FSS, but also by the incident angle, the polarisation and the nature of the structure in which the FSS is embedded.

2.8 References

[1] B. A. Munk, "Frequency selective surfaces theory and design," New York: Wiley-Interscience, 2000.

[2] B. Munk, R. Kouyoumjian, and L. Peters, "Reflection properties of periodic surfaces of loaded dipoles," *IEEE Transactions on Antennas and Propagation,* vol. 19, no. 5, pp. 612-617, 1971.

[3] E. A. Parker, "The gentleman's guide to frequency selective surfaces," *QMW Antenna symposium* pp. 1-18, 1991.

[4] T. K. Chang, R. J. Langley, and E. A. Parker, "Active frequency-selective surfaces," *IEE Proceedings-Microwaves, Antennas and Propagation,* vol. 143, no. 1, pp. 62-66, 1996.

[5] J. Romeu, and Y. Rahmat-Samii, "Fractal FSS: A novel dual-band frequency selective surface," *IEEE Transactions on antennas and propagation,* vol. 48, no. 7, pp. 1097-1105, 2000.

[6] A. K. Rashid, B. Li, and Z. Shen, "An overview of three-dimensional

frequency-selective structures," *IEEE Antennas and Propagation Magazine,* vol. 56, no. 3, pp. 43-67, 2014.

[7] C. A. Balanis, *Advanced engineering electromagnetics*: John Wiley & Sons, 1999.

[8] P. Callaghan, E. A. Parker, and R. J. Langley, "Influence of supporting dielectric layers on the transmission properties of frequency selective surfaces." *IEE Proceedings H (Microwaves, Antennas and Propagation)*, vol. 138, pp. 448-454, 1991.

[9] K. Sarabandi, and N. Behdad, "A frequency selective surface with miniaturized elements," *IEEE Transactions on Antennas and Propagation,* vol. 55, no. 5, pp. 1239-1245, 2007.

[10] Z. Sipus, and M. Bosiljevac, "Efficient analysis of curved frequency selective surfaces," *Antennas and Propagation, 2009. EuCAP 2009. 3rd European Conference on* pp. 2726-2730.

[11] S. Savia, E. A. Parker, and B. Philips, "Finite planar-and curved-ring-element frequency-selective surfaces," *IEE Proceedings-Microwaves, Antennas and Propagation,* vol. 146, no. 6, pp. 401-406, 1999.

[12] B. Philips, E. A. Parker, and R. J. Langley, "Finite curved frequency selective surfaces," *Electronics Letters,* vol. 29, no. 10, pp. 882-883, 1993.

[13] N. Marcuvitz, *Waveguide handbook*: IET, 1951.

[14] C. N. Chiu, and K. P. Chang, "A novel miniaturized-element frequency selective surface having a stable resonance," *IEEE Antennas and Wireless Propagation Letters,* vol. 8, pp. 1175-1177, 2009.

[15] F. C. Huang, C. N. Chiu, T. L. Wu, and Y. P. Chiou, "A circular-ring miniaturized-element metasurface with many good features for frequency selective shielding applications," *IEEE Transactions on Electromagnetic Compatibility,* vol. 57, no. 3, pp. 365-374, Jun, 2015.

[16] S. N. Azemi, K. Ghorbani, and W. S. T. Rowe, "Angularly stable frequency selective surface with miniaturized unit cell," *IEEE Microwave and Wireless Components Letters,* vol. 25, no. 7, pp. 454-456, 2015.

[17] G. H. Yang, T. Zhang, W. L. Li, and Q. Wu, “A novel stable miniaturized frequency selective surface,” *IEEE Antennas and Wireless Propagation Letters,* vol. 9, pp. 1018-1021, 2010.

[18] M. B. Yan, S. B. Qu, J. F. Wang, J. Q. Zhang, A. X. Zhang, S. Xia, and W. J. Wang, “A novel miniaturized frequency selective surface with stable resonance,” *IEEE Antennas and Wireless Propagation Letters,* vol. 13, pp. 639-641, 2014.

[19] H. Liu, K. L. Ford, and R. J. Langley, “Miniaturised bandpass frequency selective surface with lumped components,” *Electronics Letters,* vol. 44, no. 18, pp. 1054-U12, 2008.

[20] S. Sheikh, “Miniaturized-element frequency-selective surfaces based on the transparent element to a specific polarization,” *IEEE Antennas Wireless Propag. Lett,* vol. 15, pp. 1661-1664, 2016.

[21] B.-q. Lin, S.-h. Zhou, X.-y. Da, Y.-w. Fang, Y.-j. Li, and W. Li, “Compact miniaturised-element frequency selective surface,” *Electronics Letters,* vol. 51, no. 12, pp. 883-884, 2015.

[22] C.-N. Chiu, and K.-P. Chang, “A novel miniaturized-element frequency selective surface having a stable resonance,” *IEEE Antennas and Wireless Propagation Letters,* vol. 8, pp. 1175-1177, 2009.

[23] Y.-M. Yu, C.-N. Chiu, Y.-P. Chiou, and T.-L. Wu, “A novel 2.5-dimensional ultraminiaturized-element frequency selective surface,” *IEEE Transactions on Antennas and Propagation,* vol. 62, no. 7, pp. 3657-3663, 2014.

[24] W. Jiang, K. Zhang, S. Gong, and T. Dong, "Design of 2.5-dimensional miniaturized frequency selective surface." *Electromagnetics in Advanced Applications (ICEAA), 2016 International Conference on* pp. 491-493.

[25] Y. Shi, W. Tang, W. Zhuang, and C. Wang, “Miniaturised frequency selective surface based on 2.5-dimensional closed loop,” *Electronics Letters,* vol. 50, no. 23, pp. 1656-1658, 2014.

[26] N. Behdad, M. Al-Joumayly, and M. Salehi, “A low-profile third-order bandpass frequency selective surface,” *IEEE Transactions on Antennas and Propagation,* vol. 57, no. 2, pp. 460-466, 2009.

[27] M. Al-Joumayly, and N. Behdad, "A new technique for design of low-profile, second-order, bandpass frequency selective surfaces," *IEEE Transactions on Antennas and Propagation,* vol. 57, no. 2, pp. 452-459, 2009.

[28] S. M. A. M. H. Abadi, and N. Behdad, "Inductively-coupled miniaturized-element frequency selective surfaces with narrowband, high-order bandpass responses," *IEEE Transactions on Antennas and Propagation,* vol. 63, no. 11, pp. 4766-4774, 2015.

[29] M. A. Al-Joumayly, and N. Behdad, "Low-profile, highly-selective, dual-band frequency selective surfaces with closely spaced bands of operation," *IEEE Transactions on Antennas and Propagation,* vol. 58, no. 12, pp. 4042-4050, 2010.

[30] M. Salehi, and N. Behdad, "A second-order dual X-/Ka-band frequency selective surface," *IEEE Microwave and Wireless Components Letters,* vol. 18, no. 12, pp. 785-787, 2008.

[31] S. Çimen, "Novel closely spaced planar dual-band frequency-selective surface," *IET Microwaves, Antennas & Propagation,* vol. 7, no. 11, pp. 894-899, 2013.

[32] M. Gao, S. M. A. M. H. Abadi, and N. Behdad, "A dual-band, inductively coupled miniaturized-element frequency selective surface with higher order bandpass response," *IEEE Transactions on Antennas and Propagation,* vol. 64, no. 8, pp. 3729-3734, 2016.

Chapter 3: Asymmetrical Array Elements

3.1 Introduction

Recently, many approaches have been proposed to miniaturise FSS array element dimensions. For example, a lumped inductor and a lumped capacitor in parallel can be used to reduce the size of FSS array elements [1, 2]. Adding meander-slots to the circular ring structures can produce FSS array elements with dimensions much smaller than the wavelength [3]. A study in [4] demonstrated a miniature FSS by printing micro wire on a dielectric. Printing four symmetrical spiral patterns of metallic meander lines can increase the electrical length of the array element [5]. However, increasing the electrical length of an array element with the same physical dimensions is limited, and could increase the complexity of the FSS structure. Thus, different techniques have been used to achieve stable frequency responses in different polarisations for single and multi-layer FSSs under various angles of incident waves. Accomplishing a symmetrical FSS array element can contribute to achieving a stable resonance with respect to the polarisation and the angle of incidence [1-6]. However, using symmetrical array element shapes to avoid polarisation sensitivity can restrict FSS design options.

In this chapter, new approaches are proposed to miniaturise FSS elements and to overcome the polarisation sensitivity of unsymmetrical FSS elements. Section 3.2 describes a new approach to design FSS structure which exhibits stable resonant frequency in both vertical and horizontal polarisation, although this element is not 90^{o} symmetrical in the *xy*-plane.

In Section 3.3, the proposed miniaturised FSS is further develop. The same metal shape is fabricated on the top and bottom of the substrate. The two layers are orthogonal to each other. The elements are interconnected in one direction only. By doing so, a cross-coupling capacitor (C_{cc}) will be generated. This capacitor will greatly lower the resonant frequency. Traditionally, in single and multi-layer structures, the lower the profile, the higher the resonant frequency, due to the fact that the effective dielectric constant is gradually increased when the substrate thickness is increased. In contrast, in the proposed structure, the lower the profile, the lower the resonant frequency. The frequency response of the miniaturised FSS is

demonstrated for various incident angles and it is shown that the performance is very stable. Another significant advantage of having two layers orthogonally is that the resonator structure in either layer does not have to be rotationally symmetrical by 90º. An analytical model is derived to evaluate the resonant frequency of the proposed miniaturised FSS.

3.2 Single-layer element

This section proposes the design of a dual polarised FSS. The FSS can have a similar transmission coefficient for different polarisations, although the structure is not rotationally symmetrical by 90˚ in the xy-plane. A theoretical equivalent circuit model is proposed to characterise the structure, based on the analysis of the FSS structure geometry configuration and the distribution of the electromagnetic field on it. The FSS structure is built up by using a single-layer for easy fabrication. To demonstrate the validity of the proposed structure, the array elements are fabricated and tested in free space.

The proposed FSS resonator is realised by printing a piece of metal on one side of a dielectric substrate. It is a ring with two splits. Inside the ring, there are a pair of T-shaped strips with a gap in the centre, as shown in Fig. 3.1. At vertical polarisation, the electric field is in the direction of the *y*-axis. A mutual capacitance is induced between two adjacent cells, shown as (a) in Fig. 3.1. Half of the circumference acts as an inductor, as shown as (b) in Fig. 3.1. The two T-shaped strips with a gap between them can be represented by a capacitor in series with an inductor, shown as (c) in Fig. 3.1. The corresponding equivalent circuit of the resonator, when the incident wave is vertically polarised, is shown in Fig. 3.2. It consists of three series *LC* circuits in parallel. L_1 and L_3 are the inductance of the circumference shown as (b) in Fig. 3.1. C_1 and C_3 represent the mutual capacitances between the adjacent halves of the circumference, shown as (a) in Fig. 3.1. L_2 and C_2 are the inductance and capacitance of the T-shaped strips and the gap of the strips respectively, shown as (c) in Fig. 3.1. Similarly, for horizontal polarisation mode, the equivalent circuit of the resonator can also be described by Fig. 3.2. In this case, L_1 and L_3 are the inductance of the circumference shown as (e) in Fig. 3.1. C_1 and C_3 represent the mutual capacitances between the adjacent halves of the circumference, shown as (d) in Fig. 3.1. L_2 and C_2 are the inductance and capacitance of the parts shown as (f) in Fig. 3.1.

The designed FSS can achieve a high-value transmission coefficient, a wide operational band, an excellent band edge transition and dual polarisation performance. The resonant frequency of the proposed bandpass FSS is 5.26 GHz. The fractional bandwidth is 40% at vertical polarisation, while it is about 26% at the horizontal polarisation.

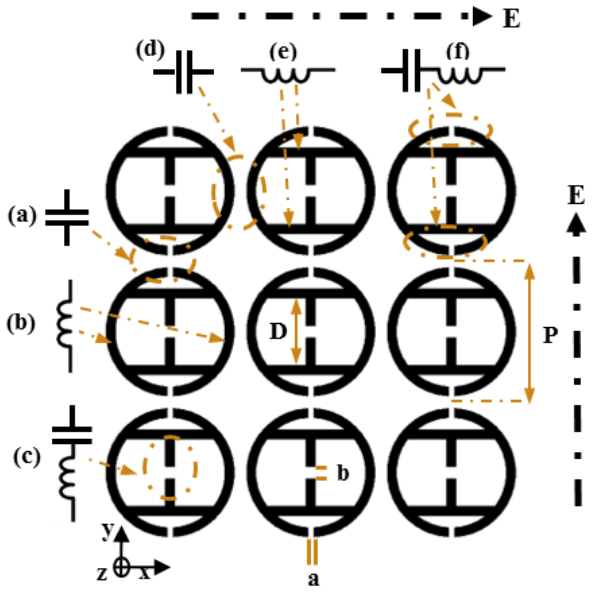

Fig. 3.1. Array elements of the proposed FSS filter.

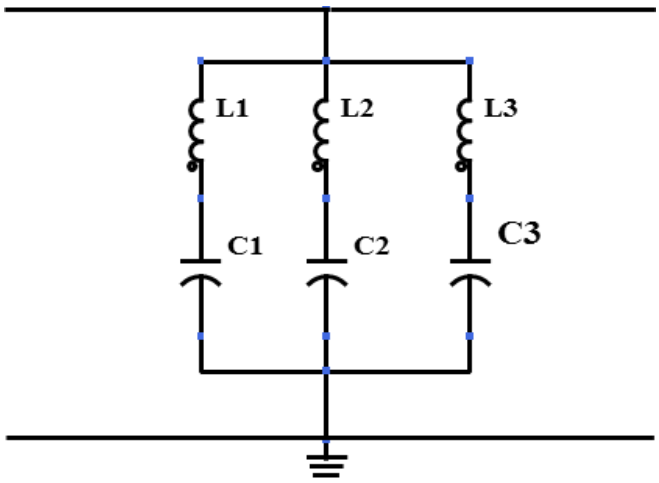

Fig. 3.2. The equivalent circuit of the proposed FSS element.

3.2.1 Experimental results

A prototype of this proposed FSS has been fabricated on a 1.5 mm thick FR4. The fabricated FSS is shown in Fig.3.7. The size of the FSS prototype is 140 mm × 140 mm and it consists of 7 × 7 elements. The simulated and measured transmission coefficients of the proposed bandpass FSS filter in vertical and horizontal

polarisation modes are in a relatively good agreement, as shown in Fig.3.4. The centre frequency is 5.26 GHz. The FSS has achieved excellent performance, characterised by high transmission of the wave, a good band-edge transition and a wide bandwidth. The 3 dB fractional bandwidth for the vertical polarisation mode is 37%, while it is 23% for

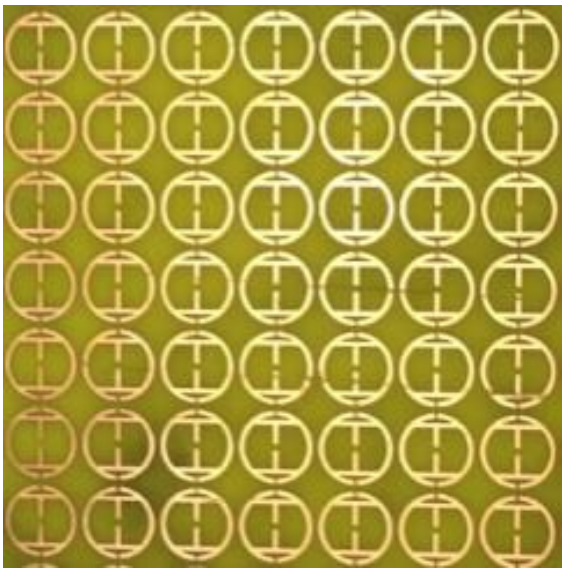

Fig. 3.3. A photograph of the fabricated FSS.

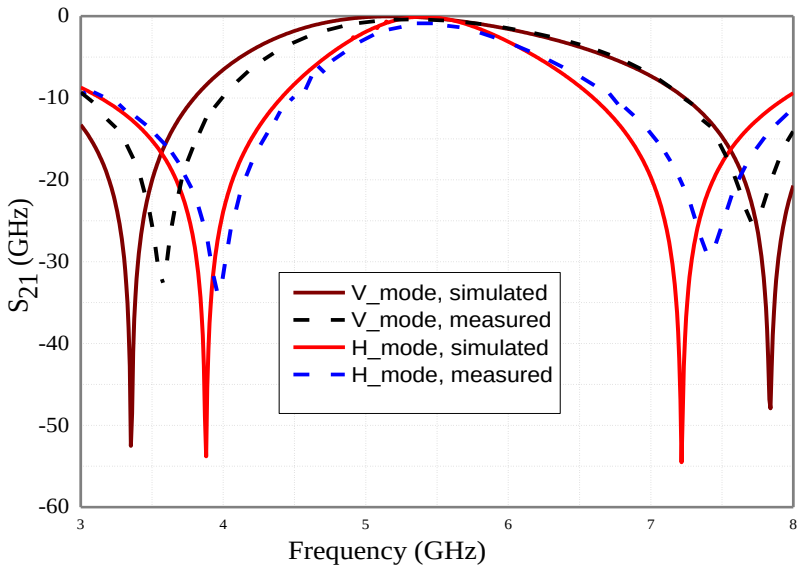

Fig. 3.4. Simulated and Measured transmission coefficients of the proposed FSS in vertical and horizontal polarisation modes.

the horizontal polarisation mode. The discrepancy between the simulation and practical measurement results is attributed to the numerical errors in simulations, tolerances and general inaccuracies involved in the fabrication process.

3.3 Interconnected adjacent elements on orthogonal layers

Traditionally, the elements of an FSS are rotationally symmetrical and the element arrays in a multi-layer FSS are aligned with each other. In this section, a new approach to miniaturise the size of the FSS array element with extreme low profile is proposed. The interconnected elements are placed orthogonally in the xy-plane to the elements on the other layer. By doing so, firstly a cross-coupling capacitance (C_{cc}) can be enhanced between the two adjacent layers. This capacitance can lower the resonant frequency of the FSS and reduce the FSS profile. This is because a smaller substrate thickness means a higher cross-coupling capacitance. Secondly, unlike traditional elements, the array element in the proposed structure does not have to be rotationally symmetrical by 90^o. This offers great flexibility in the design of array elements. The proposed resonator has a resonant frequency of 5.5 GHz on an FR4 substrate with a thickness of 0.8 mm. By interconnecting adjacent resonators in one direction and having two orthogonal layers, the resonant frequency of the array is reduced to 2.32 GHz. When the substrate thickness decreases from 0.8 mm to 0.127 mm, the resonant frequency is lowered further, from 2.32 GHz to 1.35 GHz. The frequency response of the miniaturised FSS is not sensitive to the incident angle. An analytic model is derived to validate the new approach. A theoretical equivalent circuit model is proposed to characterise the structure, based on analysis of the geometrical configuration of the FSS structure and the electric field distribution on it. The theory was verified by experimental results.

3.3.1 Miniaturisation approaches

3.3.1.1 Array element design

The miniaturisation of FSS elements is desired to enable an FSS with sufficient array elements to act as an infinite array because a practical FSS is usually fabricated in finite dimensions. It is important that the spacing of the array elements must be set less than λ/2 to avoid grating lobes, where λ is wavelength at resonant frequency. Many approaches have been used to miniaturise the FSS element. These approaches mainly depend on increasing the electrical length of array elements with the same physical area. However, this could result in a more complex FSS structure.

In this section, new approaches will be introduced to miniaturise an FSS element. Firstly, the inductance can be enhanced by connecting adjacent elements in one

direction. Secondly, an extra capacitor is introduced by having two metallic layers orthogonal to each other. This capacitance enables the FSS to have a much lower profile. The proposed array element is designed in such a way that the connection between adjacent elements is easily achievable. At the same time, the array element in the FSS is not necessarily symmetrical at 90^o rotation.

The proposed resonator is a ring with two splits. Each split is ended by two parallel strips. Inside the ring, there is a pair of T-shaped strips with a gap in the centre, as shown in Fig. 3.5. However, the structure still works if an l-shaped strip is used in the middle of the unit cell. It was found by parametric study that the whole structure is slightly smaller when using two T-shaped strips instead of the l-shaped strip and it provides flexibility to control the stopband frequency. The resonant frequency of the proposed resonator can be easily lowered by interconnecting the elements, to be discussed in detail in the following sections.

3.3.1.2 Enhanced inductance array elements

Fig. 3.5 shows the proposed structure. At the vertical polarisation, the electrical field is in the direction of the y-axis. The gaps between the two T-shaped strips can be represented by a capacitor, shown as (a) in Fig. 3.5. Half of the circumference with the parallel strips acts as an inductor, shown as (b). The gap between adjacent elements can be represented by a capacitor, shown as (c). The corresponding equivalent circuit of the resonator, when the incident wave is vertically polarised, consists of a C in series with parallel LC as shown in Fig 3.6. C_2 represents the capacitance shown as (a) in Fig. 3.5. L_1 represents the inductance shown as (b). C_1 represents the capacitance shown as (c).

Similarly, for the horizontal polarisation, the equivalent circuit of the resonator can also be described by Fig. 3.5. The corresponding equivalent circuit of the resonator, when the incident wave is horizontally polarised, is also a C in series with parallel LC. The equivalent circuit can also be represented by Fig. 3.6, although the values of the components are different. In this case, C_1 represents the mutual capacitance between the adjacent elements, shown as (d) in Fig. 3.5. L_1 is the inductance of the two T-shaped strips shown as (e). C_2 is the capacitance of the parallel strips, shown as (f).

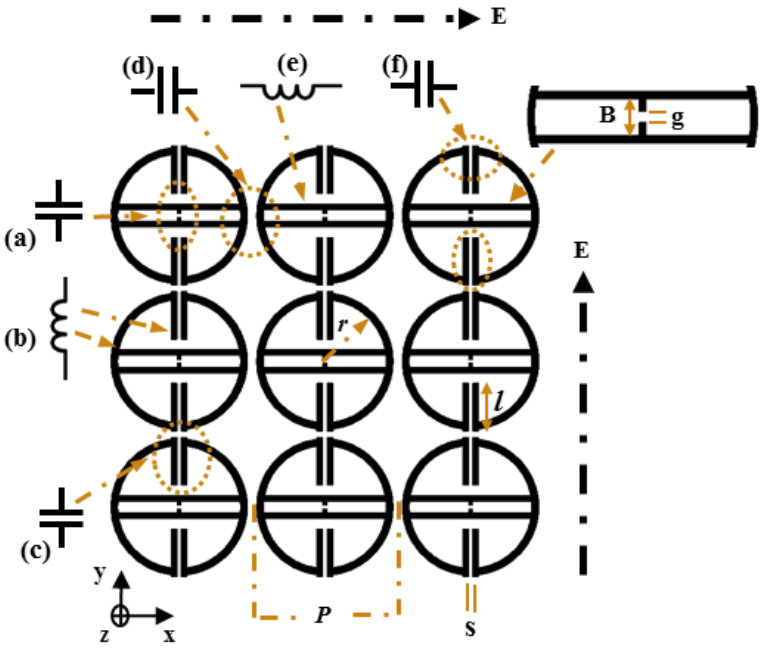

Fig. 3.5. The proposed structure with unconnected elements.

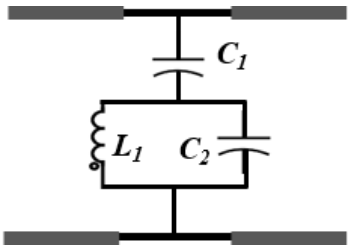

Fig. 3.6. The equivalent circuit of the proposed FSS unit.

To verify the proposed structure, numerical analysis of the proposed element was performed by CST Microwave Studio, using unit cell boundary conditions to provide periodicity along the x and y axes. The FSS is excited by an electromagnetic wave with the propagation vector (**K**) towards the z-axis direction, magnetic field vector (**H**) towards the x–axis direction and electric field vector (**E**) towards the y-axis direction, (see Chapter 1, Fig. 1.6). The frequency response of the array elements can be determined by evaluating the capacitance and inductance of the element. The approximate value of the inductance of a strip can be calculated by (1.1), whilst the approximate value of the capacitance between strips can be calculated by (1.6). The effective dielectric constant increases when the substrate thickness is increased. The capacitance between adjacent strips increases if the thickness of the substrate becomes thicker [7], although the increment will be smaller if the thickness of the substrate is much greater than the gap width. On the other hand, the inductance is

determined by the length and width of the metallic strip.

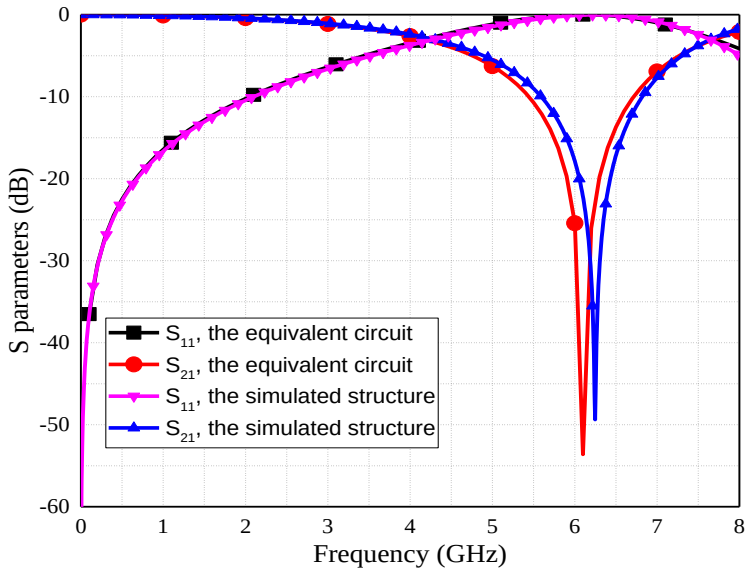

(a)

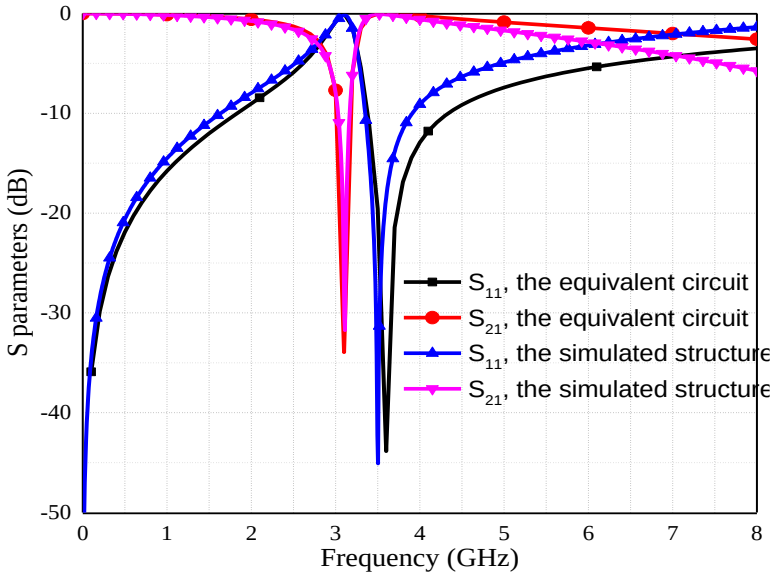

(b)

Fig. 3.7. The transmission and reflection coefficients of the structure shown in Fig. 3.5, obtained by the curve fitting and simulating the structure, (a) at the vertical polarisation, (b) at the horizontal polarisation.

An FSS was designed on a 0.127 mm thick FR4 substrate with a dielectric constant of 4.3. The strip width w is 0.3 mm, s = 0.4 mm, g = 0.25 mm, l = 3.7 mm and B = 0.6 mm, as shown in Fig. 3.5. The inner and outer ring radius is 4.4 mm and 4.7 mm, respectively. The periodic element P is 10 mm. The simulated performance of the structure of Fig. 3.5 is shown in Fig. 3.7. At the vertical polarisation, the

structure exhibits bandstop performance, and has a resonant frequency of 6.25 GHz, as shown in Fig. 3.7(a). The resonant components of the equivalent circuit, as shown in Fig. 3.6, can be calculated by using (1.1) and (1.6), where C_1 = 0.77 pF, C_2 = 0.21 pF and L_1 = 0.65 nH. To achieve a good agreement with the simulated one, as shown in Fig. 3.7 (a), a curve fitting was carried out. It was found that by taking C_1 = 0.82 pF, C_2 = 0.209 and L_1 = 0.66 nH, the calculated response will be in excellent agreement with the simulated one as shown in Fig. 3.7. These component values are very close to those obtained by calculation using (1.1) and (1.6).

At the horizontal polarisation, the structure's predicted performance is a stopband at 3.10 GHz and a passband at 3.49 GHz, as can be observed from Fig. 3.7 (b). The component values in the equivalent circuit are C_1 = 1.1 pF, C_2 = 2.6 pF and L_1 = 0.64 nH as calculated using (1.1) and (1.6). By curve- fitting, C_2 is tuned to 2.7 pf to achieve good agreement with the simulated structure, as shown in Fig. 3.7 (b).

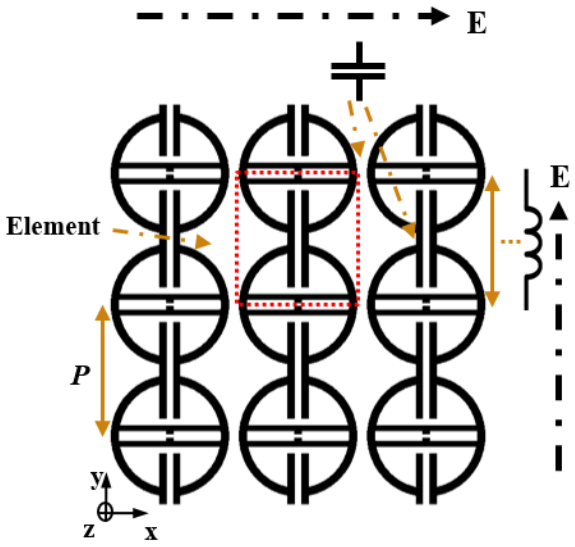

Fig. 3.8. The proposed structure with the elements interconnected in one direction.

To miniaturise the resonator, the adjacent elements of the proposed structure can be connected in one direction through two parallel strip wires, as shown in Fig. 3.8. This can enhance the inductance of the proposed structure compared to the case where the elements are not interconnected as shown in Fig. 3.5. However, the equivalent circuit of the strips in the interconnected array elements is an inductor, as shown in Fig. 3.8. While as shown in Fig. 3.5, the strips in the not-interconnected array element have series capacitance associated with the gap between adjacent elements, resulting in the equivalent circuit of a series *LC* circuit. The simulation for

the enhanced-inductance

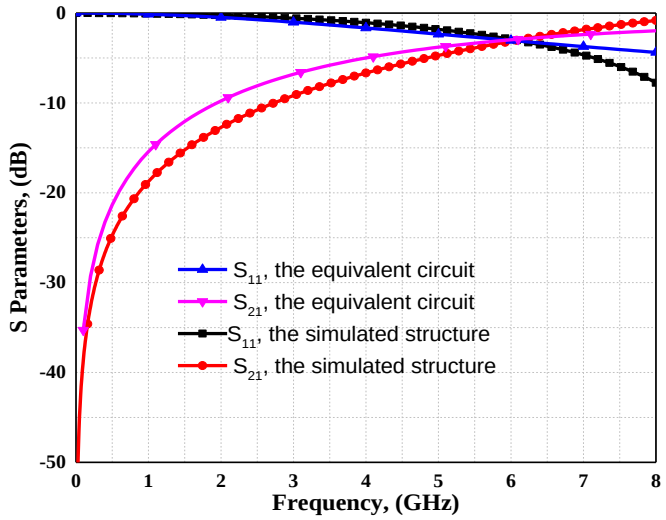

(a)

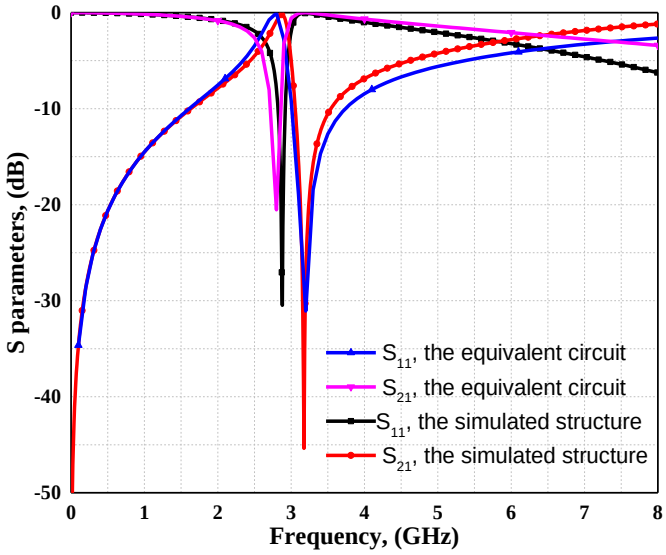

(b)

Fig. 3.9. The transmission and reflection coefficients of the structure shown in Fig. 3.8, obtained by the curve fitting and simulating the structure, (a) for the vertical polarisation, (b) for the horizontal polarisation.

(interconnected) elements, with the circuit dimensions provided above, was carried out. The E-field is assumed to be vertical as shown in Fig. 3.8. The FSS has a high pass response, as shown in Fig. 3.9(a), because the equivalent circuit is mainly an inductor as described above.

For the horizontal polarisation, the parallel strips in the interconnected circuit can be represented by a capacitor, as shown in Fig. 3.8. The simulated response of the

structure has a bandstop response with a resonant frequency of 2.9 GHz, as shown in Fig. 3.9(b). The equivalent circuit is a C in series with a parallel LC, as shown in Fig. 3.6. C_1 represents the mutual capacitance between the adjacent elements, L_1 is the inductance of the two T-shaped strips, and C_2 is the capacitance of the parallel strips, as shown in Fig. 3.8. The equivalent circuit component values are C_1 = 1.1 pF, L_1 = 0.64 nH. To achieve good agreement with the simulated performance, C_2 is tuned from 2.8 pF to 2.9 pF by curve-fitting. In fact, the interconnection between the proposed FSS array elements will not only increase the inductance, but also change the equivalent circuit.

3.3.1.3 FSS with orthogonal layers in the xy-plane

Recently, many approaches have been proposed [1-6] to miniaturise array elements by increasing the capacitance or inductance or both. These approaches include increasing the substrate thickness or the complexity of the structures. The proposed miniaturised FSS utilises a metal-dielectric-metal structure to design a passband filter by having two layers of the same shape but arranged orthogonally. In the proposed structure, the top layer of the substrate, as shown in Fig. 3.8, acts as an inductor for vertical polarisation. Meanwhile, the capacitance is achieved by the bottom layer which is the same as the top layer but with 90° rotation. That is, the interconnection contributes to making the top layer act as only an inductor (the inductance is dominant) and the bottom layer as a capacitor, as discussed in the next section. More importantly, the structure will exhibit the same transmission performance in the x and y directions.

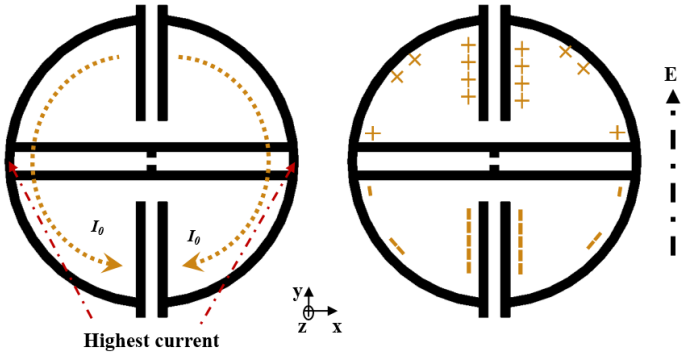

Fig. 3.10. The current and charge distribution on the top layer of the proposed structure (a) the current distribution, (b) the charge distribution.

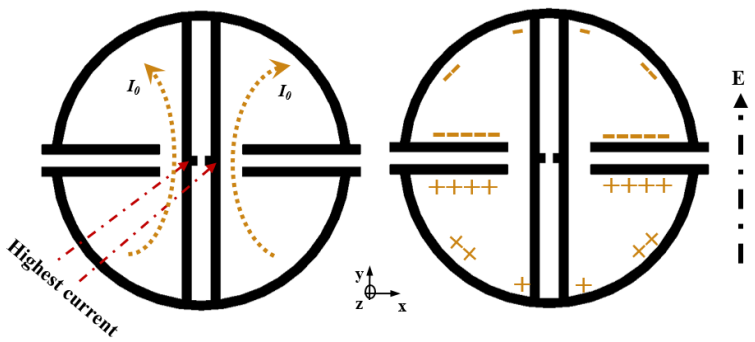

(a) (b)

Fig. 3.11. The current and charge distribution on the top layer of the proposed structure (a) the current distribution, (b) the charge distribution.

In this way, the proposed array element is insensitive to the polarisation angle. That is, in the vertical polarisation, the metal layer at the top acts as an inductor because the inductance is dominant. At the same time, the bottom metal

layer presents a capacitance because the capacitance is dominant. In the horizontal polarisation, the top metals layer acts as a capacitor and the bottom metal layer acts as an inductor.

The most important advantage is that, by having two layers orthogonally, it can induce a strong capacitance between them. This capacitor is induced because the charge distribution is different between the top and the bottom layers of the FSS. For instance, when an external electrical field, **E**, is applied in the y-axis (vertical) direction, the dominant current will be on the ring circumference toward the *y* (or -*y*) axis direction, as shown in Fig. 3.10(a). The current is the strongest at the edge of the resonator. This can induce positive charges on the top half of the proposed element and negative charges on the bottom half as shown in Fig. 3.10(b). On the other hand, for the 90^{o} rotated element on the other layer, the direction of the current is similar to the top layer, but the strongest current is in the center of the resonator, as shown in Fig. 3.11(a). As a result, the top half of the array element will have negative charges, while the bottom will have positive charges as shown in Fig. 3.11(b). This induces a strong cross-layer capacitance, C_{cc}, between the parallel layers of the proposed array element, as shown in Fig. 3.12. The equivalent circuit of the unit of the two orthogonal elements is a combination of the equivalent circuit of the top layer (enhanced inductor) and the bottom layer (*C* in series with a parallel *LC)*, as

illustrated in Fig. 3.13, where L_T is the inductance of the two T-shaped strips, C_e is the capacitance of the parallel strips, and L_e is the enhanced inductor (the interconnected parallel strips). C_s is the sum of the mutual capacitance, C_m, between the adjacent elements, and the cross-layer capacitance between the top and bottom layers, C_{cc}, where the cross-layer capacitance can be estimated by:

$$C_{cc} = \frac{\varepsilon_r \varepsilon_o A}{d} \tag{3.1}$$

where A is the area of the proposed element surface. The parallel surfaces are separated by a distance d which is the thickness of the substrate. The dielectric constant of the substrate is ε_r.

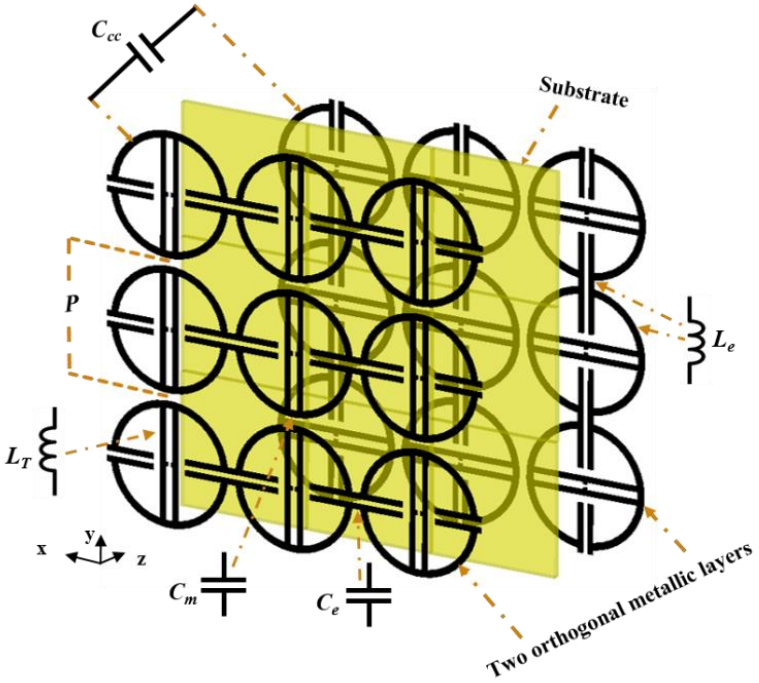

Fig. 3.12. The array elements are placed orthogonally to each other on adjacent layers. A strong cross-layer capacitance exists between the two layers.

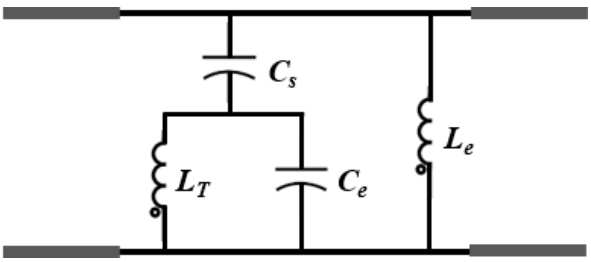

Fig. 3.13. The equivalent circuit of the proposed miniaturised FSS unit, C_s is the sum of the mutual capacitance between adjacent elements (C_m) and the cross-layer capacitance (C_{cc}).

3.3.2 Circuit design

The simulated magnitudes of S_{11} and S_{21} of the proposed structure at 0.127 mm substrate thickness are shown in Fig. 3.14. The responses in the vertical and horizontal polarisations for the TE mode are almost the same as each other. It is shown in Fig. 3.15 that the phases of S_{21} are the same as each other as well. Table 3.1 shows the simulated resonant frequency, the fractional bandwidth and the array element size as a function of the thickness of the substrate.

It is obvious that decreasing the substrate thickness from 0.8 mm to 0.127 mm can shift the resonant frequency downward from 2.32 GHz to 1.35 GHz. The array element size is miniaturised by 58% (from 0.0773λ to 0.045λ), although the bandwidth is reduced.

It should be noted that the low profile can be achieved only if C_{cc} is dominant compared to the adjacent strips' capacitance C_m and C_e. The values of the equivalent circuit components for a 0.127 mm thick substrate are C_m = 1.1 pF, C_e = 2.9 pF, and L_T = 0.64 nH, while C_{cc} is 6.2 pF as calculated from (3.1). The value of C_{cc} is much bigger than the adjacent strips' capacitances.

To obtain good agreement with the simulated structure, as shown in Fig. 3.14, a curve fitting was carried out. While other component values are very close to the calculated ones, the value of C_{cc} is found to be 7.3 pF after curve fitting. This deviation is mainly due to the fringing effect of the field between the edges of two parallel plates. This deviation increases with the thickness of the substrate, especially when $w << d$. There are several approaches to quantify the fringing effect [8, 9]. The total capacitance including the fringing effect of a circular parallel-plate capacitor can be estimated by [10]:

$$C_{cc} = \varepsilon_r \varepsilon_o [\frac{\pi r^2}{d} + r \ln(\frac{16\pi r}{d} - 1)] \tag{3.2}$$

where, r is the radius of the circular disk. As a comparison, the calculated capacitance of a circular disk with r= 4.7 mm and d= 0.127 mm would have been 7% higher by considering the fringing effect. For the proposed structure, the value of the capacitance is 17% higher compared to the value obtained by curve fitting as mentioned in Section 3.3.1.2. The deviation in the ring structure is slightly higher because the fringing effect takes place on both the inner and the outer edges of the

ring structure. The deviation would also be greater if the substrate is thicker.

Table 3.1: Resonant frequencies and element sizes with different substrate thicknesses

Thickness (mm)	f_r (GHz)	Fractional bandwidth	Element size
0.8	2.32	11%	0.077λ
0.6	2.18	9.3%	0.073λ
0.3	1.82	8.7%	0.060 λ
0.127	1.35	7.5%	0.045λ

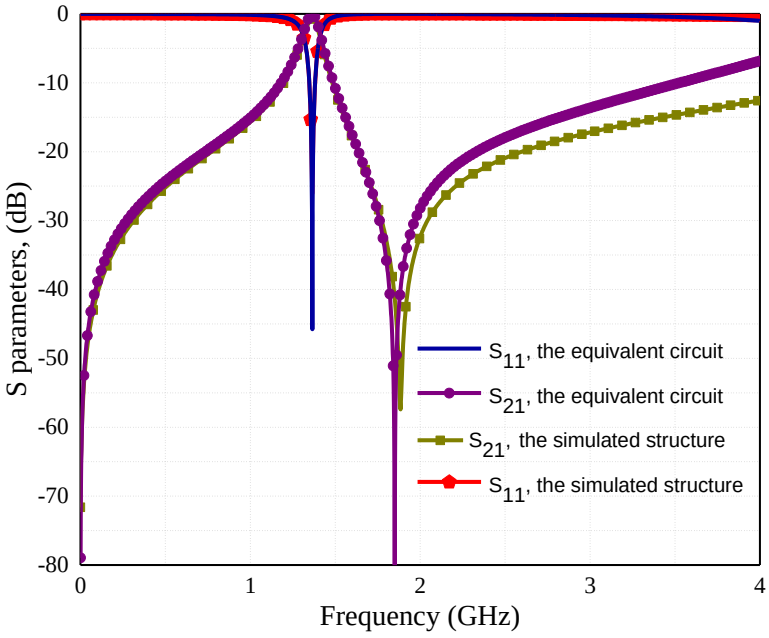

Fig. 3.14. The simulated and calculated responses of the miniaturised FSS structure. Due to the orthogonal nature of the structure, the performance is the same for both the vertical and the horizontal polarisations.

The structure was simulated under various incident angles and for different modes. The substrate thickness used in the simulation is 0.6 mm. The results show that the resonant frequency is very stable as shown in Fig. 3.16. The insertion loss is

0.33 dB at the normal incident angle and 0.69 dB at the 60˚ incident angle for the TE mode, whilst the insertion loss is 0.32 dB at the normal incident angle and 0.18 dB at 60˚ incident angle for the TM mode. As a comparison, the simulated insertion loss at a normal incident angle is 0.35 dB for the TE mode and 0.4 dB for the TM mode, while at 60˚ incident angle, it is 0.5 dB for the TE mode and 0.3 dB for the TM mode in [2]. The values at the normal incident angle are 0.2 dB for the TE mode and 0 dB for the TM mode; 0.3 dB for the TE mode and 0 dB for the TM mode at 60˚ incident angle in [3], or 1.4 dB for the TE mode and 1.2 dB for the TM mode at the normal incident angle and 1.6 dB for the TE mode and 0.8 dB for the TM mode at 60˚ in [5]. The insertion loss of the proposed structure is comparable to the results in other references.

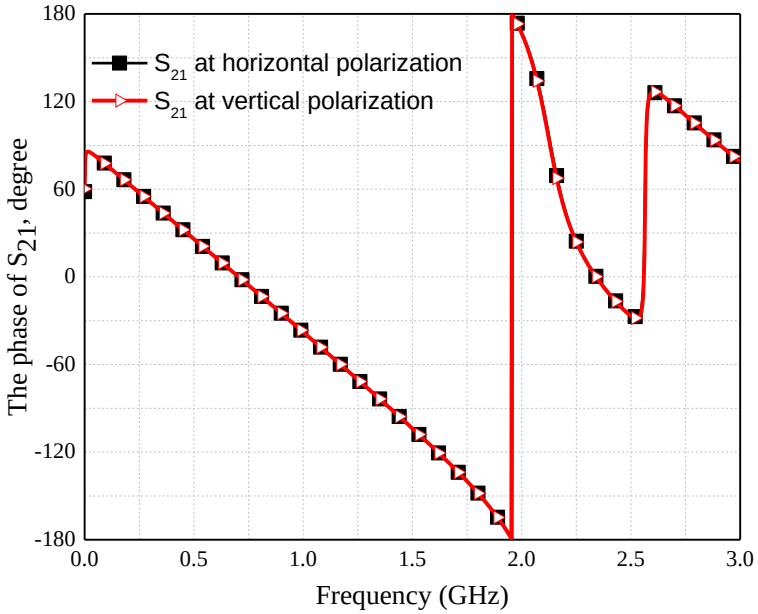

Fig. 3.15. The simulated phases of the transmission coefficients of the miniaturised FSS structure for both the vertical and the horizontal polarisations.

The cross-layer capacitance contrasts with the adjacent capacitors (C_m and C_e). C_{cc} would increase if the thickness of the substrate was reduced, while C_m and C_e would decrease. Compared with the normal incidence case, the deviations of the resonant frequency of the miniaturised FSS structure at different incident angles, for both TE and TM modes, are shown in the Table 3.2 and 3.3, respectively. The resonant frequency is shifted from 2.18 GHz to 2.25 GHz (3.2%) at the 60° incident angle for the TE mode and 0.37% for the TM mode. As a comparison, the resonant frequency deviation is 6.6% for the TE mode at 60˚ incident angle in [1], 2% for both the TE and the TM modes in [2], 0% for the TE mode and 1.3% for the TM mode in [3], and

0% fort the TE mode and 5% for the TM mode in [5].

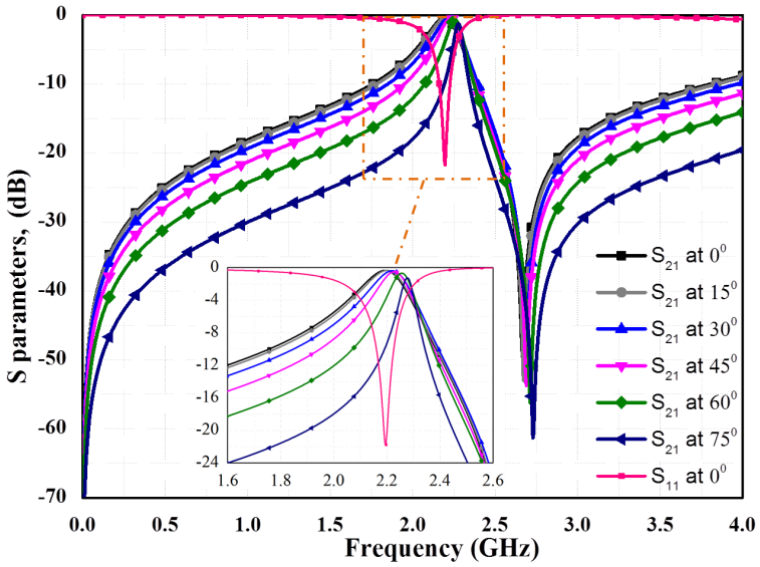

(a)

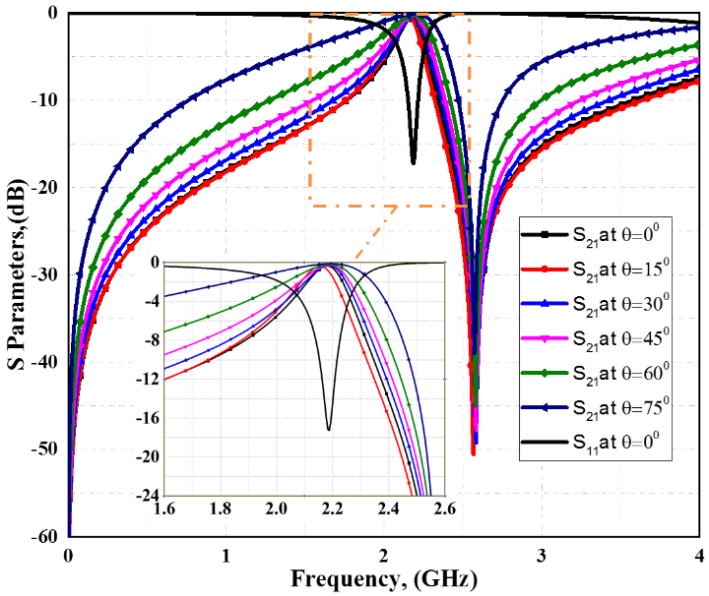

(b)

Fig. 3.16. The simulated reflection and transmission coefficients of the miniaturised FSS structure as a function of the incident angle, (a) TE mode, (b) TM mode.

The simulated result of the transmission and reflection coefficients of the miniaturised FSS structure under 45˚ incident angle and various polarisation angles is shown in Fig. 3.17. It can be seen that the transmission coefficient is hardly changed

Table 3.2: The deviation of the resonant frequency for different incident angles for the TE mode

Incident angle (degree)	f_r (GHz)	Deviation
15	2.19	0.4%
30	2.20	0.9%
45	2.22	1.8%
60	2.25	3.2%
75	2.26	3.6%

Table 3.3 shows the deviation in the resonant frequency for a wide range of incident angles for TE and TM modes.

Table 3.3: The deviation of the resonant frequency for different incident angles for the TM mode

Incident angle (degree)	f_r (GHz)	Deviation
15	2.156	1.10%
30	2.184	0.18%
45	2.188	0.36%
60	2.188	0.36%
75	2.192	0.55%

with the polarisation angle, although the array element is not rotationally symmetrical by 90˚ as for most traditional elements. This advantage offers great flexibility for the array element design. This methodology can be applied to the design of multi-layer FSSs. For example, a three-layer FSS can be designed by having each layer at an angle of 120˚ to the next layer.

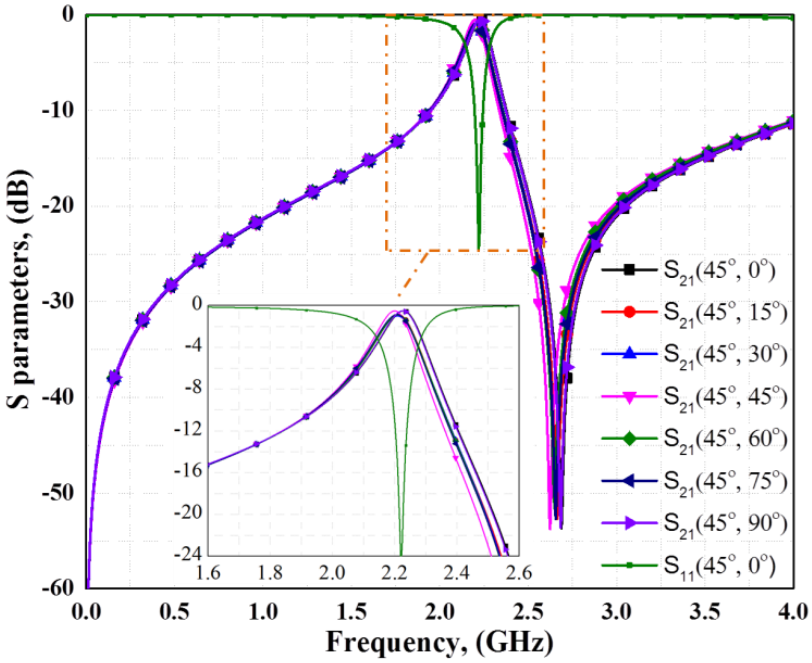

Fig. 3.17. The simulated reflection and transmission coefficients of the miniaturised FSS structure under incident angle of 45º and various polarisation angles for TE mode.

Table 3.4: Comparison of element size with other references

FSS structure	Substrate thickness (mm)	ε_r	Element size
[1]	1.6	4.3	0.22λ
[2]	1.6	4.3	0.104λ
[3]	0.5	3.55	0.088λ
[4]	0.127	2.2	0.067λ
[5]	1.6	5	0.061λ
[6]	1	3	0.058λ
[11]	0.021	1.12	0.266λ
The proposed array element	0.127	4.3	0.043λ

Cross-polarisation levels between TE and TM waves are also examined with regard to normal incident angle and varied polarisation angles (0º to 45º). The direction of polarisation is rotated from 0◦ to 45◦ to examine the cross-polarisation levels at different incident angles. The proposed orthogonal layers present a very low polarisation conversion which is generally below -25 dB The transmission

coefficients in cross polarisation at the resonant frequency is better than -45 dB at the 0° polarisation angle, -40 dB at 15°, -30 dB 30° and -27 at 45°. This confirms that when TE wave propagates through the proposed orthogonal layers, the transmitted wave is still with TE polarisation. The performance is similar for the TM case.

A comparison of the FSS array element size between the proposed design and other miniaturised FSS elements described in previous works is illustrated in Table 3.4. It can be seen that the proposed structure has the smallest size.

Moreover, the effect of the misalignment between the orthogonal layers is simulated. The simulation was carried out by shifting one layer with different distances, as show in Table 3.5. The proposed structure exhibits a stable frequency response to the misalignment. As an example, the resonant frequency was shifted from 2.018 GHz to 2.0204 GHz at 0.5 mm misalignment between the surface layers, as shown in the table.

Table 3.5: The deviation of the resonant frequency caused by the misalignment between the top and bottom layers

Misalignment (wavelength λ)	Misalignment (mm)	Deviation
0.00145	0.2	0.11%
0.00218	0.3	0.48%
0.0036	0.5	1.1%

Table 3.6: Fractional bandwidths and element sizes with different strip widths at 0.6 mm substrate thickness

W (mm)	f_r (GHz)	Fractional bandwidth	Element size
0.3	2.18	9.3%	0.077λ
0.1	2.39	14%	0.079λ
0.05	2.44	17.5%	0.081λ
0.02	2.47	19%	0.082 λ

The bandwidth of the proposed design is relatively narrow. In some applications, a wider wideband performance might be desired. The proposed techniques can be adopted to design a wideband FSS as well. This can be done by changing the dimensions of the circuit to tune the *LC* values. As the equivalent circuit is L-C in parallel, decreasing the total capacitance value will increase the bandwidth, while decreasing the inductance will decrease the bandwidth. For the proposed structure, one easy way to achieve a wider passband is to decrease the strip width to tune the *LC* values. For example, for the proposed structure with 0.6 mm thickness, the bandwidth is doubled by decreasing the strip width (*w*) from 0.3 mm to 0.02mm, as shown in Table 3.6. If it is difficult to fabricate such narrow strips, the FSS element can be revised to achieve a wider bandwidth, which can be the topic of a future publication.

3.3.3 Experimental results

The proposed FSS was fabricated as shown in Fig. 3.18. Transmission characteristics of FSS devices can be measured through a few select methods [12, 13]. The measurement setup for the proposed FSS is shown in Fig. 3.19. Two horn antennas and a vector network analyser were used. The experiment setup is composed of two broadband SATIMO horn antennas which are pointing to each other. The FSS under test is placed between the antennas. The distance is large enough to be considered as in the far field region of the horn (meeting $> 2D^2/\lambda$ condition), where D is the antenna size and λ is the free space wavelength at the resonant frequency. Thus, the wave arriving at the FSS can be considered as a plane wave. To avoid spillover at the edge of the FSS, RF absorbing materials are used around the edges. In order to ensure the measurement accuracy, a calibration was carried out. Without the FSS, the transmission coefficient was first measured as the reference for 100% transmission (S_{21} = 1 or 0 dB). When the FSS is under test, the measured transmission coefficient was normalised to the reference. In order to measure the transmission at different incident angles, the FSS holder fixture can be rotated to the angle of interest. In this case the measurement accuracy is not as good as the normal incident angle due to the limited size of the FSS. The array size of 200 mm × 200 mm (1.45λ × 1.45λ) consisting of 20 × 20 elements appeared to be large enough to give reliable results. Measurement of the fabricated FSS is performed in

two steps. Firstly, the transmission response of the system without the FSS is measured. This measurement result is used to calibrate the FSS response. Secondly, the transmission coefficient S_{21} was measured at various angles of incidence and polarisation.

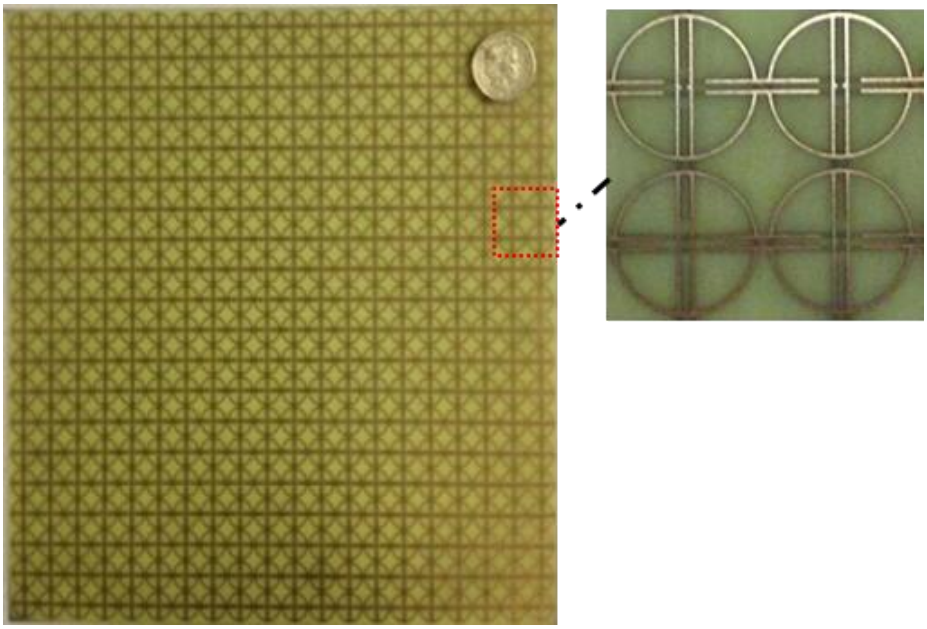

Fig. 3.18. A photograph of the fabricated FSS with the proposed miniaturized array elements.

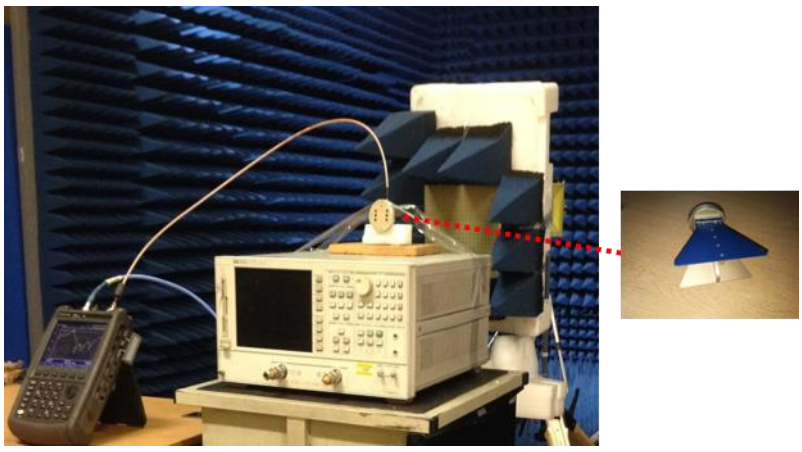

Fig. 3.19. The experimental setup to measure the transmission coefficient of the FSS.

The measured results of the miniaturised FSS are shown in Fig. 3.20 and Fig. 3.21. They show a relatively good agreement with the simulated ones. The discrepancy between the simulation and measurement results is mainly attributed to tolerances involved in the fabrication process, inaccuracies in the exact values of the parameters of the dielectric substrates used, and the small deviation due to the scattering from the stand used to hold the FSS.

The frequency response of the proposed FSS is insensitive to the angle of incidence, as shown in Fig. 3.20. It demonstrates a measured insertion loss of about 0.72 dB at its resonant frequency for normal incidence, which is mainly attributed to the dielectric and the metallic losses of the structure. The measured result of the FSS

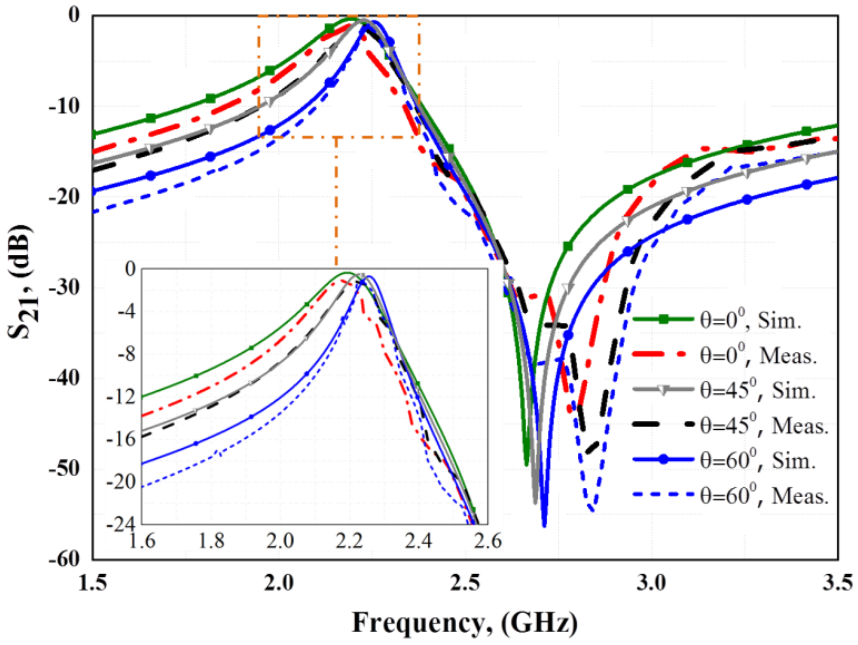

Fig. 3.20. The simulated and measured transmission coefficients of the miniaturised FSS structure at different incident angles.

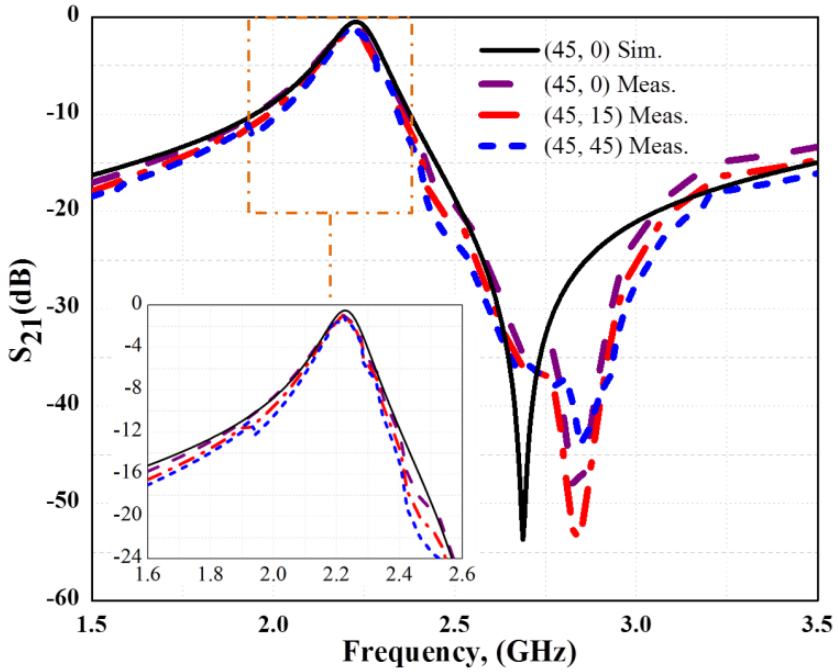

Fig. 3.21. The simulated and measured transmission coefficients of the miniaturised FSS structure under the 45º incident angle and various polarisation angles for TE mode.

with 45˚ incident angle and various polarisation angles is shown in Fig. 3.21. The proposed miniaturised FSS exhibits almost the same response at different polarisation angles with a fractional bandwidth of 9%. The measured insertion loss is about 0.92 dB for normal incidence, and 0.98 dB at 60˚ incident angle at its resonant frequency. This is comparable to the measured insertion losses in the other studies. For example, the measured insertion loss is about 0.7 dB at the normal incident angle in [15], 0.47 dB in [16], and 1.2 dB in [18].

3.4 Conclusion

Dual polarised single and two-layer FSS structures are proposed in this chapter. The single-layer is relatively easy to fabricate due to its simple structure consisting of a single metal layer on a dielectric layer. The FSS displays a high transmission, wide operational frequency band, and excellent band edge transitions. It is shown that the dual polarisation response can be achieved, although the element is not rotationally symmetrical by 90^o in xy-plane. The proposed structure is fabricated and tested to verify the design. This dual polarised bandpass FSS with broadband response can be used in absorber applications.

A few novel approaches have been combined in this chapter to miniaturise FSS elements and make the FSS insensitive to the angle of incident waves. The interconnection of the array elements in one direction can change the equivalent circuit of the FSS structure, and increase the values of the equivalent circuit component values.

In the proposed design, patterns on the layers on two sides of a substrate are arranged orthogonal to each other in the xy-plane to build up the FSS. As a result, a very strong cross-layer capacitance will be generated between the two layers. The cross-layer capacitance can miniaturise the element much further. It can offer further significant advantages because the FSS with a low profile substrate would have a lower resonant frequency. An analytical circuit model has been presented to describe the miniaturised FSS. The proposed design has the smallest size compared to other miniaturised designs.

Furthermore, using the proposed method, the array element in the FSS does not have to be rotationally symmetrical by 90^o. The method can be easily adopted in a

multi-layer FSS design. The proposed structure has been fabricated and tested. It has been shown that, by interconnecting adjacent resonators in one direction and having two orthogonal layers, the resonant frequency of the array was reduced from 5.5 GHz to 2.32 GHz. When the substrate thickness is reduced from 0.8 mm to 0.127 mm, the resonant frequency is lowered further from 2.32 GHz to 1.35 GHz. One FSS was fabricated on a 0.6 mm thick FR4 to validate the theory. The FSS was tested under different incident wave angles. It was verified that the response is insensitive to the incident angle. It exhibits polarisation insensitivity for different incident angles. In future work, a wideband performance can be achieved by revising the element structure, if desired. The proposed method can also be used for multi-layer FSS design.

3.5 References

[1] K. Sarabandi, and N. Behdad, "A frequency selective surface with miniaturized elements," *IEEE Transactions on Antennas and Propagation,* vol. 55, no. 5, pp. 1239-1245, 2007.

[2] C. N. Chiu, and K. P. Chang, "A novel miniaturized-element frequency selective Surface having a stable resonance," *IEEE Antennas and Wireless Propagation Letters,* vol. 8, pp. 1175-1177, 2009.

[3] F. C. Huang, C. N. Chiu, T. L. Wu, and Y. P. Chiou, "A circular-ring miniaturized-element metasurface with many good features for frequency selective shielding applications," *IEEE Transactions on Electromagnetic Compatibility,* vol. 57, no. 3, pp. 365-374, 2015.

[4] S. N. Azemi, K. Ghorbani, and W. S. T. Rowe, "Angularly stable frequency selective surface with miniaturized unit cell," *IEEE Microwave and Wireless Components Letters,* vol. 25, no. 7, pp. 454-456, 2015.

[5] G. H. Yang, T. Zhang, W. L. Li, and Q. Wu, "A novel stable miniaturized frequency selective surface," *IEEE Antennas and Wireless Propagation Letters,* vol. 9, pp. 1018-1021, 2010.

[6] M. B. Yan, S. B. Qu, J. F. Wang, J. Q. Zhang, A. X. Zhang, S. Xia, and W. J. Wang, "A novel miniaturized frequency selective surface with stable resonance," *IEEE Antennas and Wireless Propagation Letters,* vol. 13, pp.

639-641, 2014.

[7] B. A. Munk, "Frequency selective surfaces theory and design," New York: Wiley-Interscience, 2000.

[8] G. Parker, “What is the capacitance of parallel plates?,” *Computers in Physics,* vol. 5, no. 5, pp. 534-540, 1991.

[9] G. Carlson, and B. Illman, “The circular disk parallel plate capacitor,” *American Journal of Physics,* vol. 62, no. 12, pp. 1099-1105, 1994.

[10] L. D. Landau, and E. Lifshitz, *Course of Theoretical Physics. Vol. 8: Electrodynamics of Continuous Media*: Oxford, 1960.

[11] R. J. Langley, and E. A. Parker, “Equivalent-circuit model for arrays of square loops,” *Electronics Letters,* vol. 18, no. 7, pp. 294-296, 1982.

[12] T. Cwik, R. Mittra, K. Lang, and T. Wu, “Frequency selective screens,” *IEEE Antennas and Propagation Society Newsletter,* vol. 29, no. 2, pp. 5-10, 1987.

[13] D. K. Ghodgaonkar, V. V. Varadan, and V. K. Varadan, “A free-space method for measurement of dielectric constants and loss tangents at microwave frequencies,” *IEEE Transactions on Instrumentation and Measurement,* vol. 38, no. 3, pp. 789-793, 1989.

Chapter 4: Multi-Layer FSS

4.1 Introduction

FSSs structures can be used for many applications, such as in radomes to reduce the radar cross section (RCS) of antennas. Most antennas act as efficient radiators at the frequency band in which they are designed to operate in and also somewhat outside their desired operating frequency range. In such applications, using a bandpass FSS can reduce the RCS of antennas because it is transparent within the antenna's operating frequency and opaque at other frequencies.

Recently, there has been an interest in the design of FSSs with array element dimensions that are much smaller than the wavelength. In traditional designs, the frequency selective properties result from mutual interactions of the array elements. Therefore, the miniaturisation of an element size is desired to enable an FSS with sufficient array elements because practical FSSs are usually fabricated in finite dimensions. The miniaturisation of an FSS is mainly achieved by enhancing the values of resonant components (capacitors and inductors). Adding meander-slots to a circular ring structure can make FSS array element dimensions much smaller than the wavelength [1]. The creation of a miniature FSS by printing wire on a dielectric has been demonstrated in [2]. Printing four symmetrical spiral patterns of metallic meander lines can increase the electrical length of the array element and increase the value of resonant components [3]. Two layers, metallic patches and wire meshes, separated by a dielectric substrate are used to miniaturise the array elements in [4, 5]. An FSS element miniaturised by using lumped components is presented in [6]. Another approach is adopted in [7], by cascading interdigital capacitors on a thin substrate layer.

However, most FSSs reported in the literature suffer from practical design issues, namely sensitivity to polarisation or incident angle, the dimensions issue, or the sensitivity when attached to a wide variety of dielectric materials of varied thickness. These limitations can restrict the use of FSS in many applications. For example, the FSSs can be used in radio frequency-identification (RFID) tag applications. A tag is usually attached directly to an object that needs to be identified. Many common materials have a very strong effect on the performance of the tag antenna and can

shift the resonant frequency. In the worst case, the tag may be unreadable at normal ranges, which would cause tracking systems to miss objects [8, 9]. In some applications, the FSSs need to be attached to dielectric materials for mechanical reasons to make the structure stronger.

This chapter describes both a single and a dual polarised FSS structure. Firstly, a two-metal-layer bandpass FSS element is designed by using a step-impedance structure with very high and very low characteristic impedance transmission lines in each layer (see Chapter 2). The mesh and patch are included in the proposed array element. The novel methodology is used to miniaturise the FSS element's dimensions. The dimensions of the periodic array element are much smaller than the wavelength at the resonant frequency with a periodicity of $0.012\lambda \times 0.012\lambda$. The overall profiles (thicknesses) of the multi-layer FSS element presented in this chapter are extremely small. For example, the thickness of the FSS structure consisting of two metallic layers and one dielectric layer is less than 0.14 mm. The proposed structure is designed to display a stable frequency response when it is attached to a wide variety of dielectric materials of varied thicknesses. These particular features of the proposed structure can make it an optimal solution for many applications. In this chapter, section 4.2 describes the design of a single polarised FSS array element and the approaches to miniaturise the element. Section 4.3 explains the design of a dual polarised FSS array element. Section 4.3.1 discusses the stability of the FSS array against surrounding dielectric materials. Section 4.3.2 describes the experiment setup and results to verify the theory. Conclusions are finally given in Section 4.4.

4.2 Single polarised FSS element

Fig. 4.1 shows the structure of the proposed single polarised FSS element, consisting of two metallic layers separated by a substrate layer. Each metallic layer is printed on one side of the dielectric substrate consisting of an inductive loop with a width of w and two capacitive patches, each with an area of $b \times a$. Numerical analysis of the proposed element was performed by using CST Microwave Studio, using unit cell boundary conditions to provide periodicity along the x and y axes. The FSS is excited by an electromagnetic wave with the propagation vector (**k**) towards the z axis, magnetic field vector (**H**) towards the x axis and electric field vector (**E**) towards the y axis direction. The top and bottom layers are the same, but flipped in

the *xy* plane. In this way, the currents enter and exit from the top layer patches in opposite directions to the bottom layer patches, as shown in Fig. 4.2. This causes the charges to be distributed in different polarisations between the top and the bottom layers of the FSS, which induces a strong cross-layer capacitor, C_{cc}.

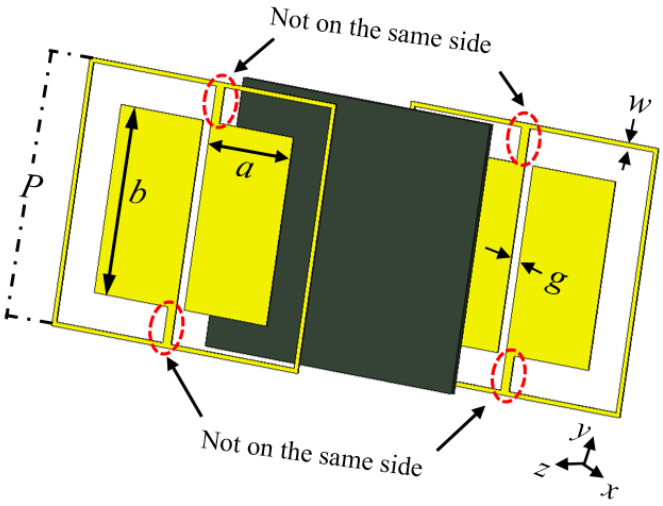

Fig. 4.1. Array element geometry of the proposed single polarized FSS.

For instance, when an external electrical field, **E**, is applied in the *y*-axis direction, the current will flow into the left patch and out from the right patch towards the (-*y*) axis direction on the top layer, as shown in Fig. 4.2(a). This can induce positive charges on the left patch of the proposed element and negative charges on the right one. On the other hand, in the bottom layer, since the structure is flipped, the current will flow into the right patch and out from the left patch towards the (-*y*) axis direction, as shown in Fig. 4.2(b). This can induce charges opposite to the top layer. Thus, there is a strong cross-layer capacitance existing between the top and the bottom layer. This capacitance offers significant advantages to the FSS element by making the structure compact, low profile (the lower the profile, the stronger the capacitance) and insensitive to surrounding dielectric materials, as discussed in the following sections. The proposed structure is designed on an FR4 PCB. The two metallic layers are etched on the top and bottom copper layers of a 0.127 mm-thick FR4 substrate with a dielectric constant of 4.4 and a loss tangent of 0.025. The length of the rectangle patch (*b*) is 4.6 mm and the width (*a*) is 4.6 mm, the gap width g is 0.2 mm and the width, w, of the short line connecting the patches is 0.2 mm and for the loop is 0.1 mm. The periodic constant P of the array is 6 mm. Fig. 4.3 shows the simulated transmission and reflection coefficients.

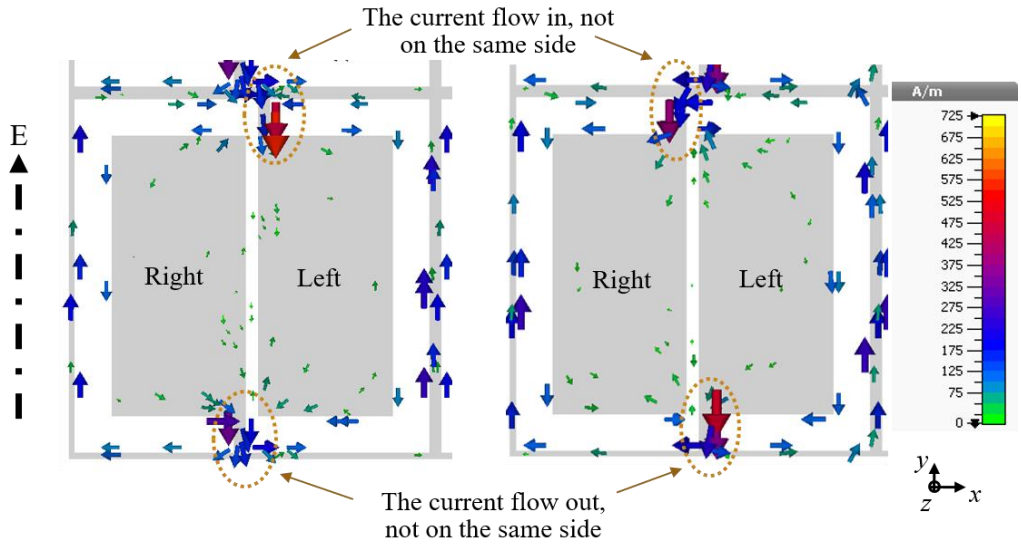

Fig. 4.2. Current distribution of the proposed element on (a) the top layer, and (b) the bottom layer.

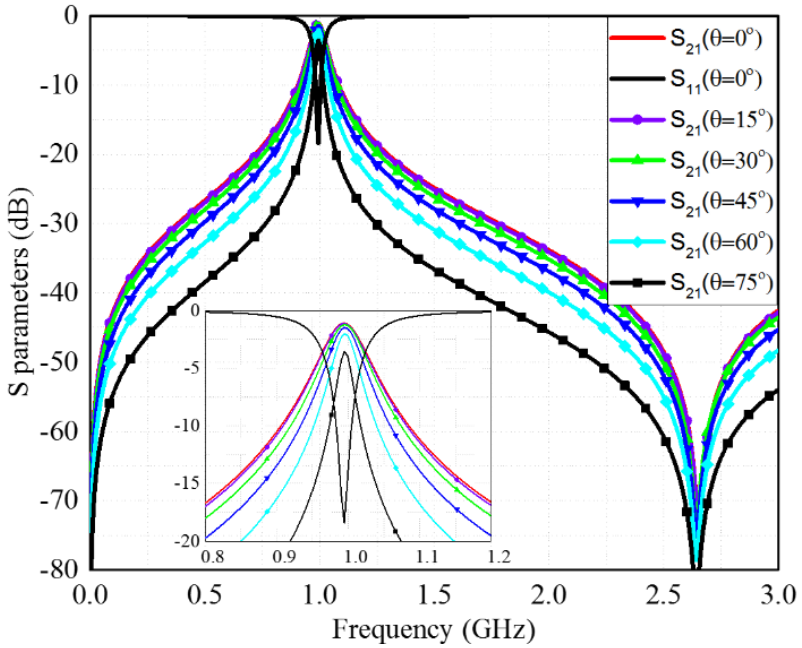

Fig. 4.3. Simulated frequency response of the proposed two-layer FSS under variable incident angles for the *E*//*y* polarisation.

The resonant frequency is 1 GHz with a fractional bandwidth of 6.1%. The reflection coefficient is -19 dB and the insertion loss is 1.13 dB at the resonant frequency. The size of the array element is found to be $0.02\lambda \times 0.02\lambda$**.** The equivalent circuit model of the proposed array element for the ***E*//*y*** polarised incident waves is shown in Fig. 4.4. It should be noted that the circuit model is only used to give a better qualitative

understanding of the proposed structure. The actual equivalent circuit is much more complicated than this circuit model. The circuit model consists of an L_1C_1 circuit for the top layer structure, an L_2C_2 for the bottom layer structure and a cross-layer capacitor C_{cc} between them. The substrate between the two metallic layers acts as a transmission line of length h (h is the substrate thickness) and a characteristic impedance of Z. The transmission line is used here as a short circuit because h is very small. For example, at the resonant frequency 1 GHz, h is $\lambda/2362$ or 0.127 mm. In the circuit model, L_1 is equal to L_2 and C_1 is equal to C_2 due to symmetry.

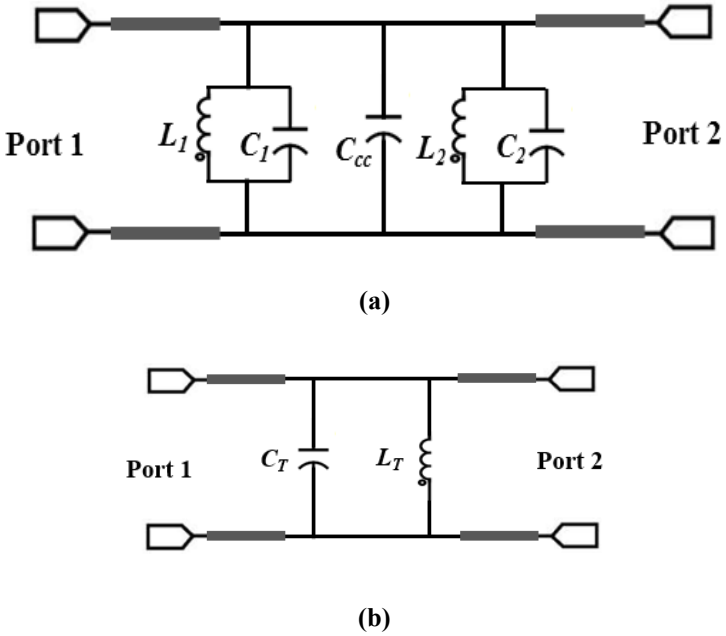

Fig. 4.4. Equivalent circuit of a two-metallic-layer structure, where $L_{T=}(L_1 \times L_2) / (L_1 + L_2)$ and $C_{r1} = C_1 + C_2 + C_{cc}$.

The cross-layer capacitance is much stronger than the intrinsic capacitance between the two adjacent patches of each layer. Any dielectric materials attached to the FSS will mainly affect the intrinsic capacitance, but not the cross-layer capacitance. Hence the performance of the proposed FSS is very insensitive to surrounding materials. This advantage will be further discussed in Section 4.3.1.

In this case, the circuit model of the FSS element is composed of the parallel LC circuits of two metallic layers and the cross-layer capacitor. This means that increasing the number of metallic layers (n) will miniaturise the structure further, although this will be accompanied with bandwidth and insertion loss penalties. The approximate values of the intrinsic inductance and capacitance for TE incident waves

can be calculated from the strip inductance and path capacitance using equations in [10],

$$L = \mu_o \mu_e \frac{P}{2n\pi} [\ln \operatorname{cosec}(\frac{\pi w}{2P})] \tag{4.1}$$

where L is the strip inductance, which is determined by the strip length P, the strip width w and the effective magnetic permeability μ_e of the structure, n is the number of metal layers. And

$$C = n\varepsilon_o \varepsilon_e \frac{2b}{\pi} [\ln \operatorname{cosec}(\frac{\pi g}{2b})] \tag{4.2}$$

where C is the intrinsic capacitance between the two adjacent patches in each layer, which is determined by the patch length b, the gap g between adjacent patches and the effective dielectric constant ε_e of the structure, $\varepsilon_e = (\varepsilon_r+1)/2$, if the substrate thickness is much greater than the gap width. While the cross-layer capacitance C_{cc} is calculated by using the parallel plates' capacitance equation:

$$C_{cc} = (n-1)\frac{\varepsilon_r \varepsilon_o \mathrm{A}}{d} \tag{4.3}$$

The overlapping area of the conducting patch is A and equal to $2(a \times b)$; the parallel conducting layers are separated by a distance d, which is the thickness of the substrate h in this case, and the dielectric constant of the substrate is ε_r. It is quite obvious that the cross-layer capacitance is much higher than the intrinsic capacitance of each layer. The approximate theoretical values for the resonator components are $L_1 = L_2 = 3.5$ nH, $C_1 = C_2 = 0.28$ pF, while the value of $C_{cc} = 6.2$ pF. The value of C_{cc} is much greater as expected. The cross-coupling capacitance C_{cc} will significantly lower the resonant frequency of the FSS array element, which makes the element much more compact.

Multi-layer structures are usually used for the design of multi-band or wideband bandpass filters. It can be seen from (4.3) that the multi-layer structure can also be used to miniaturise the array element because the value of the cross-layer capacitance will be increased with the increase of the number of metallic layers (n). It can be calculated from the equivalent circuit in Fig. 4.4 that a multi-layer structure is much less sensitive to surrounding materials. This will be further discussed below.

The cross-layer capacitance is higher with a thinner substrate (lower profile). This

is contrary to the intrinsic capacitance. The intrinsic capacitance depends on the effective permittivity of the substrate. The effective permittivity is a function of the thickness of the substrate. If the thickness is comparable with the gap width, the effective permittivity is lower with a thinner substrate. The intrinsic capacitance is lower accordingly. If the substrate thickness is much greater than the gap width, the effective permittivity is almost constant. Therefore, the proposed FSS with a lower profile is actually more compact, which is different from traditional structures.

Fig. 4.5 shows the structure with *n* metallic layers and (*n*-1) dielectric layers. The two transparent layers are only used to mechanically support assembling the multiple layers together if needed. There are alternative ways of doing this. For example, the layers can be thermally compressed together using a bonding film with a very thin thickness between them [11]. Fig. 4.6 shows the equivalent circuit of an *n*-layer FSS structure after neglecting the intrinsic capacitance of each metallic layer.

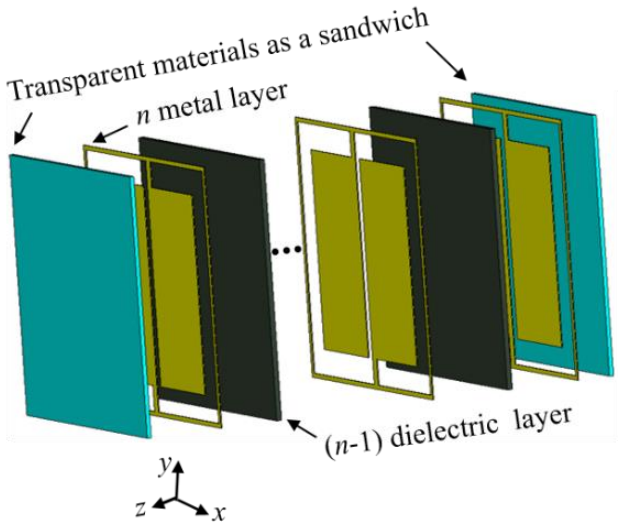

Fig.4. 5. Array element of the proposed n-metallic-layers FSS with thin dielectric supporters.

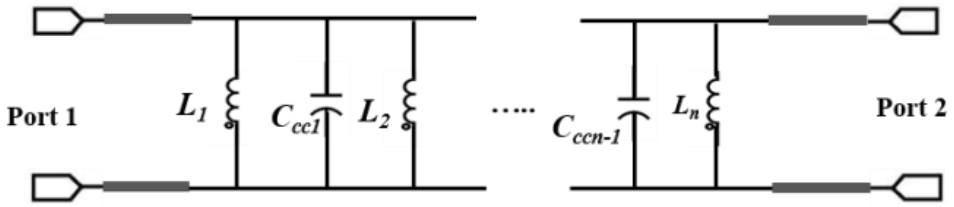

Fig. 4.6. Equivalent circuit of the proposed n-metallic-layer FSS.

The simulated resonant frequency *f*, fractional bandwidth BW, lowest values of reflection coefficients S_{11} of a multi-layer FSS using the proposed design are

summarised in Table 4.1. The periodic dimension *P* is 6 mm, the same for all of these

Table 4.1: Element size vs the number of metallic layers of single polarised FSSs

n	*f* (GHz)	BW	Insertion loss (dB)	S_{11} (dB)	Thickness (mm)	Element size
2	1	6.23%	1.15	-19	0.147	0.02λ
3	0.76	4.62%	1.3	-16.9	0.284	0.0152λ
4	0.65	3.42%	1.9	-13	0.421	0.013λ
5	0.60	2.44%	2.6	-9.7	0.558	0.012λ

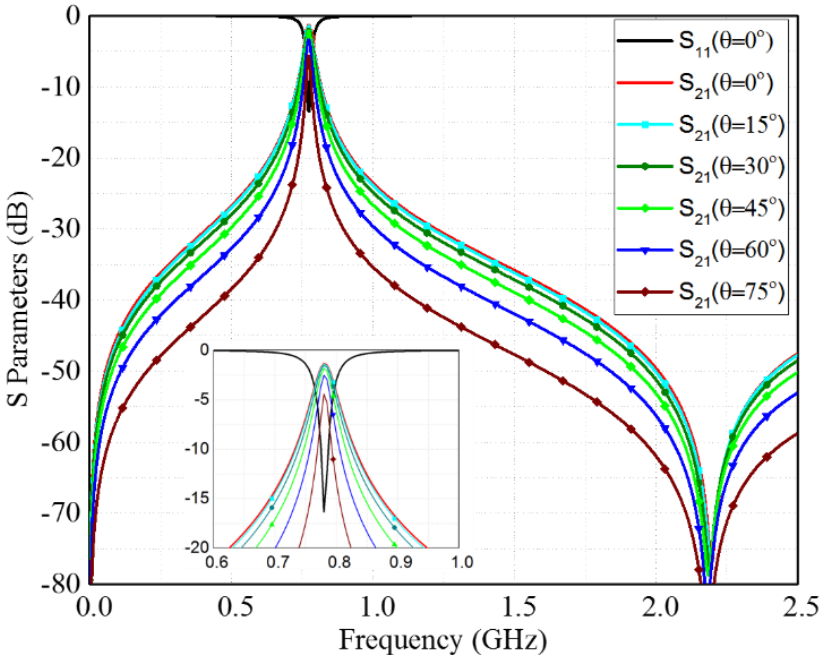

Fig. 4.7. Frequency response of the proposed three-layer FSS under variable incident angles for the *E*//*y* polarisation.

multi-layer structures. It shows that the increase of the number of layers *n* shifts the resonant frequency downward. For example, for *n* = 3 with two FR4 dielectric layers with a thickness of 0.127 mm for each, the resonant frequency is shifted downward to 0.76 GHz from 1 GHz for *n* = 2. The reflection coefficient is -16.9 dB and the fractional bandwidth is 4.62%, as shown in Fig. 4.7. The FSS array element dimensions in this case are 0.0152λ by 0.0152λ. While using five metallic layers (*n* = 5) and four dielectric layers, the resonant frequency is shifted to 0.6 GHz. The

fractional bandwidth is 2.44%, and the reflection coefficient S_{11} is -9 dB. For this case, the size of the element is 0.012λ by 0.012λ. To demonstrate the resonant stability performance of the proposed design, the structures of $n = 2$ and $n = 3$ are simulated with variable incident angles, respectively. The proposed structures are insensitive to the angle of incidence (θ) up to 60° for the ***E*//*y*** polarisations as shown in Fig. 4.3 and Fig. 4.7, respectively.

4.3 Dual polarised FSS element

The FSS element proposed in last section is suitable for single polarised incident waves. The performance of the structure is different if the *E*-field of the incident wave is along the *x*-axis. To achieve dual-polarised performance, the proposed structure can be modified to the one shown in Fig. 4.8. This structure can be used for not only dual-polarisation but also a greater fractional bandwidth. Here, the metallic structure on each layer is 90˚ rotationally symmetrical in the *xy* plane, so that the structure will achieve the same performance if the *E*-field of the incident wave is either in the *x*-axis or the *y*-axis direction. In the same way as before, the top and bottom layers are the same but flipped in the *xy* plane. Similarly, the dominant capacitor is the cross-layer C_{cc}, compared with the intrinsic capacitor. This is because only two pairs of patches will have a strong capacitance and the other two patches have relatively weak capacitance depending on the polarization.

For example, at the ***E*//*y*** polarisation, the two patches with strips along *y*-axis in each layer have a strong capacitance to the two patches on the other layer; while other two pairs of patches have weak capacitance. On the other hand, at the ***E*//*x*** polarisation, only the patches with strips along the *x*-axis have strong capacitance.

The dual polarised structure has a wider bandwidth and a higher transmission coefficient compared to the single polarized structure. This can be explained by using the quality factor (Q-factor) equation of the parallel *RLC* circuit which is given by:

$$Q = \frac{\omega}{B} = \omega\, RC \tag{4.4}$$

where ω is the resonant frequency ($\omega = 2\pi f$), and R is the half of free space impedance (Z_o). B is the bandwidth and equal to the difference between the two half power frequencies:

$$B = \omega_1 - \omega_2 = \frac{1}{RC} \tag{4.5}$$

At ω_1 and ω_2 the power on the resistor becomes half of the maximum. The quality factor increases with the increase of C and the bandwidth decreases consequently.

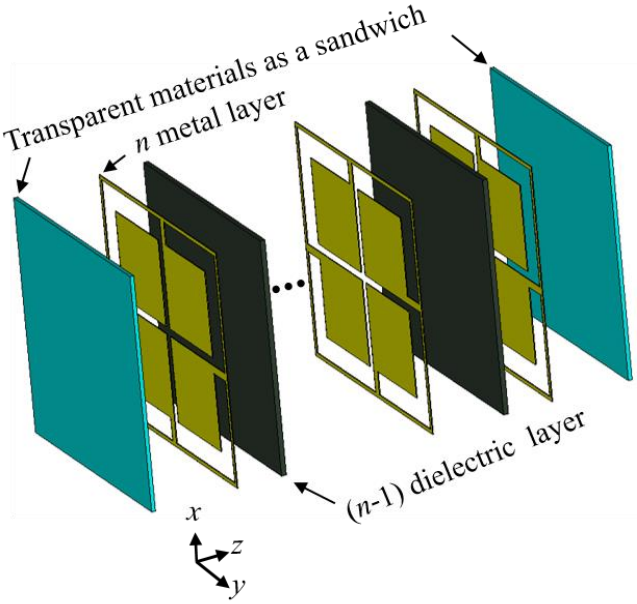

Fig. 4.8. Structure of the multi-layer bandpass FSS for dual polarisations.

The dimensions of the dual layer structure are: the gap g between adjacent patches is 0.2 mm; the width, w, of the short line connecting the patches is 0.2 mm and the loop is 0.1 mm. The periodic constant P of the array is 6 mm, but the dimension of b is halved, which means the value of the capacitance is also about halved. The patch area is a^2 since $b = 2a$.

As mentioned, increasing the number of layers will shift the resonant frequency downward. The equivalent circuit of this structure is very similar to the single polarised one, taking into consideration that the value of the C_{cc} is halved. Table 4.2 shows the variation in the resonant frequency when increasing the number of layers, n. As can be seen from the table, the resonant frequency of the two-layer (n = 2) structure is 1.98 GHz, as shown in Fig. 4.9. The same dielectric material of FR4 with 0.127 mm thickness is used in the design. The size of the array element is 0.0396λ × 0.0396λ. The resonant frequency of the structure with three metallic layers (n = 3) and two dielectric layers is 1.50 GHz, as shown in Fig. 4.10. The array element size is 0.03λ × 0.03λ.

Table 4.2: Element size vs number of metallic layers, for TE mode

n	*f* (GHz)	BW	Insertion loss (dB)	S_{11} (dB)	Overall thickness (mm)	Element size
2	1.96	10.32%	0.56	-22.5	0.147	0.038λ
3	1.50	8.42%	1.23	-22.0	0.284	0.030λ
4	1.32	6.37%	1.62	-19.2	0.421	0.026λ
5	1.21	4.45%	1.86	-16.8	0.558	0.024λ

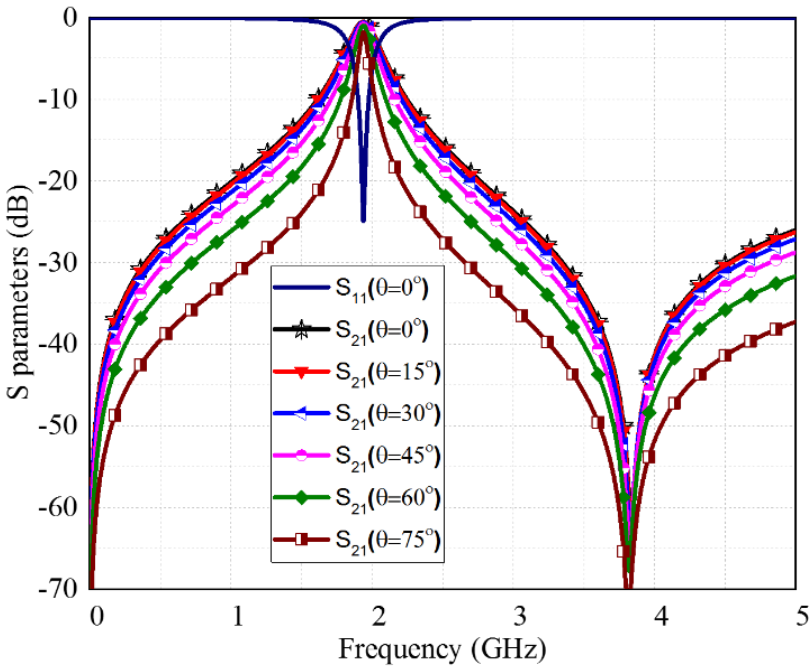

Fig. 4.9. Simulated frequency responses of the two-metallic-layer FSS (*n* = 2) under different incident angles for TE mode.

To demonstrate the resonance stability performance for the proposed FSSs with two and three metallic layers, the performance of the FSSs as a function of varied incident angles is shown in Fig. 4.9 and Fig. 4.10, respectively. The structure exhibits a polarisation independent response because it symmetrical around *z* axis. The proposed structures are insensitive to the angle of incidence (θ) up to 75° as shown.

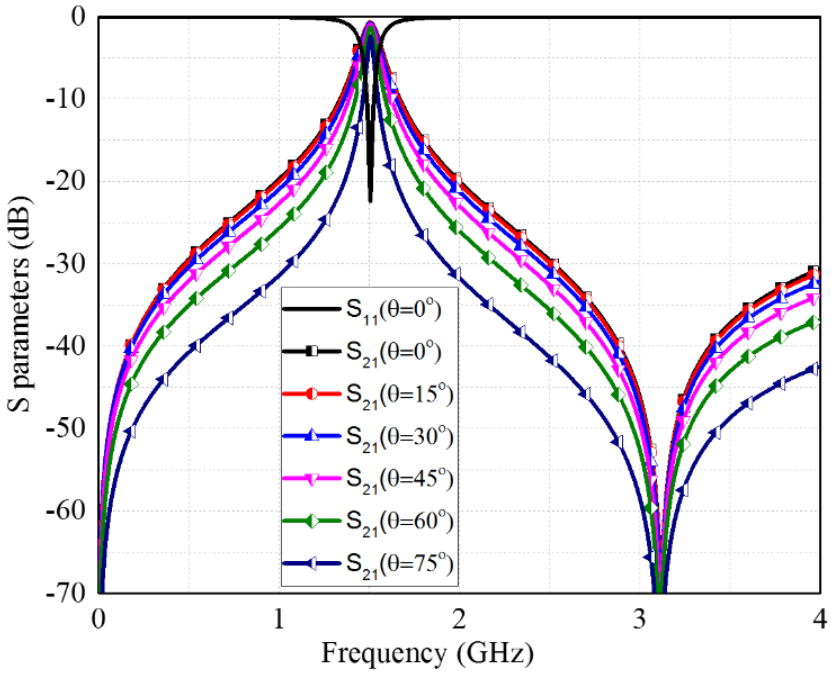

Fig. 4.10. Simulated frequency responses of the three-metallic-layer FSS (*n* = 3) under different incident angles for TE mode.

The structures were also simulated under various incident angles for the TM mode. The results show that the structures exhibit very stable performance at oblique incident angles as well. For the two-layer structure, the insertion losses are almost the same at 0.396 dB at the normal and 15˚ incident angles. The insertion losses are 0.383 dB at 30˚, 0.347 dB at 45˚, 0.287 dB at 60˚ and 0.117 dB at 75˚, respectively. The resonant frequency is always the same at 1.96 GHz. For the three-layer structure, the insertion loss is 0.645 dB at the normal incident angle. The losses are 0.582 dB at 15˚, 0.515 dB at 30˚, 0.486 dB at 45˚, 0.415 dB at 60˚ and 0.212 dB at 75˚ incident angles. The resonant frequency is the same at 1.5 GHz for all angles.

4.3.1 Surrounding dielectric materials

The performance of a conventional FSS is affected by dielectric materials attached to it. For a wide range of applications, it is desirable to design FSS structures that can achieve stable responses when the FSS is attached to dielectric materials. The proposed structures here are very stable even though they are attached to dielectric materials of varied thickness on both sides. To understand why the structure is stable when compared with traditional structures, it is necessary to understand the effect of the surrounding dielectric material on conventional FSS structures. The main reason is that the resonant components are affected by the surrounding dielectric material,

especially the intrinsic capacitance. It can be clearly concluded from (4.2) that the equivalent intrinsic capacitance of the FSS element depends on the effective dielectric constant ε_e of the structure. The surrounding dielectric directly changes the effective dielectric constant value and thus the capacitance. This can be proven by using a non-resonant FSS structure such as an inductive FSS (highpass) using planar conductor or a capacitive FSS (lowpass or bandstop) using patches. When an inductive FSS structure (planar conductor structure) is attached to a dielectric material, the frequency response is very stable, while the frequency response of the patch type FSS is shifted significantly when the structure is attached to dielectric materials. In traditional FSS structures where both wires and patches are used, the resonant frequency is very sensitive to surrounding dielectric materials.

In the proposed structure, the cross-layer capacitance is introduced and is very strong in the FSS element. This capacitor is not influenced by the surrounding dielectric material, as can be seen from (4.3). Especially for a low profile dielectric substrate, the cross-layer capacitor is dominant and diminishes the impact of surrounding materials to the intrinsic capacitance. This makes the resonant frequency very stable against surrounding dielectric materials.

The resonant frequency of the proposed structure, by ignoring the intrinsic capacitor, can be obtained by:

$$f = \frac{1}{2\pi\sqrt{LC}} \tag{4.6}$$

The values of L and C can be obtained from (4.1) and (4.3). The resonant frequency can be obtained by:

$$f = \frac{c}{\sqrt{2P\frac{(n-1)}{n}\log\left(\frac{1}{\sin\frac{\pi w}{2P}}\right)\left(\frac{\varepsilon_r A}{d}\right)}} \tag{4.7}$$

where A is equal to $2(a\times b)$ in the single polarised case and $2a^2$ for the dual polarised structure, c is the velocity of light, and n is the number of metallic layers.

To demonstrate this feature of the proposed design, the structure with dielectric materials attached is simulated using CST. Fig. 4.11 shows the comparison of frequency responses of the proposed structure shown in Fig. 4.8 with $n = 2$ in three

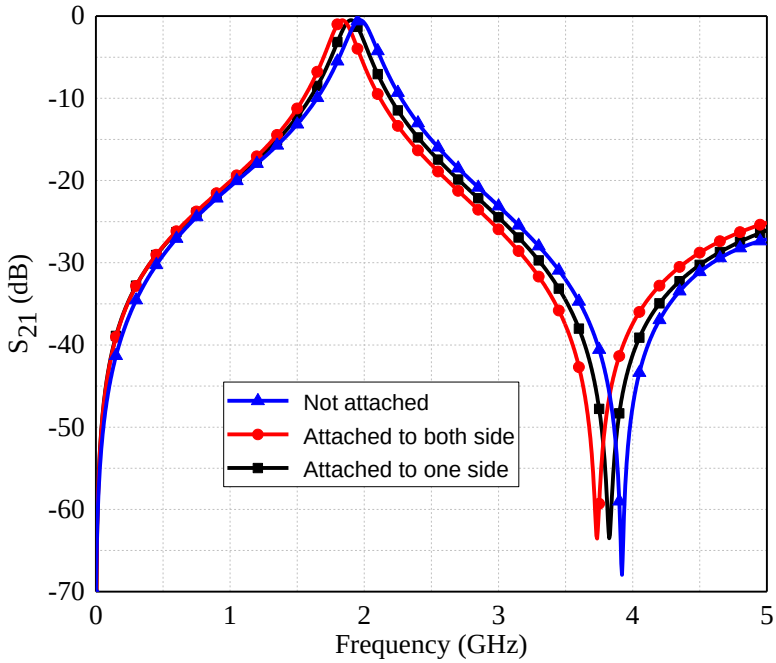

Fig. 4.11. Simulated frequency responses of the two-metallic-layer FSS (*n*=2) with or without surrounding dielectric materials attached to the FSS.

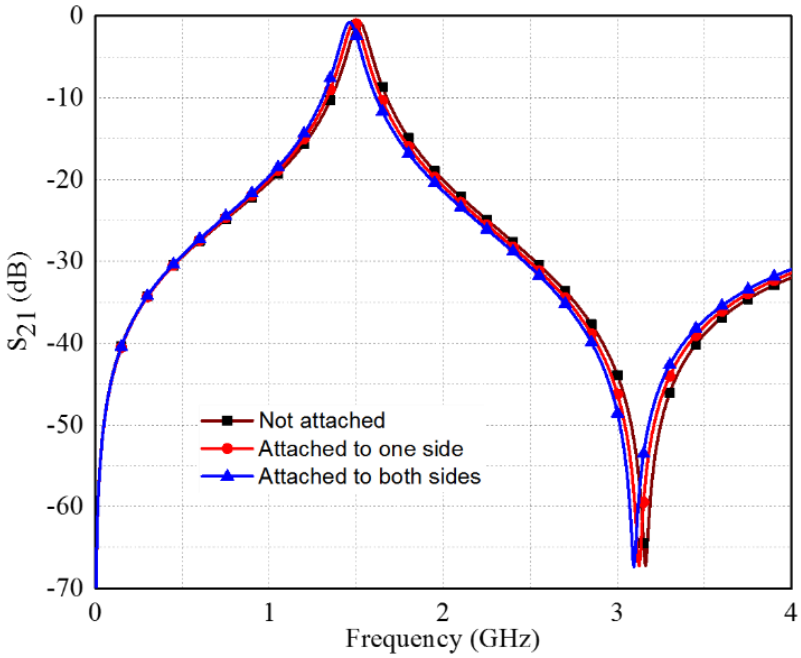

Fig. 4.12. Simulated frequency responses of the three-metallic-layer FSS (*n* = 3) with or without surrounding dielectric materials attached to the FSS.

cases: without any attaching dielectric material; with a dielectric material attached to one side; and with a dielectric material attached to both sides of the structure. The dielectric material is a 1.6 mm thick FR4. It can be seen that the resonant frequency is only shifted by 3.7% when the dielectric material is attached to one side, and

shifted by 6.7% when the dielectric material is attached to both sides. Fig. 4.12 shows the comparison of this structure in the case of n = 3. In this case, the resonant frequency is only shifted by 1.5% when the dielectric material is attached to one side, and shifted by 3.4% when the dielectric material is attached to both sides. It should be noted that the advantages of the proposed design were achieved mainly because the proposed structure on any layer is not symmetrical by itself along either the x-axis or the y-axis. The metallic layout in one layer is the flipped, or anti-parallel, version of the layout in the adjacent layer. This arrangement dramatically strengthens the cross-layer capacitance. The cross-layer capacitance makes the structure not only small, but also insensitive to surrounding dielectric materials. In contrast, in traditional FSSs, the structures in each layer are parallel to each other. The current and charge distributions on each side are the same. There is no strong capacitance between adjacent layers. To prove this, a patch-mesh FSS structure, as shown in Fig. 4.13(a), is used as an example to show the effect of surrounding dielectric materials on traditional FSSs.

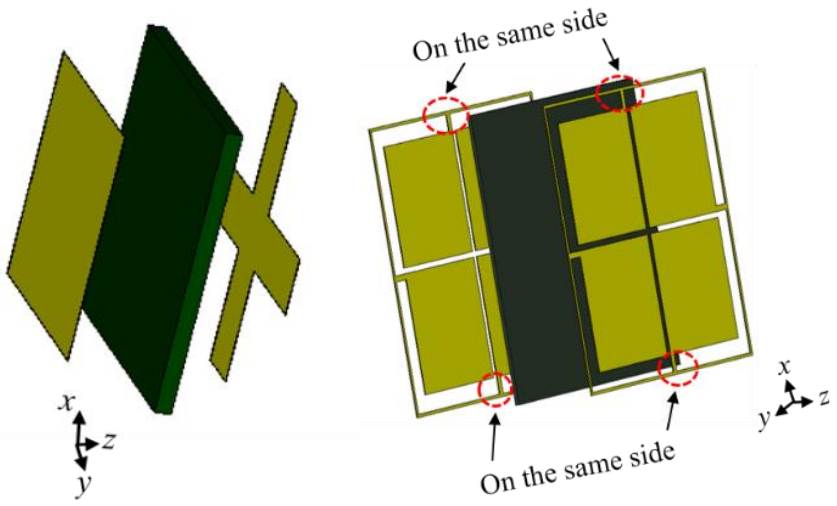

(a) **(b)**

Fig. 4.13. Traditional FSS structures as examples to demonstrate the effect of surrounding dielectric materials on the FSS's response, (a) patch-mesh structure, (b) proposed structure with identical metallic structures on adjacent layers but not flipped.

In Fig. 4.13(b), the proposed structure without flipping the shape of the bottom layer is used as another example to prove the advantage of the proposed design. To make comparison more logical, the dimensions are tuned to achieve similar resonant frequencies to the proposed structure. The substrate between metallic layers in these

examples is an FR4 with a thickness of 0.127 mm.

First of all, the array element dimensions of these two examples are much bigger than the proposed one. The periodic dimension of the patch-mesh structure is 0.22λ, and it is 0.13λ for the example in Fig. 4.13 (b). The periodic dimension of the proposed FSS element is only 0.012λ, as shown in Table 4.1. The dimension of the proposed FSS element is more than 18 times smaller than the traditional patch-mesh structure and the area is 330 times smaller.

Table 4.3 compares the performance of the proposed dualpolarised structure with the two traditional FSS structures shown in Fig. 4.13.

Table 4.3: The normalised resonant frequency deviation when the structures are attached to an FR4 dielectric substrate (ε_r=4.4) with different thicknesses. *t* is the thickness of surrounding dielectric materials. The results are obtained by simulation.

The structures	Attached to one side		Attached to both sides	
	Dev (t=1.6mm)	Dev (t=3mm)	Dev (t=1.6mm)	Dev (t=3mm)
The patch-mesh structure (Fig. 4.13(a))	0.21	0.26	0.26	0.33
The proposed structure without C_{cc} (Fig.4.13(b))	0.28	0.31	0.36	0.43
The proposed structure (n=2)	0.037	0.045	0.065	0.080
The proposed structure (n=3)	0.015	0.021	0.034	0.062
The proposed structure (n=4)	0.011	0.015	0.024	0.03

The normalised deviation (Dev) is defined as the difference between the resonant frequency of each structure before being attached to the dielectric material (f) and the resonant frequency after being attached to the dielectric (f_d) divided by f. That is, Dev = (f- f_d)/ f. It can be seen that the insensitivity of the proposed structure is about six

times better than traditional structures. The cases where they are attached to a higher dielectric constant material ($\varepsilon_r = 8$) is compared in Table 4.4.

Table 4.4: The normalised resonant frequency deviation obtained by simulation when the structures are attached to a higher dielectric constant material, $\varepsilon_r = 8$.

The structures	Attached to one side		Attached to both sides	
	Dev (t = 1.6mm)	Dev (t = 3mm)	Dev (t = 1.6mm)	Dev (t = 3mm)
The patch-mesh structure (Fig. 4.13(a))	0.27	0.33	0.36	0.41
The proposed structure without C_{cc} (Fig. 4.13(b))	0.37	0.44	0.51	0.56
The proposed structure (n=2)	0.065	0.077	0.122	0.148
The proposed structure (n=3)	0.039	0.047	0.073	0.089
The proposed structure (n=4)	0.024	0.038	0.051	0.063

It should be noted that in [21] the circuit element was also miniaturised by a cross-layer capacitance. However, the structure is still relatively sensitive to surrounding materials compared to the proposed structure. It was found by simulation that the proposed structure is two to three times less sensitive than the one in [21]. The main reason is that the proposed structure has a much lower intrinsic capacitance and a stronger cross-layer capacitance due to the charge distribution as analysed in Fig. 4.2.

It is clearly shown that the proposed structure exhibits a very stable performance compared to traditional FSSs. Increasing the number of metallic layers contributes to making the resonant frequency of the proposed structure even more stable, as shown in these tables. The resonant frequency of a four-layer structure is about 2.5 times more stable than a two-layer one. This is mainly due to the occurance that much stronger cross-layer capacitance will be induced in multi-layer ($n > 2$) structures, while the intrinsic capacitance is affected in the same way as the two-layer structure.

4.3.2 Experimental results

A prototype of the proposed FSS as shown in Fig. 4.8 has been fabricated and

measured to validate the design. The fabricated FSS is shown in Fig. 4.14. The size of the FSS prototype is 180 mm × 180 mm and it consists of 30 × 30 elements.

Two horn antennas and a vector network analyser were used for the measurement. The measurement setup is shown in Fig. 4.15. The line of sight between the two antennas passes through the centre of the FSS prototype and the antennas are located about 70 cm away from the fixture to ensure the formation of uniform plane wave impinging upon the FSS structure. When carrying out the measurement at 60˚, the absorbers at the side were adjusted so as not to block the incident wave. Measurement of the fabricated FSS is performed in two steps. Firstly, the transmission response of the system without the FSS is measured. This measurement result is used to calibrate the FSS response. Secondly, the frequency response with the presence of the FSS structure is measured. In the example of the FSS with two metallic layers (n = 2), the fabrication is performed by patterning the proposed shape on two sides of a 0.127 mm thick FR4 substrate. The measured performances with incident angles of 0^{o} and 60^{o} for this prototype are shown in Fig. 4.16.

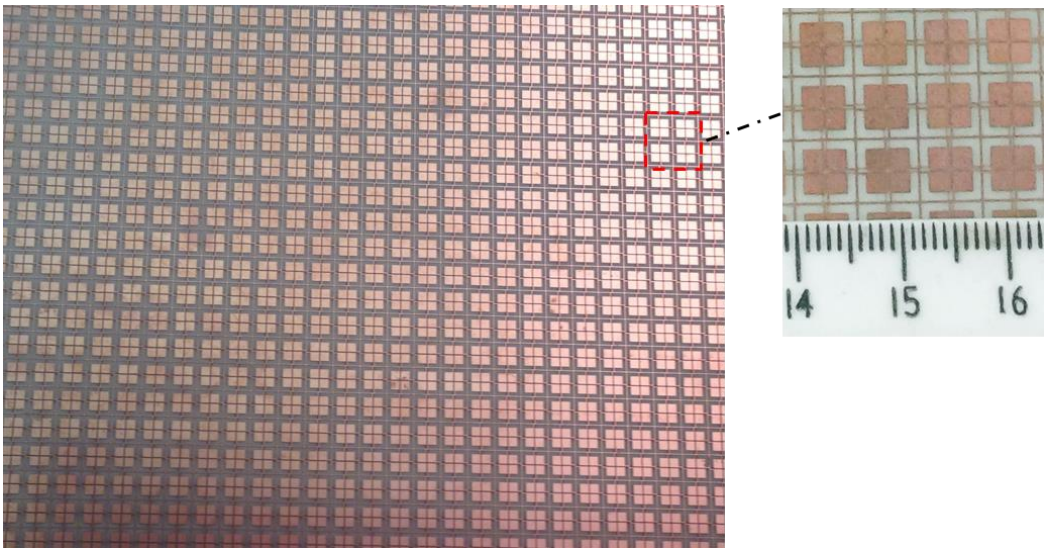

Fig. 4.14. Photograph of the prototype of the proposed FSS with n = 2.

The measured insertion loss is 0.73 dB at the resonant frequency for normal incidence, which is mainly attributed to the dielectric and the metallic losses of the structure. The measured performance is compared with the simulated one. It can be seen that very good agreement has been achieved. The transmission with other incident angles up to 75^{o} was also measured. The measured performance is also in a very good agreement with the simulated one. Such results are not shown in this figure to avoid having too many curves in the figure.

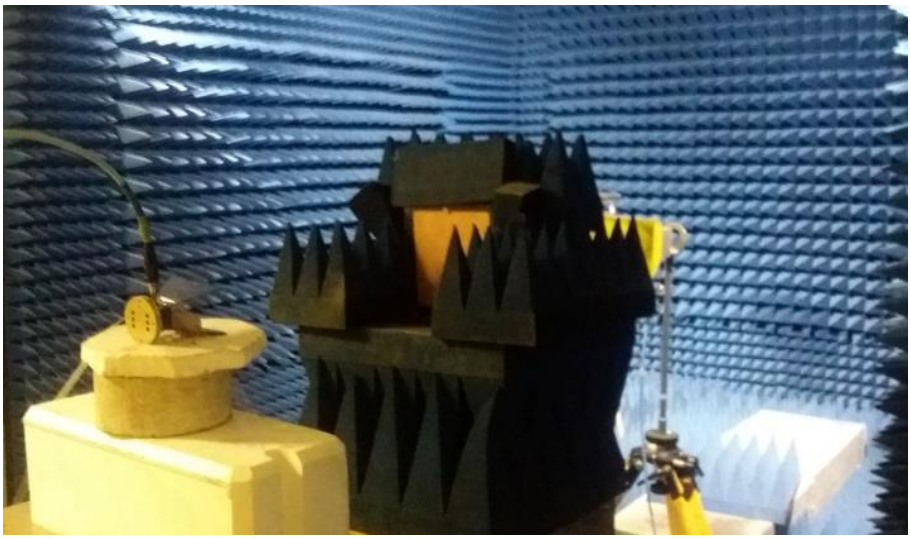

Fig. 4.15. Measurement setup to measure the transmission coefficient of the FSS.

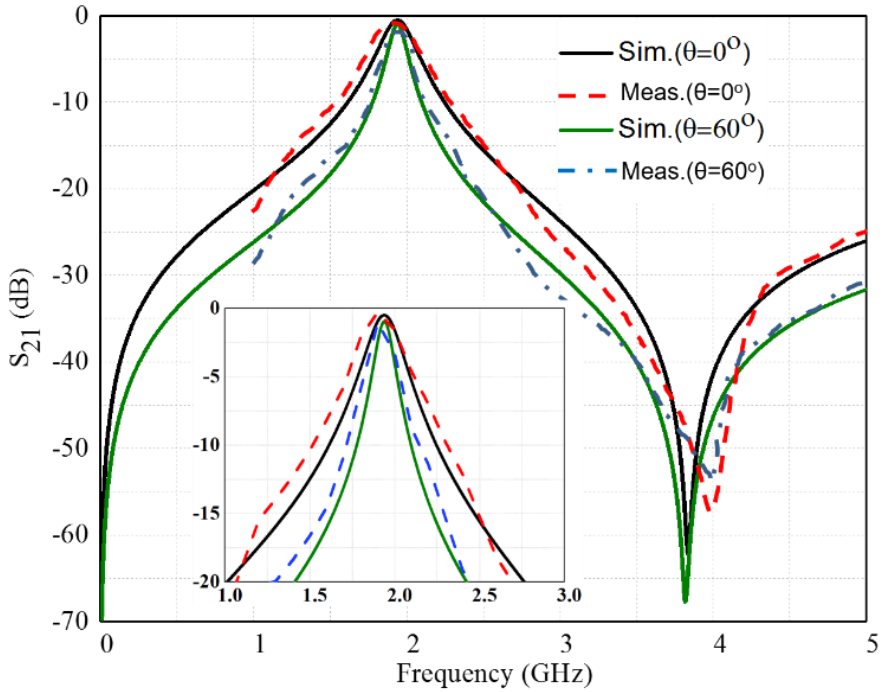

Fig. 4.16. Measured and simulated frequency responses of the two-metallic-layer (*n* = 2) FSS under different incident angles.

To measure reflection, the two horn antennas are used as the transmitter and receiver, respectively, at the same side of the FSS. They are separated by an absorber screen to eliminate the direct coupling between them. The measured reflection of the prototype of the proposed FSS is shown in Fig. 4.17. The measured result is in a relatively good agreement with the simulated performance.

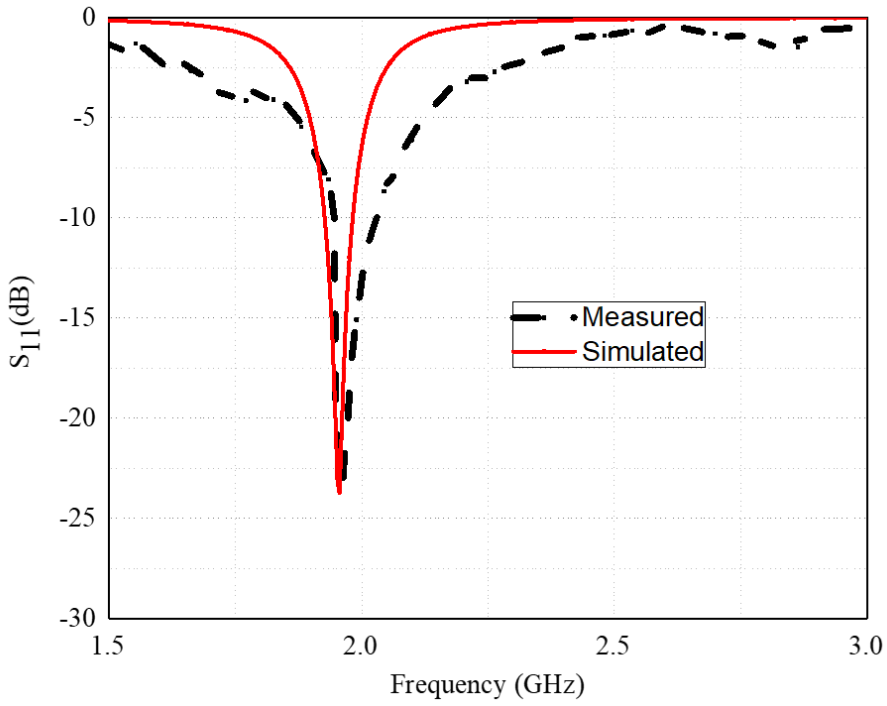

Fig. 4.17. Measured and simulated reflection coefficients of the two-metallic-layer (n = 2) FSS.

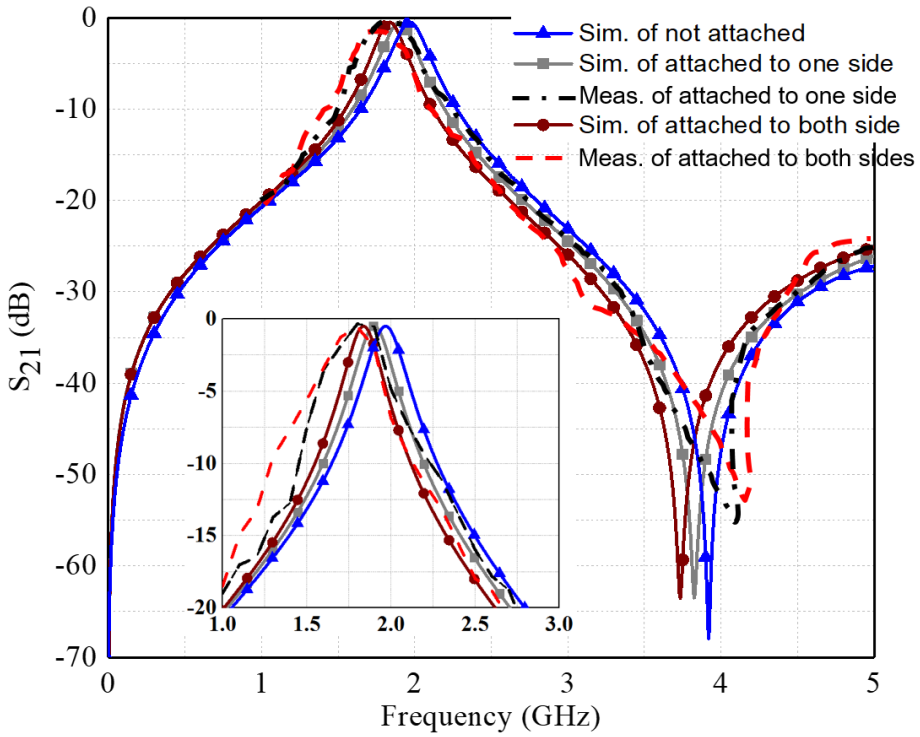

Fig. 4.18. Measured and simulated frequency responses of the two metallic layers FSS (n = 2) with or without surrounding dielectric materials.

A 1.6 mm thick FR4 dielectric material is attached to the prototype of the structure with n = 2. The dielectric material is firstly attached to one side of the

structure and then attached to both sides. The transmission coefficients were measured and shown in Fig. 4.18, to prove the stability of the proposed structure when it is attached directly to dielectric materials. It can be seen that the resonant frequency is shifted 4.0% when the dielectric material is attached to one side, and 6.9% when attached to both sides. The measured results are in good agreement with the simulated ones as summarised in Table 4.3.

4.4 Conclusion

An unconventional approach has been proposed to design miniaturised multi-layer FSS structures in this chapter. The proposed bandpass FSS exhibits a very stable frequency response when it is attached to dielectric materials of arbitrary thicknesses, about six times better than conventional FSS structures.

The overall thicknesses of the multi-layer FSSs presented are extremely small. As an example, the thickness of the FSS structure consisting of three metallic layers and two dielectric layers is less than 0.5 mm. Unlike traditional structures, the size of the proposed FSS element is smaller when the profile is lower.

The dimensions of the miniaturised element are much smaller than the wavelength at the resonant frequency, as small as $0.012\lambda \times 0.012\lambda$ which is one of the smallest reported so far. For a two-metallic-layer structure, the size of the proposed dual polarised FSS element is 330 times smaller than the traditional patch-mesh structure.

The proposed approach to design miniaturised FSSs was experimentally verified by a prototype. The simulation and measurement results verify the stable frequency response of the proposed design. These advantages of the proposed structure can be useful for many applications where circuit compactness, having a low profile and insensitivity to surrounding materials are desired.

4.5 Reference

[1] F. C. Huang, C. N. Chiu, T. L. Wu, and Y. P. Chiou, “A circular-ring miniaturized-element metasurface with many good features for frequency selective shielding applications,” *IEEE Transactions on Electromagnetic Compatibility,* vol. 57, no. 3, pp. 365-374, 2015.

[2] S. N. Azemi, K. Ghorbani, and W. S. T. Rowe, "Angularly stable frequency selective surface with miniaturized unit cell," *IEEE Microwave and Wireless Components Letters,* vol. 25, no. 7, pp. 454-456, 2015.

[3] G. H. Yang, T. Zhang, W. L. Li, and Q. Wu, "A novel stable miniaturized frequency selective surface," *IEEE Antennas and Wireless Propagation Letters,* vol. 9, pp. 1018-1021, 2010.

[4] C. N. Chiu, and K. P. Chang, "A novel miniaturized-element frequency selective surface having a stable resonance," *IEEE Antennas and Wireless Propagation Letters,* vol. 8, pp. 1175-1177, 2009.

[5] K. Sarabandi, and N. Behdad, "A frequency selective surface with miniaturized elements," *IEEE Transactions on Antennas and Propagation,* vol. 55, no. 5, pp. 1239-1245, 2007.

[6] H. Liu, K. L. Ford, and R. J. Langley, "Miniaturised bandpass frequency selective surface with lumped components," *Electronics Letters,* vol. 44, no. 18, pp. 1054-U12, 2008.

[7] S. Sheikh, "Miniaturized-element frequency-selective surfaces based on the transparent element to a specific polarization," *IEEE Antenna and Wireless Propgation Letters*, vol. 15, pp. 1661-1664, 2016.

[8] D. M. Dobkin, and S. M. Weigand, "Environmental effects on RFID tag antennas," *2005 IEEE MTT-S International Microwave Symposium,* vol. 1-4, pp. 135-138, 2005.

[9] S. Shao, R. J. Burkholder, and J. L. Volakis, "Design approach for robust UHF RFID Tag antennas mounted on a plurality of dielectric surfaces," *IEEE Antennas and Propagation Magazine,* vol. 56, no. 5, pp. 158-166, 2014.

[10] N. Marcuvitz, *Waveguide handbook*: IET, 1951.

[11] M. Al-Joumayly, and N. Behdad, "A new technique for design of low-profile, second-order, bandpass frequency selective surfaces," *IEEE Transactions on antennas and propagation,* vol. 57, no. 2, pp. 452-459, 2009.

Chapter 5: Multi-Band FSS

5.1 Introduction

The use of FSSs has contributed to improvement of the communication capabilities of satellite platforms [1-4]. The use of dual-reflector antennas in space missions such as Galileo, Cassini and Voyager, sharing the main reflector among different frequency bands has been made possible by using an FSS [8-11]. A dual passband FSS for WLAN applications at the frequencies of 2.4 and 5.2 GHz by using the complementary structure has been proposed in [12], and to shield the GSM 1800 MHz band [13]. Several types of design have been proposed to design dual band filters. Gosper prefractals based on a hexagonal geometry display a dual bandstop frequency response [14]. A dual band FSS is built by cascading a metal loop shaped layer and its complementary structure in [15]. Cascading two layers of conducting patches with slots to design dual bandstop FSS is used in [16]. Left-handed structures and capacitive grids are used to design dual band FSSs in [17].

FSSs have been used as frequency diplexers in satellite reflector antenna systems with feeds placed on either side of an FSS [4-6]. Multichannel space-borne sounders were employed for spectroscopic characterisation of the Earth's atmosphere [7]. These devices carry out molecular emission spectroscopy at millimeter and sub millimeter-waves in narrow frequency channels. To meet the satellite restrictive payload on cost, mass and energy consumption, passive remote sensing radiometers traditionally employ a single mechanically scanned reflector antenna to collect radiation over a wide frequency range. FSSs can play an essential role as an enabling technology for these advanced instruments. They can be used in quasi-optical receivers to spectrally separate the signals that are collected by the scanning antenna [7].

The FSS can exhibit very low insertion loss and simultaneously meet the inconsistent requirements for high isolation between adjacent frequency channels. This should be accompanied by minimising the overall noise performance of the instrument and then achieve high receiver sensitivity which is necessary to detect weak molecular emissions at millimeters waves.

Recently, satellite systems tend to operate in the Circular Polarisations (CP) mode, which is advantageous in communication and sensing systems as it can provide resilience to effects such as Faraday rotation [8]. It can also remove the requirement for alignment in polarisation between the transmitter and receiver. The design of polarization independent FSSs has attracted a lot of interest. These surfaces have near identical transmission and reflection coefficient magnitudes for TE and TM polarised waves. Several FSS geometries with such properties have been presented for millimeter- and sub-millimeter waves including crossed dipoles [9], Jerusalem crosses [10], rings [2], two layers of the semi-circle surfaces [11], double square loop arrays and gridded double square loop arrays [12]

The objective of this Chapter is to use novel methodology to design dual band spatial filters by using FSS periodic arrays composed of a bandpass and a bandstop element. The fabrication of the dual band filters is significantly simplified by using a single metal layer on a dielectric substrate.

In Section 5.2, a novel technique is proposed to design a dual-band bandstop FSS by combining a bandpass structure with its complementary structure in series. It displays flexibility to control the stopband frequencies, which is the most attractive feature of this design. The proposed FSS filter is also very easy to fabricate, consisting of a single metal layer on a dielectric layer. A theoretical equivalent circuit model is proposed to characterise the structure. In section 5.3, a new method to implement FSS with sharp band edge transitions suitable for millimeter wave applications is introduced. A high selectivity bandpass FSS can be realised by combining two bandstop FSS structures on the same plane. By choosing appropriate dimensions of the structures, the passband and stopbands of the FSS can be controlled to obtain desired characteristics. With this method, multiple passbands and stopbands of an FSS can be achieved simultaneously. A prototype FSS is designed at the Ka band. The FSS is fabricated and tested in free space to verify the proposed design. The structure is polarisation independent and exhibit low insertion loss at around 40 GHz.

5.2 Dual-band bandstop FSS

Arrays of rings are of interest as FSSs for dichroic reflector antennas [13]. The

equivalent circuit of the ring is an inductor L_s in series with the mutual capacitance with adjacent cells C_m. It works as a bandstop filter as shown in Fig. 5.1a [13]. The

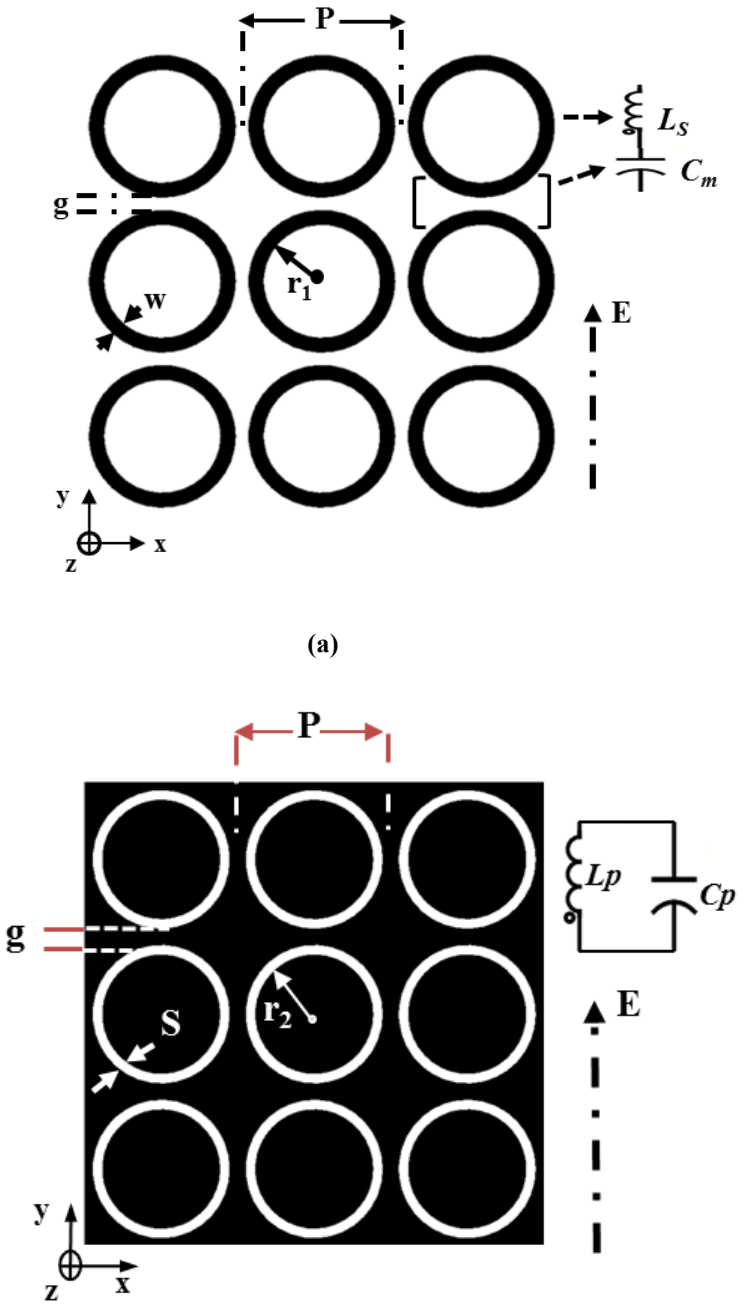

Fig. 5.1. Grid and equivalent circuit of the element (E is the electric field), (a) Ring shape (bandstop filter), (b) Complementary structure (bandpass filter).

first step to design a desired dual bandstop FSS using the proposed architecture is to design the constituting resonator. The ring is designed on a 1.5 mm thick FR4 substrate with a dielectric constant of 4.3. The radius of the ring r_1, as shown in Fig.

5.1(a), is 10 mm, the width of the circumference of the ring w is 0.5 mm; the periodic constant *P* is 22 mm. At the same band approximately, the complementary of the ring structure works as a bandpass. The equivalent circuit of the complementary of the ring is an inductor *Lp* in parallel with a capacitor *Cp* as shown in Fig. 5.1(b), where S is the aperture and r_2 is the radius of the circular patch. The structure of the proposed filter is built up by using half of the ring and half of the slot, the complementary of the ring, as shown in Fig 5.2(a). The equivalent circuit of the proposed filter is based on series connecting of a parallel *LC* with a series *LC* as shown in Fig. 5.2(b).

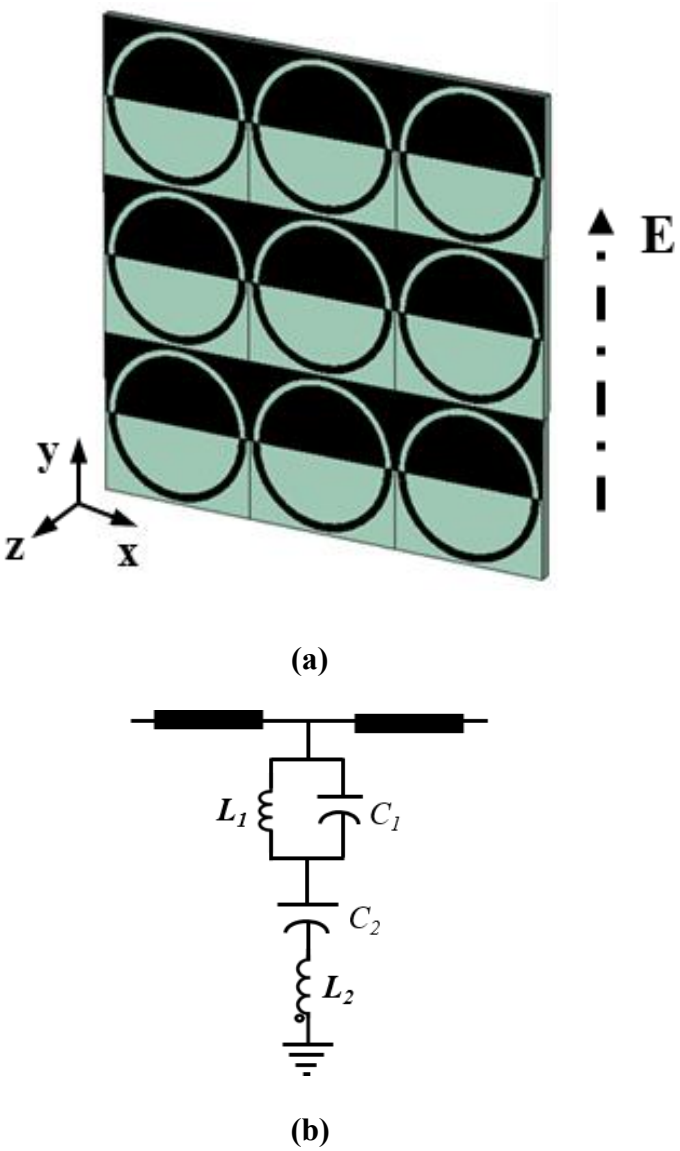

Fig. 5.2. (a) The proposed structure of the dual bandstop filter (b) Equivalent circuit model of the proposed dual bandstop filter.

As shown in Fig. 5.2, L_1 and C_1 are the equivalent circuit components of half of the slot. L_2 and C_2 are the equivalent circuit components of half of the ring.

It is found in the simulation that the resonant frequency of the ring is 3.15 GHz; the resonant frequency of half of the ring is 3.28 GHz as shown in Fig. 5.3; while the resonant frequencies of the slot and half of the slot are 3 GHz and 2.96 GHz, respectively, as shown in Fig. 5.3.

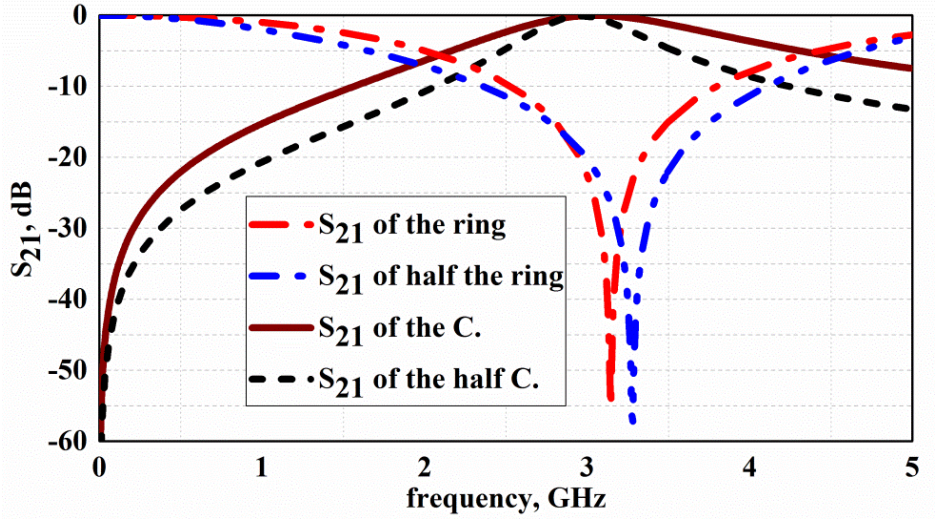

Fig. 5.3. Transmission coefficient (S21) of the whole and half structure of the bandstop resonator (ring shaped) and the bandpass filter resonator (C. is complementary).

The impedance of the parallel connection of LC at frequency f ($\omega=2\pi f$) is:

$$Z_{pass} = \frac{j\omega L_1}{1-\omega^2 L_1 C_1} \tag{5.1}$$

It is infinite (open-circuit condition) when $\omega=\omega_0=1/\sqrt{L_1C_1}$

The impedance of the series connection of LC is:

$$Z_{stop} = -j\frac{1-\omega^2 L_2 C_2}{\omega C_2} \tag{5.2}$$

The impedance of the dual-band bandstop FSS resonator is:

$$Z_T = Z_{pass} + Z_{stop} = \frac{j\omega L_1}{1-\omega^2 L_1 C_1} - j\frac{1-\omega^2 L_2 C_2}{\omega C_2} \tag{5.3}$$

The first stopband frequency f_1, and second stopband frequency f_2 of the proposed dual-band bandstop can be computed from solving (5.3):

$$f_{1,2}^2 = \left| \frac{(L_1C_1 + L_1C_2 + L_2C_2) \pm \sqrt{(L_1C_1 + L_1C_2 + L_2C_2)^2 + 4L_1C_1L_2C_2}}{8\pi^2 L_1C_1L_2C_2} \right| \tag{5.4}$$

At around f_0 (the resonant frequency of the bandpass structure), the magnitude of the impedance of the parallel LC is infinity or open circuit, so all energy is transmitted, where f_o can be calculated from (5.5).

$$f_o = \frac{1}{2\pi\sqrt{L_1 C_1}} \tag{5.5}$$

In this design, the resonant frequencies of the parallel LC circuit and the series LC circuit are very close to each other. At $f < f_0$, the impedance of parallel LC circuit in (5.1) is inductive. This effective inductance, being in series connection with the series LC circuit, will lower the resonant frequency of the series circuit. It can be calculated from (5.4) that the impedance of the equivalent circuit is zero at the lower stopband frequency f_1 ($< f_0$). f_1 is found to be 2.36 GHz by simulation. Similarly, at $f > f_0$, the impedance of parallel LC circuit in (5.1) is capacitive. This effective capacitance will increase the resonant frequency of the series LC circuit. It can be calculated from (5.4) that the impedance of the equivalent circuit is zero at the upper stopband frequency f_2 ($> f_0$). f_2 is found to be 3.36 GHz by simulation. The structure exhibits flexibility to control the stopband as well as the passband frequencies by changing the dimensions of either the rings or the slots or both. In Table 5.1, three cases are given to demonstrate how to control the frequency response of the dual-band bandstop filter as illustrated in Fig. 5.4. Case A can be regarded as a reference to other cases. The stopband frequencies f_1 and f_2 can be changed without changing the bandpass frequency f_0 by changing the ring dimensions (r_1 and w), as shown in case **B**. The changes in f_1 and f_2 are because of the changes in the values of the L_2 C_2, as can be observed from (5.4), which will change with r_1 and w (ring dimensions). f_o does not change as long as the (L_1 C_1) have fixed values, as can be seen from (5.5). Changing the dimensions of the complementary structure (r_2, S) will shift the stopband frequencies f_1 and f_2 and the passband frequency f_0 as illustrated in case **C.** This is because the values of L_1 C_1 are changed, as can be observed form (5.4) and (5.5).

The maximum attenuations at f_1 and f_2 are more than 50 dB in all cases. The 10 dB attenuation bandwidth for f_1 is 28% and for f_2 is 24%. The resonant frequency of bandpass (f_o) is 2.87 GHz with 0.19 dB insertion loss.

Table 5.1: Dimensions of the proposed filter in three cases (Unit: mm)

(mm)	Ring parameters (mm)		C. ring parameters	
Case	r_1	W	r_2	S
A	9.5	1	9.5	1
B	9	1.5	9.5	1
C	9.5	1.5	9	1

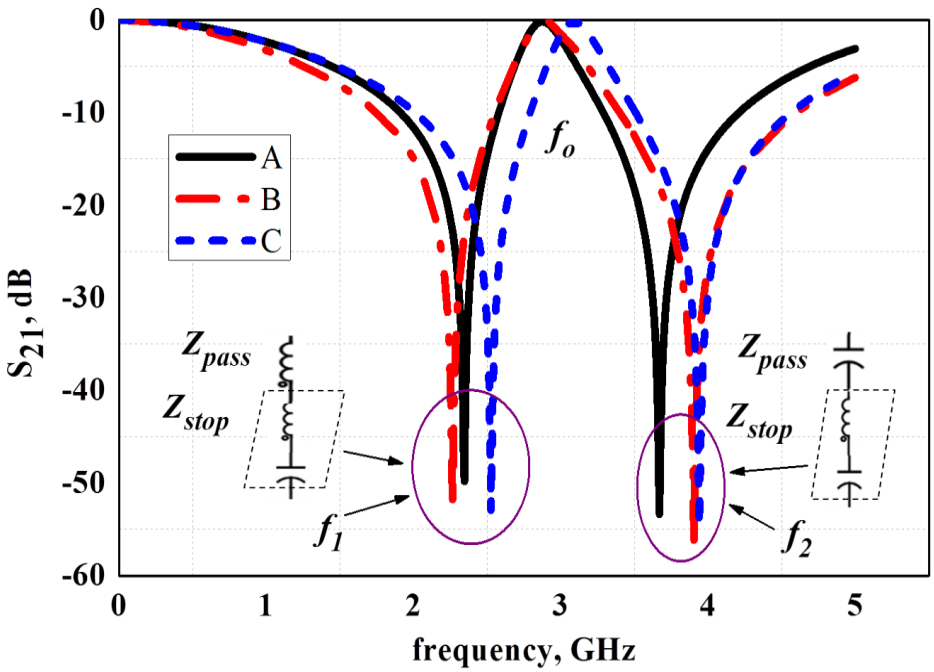

Fig. 5.4: Simulated transmission coefficients of the proposed dual-band bandstop filter in three cases.

The unit cell size of the proposed FSS is $0.17\lambda \times 0.17\lambda$, where λ is the wavelength at the passband frequency. The transmission coefficients of the dual-band bandstop FSS with case **A** parameters were tested under various angle of incidence. It is observed in simulation that the resonant frequencies of the filter are not strongly sensitive to the angle of incidence (θ). This is especially valid for $-45 \leq \theta \leq 45$.

5.2.1 Experimental results

A prototype of the proposed case **A** FSS has been fabricated and measured to validate the design. The size of the FSS prototype is 176×176 mm^2 and the whole structure consists of 8×8 elements. Two horn antennas and a vector network analyser

were used for the measurement. The transmission coefficient S_{21} was measured at various angles of incidence. The frequency response of the proposed structure exhibits a relatively stable frequency response for various angles of incidence. The measured frequency response of the proposed FSS shows a good agreement with the simulated result as shown in Fig. 5.5. The maximum attenuations at f_1 and f_2 are around 35 dB and 45 dB, respectively. The insertion loss at f_0 is 0.6 dB. The minor discrepancies between the simulated and measured results can be attributed to errors which occurred during the fabrication and measurement environment.

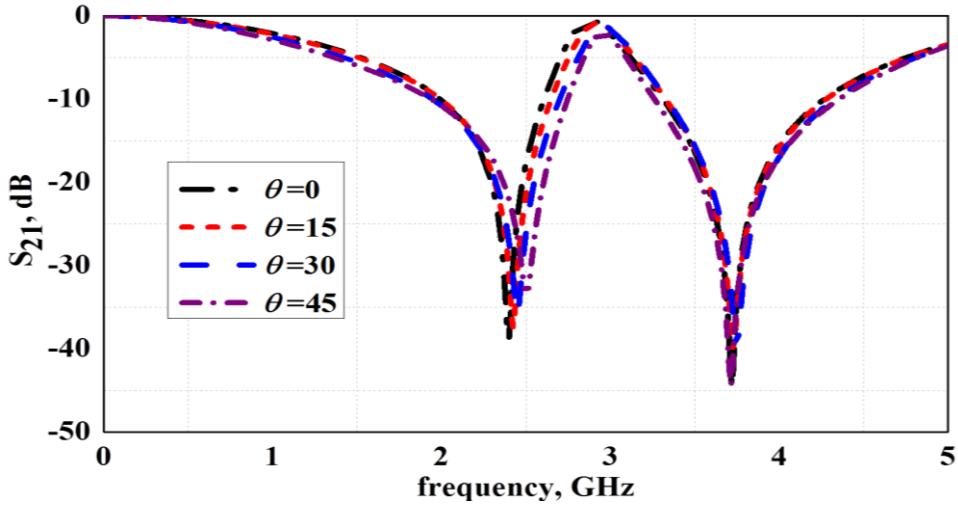

Fig. 5.5. Measured transmission coefficients of the proposed dual-band bandstop FSS with different angles of incidence (θ).

5.3 High selectivity FSS

An FSS is essentially a spatial filter [14]. Compared to a connectorised filter with fixed ports, an FSS has two distinctive features. One feature is that signals can be separated by both transmission and reflection as shown in Fig. 5.6. If connectorised filters were used, the signals would have to be split by a wideband divider and filtered individually. A three-way power divider has an intrinsic insertion loss of 3 dB, while the maximum measured insertion loss is 0.65 dB for an FSS in the transmission band of 320 GHz in [15]. The other distinctive feature is that two FSSs can co-exist on the same structure without significantly affecting each other. Therefore, a bandstop filter can be realised by combining two bandpass filters. A bandpass filter can be implemented by combing two bandstop filters, and so on.

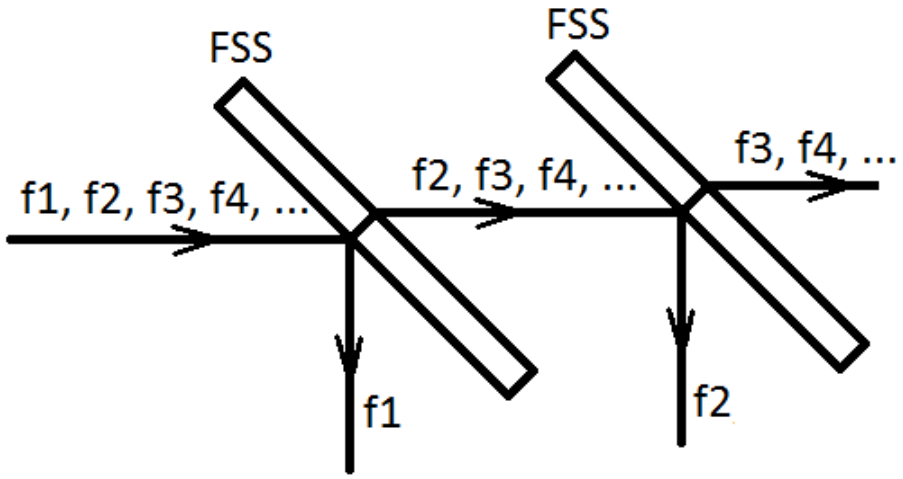

Fig. 5.6. An FSS is essentially a spatial filter. Signals can be separated by both transmission and reflection

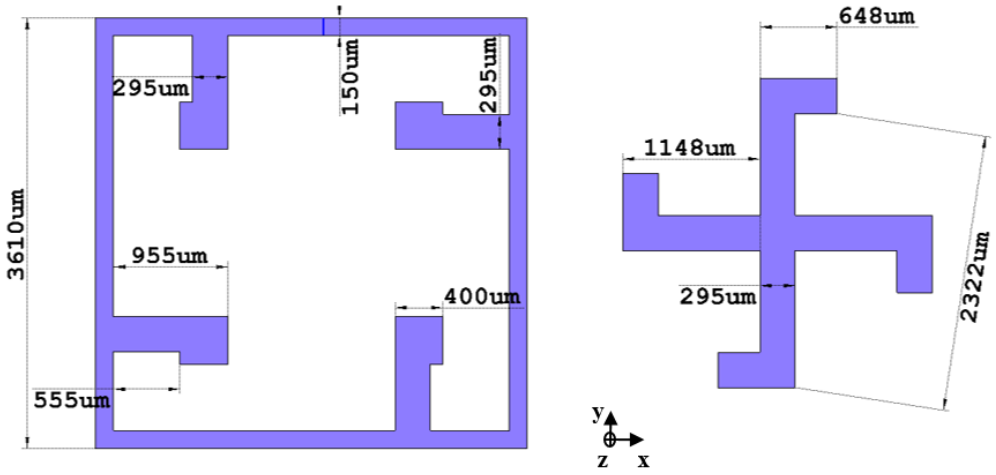

(a) **(b)**

Fig. 5.7. Top view and dimensions of the array element of the proposed FSS. The host structure is shown on the left-hand side and the secondary structure is shown on the right-hand side.

A bandpass FSS is realised by combining two bandstop ones. The proposed FSS can be designed with a simple three-step procedure described in this section. The first step in this approach is to obtain the appropriate bandstop structure based on the desired frequency response. The structure should be chosen with a shape to be appropriate to host of a secondary structure. Fig. 5.7(a) shows the host structure. More details on the design of this structure can be found in [16]. The second step is to design an appropriate secondary structure with suitable characteristics, such as the frequency response, the array element size and the shape. The four-leg structure shown in Fig. 5.7(b) is used as the secondary structure in this design. The final step is to combine the host and the secondary structure, as shown in Fig. 5.8, and tune the

performance.

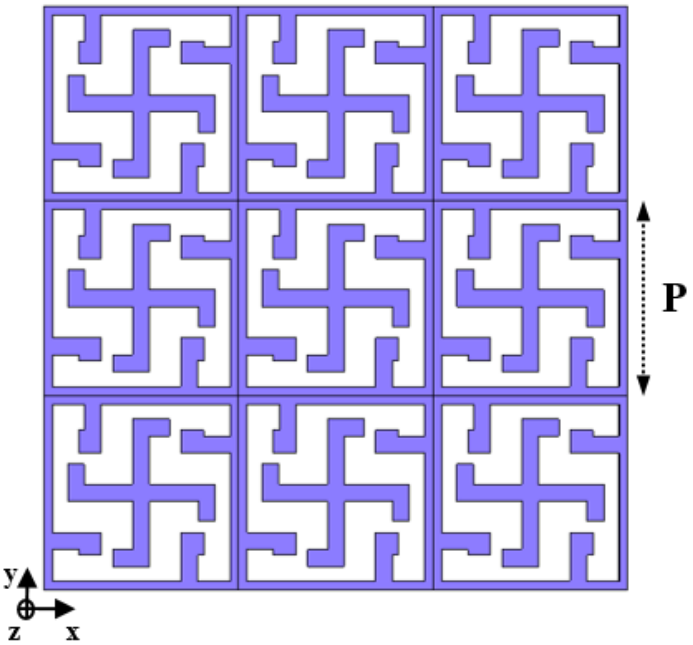

Fig. 5.8. 3×3 array elements of the proposed dual-stopband FSS.

For example, to obtain a narrow bandpass FSS with a centre frequency of 40 GHz and a fractional bandwidth of 5%, the dimensions of the structures shown in Fig. 5.7 can be used. The substrate is a 0.81 mm thick Rogers RO4003 with a dielectric constant of 3.38. The structures are simulated separately. The shape of the FSS transfer functions can be optimised using simple circuit based simulations. To verify the responses of these structures, the proposed structure was simulated with CST Microwave Studio, using unit cell boundary conditions to provide periodicity along the x and y axes. The structure is excited by an electromagnetic wave with the propagation vector (**K**) towards the z-axis direction, magnetic field vector (**H**) towards the x–axis direction and electric field vector (**E**) towards the y-axis direction as shown in Fig. 5.7.

Fig. 5.9 shows the simulated response of the host structure. The resonant frequency is at 43 GHz. The transmission coefficient of the four-leg secondary structure is shown in Fig. 5.10. The structure exhibits performance with a stopband at 35 GHz. Fig. 5.11 shows response of the combined structures. It can be observed that a dual-stopband performance is achieved. Put it in another way, a bandpass performance is achieved at 20 GHz and 40 GHz. The bandpass FSS has a very sharp selectivity due to the two stopbands introduced by the host and the secondary

structures, respectively.

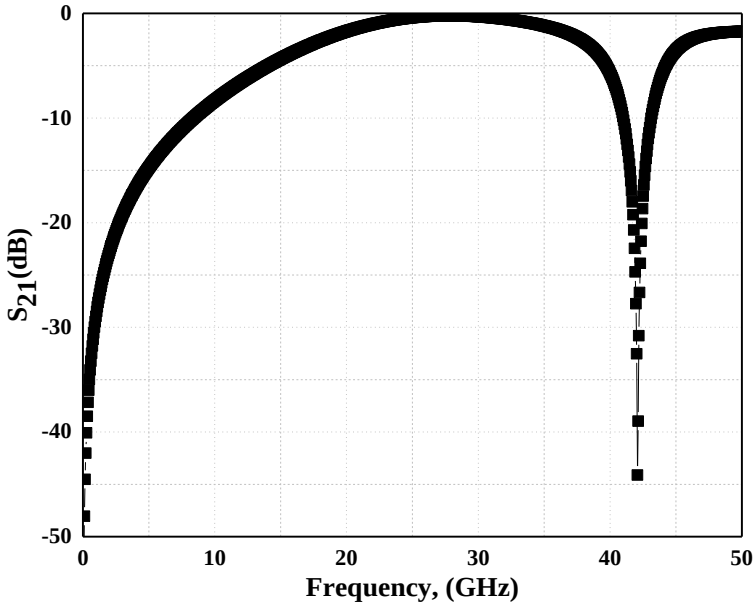

Fig. 5.9. Simulated transmission response of the host structure.

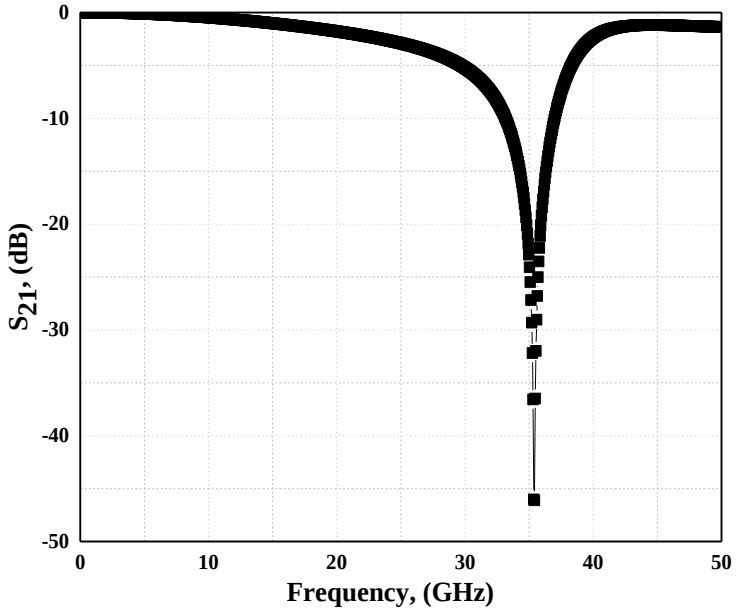

Fig. 5.10. Simulated transmission coefficients of the secondary structure.

In fact, both the lower and the higher stopband can be shifted downwards or upwards independently by changing of the geometric dimensions of structures. Also, as discussed in Fig. 5.6, both reflection and transmission of FSSs are useful for signal separation. The proposed is effectively a dual-bandpass filter as well if the reflected signals are received.

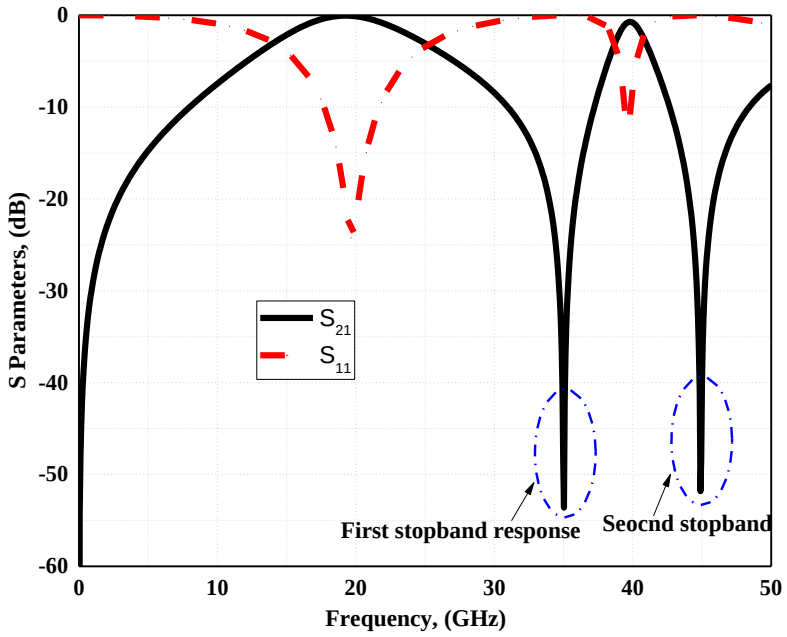

Fig. 5.11. Simulated transmission coefficients of the proposed FSS.

5.3.1 Experimental results

A prototype of the proposed structure has been fabricated and tested to validate the design. The fabricated FSS is shown in Fig. 5.12. The elements are enlarged and shown in the inset. The array element dimensions of the prototype are measured by using a microscope and is shown to be in good agreement with the simulated structure. The size of the FSS prototype is 102.6 mm × 102.6 mm. It consists of 30 × 30 elements. Two horn antennas and a vector network analyser were used for the measurement. To ensure the accuracy of the experiment, the transmission coefficient between the two horn antennas was measured without the FSS. The transmission coefficient was then measured again with the FSS prototype. Then the measured transmission with the FSS is normalised with respect to the measured data without the FSS. The FSS was measured between 26.5 GHz and 40 GHz due to the bandwidth of the antennas. The measured response after smoothing is shown in Fig. 5.13. As can be seen in Fig. 5.13, the response has two stopbands at 35 GHz and 45 GHz and a narrow bandpass at 40 GHz. The insertion loss at the passband is 0.7 dB. The FSS was also tested under various polarisation angles. The performance is almost independent from polarisation angles due to the symmetrical nature of the proposed element.

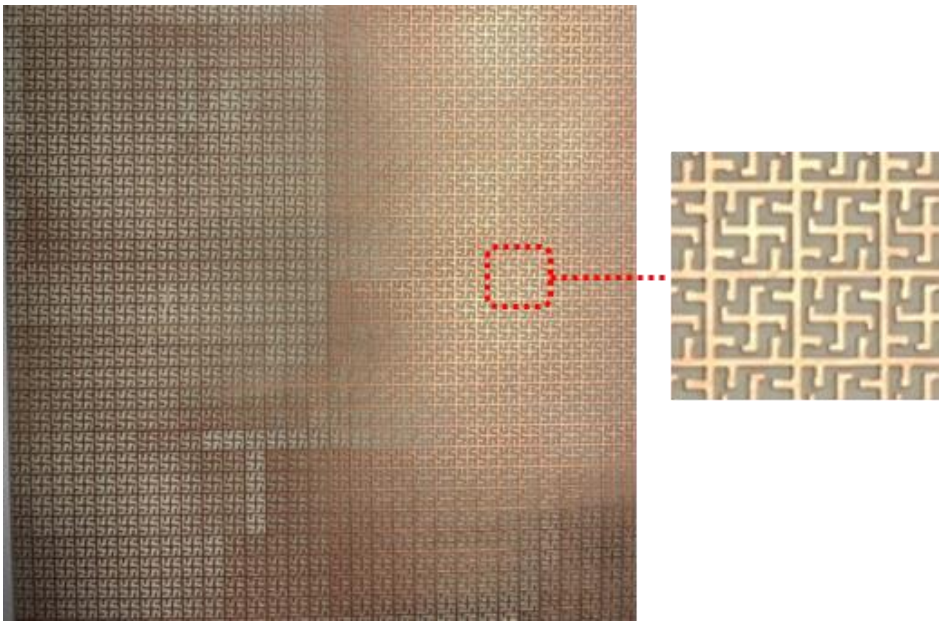

Fig. 5.12. A photograph of the fabricated FSS with the proposed miniaturised array elements.

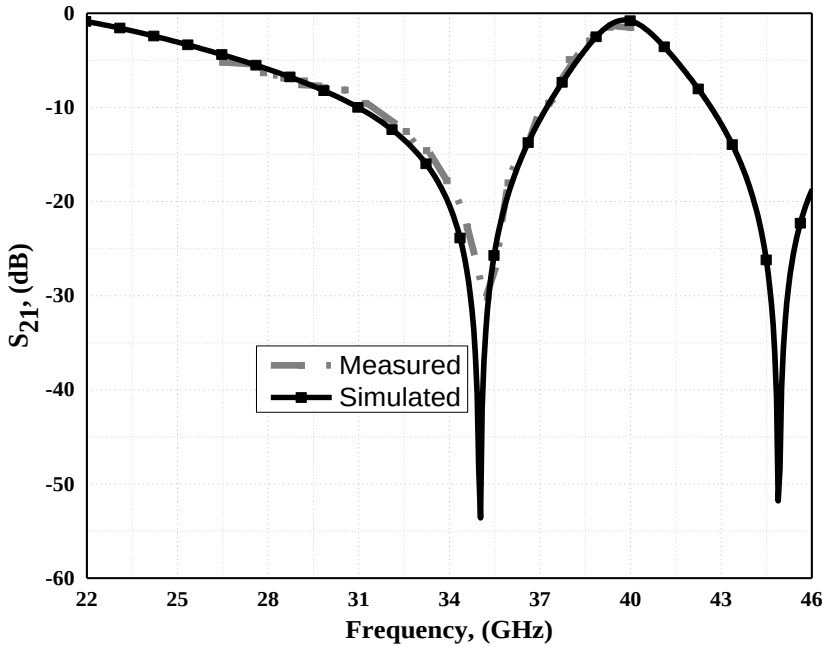

Fig. 5.13. The simulated and measured transmission coefficients of the proposed FSS structure.

5.4 Conclusion

A novel methodology to design dual-band bandstop FSS structure is proposed in this chapter. The proposed filter is relatively easy to fabricate due to its simple structure consisting of a single metal layer on a dielectric layer. It is shown that the

dual-band bandstop filter can be built up by combining the structure of half a ring and its complementary. The proposed structure is tested under different incident wave angles to verify that the response is insensitive to the incident angle. It is also shown that the proposed structure is very flexible in changing the stopband and passband frequencies.

In this chapter, a novel schematic is used to design FSS with desired characteristics. This FSS is built by using a simple configuration of single surface layers. The structure exhibits low insertion loss at the millimeter waves. The frequency response of this test sample was measured both for normal incidence and for oblique angles of incidence. The measurement result for the protype demonstrates a restively good agreement with simulation one. The discrepancy between the simulation and measurement results is attributed to the tolerances involved in the fabrication process and numerical errors in simulations. The proposed approach with these features is very attractive for a wide range of applications.

5.5 References

[1] T.-K. Wu, “Cassini frequency selective surface development,” *Journal of electromagnetic waves and applications,* vol. 8, no. 12, pp. 1547-1561, 1994.

[2] Y. Rahmat-Samii, and A. N. Tulintseff, “Diffraction analysis of frequency selective reflector antennas,” *IEEE Transactions on Antennas and Propagation,* vol. 41, no. 4, pp. 476-487, 1993.

[3] Y. Rahmat-Samii, and M. Gatti, “Far-field patterns of spaceborne antennas from plane-polar near-field measurements,” *IEEE Transactions on Antennas and Propagation,* vol. 33, no. 6, pp. 638-648, 1985.

[4] G. Schennum, “Frequency-selective surfaces for multiple-frequency antennas,” *Microwave Journal,* vol. 16, pp. 55-57, 1973.

[5] V. Agrawal, and W. Imbriale, “Design of a dichroic Cassegrain subreflector,” *IEEE Transactions on Antennas and Propagation,* vol. 27, no. 4, pp. 466-473, 1979.

[6] C.-C. Hunag, and N.-W. Chen, "Frequency selective surface for reflector antenna with multiple feeds." *Antennas and Propagation Society*

International Symposium (APSURSI) pp. 1-2, 2012.

[7] R. Martin, and D. Martin, “Quasi-optical antennas for radiometric remote-sensing,” *Electronics & Communication Engineering Journal,* vol. 8, no. 1, pp. 37-48, 1996.

[8] F. E. Nathanson, J. P. Reilly, and M. N. Cohen, “Radar design principles-Signal processing and the Environment,” *NASA STI/Recon Technical Report A,* vol. 91, 1991.

[9] E. A. Parker, A. D. Chuprin, J. C. Batchelor, and S. Savia, “GA optimisation of crossed dipole FSS array geometry,” *Electronics Letters,* vol. 37, no. 16, pp. 996-997, 2001.

[10] A. Kesavan, R. Karimian, and T. A. Denidni, “A novel wideband frequency selective surface for millimeter-wave applications,” *IEEE Antennas and Wireless Propagation Letters,* vol. 15, pp. 1711-1714, 2016.

[11] J.-Q. Hou, L.-F. Shi, S. Chen, and Z.-R. Gou, “Compact broadband circular polariser based on two-layer frequency-selective surfaces,” *Electronics Letters,* vol. 51, no. 15, pp. 1134-1136, 2015.

[12] C. Lee, R. J. Langley, and E. A. Parker, "Technical memorandum. Single-layer multiband frequency-selective surfaces." *IEE Proceedings H-Microwaves, Antennas and Propagation* pp. 411-412, 1985.

[13] R. J. Langley, and E. A. Parker, “Equivalent circuit model for arrays of square loops,” *Electronics Letters,* vol. 18, no. 7, pp. 294-296, 1982.

[14] B. A. Munk, "Frequency selective surfaces theory and design," NewYourk: Wiley-Interscience, 2000.

[15] R. Dickie, R. Cahill, V. Fusco, H. Gamble, P. Huggard, M. Henry, M. Oldfield, P. Howard, Y. Munro, and P. De Maagt, “Micromachined sub-mm wave frequency selective surface for polarimetric space science instruments,” 31st ESA Workshop on Antennas for Millimetre Wave Technology and Applications, Netherlands.2009.

[16] M. Hussein, J. Zhou, Y. Huang, A. Sohrab, and M. Kod, "Frequency selective surface with simple configuration stepped-impedance elements." *Antennas and Propagation (EuCAP),* pp. 1-4, 2016.

Chapter 6: High Order FSS

6.1 Introduction

FSSs with bandpass responses have gained more and more attention. Many design methods and structures are adopted to achieve bandpass characteristics. They can be designed by using slot elements since they are transparent at the resonant frequency and opaque below and somewhat above the resonance, Chapter 1, Section 1.1 [1]. They can also be built by multiple layers in parallel, separated by dielectric slabs. The thickness of the dielectric slabs should be around a quarter of the wavelength to obtain a fast roll-off and flat in-band frequency response. Recently, a number of high order FSSs have been developed to achieve flat response and fast roll-off [2-8]. These structures have thick substrate and relatively large element dimensions, as discussed in Chapter 2.

This chapter illustrates high order bandpass FSSs ($N \geq 2$) with low profiles and miniaturised dimensions. It is achieved by using two different techniques as described in Section 6.2 and 6.3 respectively.

6.2 Miniaturised second order FSS

High order bandpass FSSs ($N \geq 1$) can achieve high performance with a flat in-band frequency response and fast roll-off. One particular practical issue of designing bandpass FSSs using resonant surfaces is that the thickness of the substrate would be around a quarter of the wavelength. On the other hand, the size of a non-resonant FSS array element is usually large.

A new miniaturised FSS capable of exhibiting a second order bandpass response is proposed in this section. Two miniaturised resonant surfaces coupled by a non-resonant inductive layer are used to build the proposed FSSs. An FSS operating at around 3.8 GHz is designed to verify the method. The element size is smaller than $0.076\lambda \times 0.076\lambda$ for the proposed structure. This is significantly smaller than the element size of second-order FSSs designed using conventional approaches. The overall thickness is less than $\lambda/24$. The method could be particularly useful for the design of FSSs at lower frequencies with longer wavelengths.

6.2.1 Circuit design

Fig. 6.1 shows the proposed structure with three surface layers. Two dielectric slabs are used to separate them. The first and third surface layers, as introduced in [9], are identical. They are formed by four stepped-impedance transmission lines connected to a square ring. The middle layer is built using grids to present inductance. Two dielectric slabs of FR4 with a thickness of 1.6 mm and a dielectric constant ε_r of 4.4 were used to separate the three metallic layers.

For normal incident waves, the equivalent circuit as shown in Fig. 6.2 can be used to explain the operation principles of the proposed structure. The dielectric slabs, separating the surfaces layers, can be represented by two short pieces of transmission lines h_1 and h_2. The characteristic impedance of the transmission lines is $Z_d = Z_o/\sqrt{\varepsilon_r}$, where Z_o is the free space impedance. In Fig. 6.2(a), C_1 and C_3 represent the mutual capacitance between adjacent elements in the first and third layers, respectively. C_2 and C_4 represent the capacitance between the patches of an element in the first and third layers, respectively. L_1 represents the inductance of strips on the first layer which are parallel to the E-field, and L_3 represents the inductance of strips on the third layer. L_2 represents the inductance of the inductive layer (the middle layer). The short transmission line sections, h_1 and h_2 in Fig. 6.2(a), can be replaced with their equivalent circuit model [10] which consists of a shunt capacitor and a series inductor. The revised equivalent circuit is shown in Fig. 6.2(b). The three inductors, L_{t1}, L_2 and L_{t2} in Fig. 6.2(b) can be transformed into the T-configuration as shown in Fig. 2(c) by using the well-known star-delta transformation [11]. It is assumed that each resonant circuit is coupled only with the circuit adjacent to it.

As can be observed, the circuit shown in Fig. 6.2(c) is composed of two resonators coupled to one another with a single inductor. This circuit presents a second-order coupled-resonator bandpass filter, as described in [11]. The resonant frequency can be calculated as [8].

$$f \approx \frac{1}{2\pi\sqrt{C_1(C_2+\varepsilon_r\varepsilon_o h/2)(2L_1+2L_2+2\mu_r\mu_o h)/(C_1+C_2)}} \tag{6.1}$$

where ε_r and μ_r are the relative permittivity and permeability of the substrate, respectively. It is obvious from (6.1) that L_1 the inductance of the resonant structure layer contributes significantly to the miniaturisation of the proposed structure. This inductance (L_1) is designed to be relatively big, much stronger than the inductance of

the inductive layer to lower the resonant frequency or miniaturise the element size.

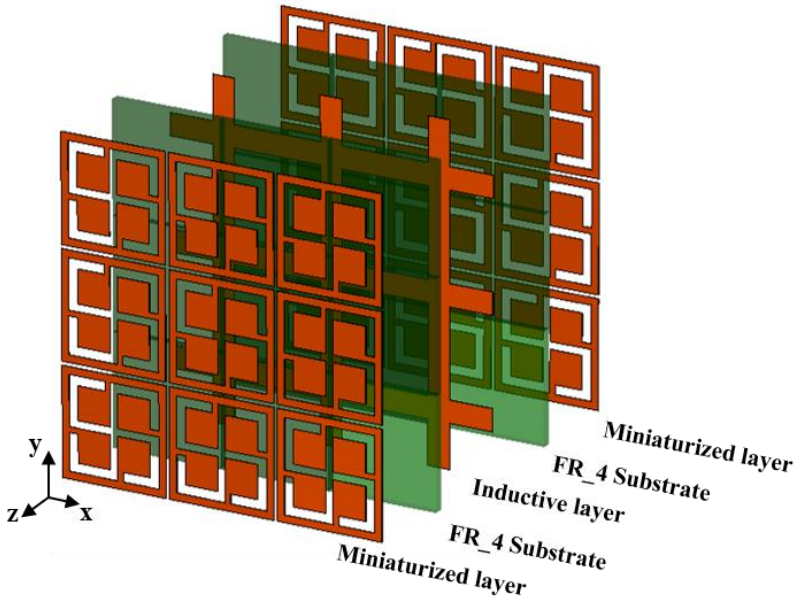

Fig. 6.1. Topology of the proposed second-order bandpass FSS.

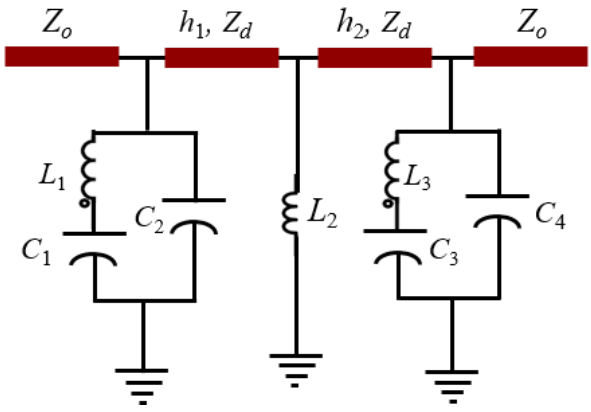

(a)

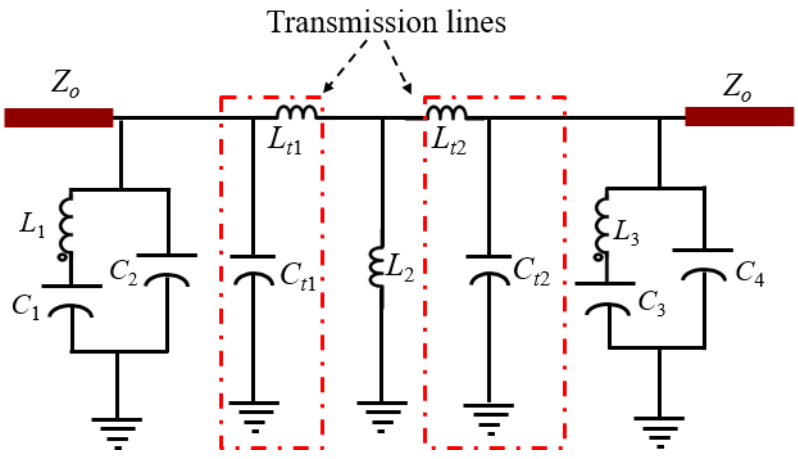

(b)

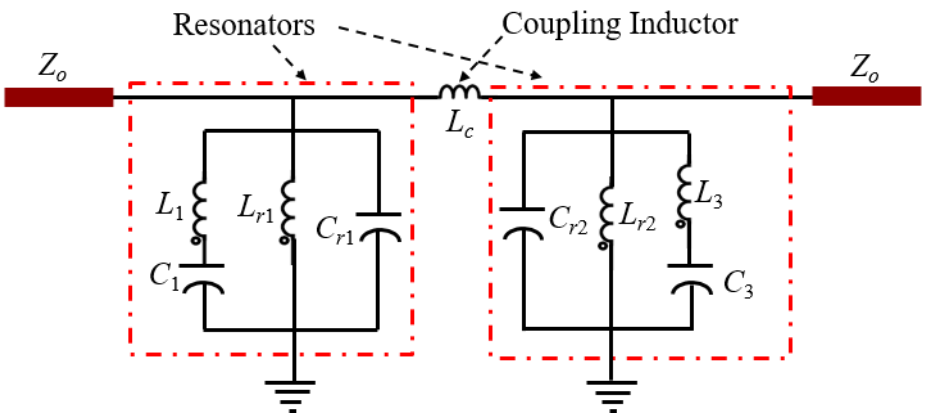

(c)

Fig. 6.2. Equivalent circuit model of the proposed second-order bandpass FSS. (a) With transmission lines. (b) Using shunt capacitors and series inductors instead of transmission lines. (c) After star-delta transformation.

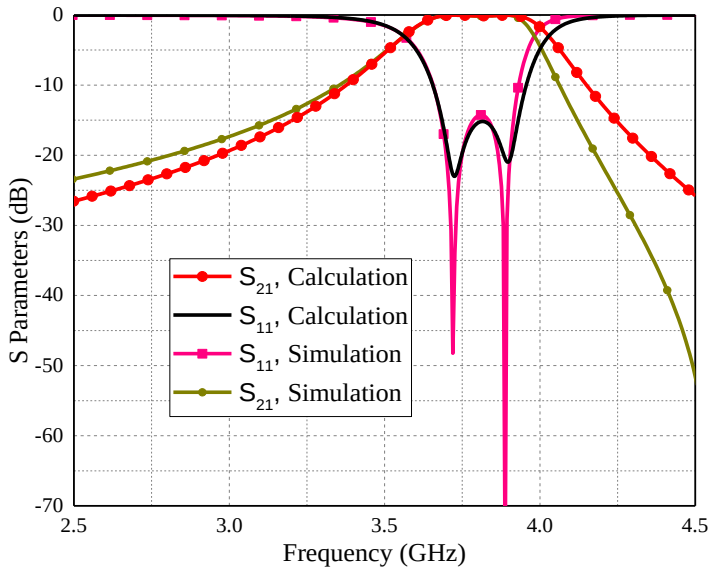

Fig. 6.3. Comparison between the calculated and simulated transmission and reflection coefficients of the proposed second-order bandpass FSS.

The values of the inductors L_{r1}, L_{r2}, and L_1 are related to L_{t1}, L_{t2}, and L_c by: $L_{r1}= L_{t1}+ L_2 (1+ L_{t1}/L_{t2})$ and $L_{r2}= L_{t2}+ L_2 (1+ L_{t2}/L_{t1})$. The coupling inductor $L_c = L_{t1}+L_{t2}+ (L_{t1}L_{t2})/L_2$, while $C_{r1}=C_2+C_{t1}$ and $C_{r2}= C_4+C_{t2}$. The values of lumped-element components in Fig. 6.2 (a), to achieve the desired response, can be determined. By taking $C_1= C_3$=0.30 pF, $C_2 =C_4=$ 0.25 pF, $L_1=L_3$ = 2.34 nH and L_2 =0.27 nH, the calculated reflection and transmission coefficients of the equivalent circuit are shown in Fig. 6.3.

To design the proposed miniaturised FSS with the desired response, one can first

determine the values of the elements used in the equivalent circuit model of Fig. 6.2, then the initial dimensions of these *LC* components can be approximated using the formulas in [12].

Finally, based on the results obtained from full-wave simulation on the array element of the proposed FSS, the dimensions of the inductive and resonant structures can be tuned to achieve the desired frequency response.

Fig. 6.4 shows the dimensions of each layer of the proposed FSS after tuning. D_x and D_y are the dimensions of the array element on the inductive layer toward the x and y axis, respectively. D_x-s and D_y-s are the dimensions of the elements on the first and the third layers; s represents the separation between two adjacent elements on the same layer. W_p is the width of the square patch.

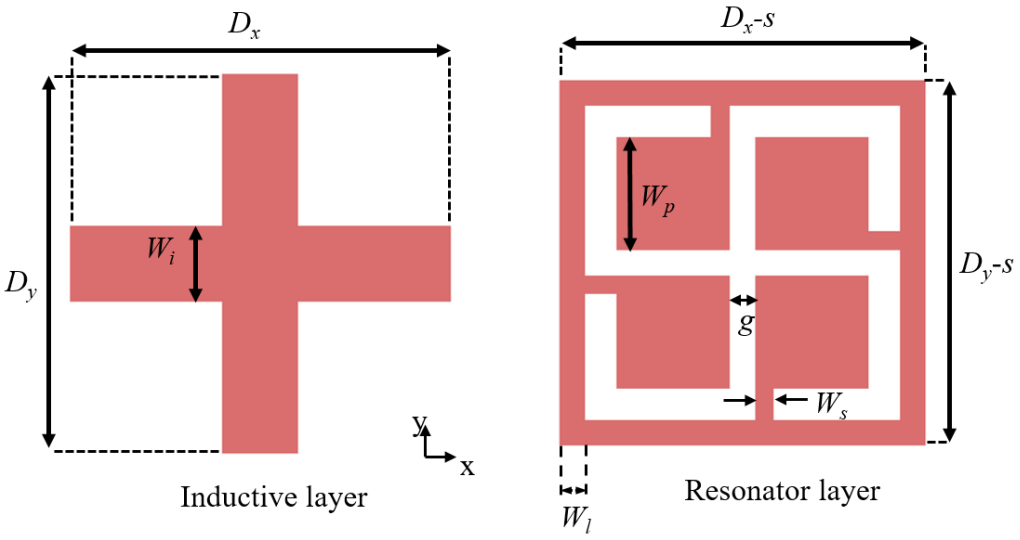

Fig. 6.4. Top view of the array element of the second-order bandpass FSS. The resonant layer is shown on the right-hand side and the inductive (grid) layer is shown on the left-hand side.

Table 6.1: Physical parameters of an element of the proposed second order bandpass FSS

Parameter	D_x	D_y	h_1	h_2
Value	6 mm	6 mm	1.6 mm	1.6 mm
Parameter	W_s	W_i	W_p	W_l
Value	0.2 mm	2.4 mm	2.3 mm	0.2 mm
Parameter	ε_r	S	g	
Value	4.3	0.1 mm	0.2 mm	

W_i is the width of the wire grid. A 1.6 mm thick FR4 substrate with a dielectric constant of 4.4 and a loss tangent of 0.027 at 10 GHz is used in the design. The final design parameters of the structure and its unit cell are listed in Table 6.1.

Fig. 6.3 shows the comparison between the calculated transmission and reflection coefficients and the simulated ones. The discrepancy in results between the simulation and the calculation is mainly attributed to use of the approximation equations (1.1) and (1.6). Fig. 6.5 and Fig. 6.6 show the simulated frequency responses of the proposed FSS for the TE and TM modes, respectively. The resonant frequency is 3.8 GHz, and the fractional bandwidth is about 10% at normal incidence angle. The insertion loss is 0.10 dB (assuming a lossless FR4). Whereas, using a lossy FR4 with a loss tangent of 0.027, the simulated insertion loss in the passband is about 1.05 dB.

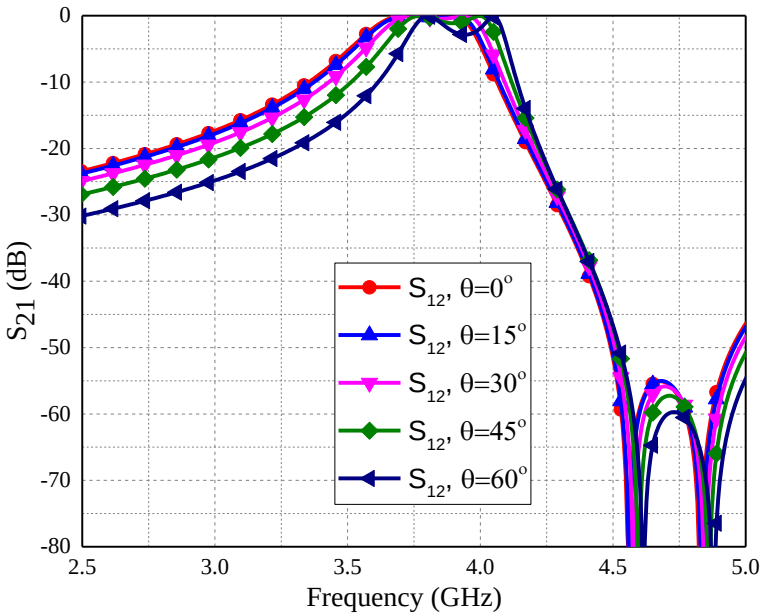

Fig. 6.5. Simulated transmission coefficients of the proposed second-order FSS with variable incident angles for the TE mode.

The simulation results show that the response of the proposed FSS is not very sensitive against incident angles. The frequency shift of the FSS at the TE mode with different incident angles is shown in Fig. 6.5. It can be seen that the centre frequency is shifted only by 2.6% from 0˚ to 60˚. The response is stable at the TM mode as well, as shown in Fig. 6.6. The comparison with works that have been used to design miniaturised second order bandpass FSS are shown in Table 6.2. It can be observed that the proposed structure is very stable, especially when the incident angle is high

as 60˚. This is expected because FSSs with miniaturised array elements usually exhibit stable responses for non-zero incident angles [13]. Due to symmetry, the frequency response of the proposed structure is independent from the polarisation angle. These features offer great flexibility for the proposed structure to be used for many applications.

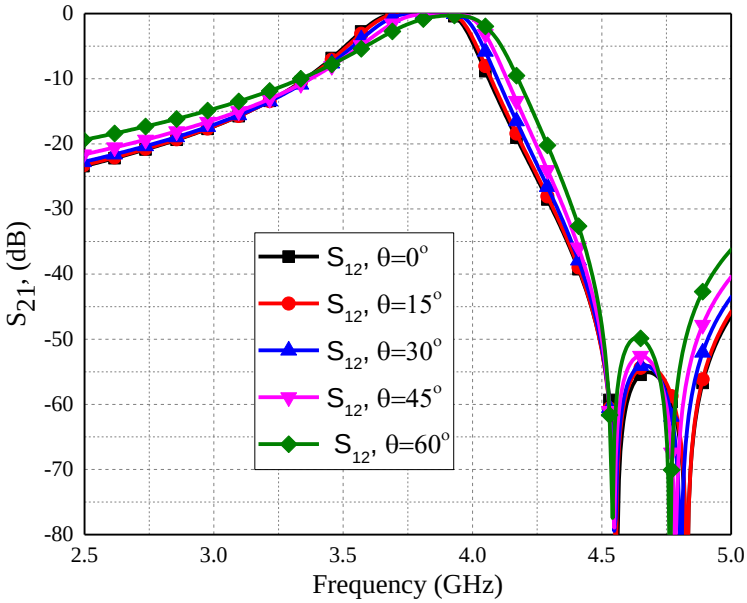

Fig. 6.6. Simulated transmission coefficients of the proposed second-order FSS with variable incident angles for the TM mode.

Table 6.2: Comparison with other work regarding the center frequency deviations with incident angles

FSS	f_o (GHz)	Incident angle (degree)	TE Tuning	TM Tuning
[3]	10	60	7%	10%
[2]	21	40	2.5%	2.3%
[14]	10	60	18%	16%
This work	3.8	40	2%	1.8%
This work	3.8	60	2.6%	2.6%

A comparison of the proposed FSS filter with other reported ones is illustrated in Table 6.3. It can be seen that the proposed structure has the smallest size. The overall

thickness is one of the lowest as well. The thickness is only slightly thicker than that in [3] and [8]. However, the fractional bandwidth is about half. Had the FSS been designed with the same fractional bandwidth, the thickness would have been thinner than them.

Table 6.3: Comparison with other work regarding the size, thickness and factional bandwidth (BW) of array elements

FSS	Order	f_o (GHz)	Element size	Overall thickness	BW%
[3]	2	10	0.15λ	0.033λ	20
[4]	2	16.5	0.104 λ	0.22λ	10
[2]	2	21	0.21 λ	0.273λ	5
[14]	2	10	0.1λ	0.067λ	21
[8]	2	24	0.16 λ	0.033λ	19
[15]	3	8.5	0.2λ	0.257λ	15
This work	2	3.8	0.076 λ	0.038 λ	10

Because of their relatively large size, most traditional high order bandpass FSSs are designed at the X, Ku, K and Ka band, rather than at lower frequencies, as can be observed from Table 6.3. The size of the proposed element is very compact and the overall thickness is small, which make the proposed design very suitable for low frequency applications.

6.2.2 Experimental results

A prototype of the proposed FSS filter has been fabricated and tested to validate the design method. The fabricated FSS is shown in Fig. 6.7. The size of the FSS prototype is 198 mm × 198 mm. It consists of 33 × 33 elements. The dimensions of the array element of the prototype are measured to ensure that they are in good agreement with the simulated elements. A vector network analyser and two horn antennas were used for the measurement. The measurement was done in two steps. First, the transmission coefficient between the two horn antennas was measured without the FSS. Second, the transmission coefficient was measured with the FSS

prototype between the antennas. Then the measured transmission with the FSS is normalised with respect to the measured data without the FSS. The transmission coefficient S_{21} was measured at

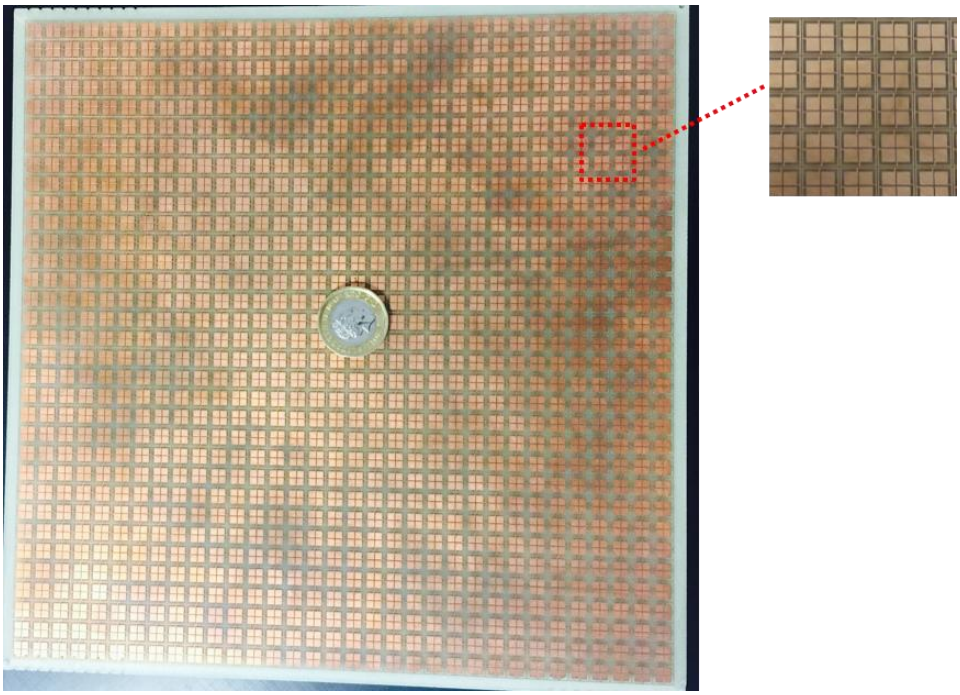

Fig. 6.7. Photograph of the fabricated prototype of the proposed second-order bandpass FSS.

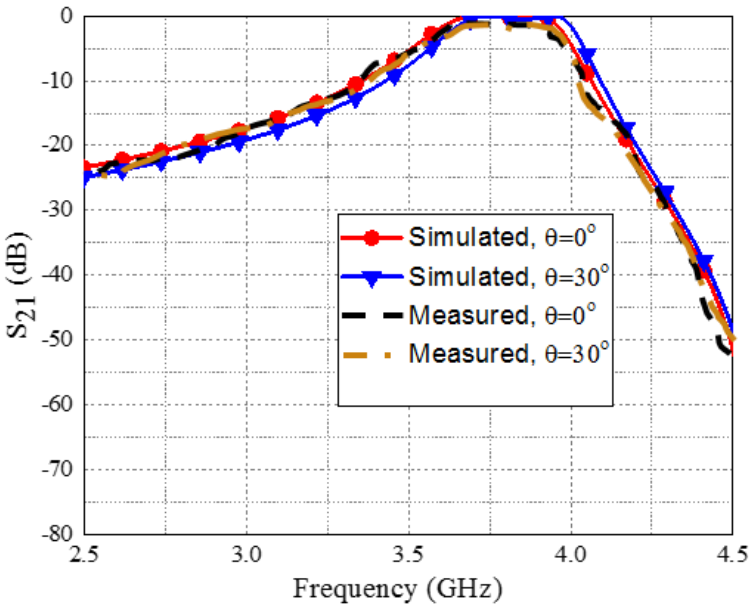

Fig. 6.8. Simulated and measured responses of the proposed second-order bandpass FSS.

various angles of incidence. The measured results are shown in Fig. 6.8 for the incident angles of 0˚ and 30˚. They show very good agreement with the simulated ones. As can be observed, the structure exhibits a bandpass response. The centre

frequency of the passband is 3.8 GHz with a fractional bandwidth of 10%. The frequency response of the proposed FSS is insensitive to the wave incident angle. The FSS was also tested under various polarisation angles. The performance is almost independent from polarisation angles due to the symmetrical nature of the proposed element.

6.3 Low profile second order FSS

In high-order FSSs, the surfaces should be cascaded vertically and separated by a dielectric substrate to achieve the desired responses. For that, the dielectric substrate thickness will matter in designing such structures. We present a novel approach for designing extremely low profile high-order bandpass FSSs. The structure is built in such a way to obtain bandpass response by using the coupling of the third harmonic of the resonators instead of the fundamentals. By parameter study of the proposed structure, it is found that a flat response can be achieved at a very thin substrate because the coupling between the third harmonics is very weak. The overall thickness of a second-order FSS can be reduced to λ/75. A prototype of the proposed second order bandpass FSS is designed, fabricated, and experimentally characterised. The measurement results of this device show a stable frequency response with respect to the angle of incidence up to ±45°.

6.3.1 Circuit design

The thickness of dielectric substrate layers, which are used to separate the metallic surfaces of an FSS, is reduced by using the third harmonics of the resonant surfaces as the main operation mode. In the proposed structure, two quarter-wavelength resonators are coupled by an inductive surface. Conventional quarter-wavelength resonators with uniform impedance resonate at an odd number times of the fundamental frequency (f_o), i.e., $(2n + 1)f_o$ with $n = 1,2,3 \ldots$ where f_o is the fundamental resonating frequency. In this study, it will be demonstrated how to enhance the third harmonic of a resonator and how to design extreme low profile high order FSS with such resonators.

The proposed second-order FSS is designed by using three surface layers and two dielectric slabs to separate them, as shown in Fig. 6.9. The first and third surface layers, as introduced in [9], are identical and present mutual capacitance in parallel

with series *LC*. The mutual capacitance is induced when the electric field of the illuminated wave is normal to the gap between adjacent elements. Regarding the series *LC*, the inductance is induced due to the magnetic field normal to the square loop strip, while *C* presents the capacitance between the adjusted patches. Each resonator is formed by using a square loop with four stepped-impedance transmission lines. The middle surface is built by using grid to provide inductance. Two dielectric slabs with a relative dielectric constant of 4.4 (FR-4) are used to separate the two resonating surfaces and the non-resonant (inductive) surface.

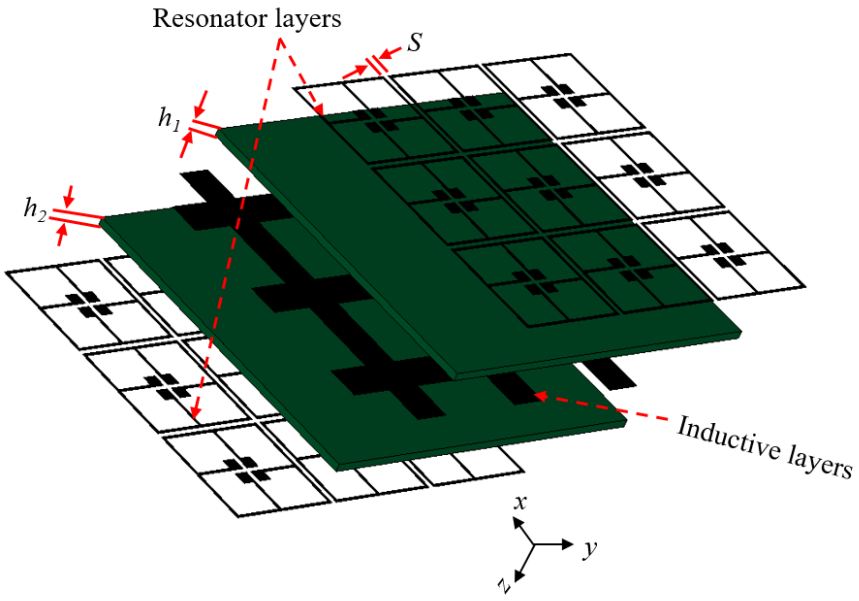

Fig. 6.9. Topology of the proposed second-order bandpass FSS.

For normal incident waves, the equivalent circuit as shown in Fig. 6.10 can be used to explain the operation principles of the proposed structure. The dielectric slabs are represented by two short pieces of transmission lines h_1 and h_2. The characteristic impedance of the dielectric slab is $Z_d = Z_o/\sqrt{\varepsilon_r}$, where Z_o is the free space impedance. C_1 and C_3 represent the mutual capacitance between adjacent elements in the first and third layers, respectively. C_2 and C_4 represent the capacitors between the patches of an element in the first and third layers, respectively. L_1 represents the inductance of the strip wire in an element of the first layer, and L_3 represents the inductance of the third layer. L_2 represents the inductance of the grid in the middle layer (inductive layer). It has been explained in detail that the inductance L_2 will significantly weaken the coupling between the first and the third layer.

This circuit is a second-order coupled resonator bandpass filter. Fig. 6.11 shows the

geometry dimensions of different layers of the proposed FSS, where D_x and D_y are the dimensions of the array element toward the x and y axis, respectively. D_x-s and D_y-s are dimensions of the square ring (first and third layer). w_p is the width of the square patches inside the square ring; w_s is the width of the strips inside the square ring; w_l is the width of the square ring perimeter.

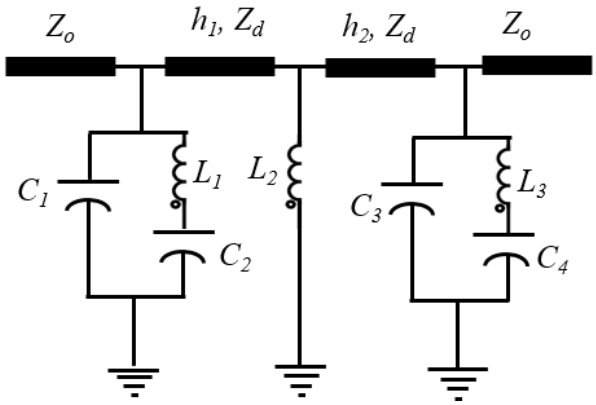

Fig. 6.10. Equivalent circuit model of the proposed second-order bandpass FSS.

Assuming that the structure has the same period in x and y directions, the inductive layer will be in the form of two metallic strips cross to each other with a length of $D_x = D_y = D$, and width of w_i.

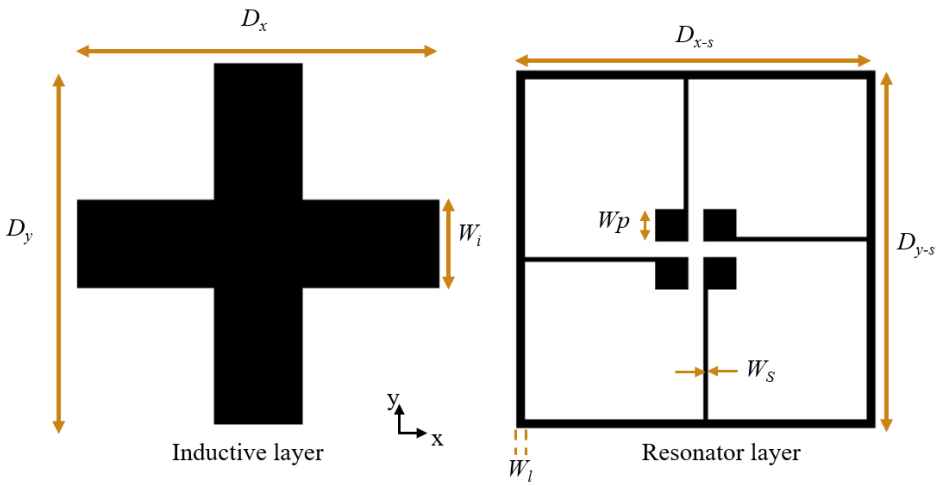

Fig. 6.11. Top view of the array elements of the second-order bandpass FSS: (a) The capacitive patch, (b) The inductive (grid) surface layer.

Dimensions of the FSS structures are optimised by full-wave simulation to achieve the desired frequency response. The final design parameters of the structure

and its unit cell are listed in Table 6.4.

Table 6.4: Physical parameter of the element of the proposed second order bandpass FSS (Unit: mm)

Parameter	D_x	D_y	W_p	W_1	h_1
Value	18	18	2	0.4	0.8
Parameter	W_s	W_i	S	g	h_2
Value	0.2	4	0.2	0.8	0.8

Fig. 6.12 shows the FSS frequency response for the normal incident wave obtained using a full-wave simulation tool (CST Microwave Studio). It can be observed that a flat bandpass response is achieved at around the third harmonic frequency, while two peaks can be observed at around the fundamental frequency. This is because with a thin substrate, the coupling between the first and the third layer is very strong at the fundamental frequency. Thus, although the coupling through the effective transmission line (h_1+h_2) is weakened by the shunt inductance L_2 of the middle layer, the direct coupling between the first and third layers will introduce two peaks at the fundamental frequency. It will be explained below that at the third harmonic, the coupling between the two layers at the third harmonic frequency is much weaker. This can be observed from the current distributions on the FSS surfaces as shown in Fig. 6.13. It can be seen that at the fundamental frequency, the current is mainly distributed in the parameter of the square rings on the first and third layers, as can be seen in Fig. 6.13(a). The coupling between these two layers is very strong. At the third harmonic, the current is mainly distributed at the centre of the rings on both sides and on two of the four step-impedance transmission lines inside the square ring, as shown in Fig. 6.13(b). The couplings between the first and third layers at these four places should have been very strong. However, due to the design, there are metallic strips on the middle layer. The middle layer will significantly weaken the coupling. Thus, a flat bandpass response can be achieved with a very thin substrate. The centre of the third-harmonic passband is at 3.86 GHz; the fractional bandwidth is 4.5%. On the contrary, at the fundamental frequency, the coupling is too strong.

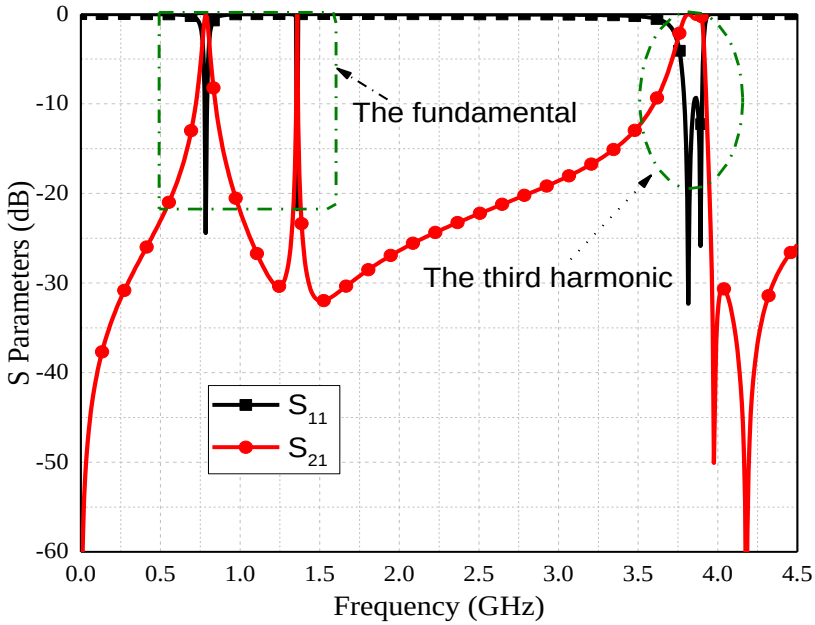

Fig. 6.12. Simulated magnitudes of transmission and reflection coefficients at thinner substrate.

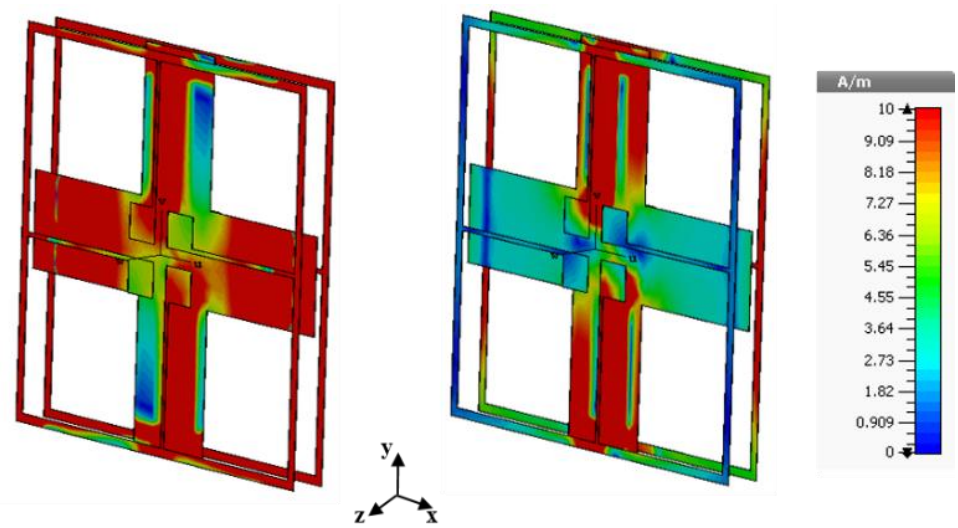

(a) **(b)**

Fig. 6.13. Current distribution of the proposed structure: (a) At the fundamental resonant (1.35 GHz), (b) At the third harmonics response (3.9 GHz).

It is worth mentioning that the structure still exhibits a very good second-order response even with a further reduced substrate thickness. The structure is simulated with different substrate thicknesses while other parameters are provided in Table 6.4. Fig. 6.14 shows the simulated results of the structure with three different substrate thicknesses (h_1 and h_2). It can be observed that the structure still exhibits a second-order bandpass response with a substrate thickness equal to $\lambda/75$, $h_1 = h_2 = 0.5$ mm.

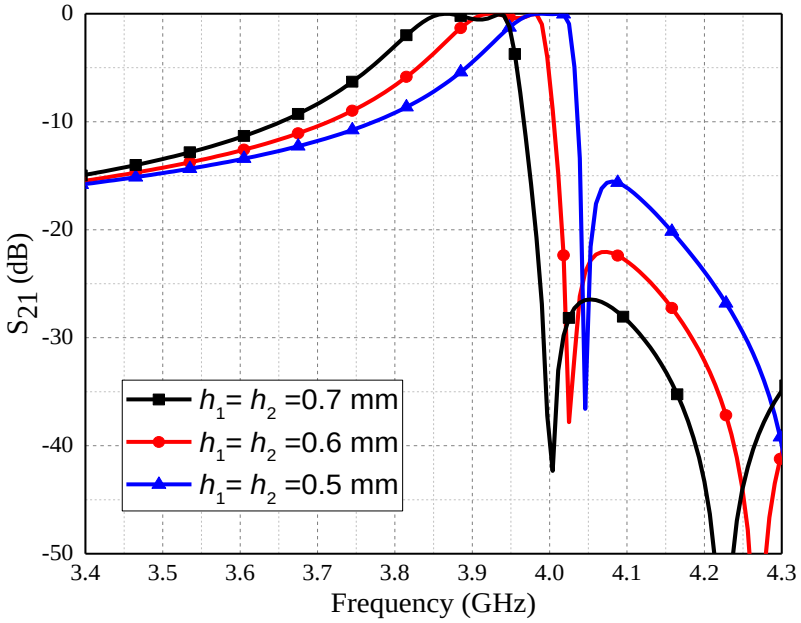

Fig. 6.14. Simulated transmission coefficients of the third harmonic of the proposed second-order FSS with different substrate thicknesses.

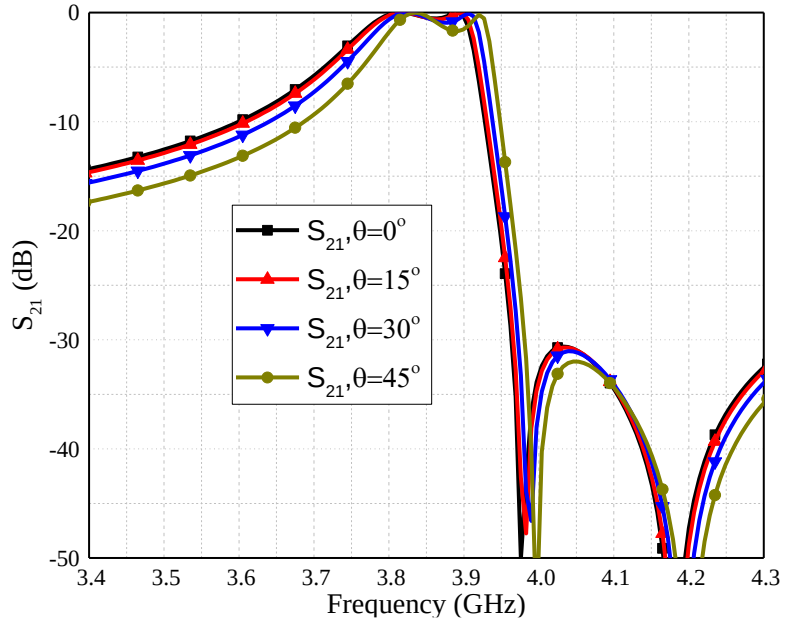

Fig. 6.15. Simulated transmission coefficients of the proposed second-order FSS with varied incident angle for TE mode response.

The thickness could be further decreased by optimizing the structure on the middle layer. The proposed FSS element was designed to be symmetrical in the *xy*-plane. For this reason, it is independent from the polarisation angle. The structure was also simulated under various incident angles.

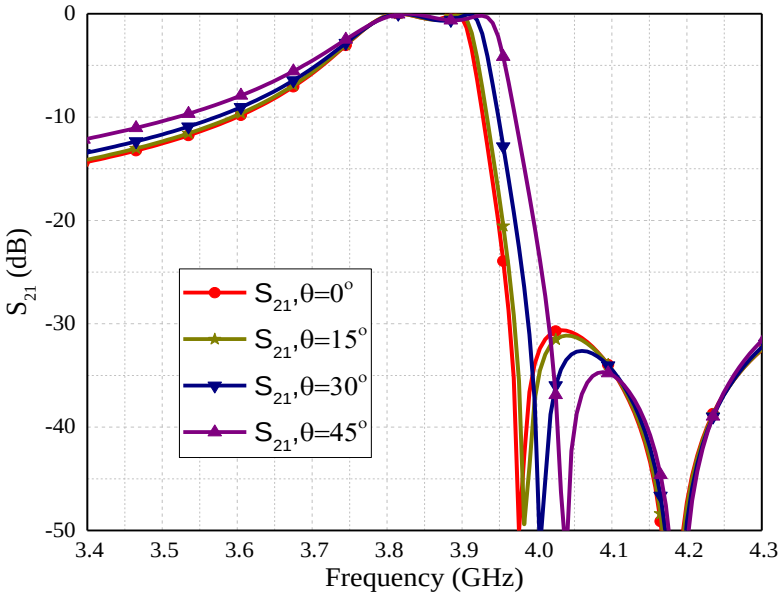

Fig. 6.16. Simulated transmission coefficients of the proposed second-order FSS with varied incident angle for TM mode response.

The results indicate that the response is very stable as shown in Fig. 6.15 and Fig. 6.16. Fig. 6.15 shows the result for the TE mode under 0º, 15º 30º and 45º incident angles. The insertion loss at the centre frequency response is 0.0115 dB at the normal incident angle. Fig. 6.16 shows the result for TM mode under 0º, 15º 30º and 45º, as well. These advantages offer great flexibility for the proposed structure to be suitable for many applications.

6.3.2 Experimental results

A fabricated sample of the proposed structure has been tested to validate the design.

The fabricated FSS is shown in Fig. 6.17. The dimensions of the FSS prototype are 216 mm × 216 mm. It consists of 12 × 12 elements. A vector network analyser and two horn antennas were used for the test. Two steps were used in the measurement procedure. First, in the free space case, the transmission coefficient between the two horn antennas was measured without the FSS. Second, the transmission coefficient was measured with the FSS prototype between the antennas. Then the measured transmission coefficient with the FSS is normalised with respect to the measured data without the FSS.

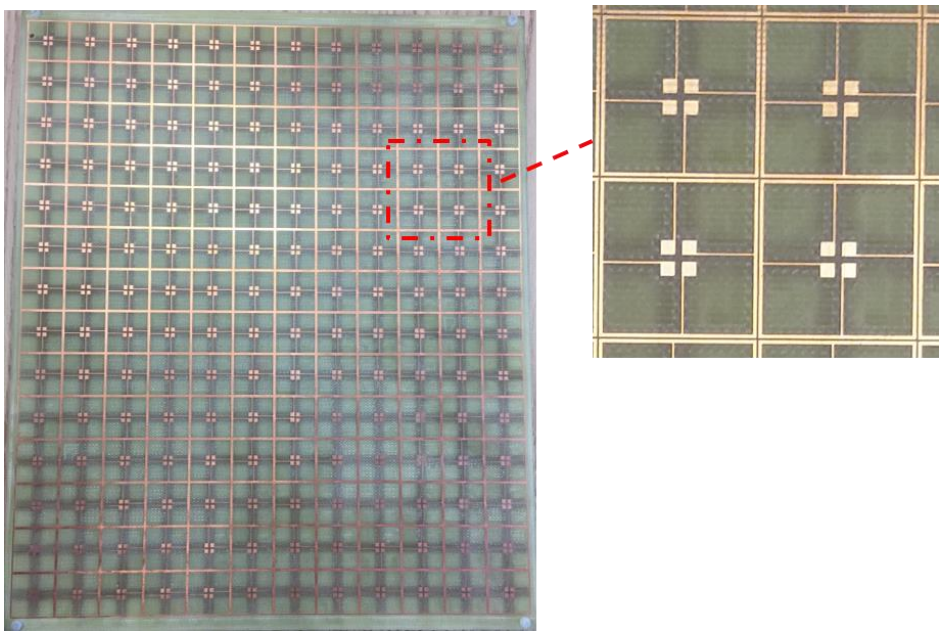

Fig. 6.17. Photograph of the prototype of the proposed FSS.

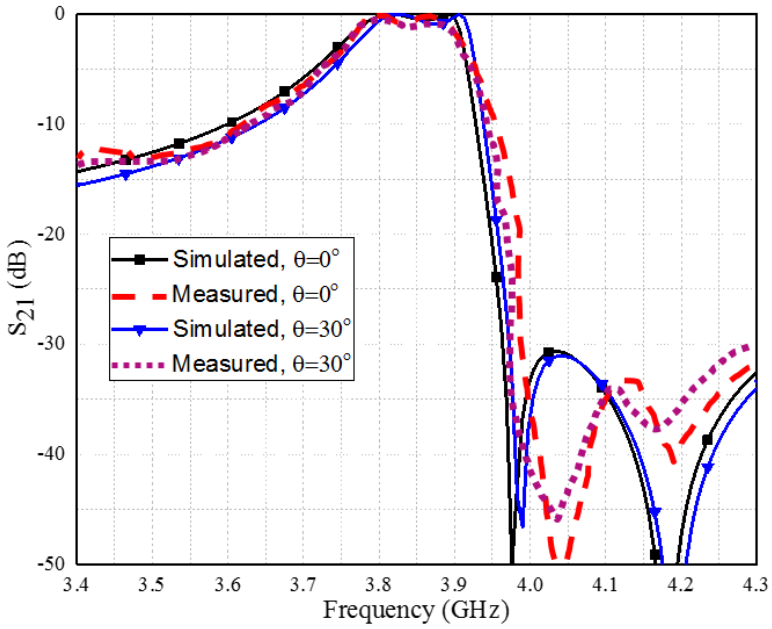

Fig. 6.18. Measured and simulated transmission coefficient of the third harmonic of the second order bandpass FSS.

The transmission coefficient S_{21} was measured at various angles of incidence. The measured results are shown in Fig. 6.18 for the incident angles of 0˚ and 30˚. They show very good agreement with the simulated results. As can be seen, the structure exhibits a bandpass response at the third harmonic. The centre frequency of the passband is 3.86 GHz with a fractional bandwidth of 4.4%. The proposed FSS exhibits insensitive frequency response to the wave incident angle up to ±45º.

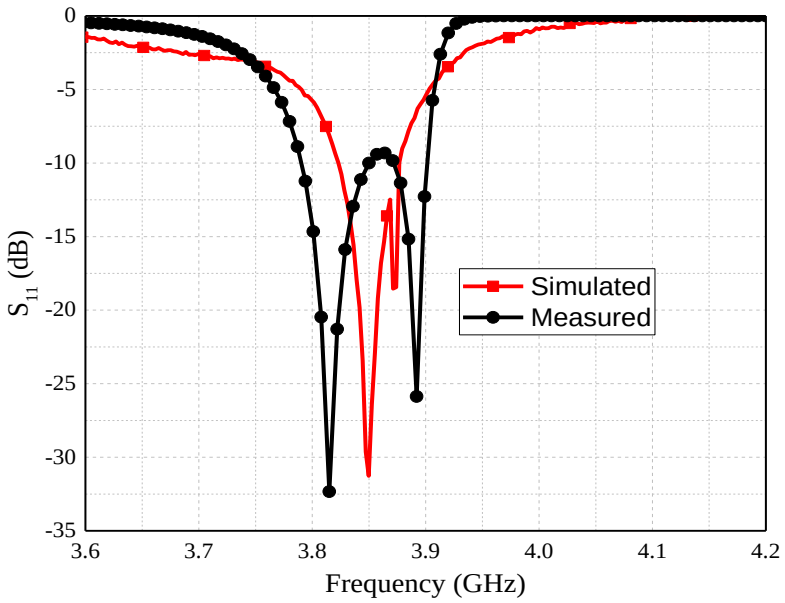

Fig. 6.19. Measured and simulated reflection coefficients of the third harmonic of the second order bandpass FSS.

The FSS was also tested under various polarisation angles. It was shown that the performance is almost independent from polarisation angles. This is expected because of the symmetrical shape of the proposed element. The two horn antennas are used as the transmitter and receiver, respectively, at the same side of the FSS to measure the reflection coefficient. An absorber screen is used between the two horn antennas to eliminate the direct coupling between them. The measured reflection of the prototype of the proposed FSS is shown in Fig. 6.19. The measured result is in relatively good agreement with the simulated performance. The discrepancy between the measurement and simulation results is mainly due to inaccuracies in the exact values of the dielectric substrates used (±1.5% as specified by the manufacturer), the finite size of the prototype, tolerances and general inaccuracies involved in the fabrication process, inaccuracies involved in the measurement, and the numerical errors in the simulation.

6.4 Conclusion

In this chapter, a new approach to design a miniaturised second-order bandpass filter has been proposed. The miniaturised FSS has been built by using a configuration of three surfaces layers. The overall thickness of the proposed structure is 0.038λ, and the element dimensions are 0.076λ × 0.076λ for the prototype, which

is one of the smallest reported so far. The miniaturisation was realised by using resonant structures on the first and third layers. The proposed technique is particularly useful for low frequency applications. The structure exhibits very good features as an FSS, such as insensitivity to the incident angle and independence from the polarisations. The proposed design method with these features is very attractive for a wide range of applications.

A new approach to design high order bandpass FSSs with extremely thin dielectric substrates has been introduced. The proposed approach is built based on the coupling between the third harmonics of the quarter wavelength resonators. The overall thickness of the proposed structure is λ/75, which is the lowest profile has been reported so far. As a result, the structure can be classified as a very low profile multi-layered structure. The proposed method can also be useful for millimeter wave and terahertz application, where the substrate comprises the most significant loss to such structures. It has been shown that the transmission and reflection coefficients are almost independent from polarisations and insensitive to the incident angles Such an FSS can be very attractive for a wide range of applications.

6.5 References

[1] B. A. Munk, "Frequency selective surfaces theory and design," New York: Wiley-Interscience, 2000.

[2] S. M. A. M. H. Abadi, and N. Behdad, “Inductively-coupled miniaturized-element frequency selective surfaces with narrowband, high-order bandpass responses,” *IEEE Transactions on Antennas and Propagation,* vol. 63, no. 11, pp. 4766-4774, 2015.

[3] M. Al-Joumayly, and N. Behdad, “A new technique for design of low-profile, second-order, bandpass frequency selective surfaces,” *IEEE Transactions on Antennas and Propagation,* vol. 57, no. 2, pp. 452-459, 2009.

[4] M. Gao, S. M. A. M. H. Abadi, and N. Behdad, “A dual-band, inductively coupled miniaturized-element frequency selective surface with higher order bandpass response,” *IEEE Transactions on Antennas and Propagation,* vol. 64, no. 8, pp. 3729-3734, 2016.

[5] M. A. Al-Joumayly, and N. Behdad, “Low-profile, highly-selective, dual-

band frequency selective surfaces with closely spaced bands of operation," *IEEE Transactions on Antennas and Propagation,* vol. 58, no. 12, pp. 4042-4050, 2010.

[6] S. Çimen, "Novel closely spaced planar dual-band frequency-selective surface," *IET Microwaves, Antennas & Propagation,* vol. 7, no. 11, pp. 894-899, 2013.

[7] N. Behdad, M. Al-Joumayly, and M. Salehi, "A low-profile third-order bandpass frequency selective surface," *IEEE Transactions on Antennas and Propagation,* vol. 57, no. 2, pp. 460-466, 2009.

[8] M. Salehi, and N. Behdad, "A second-order dual X-/Ka-band frequency selective surface," *IEEE Microwave and Wireless Components Letters,* vol. 18, no. 12, pp. 785-787, 2008.

[9] M. Hussein, J. Zhou, Y. Huang, A. Sohrab, and M. Kod, "Frequency selective surface with simple configuration stepped-impedance elements." *Antennas and Propagation (EuCAP),* Davos, 2016, pp.1-4.

[10] R. W. P. King, *Fundamental electromagnetic theory*: Dover Publications, 1963.

[11] A. I. Zverev, *Handbook of filter synthesis*: Wiley-Blackwell, 2005.

[12] N. Marcuvitz, *Waveguide handbook*: IET, 1951.

[13] K. Sarabandi, and N. Behdad, "A frequency selective surface with miniaturized elements," *IEEE Transactions on Antennas and Propagation,* vol. 55, no. 5, pp. 1239-1245, 2007.

[14] M. Yan, S. Qu, J. Wang, A. Zhang, L. Zheng, Y. Pang, and H. Zhou, "A miniaturized dual-band FSS with second-order response and large band separation," *IEEE Antennas and Wireless Propagation Letters,* vol. 14, pp. 1602-1605, 2015.

[15] M. Gao, S. M. A. M. H. Abadi, and N. Behdad, "A hybrid miniaturized-element frequency selective surface with a third-order bandpass response," *IEEE Antennas and Wireless Propagation Letters,* vol. PP, no. 99, pp. 1 - 1 2016.

Chapter 7: THz FSS

7.1 Introduction

Terahertz (THz) is the band of frequencies between microwave and infrared in the range from 0.3 to 3 THz. The wavelength of radiated signal at 1 THz is 300 μm in free space. Medical imaging, THz spectroscopy, security scanning, high speed and wireless communication are typical applications of THz systems [1-3].

Recently, filter components have been proposed for some of these applications [1-7]. Similar to microwave FSSs, THz FSSs can be realised by printing metal on one or both sides of a dielectric slab. Metal mesh and related structures have been shown to be suitable for the construction of THz filters. Several types of design have been proposed to achieve a desired THz filter. Dielectric-metal-dielectric has been used to achieve a dual band and low loss bandpass filter with a transmission coefficient of up to 90%[8].

The bandpass filter based on meta-material could exhibit very narrow bandwidths [9-11]. The 3 dB fractional bandwidth of the passband by using two layers of the cross-slot structure and four layers of the wire-plate structure is less than 25% in each case. The amplitude of transmission is over 80% [12]. In the past, the researchers were focused on the analysis and design of single resonance THz FSS. The extension of FSS technology for multiband and tunable capabilities is of great interest. One interesting approach is to use fractal FSSs which are achieved by using a genetic algorithm [13]. Although they exhibit good performance, there is no obvious direct relationship between the performance and the geometry. It relies decisively on time-consuming computational trials.

Conventionally, millimeter-wave and THz bandpass FSSs with an almost flat top and a fast roll-off frequency response can be implemented by using two or more cascaded surfaces (the same procedure which is used at microwave frequencies) [14]. The surfaces would be resonant or non-resonant, separated by dielectric layers. The thickness of the dielectric slab is usually around a quarter wavelength to obtain a flat frequency response and fast roll-off [15]. Generally, the thinner substrates are better to minimising radiation loss [16]. Also, satellite systems tend to operate in the

Circular Polarisations (CP) mode, which can provide flexibility to effects such as Faraday rotation [17]. It can make the alignment in polarisation between the transmitter and receiver easier. Polarisation independent FSSs have attracted a lot of interests. Several FSS geometries with such characteristics have been proposed at millimeter and sub-millimeter waves including crossed dipoles [18], Jerusalem crosses [19], rings [20], two layers of semi-circle surfaces [21], double square loop arrays and gridded double square loop arrays [22].

In this chapter, a new approach to design FSSs with sharp transition edges will be described in Section 7.2. In Section 7.3, a low loss bandpass FSS with symmetrical shape in the *xy*-plane will be discussed.

7.2 Sharp transition edge FSS

In this section, a bandpass FSS is realised by combining a bandstop and a bandpass structures. The FSS can be applied to separate signals in THz frequencies. For example, it will be used to separate signals at 166 GHz and 183 GHz. Circular ring and circular slots are used here. The two structures can co-exist on the same layer without significantly affecting each other. It is demonstrated that using the proposed technique, second-order FSSs with an overall thickness of less than λ/7 can be designed. The proposed method focuses on designing a second order bandpass FSS with desired features, such as: low insertion loss, flat passband and sharp transition edges.

7.2.1 Circuit design

The proposed single-layer FSS is shown in Fig. 7.1. The element of the proposed FSS consists of two circular rings and their complementary structures on the same plane. D_x and D_y are the dimensions of the array element toward the x and y axes, respectively. D_x and D_y are 560 μm. The two rings and two slots are arranged to be rotationally symmetrical around the *xy*-plane shown in Fig. 7.1. By using this arrangement, the performance is insensitive to the polarisation of the normal incident waves.

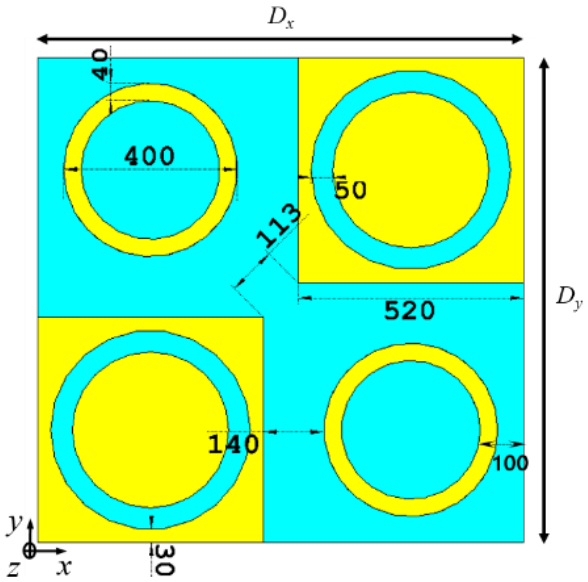

Fig. 7.1. Geometric parameters of the proposed surface, unit: µm.

The proposed structure can be designed in three steps. The first step is to achieve the appropriate bandpass structure based on the desired frequency response. A circular slot, as shown in Fig. 7.2, is used as the bandpass structure. By cascading two such structures in two layers, the desired frequency response with a flat top can be achieved.

The second step is to design an appropriate structure with suitable bandstop characteristics, such as the frequency response, the array element size and the shape. The circular slot structure shown in Fig. 7.3 is used as the secondary structure in this design.

The final step is to combine the two structures, the circular slot and the ring. It is worth mentioning here that the frequency response of the combined structure will be different from two individual circuits combined. This is mainly because of the coupling between the two structures. For that reason, tuning is needed to achieve the desired response. To verify the response of the combined structures, simulation was carried out on both the bandpass and stopband structures. It was done with a CST Microwave Studio, using unit cell boundary conditions to provide periodicity along the x and y axes.

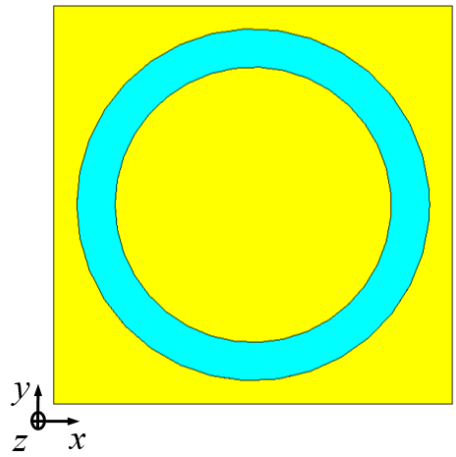

Fig. 7.2. Top view of the passband FSS element (metal is shown in yellow and the slot is shown in cyan).

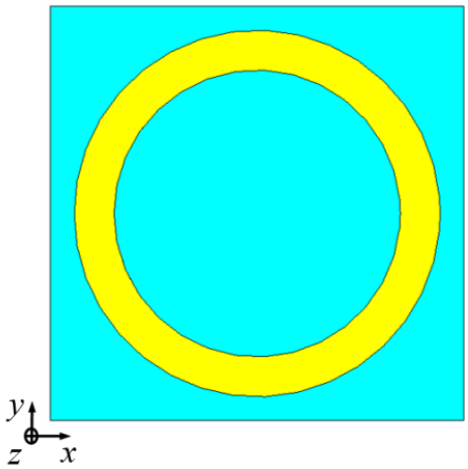

Fig. 7.3. Top view of the stopband FSS element.

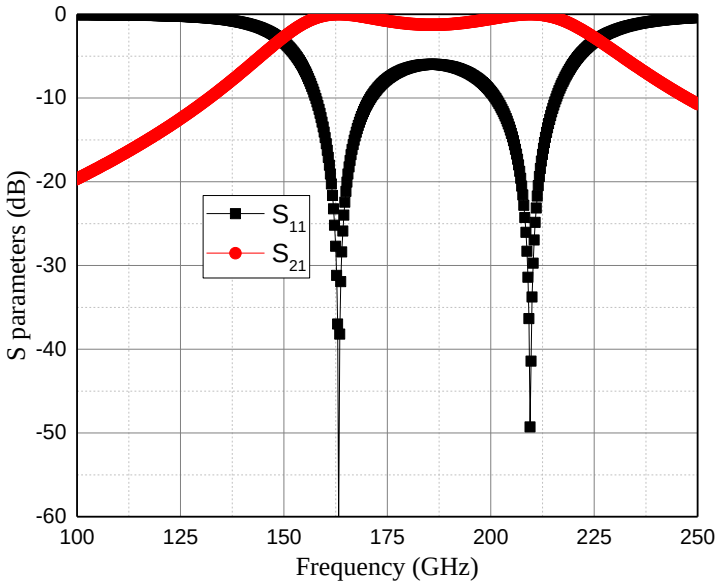

Fig. 7.4. Simulated transmission and reflection coefficients of the slot structure (bandpass).

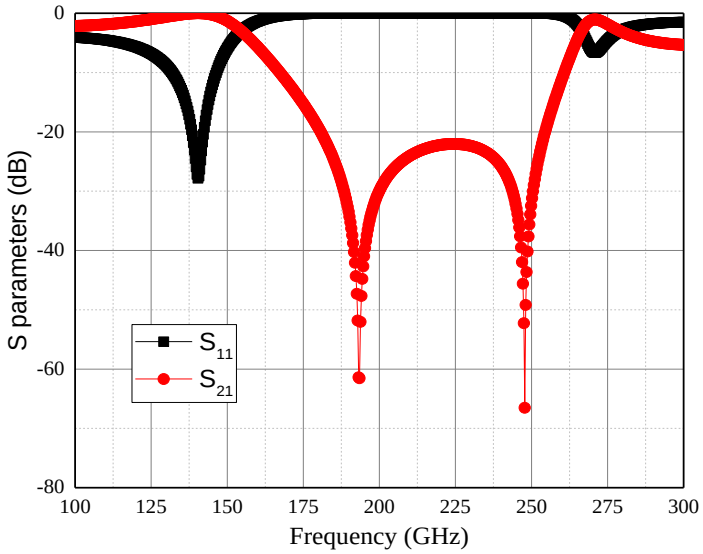

Fig. 7.5. Simulated transmission and reflection coefficients of the ring structure (bandstop).

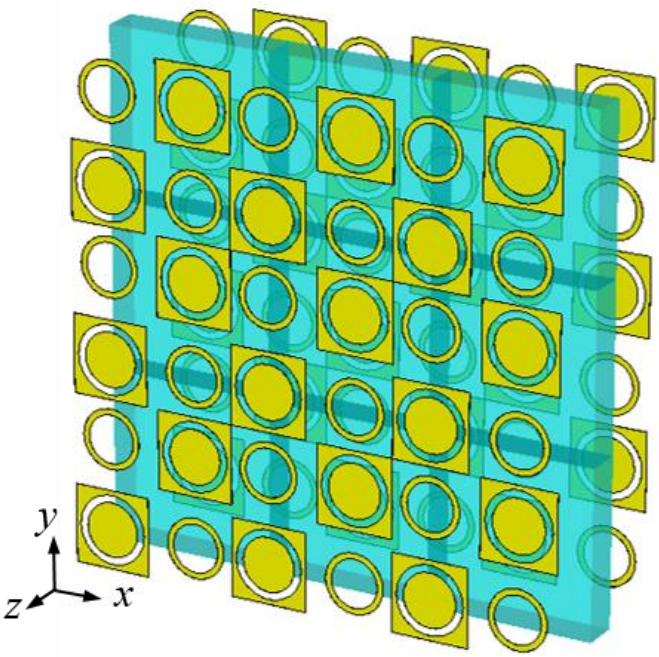

Fig. 7.6. Schematic view of the two-layer FSS with 3×3 array elements.

The structure is excited by an electromagnetic wave with the propagation vector (**K**) towards the z-axis direction, magnetic field vector (**H**) towards the x–axis direction and electric field vector (**E**) towards the y-axis direction. The bandpass response was achieved by cascading two layers of circular slots, which were separated by a Polyethylene Naphthalate (PEN) substrate with a 2.9 dielectric constant [23], 250 μm thick. The filter has a fraction bandwidth of 40% (150 GHz - 225 GHz), as can be observed from the simulated results of the transmission and reflection coefficients shown in Fig. 7.4. The simulated results of the cascaded rings,

which are separated by the same PEN substrate, are shown in Fig. 7.5. The structure exhibits performance with a stopband from 150 GHz to 266 GHz. Fig. 7.6 shows the proposed two-layer combined structure with 3×3 array elements. Each element consists of two rings and two circular slots on two layers. It should be noted here that the dimensions of the circular slots and the rings are slightly different.

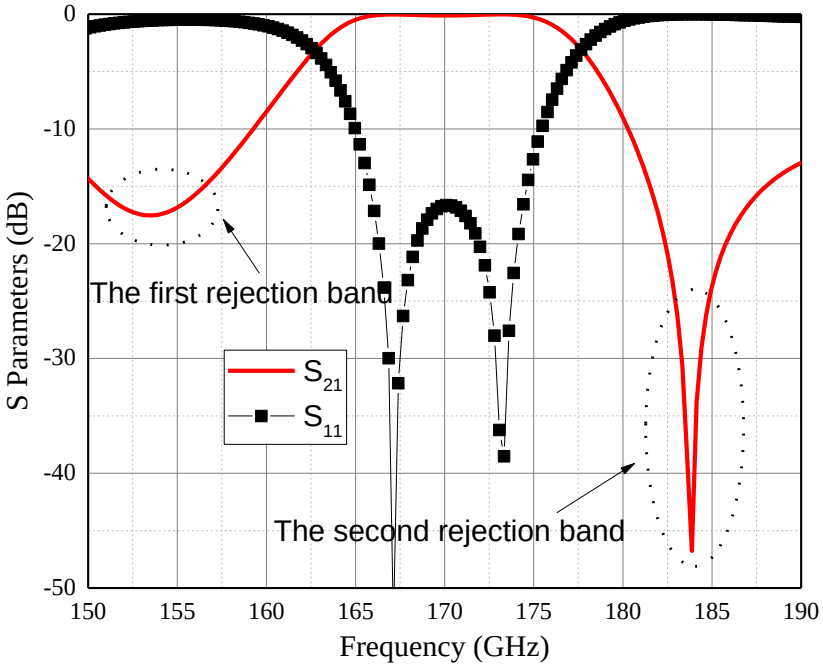

Fig. 7.7. Simulated transmission response of the two-layer FSS structure for TE and TM polarisations.

The transmission characteristics of the FSS are predicted and obtained by simulation. The simulated response is shown in Fig. 7.7. It can be seen that the response has a flat passband from 162 to 177 GHz, with very high selectivity and low insertion loss. The insertion loss is less than 0.2 dB, the first rejection band is at around 152 GHz with an attenuation of 17 dB. The second rejection band is at around 183.5 GHz as specified with a high attenuation of better than - 40 dB. The structure exhibits the same response for TE and TM polarisations at normal incidence.

Standard photolithography and lift-off processes were used to pattern the single-layer FSS on a PEN. For the metallic layer, a bilayer of approximately 25 nm thick Ti and 100 nm of Au was deposited by e-beam evaporation. The array element dimensions are 1120 µm ×1120 µm. A prototype of the size of 3 cm × 3 cm has been fabricated. A two-layer FSS is also being fabricated. The measurement will be carried

out as future work.

7.3 Low loses high order bandpass FSS

One of the most popular FSS grid geometry and element is a cross-dipole as shown in Fig. 7.8(a). The geometry is defined by periodicity *P*, cross-member length *d,* and cross-member width *W*. A 3×3 cross-dipole array element is shown in Fig. 7.8(b). The cross-dipole dimensions determine the frequency response of the filter. Linearly scaling the dimensions *P, d* and *W* can shift the filter profile, provided that *P* is much smaller than the wavelength[24, 25]. This structure exhibits bandstop response.

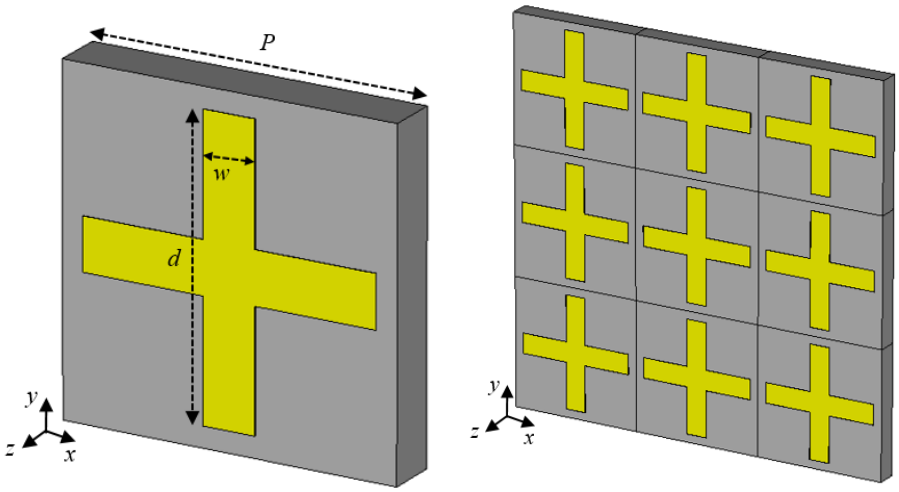

(a) **(b)**

Fig. 7.8. Cross shaped filter.

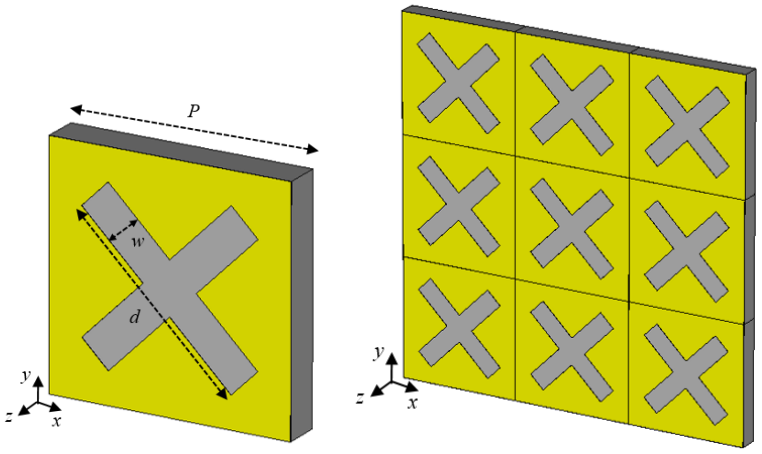

Fig. 7.9. (a) Schematic view of the single-layer FSS array element, (b) Schematic view of the single-layer FSS with 3×3 array elements

Fig. 7.9 (a) shows a single-layer FSS array element, which is the complementary of the cross-dipole. The schematic view of the single-layer complementary structure with 3×3 elements is shown in Fig. 7.9(b). The dimension of a single element is 0.662 × 0.662 mm^2. Each cross is rotated by 45^o in the *xy*-plane. The slot width is $W = 0.15$ mm, and the slot length is $d = 0.662$ mm. With this arrangement, the performance of the FSS is insensitive to polarisation of incident waves.

7.3.1 Fabrication and measurements

Our single-layer FSS structure consists of 3 × 3 elements which have been fabricated. Standard photolithography and lift-off processes were used to pattern the single-layer FSS array on a 0.75-mm-thick Polyimide substrate, as shown in Fig. 7.10. For the metallic layer, a bilayer of approximately 25 nm Ti coated with 100 nm of Au was deposited by e-beam evaporation. The measurement setup is shown in Fig. 7.11. Interferograms were acquired at a range of emitter frequencies by adjusting the THz beam path length between the emitting and receiving antennas and recording the amplitude of the THz field over an 80-ps delay length, with 0.83-ps step size.

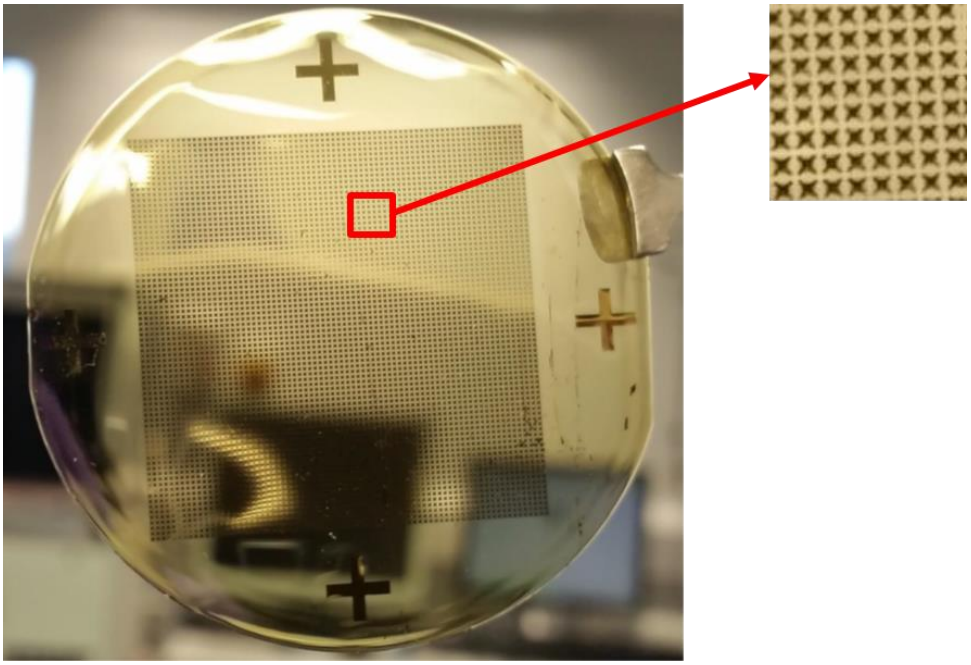

Fig. 7.10. The fabricated THz FSS on a 7.5 µm thick Polyimide substrate.

The transmission spectrum was obtained by comparing the interferogram amplitudes, both with and without the FSS present, at each frequency. The measured transmission response of the fabricated single-layer FSS array is shown in Fig. 7.12. The red line shows high-resolution scans over a narrow range of frequencies, while

the black line shows low-resolution scans over a wide range of frequencies. The passband can be clearly observed at 166 GHz as expected. The loss is relatively high at around 5 dB. To improve the performance, a new method is proposed to design a low-loss second-order FSS bandpass filter. The two layers of the array element are separated from each other by an air gap, as shown in Fig. 7.13(a). The schematic view of the two-layer FSS with 3×3 array elements is shown in Fig. 7.13(b). The simulated response is shown in Fig. 7.14. It can be seen that the response has a flat passband, much better selectivity and lower loss. This design will be fabricated and tested in the near future.

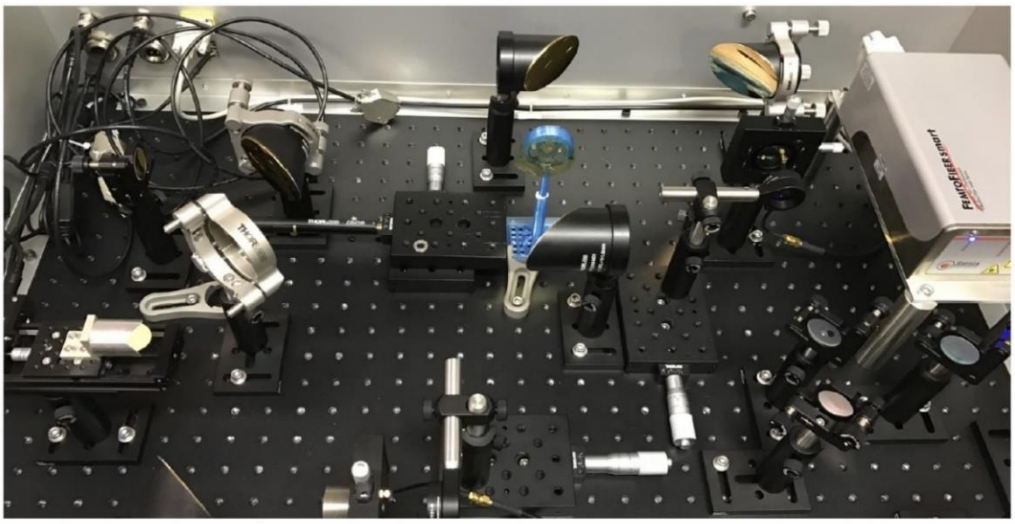

Fig. 7.11. Measurement setup of an FSS at millimetre-wave and THz.

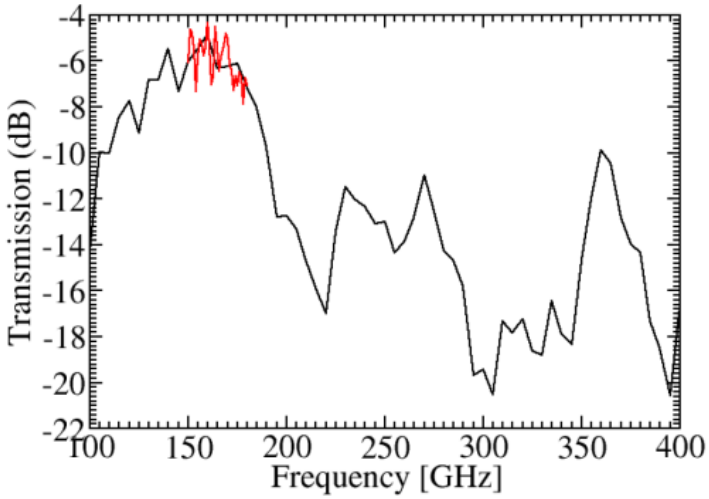

Fig. 7.12. The measured result of the transmission response of the single-layer FSS array, the red lines show high-resolution scans over a narrow range of frequencies, while the black lines show low-resolution scans over a wide range of frequencies.

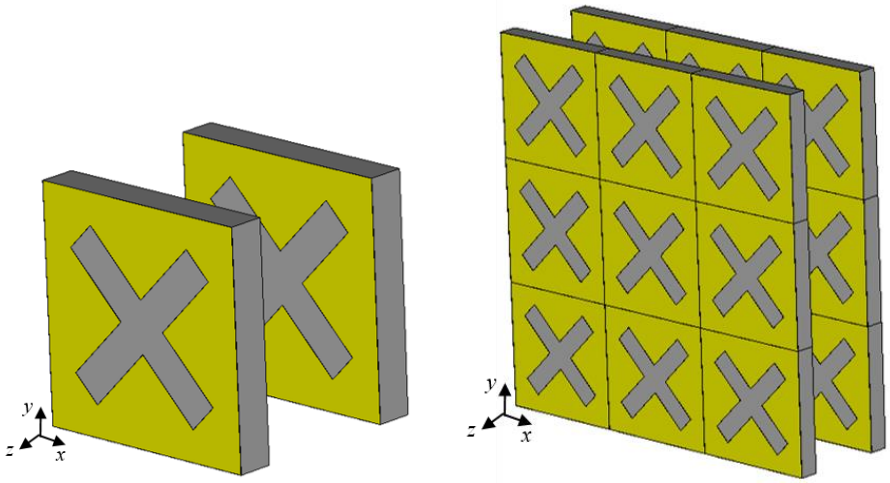

Fig. 7.13. (a) Schematic view of the two-layer FSS array structure with an air gap, (b) Schematic view of the two-layer FSS with 3×3 array elements.

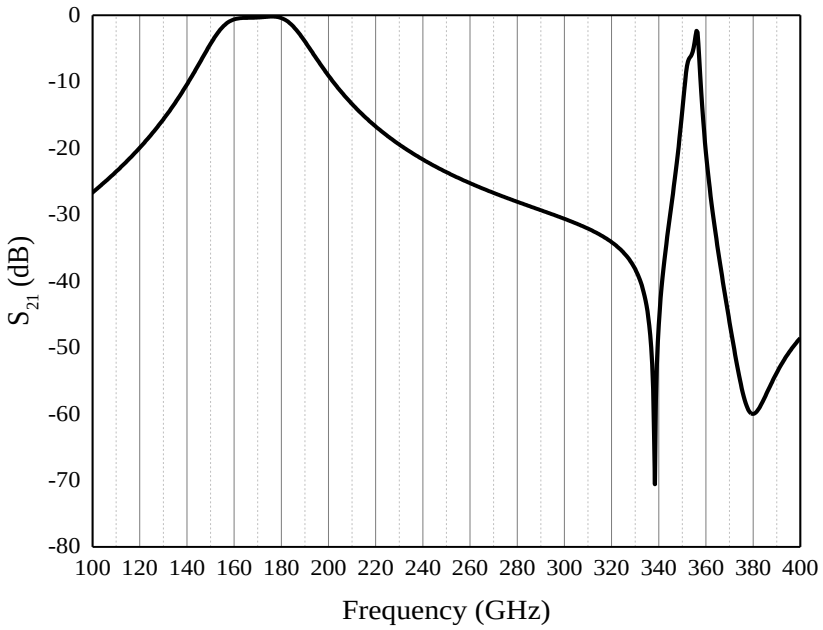

Fig. 7.14. Simulated transmission response of the two-layer FSS array structure.

7.4 Conclusion

In this chapter, a new approach to design bandpass FSSs with high selectivity for submillimeter wave applications has been proposed. The proposed approach is built by using a simple configuration of two different structures on the same layer. One structure has a bandpass response and the other has a bandstop response. It is shown that the transmission coefficient is independent from polarisation angles. The proposed FSS exhibits excellent characteristics such as low insertion loss, sharp roll-off and flat passband.

Another method is proposed to design a low-loss high order bandpass FSS. The proposed structure is constructed by cascading two of the same surfaces separated from each other by an air gap. The device will be fabricated and measured in the future work.

7.5 References

[1] T. K. Nguyen, H. Han, and I. Park, "Highly efficient resonant antennas for terahertz photomixers." *Antenna Technology (iWAT), IEEE International Workshop on* pp. 315-318, 2012.

[2] B. S. Rawat, A. Bhat, and J. Pistora, "THz band nanoantennas for future mobile communication." *Signal Processing and Communication (ICSC), International Conference,* pp. 48-52, 2013.

[3] Y. Chianga, and T. Yena, "A high-transmission dualband terahertz bandpass filter by exciting multiresonance of metamaterials." *Proc.* SPIE 8070, Metamaterials VI, 80700V, 2011.

[4] C. Winnewisser, F. Lewen, and H. Helm, “Transmission characteristics of dichroic filters measured by THz time-domain spectroscopy,” *Applied Physics A: Materials Science & Processing,* vol. 66, no. 6, pp. 593-598, 1998.

[5] S. Govindaswamy, J. East, F. Terry, E. Topsakal, J. L. Volakis, and G. I. Haddad, “Frequency-selective surface based bandpass filters in the near-infrared region,” *Microwave and Optical Technology Letters,* vol. 41, no. 4, pp. 266-269, 2004.

[6] C. Debus, and P. H. Bolivar, “Frequency selective surfaces for high sensitivity terahertz sensing,” *Applied Physics Letters,* vol. 91, no. 18, pp. 184102, 2007.

[7] N. Liu, L. Langguth, T. Weiss, J. Kästel, M. Fleischhauer, T. Pfau, and H. Giessen, “Plasmonic analogue of electromagnetically induced transparency at the Drude damping limit,” *Nature materials,* vol. 8, no. 9, pp. 758, 2009.

[8] Y. Chiang, and T. Yen, "A high-transmission dualband terahertz bandpass filter by exciting multiresonance of metamaterials." *SPIE Optics+ Optoelectronics* pp. 80700V-80700V-6.

[9] N. Jin, and J. S. Li, “Terahertz wave bandpass filter based on metamaterials,” *Microwave and Optical Technology Letters,* vol. 53, no. 8, pp. 1858-1860, 2011.

[10] L. M. Si, Y. Yuan, H. J. Sun, and X. Lv, “Characterization and application of planar terahertz narrow bandpass filter with metamaterial resonators,” *Proceedings, International Workshop on Metamaterials*, pp. 351-354, 2008.

[11] I. A. I. Al-Naib, C. Jansen, and M. Koch, “Very compact bandpass filter based on spiral metamaterial resonators,” *International Conference on Infrared, Millimeter and Terahertz Waves, Vols 1 & 2*, pp. 7-8, 2009.

[12] O. Paul, R. Beigang, and M. Rahm, “Highly selective terahertz bandpass filters based on trapped mode excitation,” *Optics Express,* vol. 17, no. 21, pp. 18590-18595, 2009.

[13] J. A. Bossard, D. H. Werner, T. S. Mayer, J. A. Smith, Y. U. Tang, R. P. Drupp, and L. Li, “The design and fabrication of planar multiband metallodielectric frequency selective surfaces for infrared applications,” *IEEE Transactions on Antennas and Propagation,* vol. 54, no. 4, pp. 1265-1276, 2006.

[14] A. Ebrahimi, S. Nirantar, W. Withayachumnankul, M. Bhaskaran, S. Sriram, S. F. Al-Sarawi, and D. Abbott, “Second-order terahertz bandpass frequency selective surface with miniaturized elements,” *IEEE Transactions on Terahertz Science and Technology,* vol. 5, no. 5, pp. 761-769, 2015.

[15] B. A. Munk,"*Frequency selective surfaces: theory and design*", New York: Wiley-Interscience, 2000.

[16] J. Coonrod, “Choosing circuit materials for millimeter wave applications,” *High Frequency Electronics*, pp. 22-30, 2013.

[17] F. E. Nathanson, J. P. Reilly, and M. N. Cohen, “Radar design principles-Signal processing and the Environment,” *NASA STI/Recon Technical Report A,* vol. 91, 1991.

[18] E. A. Parker, A. D. Chuprin, J. C. Batchelor, and S. Savia, “GA optimisation of crossed dipole FSS array geometry,” *Electronics Letters,* vol. 37, no. 16, pp. 996-997, 2001.

[19] A. Kesavan, R. Karimian, and T. A. Denidni, “A Novel Wideband Frequency Selective Surface for Millimeter-Wave Applications,” *IEEE Antennas and Wireless Propagation Letters,* vol. 15, pp. 1711-1714, 2016.

[20] Y. Rahmat-Samii, and A. N. Tulintseff, “Diffraction analysis of frequency selective reflector antennas,” *IEEE Transactions on Antennas and Propagation,* vol. 41, no. 4, pp. 476-487, 1993.

[21] J.-Q. Hou, L.-F. Shi, S. Chen, and Z.-R. Gou, “Compact broadband circular polariser based on two-layer frequency-selective surfaces,” *Electronics Letters,* vol. 51, no. 15, pp. 1134-1136, 2015.

[22] C. Lee, R. J. Langley, and E. A. Parker, "Technical memorandum. Single-layer multiband frequency-selective surfaces." *IEE Proceedings H-Microwaves, Antennas and Propagation* pp. 411-412, 1985.

[23] J. Ulrych, R. Polansky, and J. Pihera, "Dielectric analysis of polyethylene terephthalate (PET) and polyethylene naphthalate (PEN) films." *Electric Power Engineering (EPE), Proccedings of the 2014 International Scientific Conference on* pp. 411-415.

[24] A. M. Melo, A. L. Gobbi, M. H. Piazzetta, and A. M. Da Silva, “Cross-shaped terahertz metal mesh filters: Historical review and results,” *Advances in Optical Technologies,* vol. 2012, 2012.

[25] R. Ulrich, “Far-infrared properties of metallic mesh and its complementary structure,” *Infrared Physics,* vol. 7, no. 1, pp. 37-55, 1967.

Chapter 8: FSS for HIS and Antenna Applications

8.1 Introduction

This chapter focuses on applications of FSSs. Periodic structures are often used to improve antennas' performance. A U-slot patch antenna was integrated to a modified Jerusalem cross FSS in [1] to improve the antenna gain, bandwidth and return loss at 2.45 and 5.8 GHz for Bluetooth and WLAN applications. A split ring-shaped slot based frequency selective surface (FSS) is applied to increase the bandwidth and gain of an antenna [2].

In Section 8.2, a high impedance surface (HIS) is implemented by using two layers which are symmetrical in the *xy* plane, but flipped by 180^o in the *yz* plane (see Chapter 4). As a result of doing this, the HIS has miniaturised element size with a low profile. The dimensions of the miniaturised element are as small as 0.0592λ×0.0592λ and the overall thickness is 0.006λ. The proposed structure is polarisation independent. These features of the proposed HIS structure can make it desirable for many applications.

In Section 8.3, a design approach of FSS is presented for passive radio frequency identifier (RFID) tag antennas to function efficiently when mounted on a wide variety of dielectric materials of varied thickness. It is well known that the presence of materials can detune an antenna by shifting its operational frequency.

8.2 A low profile miniaturised HIS

HIS or artificial magnetic conductor (AMC) consists of an FSS placed above a perfect electric conductor (PEC) ground plane, with a dielectric material in between [3]. It exhibits selectivity in supporting surface wave currents, which is different from traditional metallic conductors. It displays a 0^o reflection coefficient phase at a given frequency [4]. While using a conventional conductor as the ground plane of a planar antenna, the power transferred into the surface waves does not contribute to the main radiation of the antenna, it is scattered off the edges of the finite ground

plane and leads to ripples in radiation patterns, increased back radiation, and lower polarisation purity. This is because the electromagnetic energy trapped between the conductor-dielectric interfaces is formed into surface waves. Secondly, when the electromagnetic waves radiated into the substrate reaching the dielectric-air interface, any wave at angles greater than $[sin(\sqrt{\varepsilon_r})]^{-1}$ will be reflected [5]. The bandwidth of a HIS structure is considered as the frequency band where the reflection phase shift varies from -90 to +90. Traditionally, at microwave frequencies, the HIS structure has an array element size of about half to a quarter of a wavelength, making the overall HIS prohibitively large if it is used a backing plane for antennas [6]. Designing HIS structures operating at low frequencies is relatively challenging because the array element is physically large and because the wavelength is long. Modern communication systems require small microwave components, so miniaturisation has become increasingly important for applications of AMCs where physical space is constrained [7].

Recently, many approaches have been proposed to overcome on the size limitation. For example, a miniaturised AMC by using lumped capacitors is introduced [8]. Interdigitated-capacitor and spiral-inductor lumped elements are used to reduce the array element's dimensions in [9].

8.2.1 The structure

The proposed FSS structure, formed by two metallic layers separated by a single substrate layer, was described in Chapter 4.

The HIS surface can be built by cascading the FSS structure with ground separated by a dielectric substrate. In this case the surface does not have via pins connected to the ground plane. The FSS was designed on a 0.127 mm thick FR4 substrate with a dielectric constant of 4.3. The grounded substrate is RO3003 with a dielectric constant of 3.0 and a thickness of 0.5mm. The strip width w is 0.1 mm, g = 0.2 mm, a = 2 mm and D = 6 mm, as shown in Fig. 8.1. The equivalent circuit of the HIS is shown in Fig. 8.2. The FSS impedance (Z_{FSS}) is in parallel with the input impedance of the grounded dielectric slab [10], where the impedance of the thin grounded dielectric slab behaves as an inductor ($Z_s = L_s = j\mu d$, d is the dielectric slab thickness, μ is the permeability).

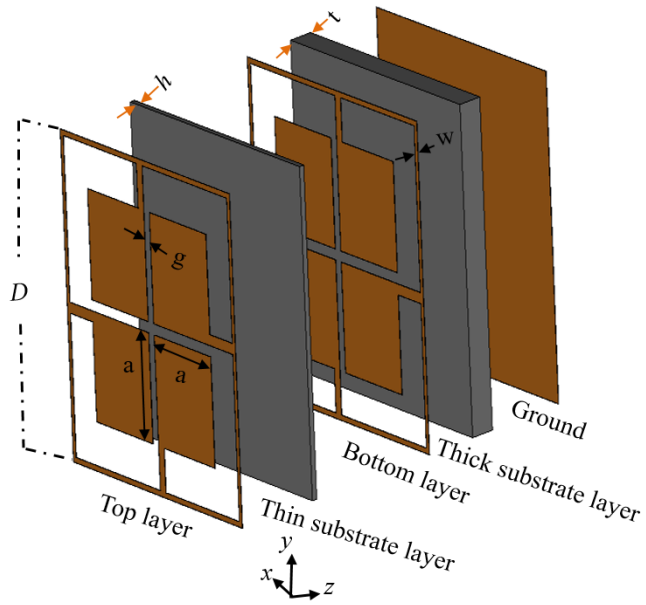

Fig. 8.1. Array element of the proposed HIS.

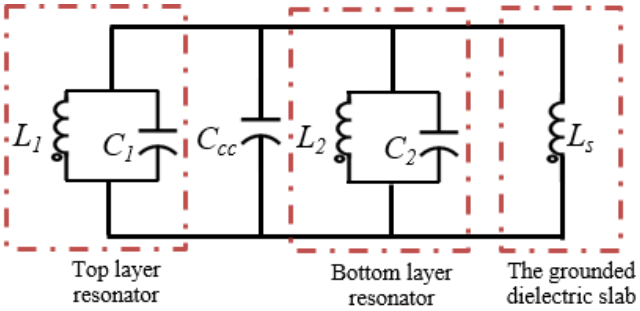

Fig. 8.2. Equivalent circuit model the proposed HIS array element.

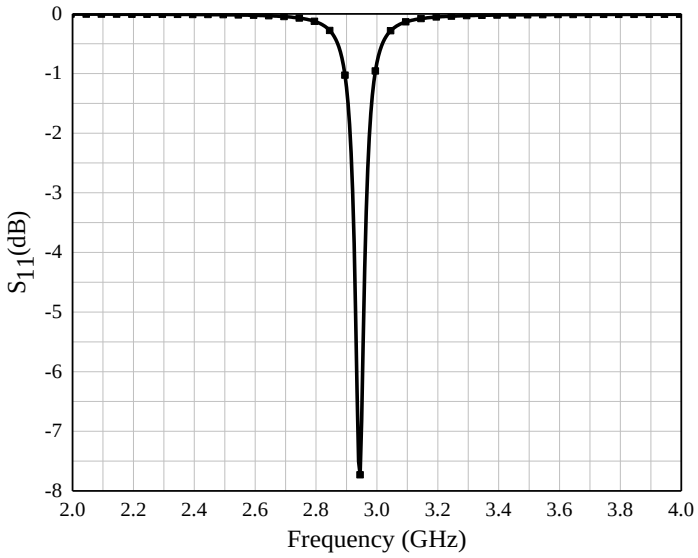

Fig. 8.3. The simulated reflection coefficient of the miniaturised HIS for vertical and horizontal polarisation angles.

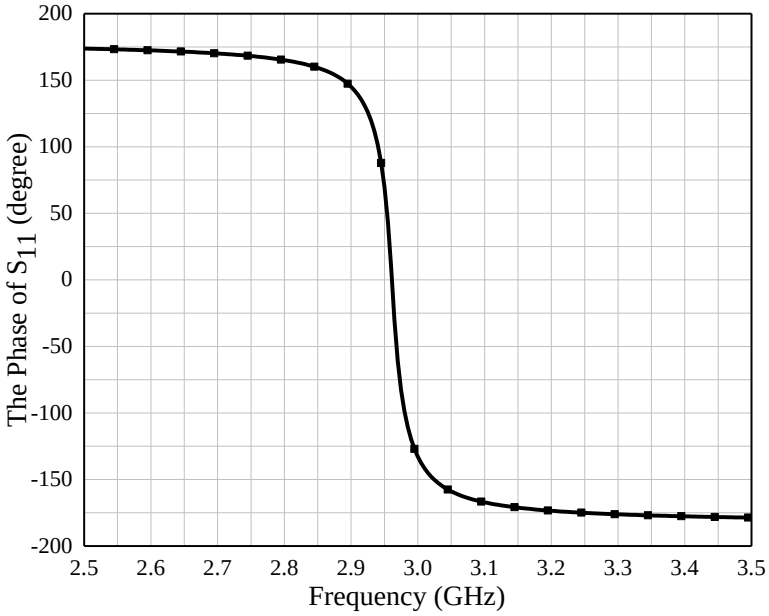

Fig. 8.4. The simulated reflection phase of the miniaturised HIS for vertical and horizontal polarisation angles.

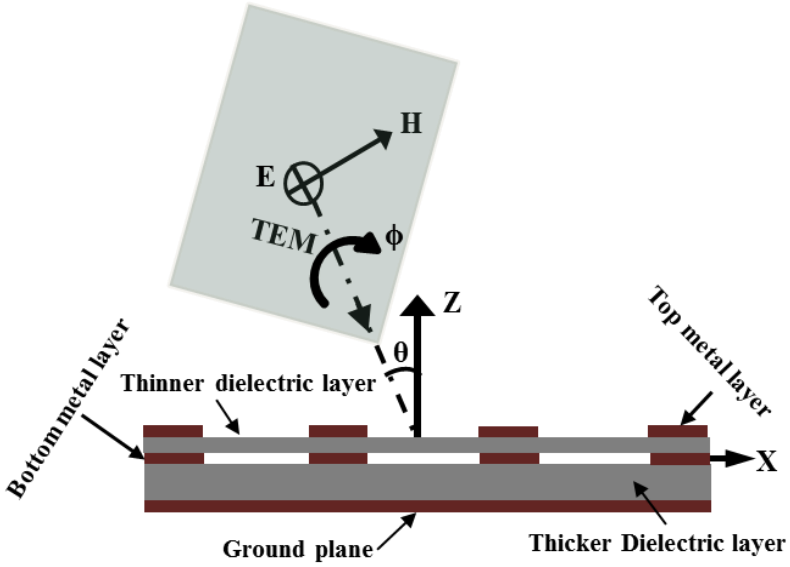

Fig. 8.5. Side view of the topology of the two-layer HIS formed by periodically repeating element.

Thus, decreasing the thickness of the substrate will shift the resonant frequency upwards because the value of L_s will decrease, and then the size of the HIS array element will be bigger to achieve the desired resonant frequency. It is a trade-off to have a very small HIS element and a low profile of the HIS structure.

Fig. 8.3 shows the magnitude of the reflection coefficient of the proposed HIS for normal incident waves of vertical or horizontal polarisations. The resonant frequency

is 2.96 GHz. The power loss at the resonant frequency is mainly because of the substrate losses and the scattering in the incident wave between the cascaded layers (top and bottom). Fig. 8.4 shows the phase of the reflection coefficient for the normal incident wave. The ± 90º phase bandwidth is 33.5 MHz. The dimension of the array element is 0.0592λ×0.0592λ**.**

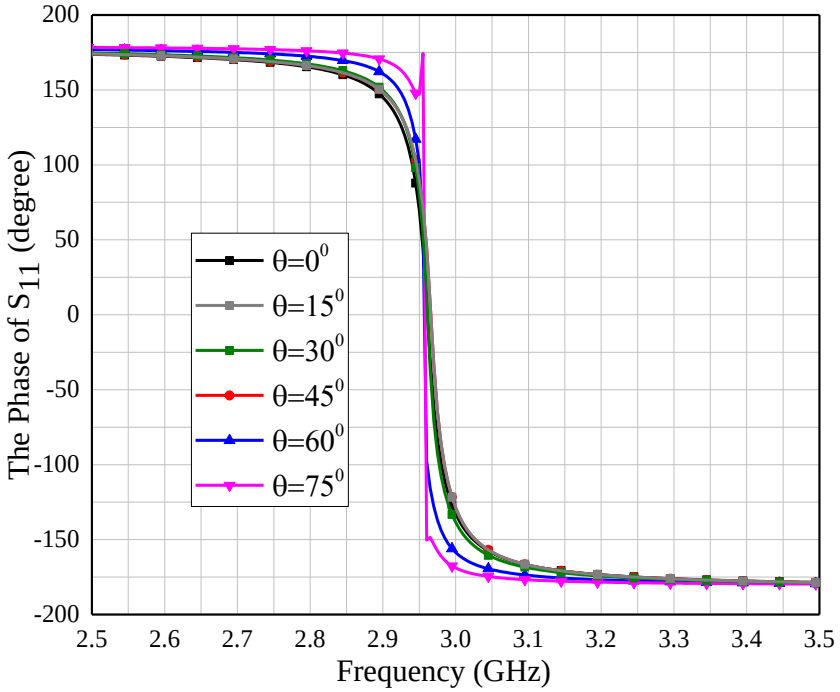

Fig. 8.6. The simulated reflection phase of the miniaturised HIS at different angles of the incident wave and for vertical and polarisation angles.

Table 8.1: Comparison with other miniaturised HISs

HIS structure	Substrate Thickness (mm)	ε_r	Element size
[8]	22.4	4.4	0.0137λ
[9]	1.524	4.5	0.0938λ
[11]	1.51	3	0.13λ
[12]	1.27	10	0.0588 λ
[13]	1.58	10.7 & 3.4	0.051λ
The proposed structure	0.627	4.5	0.0572λ

For non-normal incident waves, the incident angles (θ) and polarisation angle (ϕ)

are defined as shown in Fig. 8.5. Fig. 8.6 shows the resonant frequencies of the structure under variable incident angles for the proposed HIS. It can be seen that the performance is very stable under different incident angles up to 75˚.

The dimensions and the overall thickness of the proposed structure is compared with other approaches that have been used to design miniaturised HISs, as shown in Table 8.1.

8.3 FSS for antennas

It is well known that the presence of unknown materials can detune the performance of an antenna, thereby degrading its performance. For example, passive UHF RFID tag antennas are extensively used for inventory tracking and sensing in a variety of applications and environments. In general, an RFID tag antenna is designed for a given type of material, to optimise its gain, impedance, and efficiency. Examples include tags designed for near body applications [14], metallic surfaces [15, 16], bottled water [17], paper-based applications [18], and tags for specific products [19]. A tag antenna designed for a certain material (specific application) may not be applicable to another. This is mainly because the antenna frequency response is detuned when embedded or attached to materials with different dielectric properties. The thickness of the material also detunes RFID tag antennas.

The target of this study is to suggest an extreme low profile FSS design for antennas to avoid the detuning due to surrounding materials. The antenna should have a wide bandwidth and a radiation pattern uniform around the broadside direction. Section 8.3.1 discusses the effect of dielectric materials on periodic structures. Section 8.3.2 describes the procedure to design FSS for RFID tag antennas. Section 8.3.3 focuses on the performance of the antenna when loaded with the proposed FSS. The measurement setup and experimental results to verify the theory are described in Section 8.3.4.

8.3.1 Dielectric effect on patch-mesh FSS

In this subsection, the effect of dielectric materials on a multi-layer (patch-mesh) FSS, as shown in Fig. 8.7, will be investigated. The inductive surface is constructed by square rings with a strip width of 0.3 mm. Square patches with a gap of 0.4 mm are used as the capacitive surface. The array element size is 6 mm.

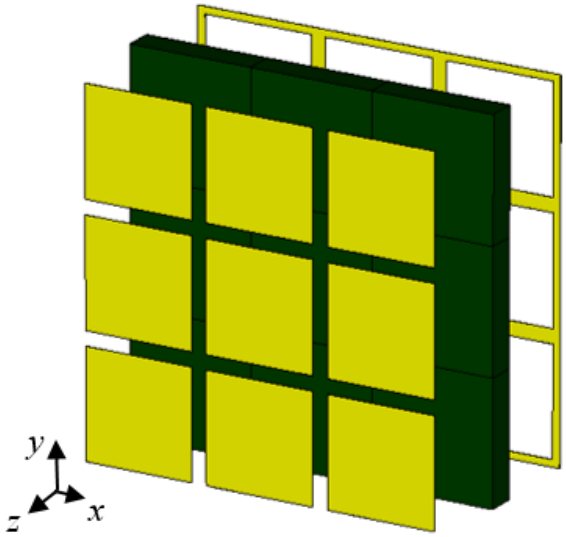

Fig. 8.7. 3×3 array element of the inductive FSS type.

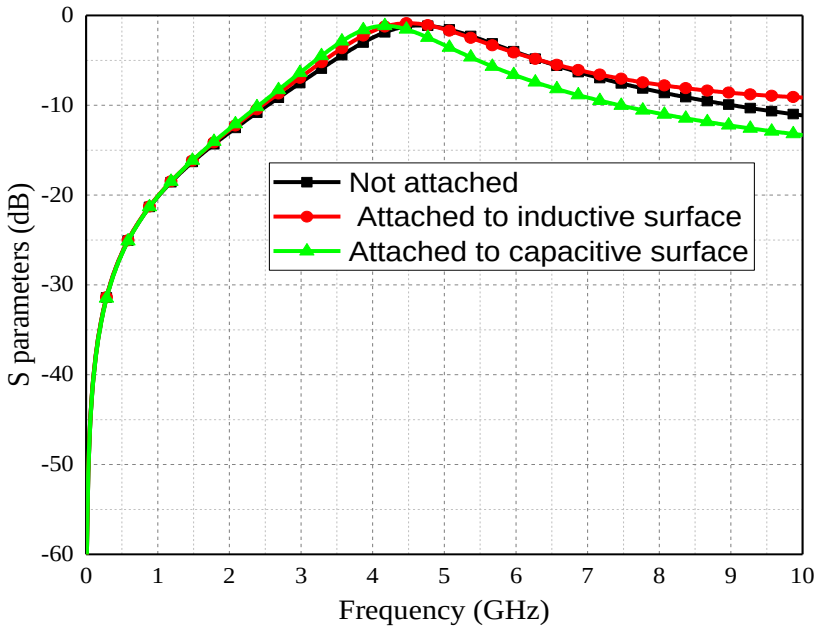

Fig. 8.8. The reflection coefficient of the Patch-mesh FSS when placed on the surface of a material with ε_r = 6 and 2mm thick.

A dielectric substrate with $\varepsilon_r = 4$ is uesed to separate the two surfaces. The structure is simulated under three cases. Firstly, when it is not attached to any other material; secondly when the inductive surface side is attached to a dielectric material ($\varepsilon_r = 6$); thirdly, when the patch surface side is attached to the dielctric material.

The simulation result is shown in Fig. 8.8. It can be observed that the frequency response of the structure is very stable when it is attached to the dielectric slab from the inductive side, while the frequency response shifted significantly when the

dielctric slab is attached to the capacitive side. The stable resonant frequency response of the patch-mesh structure when a dielectric slab is attached to the inductive side occurs for two reasons. Firstly, the intrinsic inductance of the FSS is not influenced by the dielectric material as mentioned in Chapter 1, Section 1.4.1. Secondly, the equivalent inductance and capacitance values of the transmission line (dielectric slab) are very small compared to the intrinsic inductance and capacitance. The resonant frequency is shifted significantly in the case where the dielectric slab is attached to the capacitive side. This is because the effective dielectric constant of the FSS structure is changed and then the intrinsic capacitance is also changed.

8.3.2 Circuit design

The choice of the proper element may be of most importance when designing either a bandpass or band-stop FSS. Some elements are inherently more narrow-band or more broadband than others, while some can be varied considerably by design. Different FSS types can be chosen based on the application requirements. These requirements usually include a level of dependence on the polarisation and incidence angle of the incoming wave, and bandwidth.

In this section, a new approach to implement an FSS structure which can exhibit an insensitive response to nearby dielectric materials of arbitrary thickness can be shown. Under the assumption that the dielectric materials will be attached to a one side only, let it be the bottom side of the proposed FSS.

The structure is designed by using a resonator surface (the top side) and an inductive surface (the bottom side). They are separated by a dielectric substrate. The inductive surface will minimise the effect on the whole structure from any changes in the frequency response.

To design the proposed FSS with the desired response, the values of the elements used in the equivalent circuit model of Fig. 8.9 should be determined. The initial values of these *LC* components can be approximated using those formulas in (1.1) and (1.6). The values of lumped-element components in Fig. 8.9, to achieve the desired response, can be obtained as $C_1 = C_3 = 0.30$ pF, $C_2 = C_4 = 0.25$ pF, $L_1 = L_3 = 2.34$ nH and $L_2 = 0.27$ nH. The calculated reflection and transmission coefficients of the equivalent circuit are shown in Fig. 8.10.

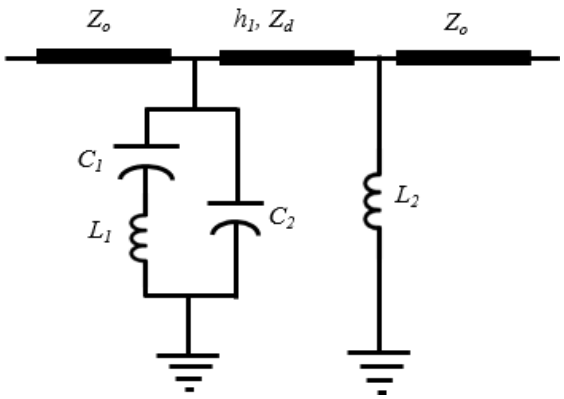

Fig. 8.9. Equivalent circuit model of the proposed FSS.

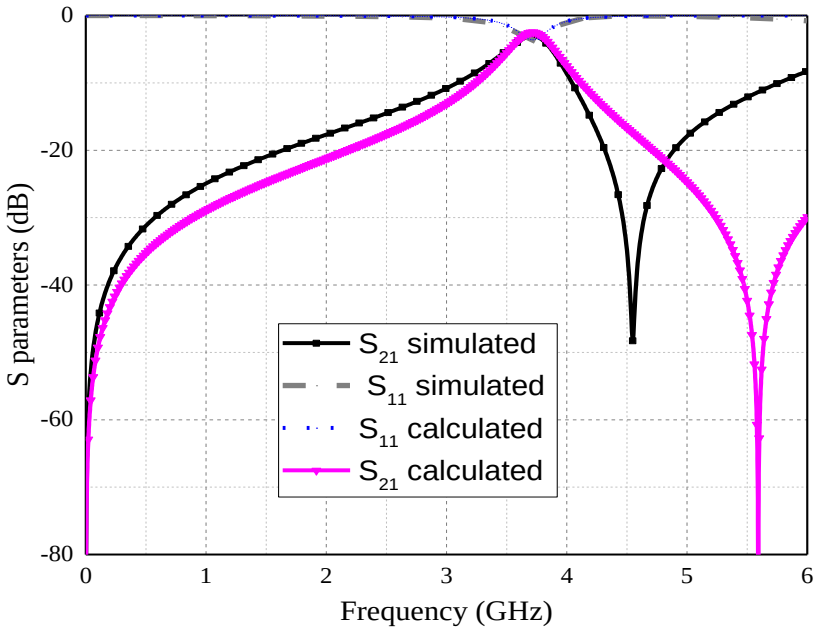

Fig. 8.10. The calculated and simulated S parameters of the proposed structure.

The response of the FSS is the result of combining the top resonator layer and the bottom inductive layer. The resonator surface exhibits a bandstop characteristic at 4.5 GHz, as can be observed from the simulation result shown in Fig. 8.11. It is worth mentioning that cascading the resonant bandstop layer with the non-resonant inductive layer (L_2) through the substrate will not only achieve an insensitive frequency response to nearby materials, but will also miniaturise the array element. The value of the inductance surface (L_1) plays an essential role in shifting the bandpass frequency downwards. The proposed structure is designed to obtain a big value of L_1 by using thin wires on the bottom layer.

Based on the results obtained from the full-wave simulation on the array element of the proposed FSS, the dimensions of the inductive and resonator surfaces are

tuned to achieve the desired frequency response.

The resonator surface as introduced in [20, 21], consisting of an inductive mesh and four capacitive patches as shown in Fig. 8.12 (a), are used for the design. Thin wires (grid) as shown in Fig. 8 12(b) are used as the inductive surface. The mutual capacitance between adjacent surfaces presents C_1; the square wire inductor presents L_1; and the capacitance between adjacent patches in one element presents C_2.

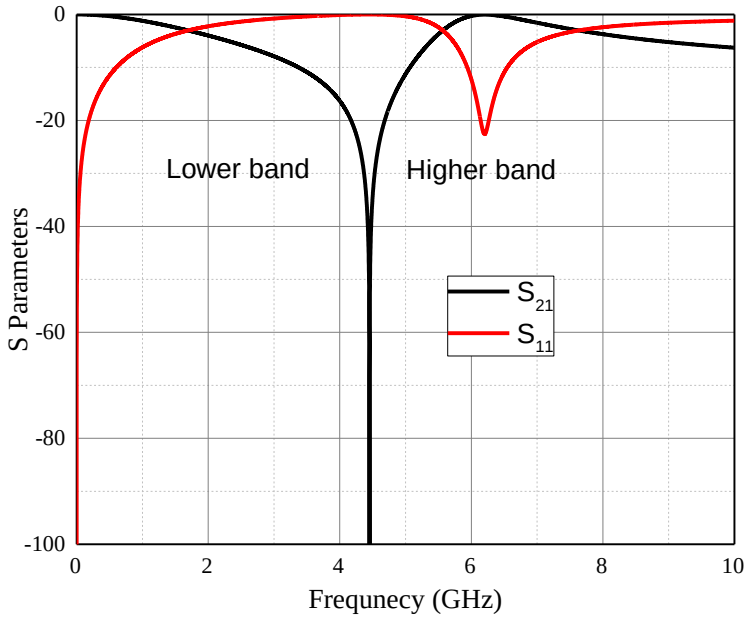

Fig. 8.11. The calculated transmission coefficient of the resonator surface.

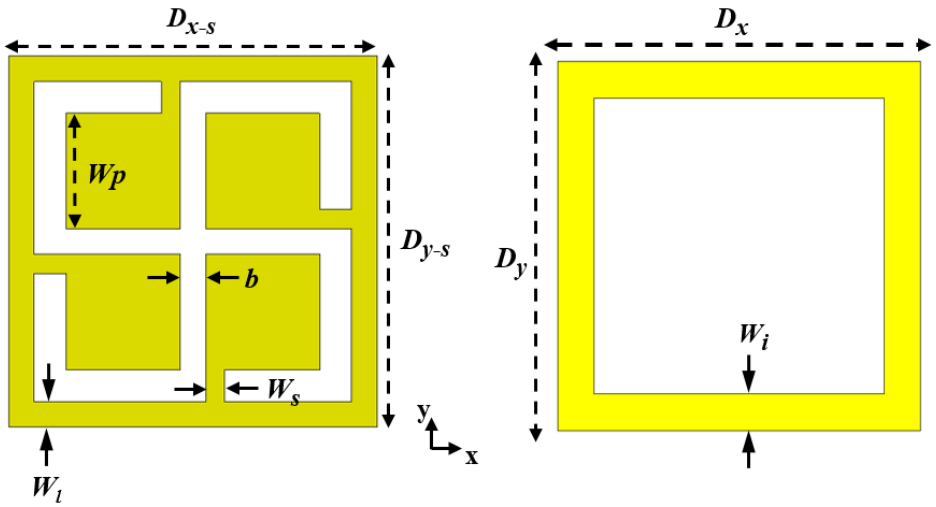

(a) **(b)**

Fig. 8.12. (a) The resonator surface, (b) the inductive surface.

The structure was designed on a 1.6 mm thick FR4 substrate with a dielectric

constant of 4.3. The geometry parameters are shown in Table 8.2. 3×3 array elements of the proposed structure are shown in Fig. 8.13. The simulation result of the proposed structure is shown in Fig. 8.14. It can be seen that the proposed structure exhibits a bandpass response at 3.73 GHz.

Table 8.2. Geometry parameters of the proposed resonator surface (unit:mm)

Parameter	D_x	D_y	h_1	h_2
Value	6	6	1.6	1.6
Parameter	W_s	W_i	W_p	W_l
Value	0.2	0.2	2.3	0.5
Parameter	ε_r	s	g	
Value	4.4	0.1	0.2	

Performance of the proposed structure as a function of incident wave angles has been simulated. It exhibits a very stable response for incident angles (θ) up to 60^o for both vertical and horizontal polarizations.

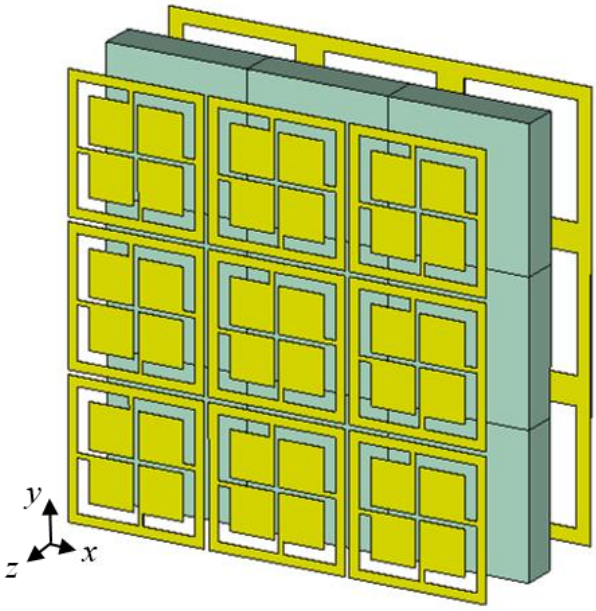

Fig. 8.13. 3×3 Array element of the proposed FSS.

As mentioned, the bottom layer (inductive surface) is not influenced by the surrounding dielectric material. To demonstrate this feature of the proposed structure, the structure is simulated when: Not attached to dielectric material, and the inductive (mesh) side placed on a 2 mm dielectric slab with various dielectric constants, $\varepsilon_r = 3$ and 8.

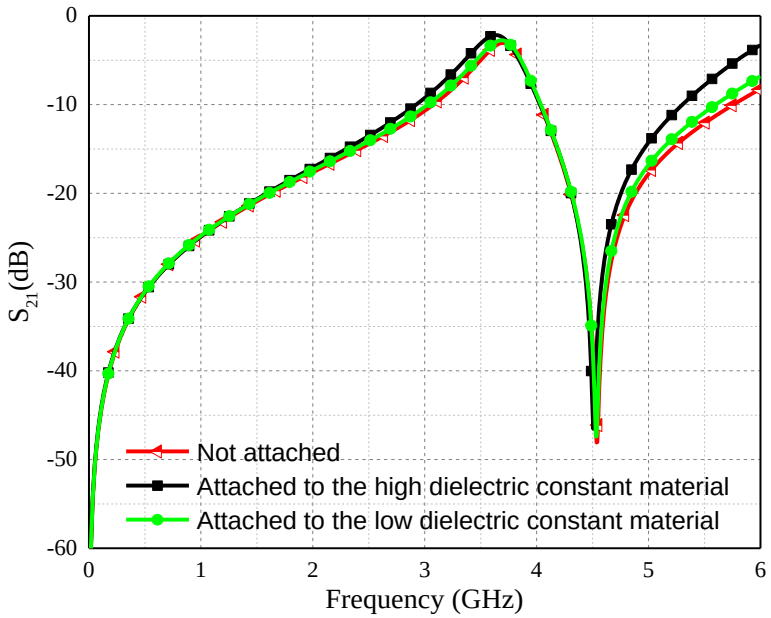

Fig. 8.14. The simulated transmission coefficient of the proposed structure when placed on a 2mm dielectric slab with varying dielectric constants.

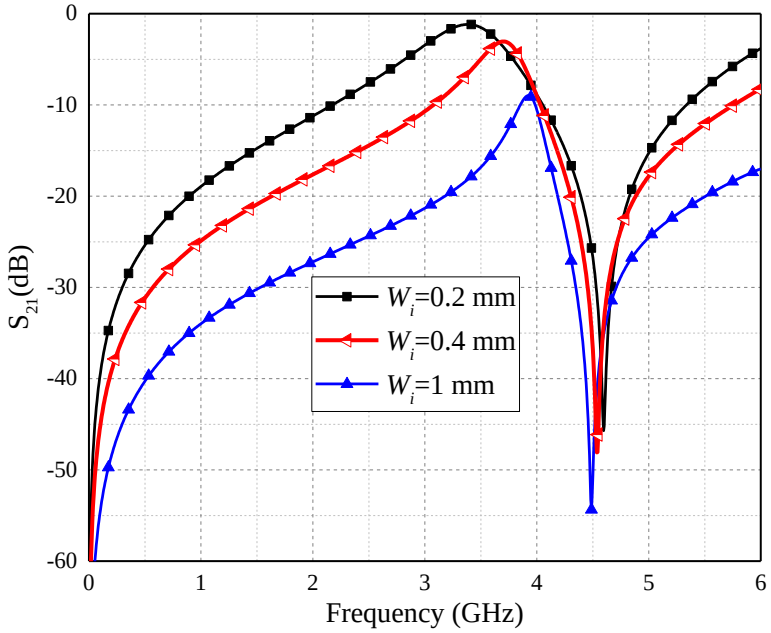

Fig. 8.15. Simulated transmission coefficient of the proposed FSS for different inductive strip width.

It can be seen from Fig. 8.14 that the resonant frequency is only shifted by 0.3% when the proposed structure is attached to the low dielectric constant material, and shifted by 1.7% at the high dielectric constant material case.

Decreasing the strip width (W_i) of the inductive layer, or increasing the inductance (L_2) at the equivalent circuit, will increase the bandwidth and decrease the surface

impedance. Fig. 8. 15 shows the simulated performance of the proposed structure with three different strip widths (W_i = 0.2, 0.4 and 1 mm). It is obvious that the transmission is higher with thinner wires. Thus, at the lower values of L_2, the bottom layer will be closer to a ground plane than an inductive surface. The proposed structure will work as an HIS when the bottom side is attached to a metal plane.

8.3.3 A dipole antenna loaded with the proposed FSS

In this section, the proposed FSS is presented to antennas to function efficiently when the whole structure is mounted on a wide variety of dielectric materials of arbitrary thickness. A simple planar dipole antenna is used in this work. Fig. 8.16 shows the physical arrangement of the dipole antenna loaded with the proposed FSS structure. As can be seen, the top layer is the dipole antenna on a 0.81 mm thick Roger 3004C substrate. The dielectric constant is 3.38. The resonator surface on an FR-4 substrate is located in the middle of the combination.

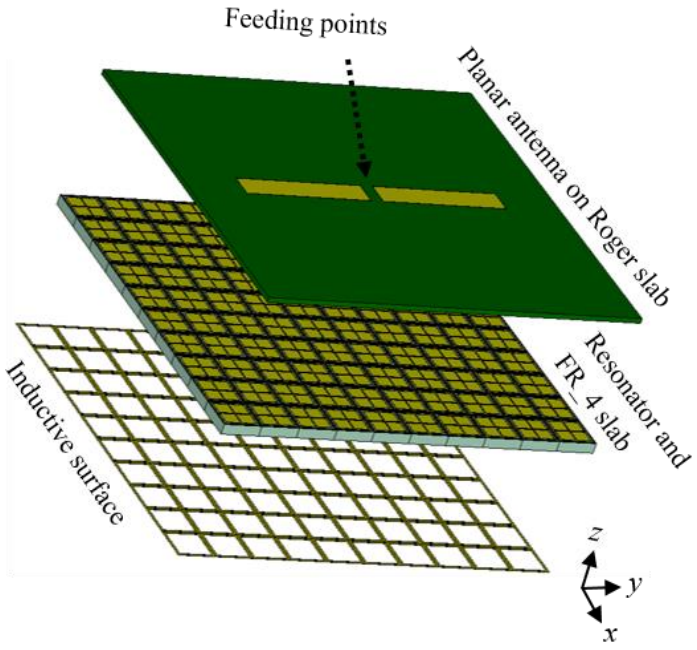

Fig. 8.16. The dipole antenna loaded on 10×10 array element of the proposed structure.

The dipole length is about λ/2 (42 mm). The simulated reflection coefficient of the dipole antenna when supported by the proposed FSS is shown in Fig. 8.17. As expected, the resonant frequency of the proposed structure will be shifted downwards. It is mainly because the antenna substrate is attached to the top layer of the FSS structure. The top layer is sensitive to dielectric materials as mentioned above. It is also because the equivalent circuit of the FSS as shown in Fig. 8.9 will be

changed by adding a series LC (the equivalent circuit of the dipole antenna). The resonant frequency of the FSS will shifts from 3.36 GHz to 2.72 GHz, as can be seen in Fig. 8.17. The stability of the combined structure when attached directly to a variety of dielectric materials of arbitrary thicknesses is demonstrated as shown in Fig. 8.17 and Fig. 8.18. Fig. 8.17 shows the simulation result of the combined structure with three cases: Not attached to dielectric materials; attached to a 4-mm thick low dielectric constant material ($\varepsilon_r = 3.38$) and; attached to a 4 mm thick high dielectric constant material ($\varepsilon_r = 8$). It can be observed from Fig. 8.17 that the frequency response of the combination is very stable in all three cases.

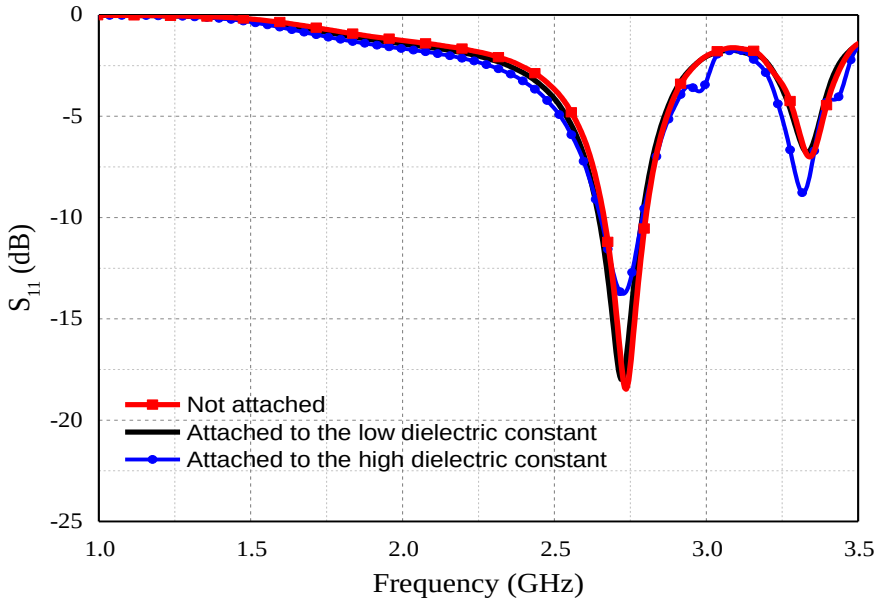

Fig. 8.17. The simulated return losses of the dipole antenna loaded with the proposed FSS when placed on a 4 mm thick dielectric slab with a variety of dielectric materials.

Fig. 8.18 shows the simulation result of the combined structure when attached to the high dielectric constant material ($\varepsilon_r = 8$) with variable thickness (4 and 8 mm). Simulation was then carried out to obtain the return losses of the combined structure when the attached to metal through thin dielectric slabs (0.1 mm and 0.3 mm). The simulated results are shown in Fig. 8.19. It is very obvious that the bandwidth is decreased and the array element size becomes bigger. Table 8.3 shows the resonant frequency (f_o), the fractional bandwidth (BW) and the array element size of the antenna when loaded with the proposed FSS for variable strip width of the inductive surface.

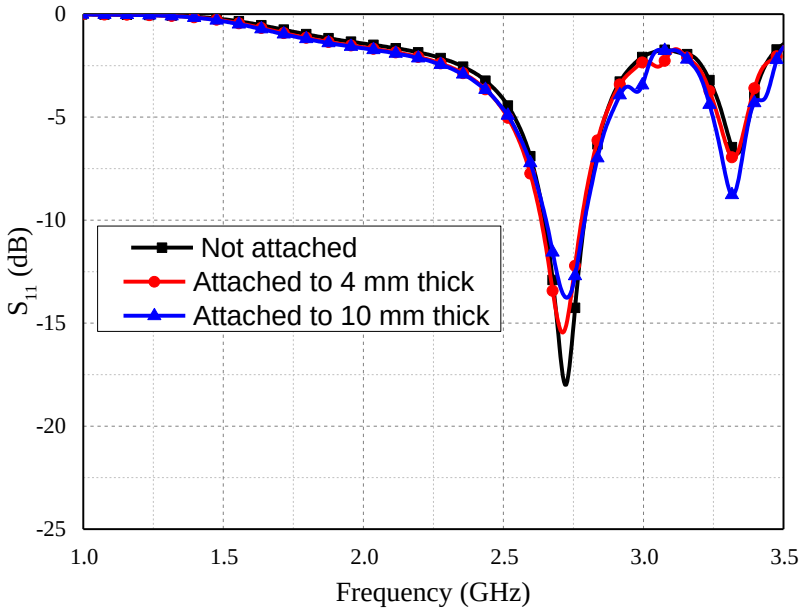

Fig. 8.18. The simulated return losses of the dipole antenna loaded with the proposed FSS, when the bottom layer is attached directly to the high dielectric constant material of varied thicknesses.

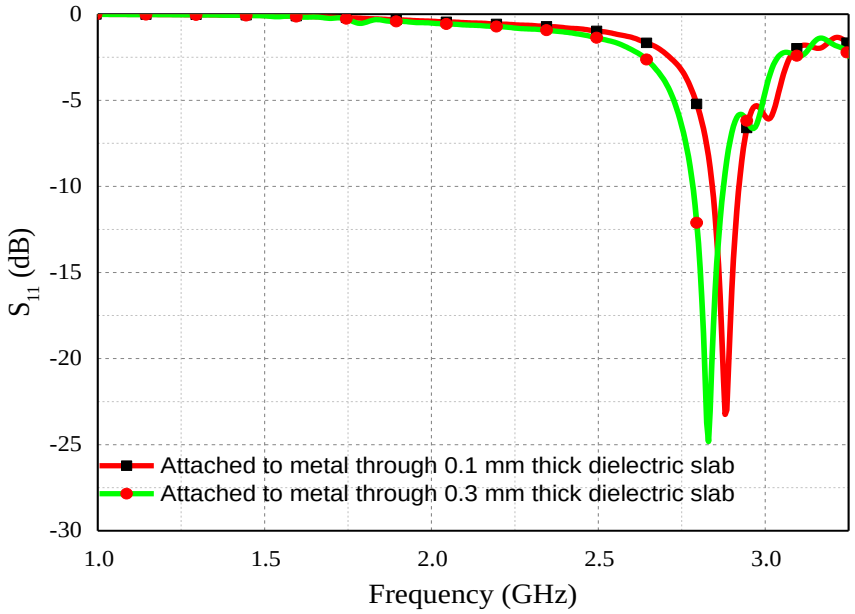

Fig. 8.19. The simulated return losses of the dipole antenna loaded with the proposed FSS when the bottom layer is attached to metal through thin dielectric slabs.

It can be seen that the 10 dB fraction bandwidth (BW) in the case using the inductive surface with thinner wires (W_i = 0.1 mm) is twice as wide as that when using the ground plane. The radiation pattern is uniform in the broadside direction, as can be seen from Fig. 8.20. The total radiation efficiency is more than 90% at the resonant frequency. It should be mentioned that the centre of the antenna is aligned with the centre of the 10 × 10 proposed FSS elements. The effect of the misalignment

between the antenna and the FSS elements is simulated. The simulation was carried out by shifting the antenna from the centre of the FSS.

Table 8.3. The frequency response and the element size for variable strip width of the inductive surface

W_i (mm)	f_o (GHz)	BW%	Element size	Overall thickness
0.1	2.64	6.65	0.052λ	0.0211λ
0.4	2.72	5.67	0.054λ	0.0217λ
1	2.83	4.03	0.057λ	0.0226λ
Ground plane	2.9	3.01	0.067λ	0.0232λ

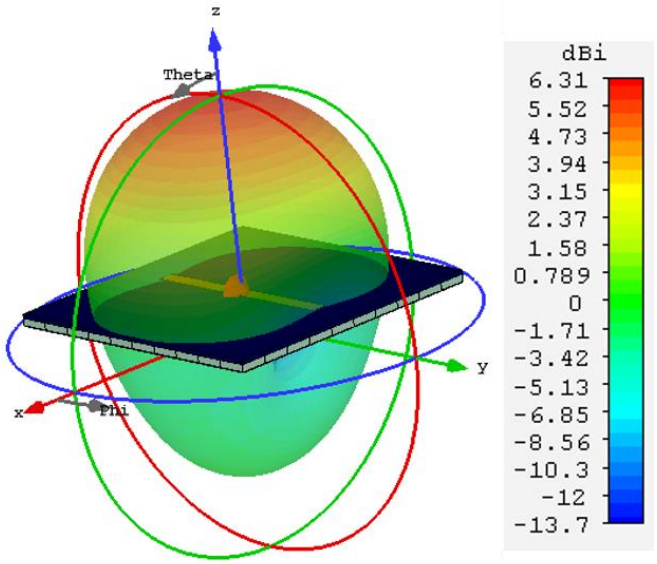

Fig. 8.20. Radiation pattern of the dipole antenna loaded with proposed FSS in free space.

The proposed structure exhibits a stable frequency response to the misalignment. For example, the deviation in resonant frequency was 0.5% when the misalignment between the antenna and the centre of the FSS is 2 mm (0.018λ), or 3% at 4 mm (0.036λ), toward either the *x* or the *y* axis.

8.3.4 Experimental results

Firstly, an FSS consisting of 30 × 30 elements is etched on a 180 mm × 180 mm FR-4 substrate. The parameters are given in Table I. The fabricated circuit is shown in Fig. 8.21. The resonator surface (top side) is shown in Fig. 8.21 (a), while Fig. 8.21 (b) shows the inductive surface (bottomed side). A vector network analyser and

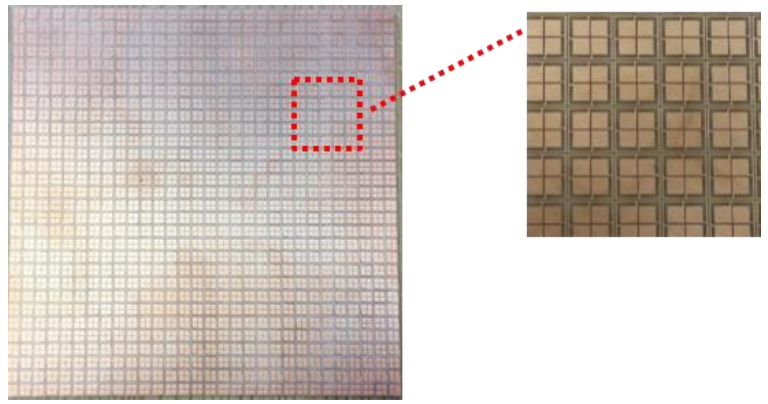

(a)

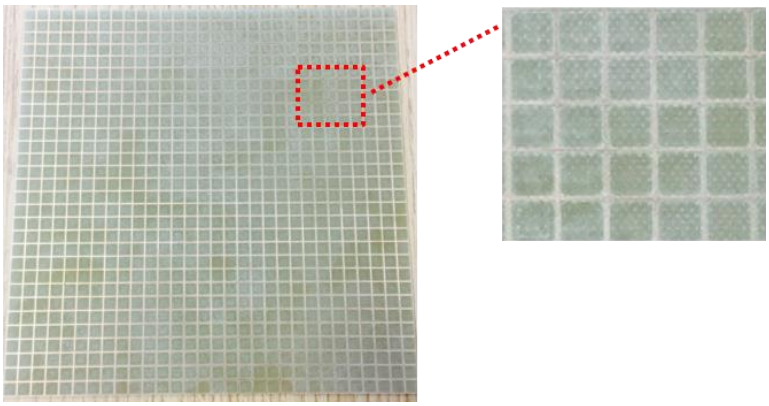

(b)

Fig. 8.21. A photograph of the fabricated prototype of the proposed second-order bandpass FSS (a) the resonant surface, (b) the inductive surface.

two horn antennas were used for the measurement. The transmission coefficient between the two horn antennas was measured without the FSS, and then the transmission coefficient was measured with the FSS prototype between the antennas. Thereby, the measured transmission with the FSS is normalised with respect to the measured data without the FSS. The prototype FSS was measured when it was attached to 2 mm thick Glass with dielectric constant 5.75 at 10 GHz and 1.6 mm thick Rogers (RO4003C), respectively. It can be seen from Fig. 8.22 that the resonant frequency of the proposed FSS is very stable when it is placed on different dielectric materials. The structure exhibits a bandpass response. The centre frequency of the passband is 3.8 GHz. The FSS was also tested under various polarisation angles. The performance is almost independent from polarisation angles due to the symmetrical nature of the proposed element. Secondly, another prototype of proposed FSS, with a smaller element number, was fabricated.

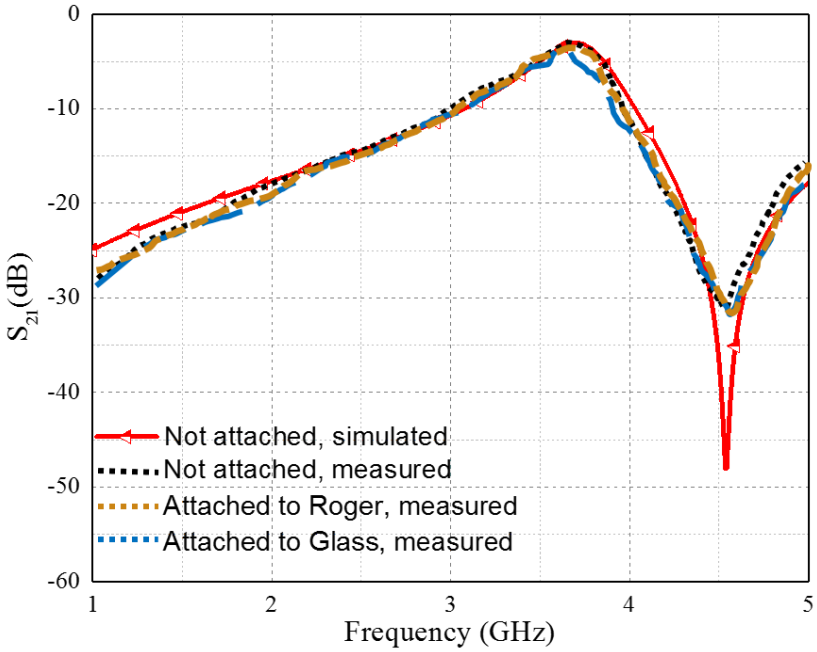

Fig. 8.22. Simulated and measured transmission coefficient of the proposed FSS when placed on a 2 mm thick dielectric slab with various dielectric constants.

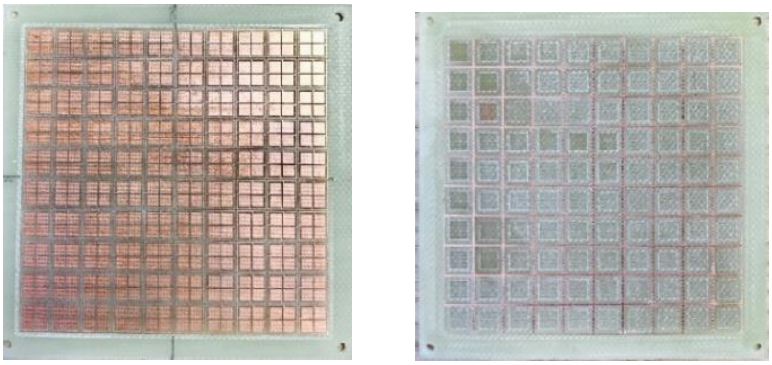

(a) **(b)**

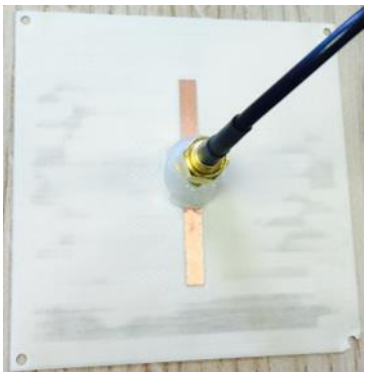

(c)

Fig. 8.23. Photographs of the fabricated antenna loaded the FSS prototype: (a) The top (resonator surface) layer of the FSS, (b) the bottom (inductive surface) layer of the FSS, and (c) the planar dipole antenna.

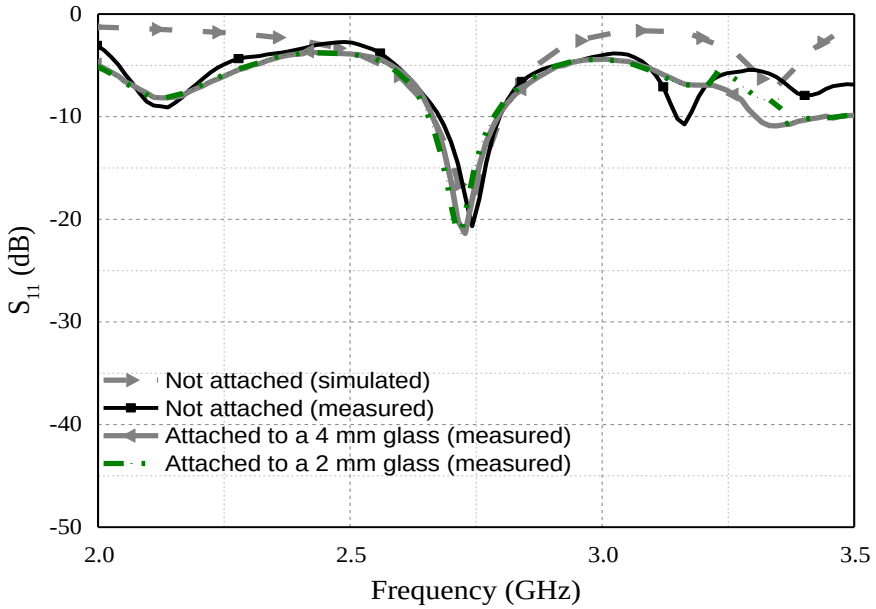

Fig. 8.24. The simulated and measured return losses of the dipole antenna loaded with the proposed FSS in different cases: No materials nearby; placed on glass of surface of variable thicknesses; and placed on metal.

This prototype was coupled with an antenna. The size of this FSS prototype is 60 mm × 60 mm, consisting of 10 × 10 elements. The prototype antenna was fabricated using the parameters as given in first paragraph in Section 8.3.3. Fig. 8.23 shows photographs of the prototype of the antenna loaded with the FSS. The dipole antenna was designed on a 0.81 mm thick Roger (RO4003C) substrate as shown in Fig. 8.23 (c). The antenna and the FSS (the two PCBs) are then compressed together by using screws on their corners. The overall size of the combined structure (the dipole antenna loaded with the proposed FSS) was 60 mm× 60 mm × 2.4 mm. Fig. 8.24 depicts the measured and simulated S_{11} of the dipole antenna loaded with the proposed FSS in three cases: No material nearby; placed on the 2 mm glass; placed on metal surface. It can be observed that the antenna shows robustness to challenging dielectric materials. Thus, the measurement of the antenna loaded with the FSS when placed on metal is in a very good agreement with the simulated one. Thus, the structure exhibits an insensitive response when attached directly to varied dielectric materials of arbitrary thickness. The centre frequency of the passband is 2.73 GHz with a fractional bandwidth of 5.6%.

8.4 Conclusion

A new low profile and miniaturised HIS is presented in this chapter. The novel compact HIS consists of two metallic layers and two thin dielectric substrates. The overall thicknesses of the proposed HISs are extremely small, at just 0.627 mm. The dimensions of the miniaturised element are much smaller than the wavelength at the resonant frequency, as low as 0.059λ.

A comparison with similar work has been carried out to demonstrate that the proposed AMC is low profile and of compact size. It is also shown that the proposed AMC is polarisation independent and has a very stable performance against incident waves from variable angles. Also in this chapter, the effect of dielectric materials on periodic structures is discussed. A theoretical model is introduced to analyse the structure based on the transmission line theory. A dipole antenna is mounted on the proposed FSS. The antenna can achieve a much wider bandwidth with a smaller size compared to the structure using an HIS. The dimensions of the antenna loaded with the proposed FSS are 60× 60 × 2.4 mm^3 at 2.73 GHz. The theoretical and experimental results show that the proposed antenna loaded with the proposed FSS was more robust against surrounding materials than a conventional antenna. The proposed method can be very useful for a wide range of applications, for example, to design antennas for RFID tags.

8.5 References

[1] H.-Y. Chen, and Y. Tao, “Performance improvement of a U-slot patch antenna using a dual-band frequency selective surface with modified Jerusalem cross elements,” *IEEE Transactions on Antennas and Propagation,* vol. 59, no. 9, pp. 3482-3486, 2011.

[2] B. Mandal, A. Chatterjee, and S. K. Parui, "A wearable button antenna with FSS superstrate for WLAN health care applications." *RF and Wireless Technologies for Biomedical and Healthcare Applications (IMWS-Bio), IEEE MTT-S International Microwave Workshop Series,* pp. 1-3, 2014.

[3] D. J. Kern, D. H. Werner, A. Monorchio, L. Lanuzza, and M. J. Wilhelm, “The design synthesis of multiband artificial magnetic conductors using high

impedance frequency selective surfaces," *IEEE Transactions on Antennas and Propagation,* vol. 53, no. 1, pp. 8-17, 2005.

[4] D. Sievenpiper, L. J. Zhang, R. F. J. Broas, N. G. Alexopolous, and E. Yablonovitch, "High-impedance electromagnetic surfaces with a forbidden frequency band," *IEEE Transactions on Microwave Theory and Techniques,* vol. 47, no. 11, pp. 2059-2074, 1999.

[5] R. E. Collin, "Field theory of guided waves," 2nd ed. New Yourk: Wile, 1984.

[6] F. Yang, and Y. RahmatSamii, "Electromagnetic band gap structures in antenna engineering," *Electromagnetic Band Gap Structures in Antenna Engineering*, pp. 1-266, 2009.

[7] R. C. Hadarig, M. E. D. Gomez, Y. Alvarez, and F. Las-Heras, "Novel bow-tie-AMC combination for 5.8-GHz RFID tags usable with metallic objects," *IEEE Antennas and Wireless Propagation Letters,* vol. 9, pp. 1217-1220, 2010.

[8] H. Liu, K. L. Ford, and R. J. Langley, "Miniaturised artificial magnetic conductor design using lumped reactive components," *Electronics Letters,* vol. 45, no. 6, pp. 294-U2, 2009.

[9] S. Raza, M. A. Antoniades, and G. V. Eleftheriades, "A compact low-profile high-impedance surface for use as an antenna ground plane." *Antennas and Propagation (APSURSI), IEEE International Symposium,* pp. 1832-1835, 2011.

[10] F. Costa, S. Genovesi, and A. Monorchio, "On the bandwidth of high-impedance frequency selective surfaces," *IEEE Antennas and Wireless Propagation Letters,* vol. 8, pp. 1341-1344, 2009.

[11] A. Presse, X. Zhang, M. Mantash, A.-C. Tarot, and J. M. Floc'h, "Miniaturization of an artificial magnetic conductor with interdigital capacitances." *Antennas & Propagation Conference (LAPC), Loughborough* pp. 1-4, 2015.

[12] R. C. Hadarig, M. E. de Cos, and F. Las-Heras, "Novel miniaturized artificial magnetic conductor," *IEEE Antennas and Wireless Propagation Letters,* vol. 12, pp. 174-177, 2013.

[13] M. Grau, R. Serra, and J. Parron, “Miniaturisation of artificial magnetic conductors: comparison methodology and realisation of compact unit cell,” *Electronics Letters,* vol. 50, no. 19, pp. 1340-1342, 2014.

[14] A. G. Santiago, J. R. Costa, and C. A. Fernandes, “Broadband UHF RFID passive tag antenna for near-body applications,” *IEEE Antennas and Wireless Propagation Letters,* vol. 12, pp. 136-139, 2013.

[15] A. A. Babar, T. Bjorninen, V. Bhagavati, L. Sydanheimo, P. Kallio, and L. Ukkonen, “Small and flexible metal mountable passive UHF RFID tag on high-dielectric polymer-ceramic composite substrate,” *IEEE Antennas and Wireless Propagation Letters,* vol. 11, pp. 1319-1322, 2012.

[16] H.-W. Son, H.-G. Jeon, and J.-H. Cho, “Flexible wideband UHF RFID tag antenna for curved metal surfaces,” *Electronics Letters,* vol. 48, no. 13, pp. 749-750, 2012.

[17] T. Bjorninen, A. Z. Elsherbeni, and L. Ukkonen, “Low-profile conformal UHF RFID tag antenna for integration with water bottles,” *IEEE Antennas and Wireless Propagation Letters,* vol. 10, pp. 1147-1150, 2011.

[18] V. Lakafosis, A. Rida, R. Vyas, L. Yang, S. Nikolaou, and M. M. Tentzeris, “Progress towards the first wireless sensor networks consisting of inkjet-printed, paper-based RFID-enabled sensor tags,” *Proceedings of the IEEE,* vol. 98, no. 9, pp. 1601-1609, 2010.

[19] S. Wang, Y. Tao, and G. Wang, “UHF RFID tag for integration into a cigarette pack,” *IEEE Antennas and Wireless Propagation Letters,* vol. 10, pp. 1433-1436, 2011.

[20] M. Hussein, J. Zhou, Y. Huang, A. Sohrab, and M. Kod, "Frequency selective surface with simple configuration stepped-impedance elements." *European Conference on Antennas and Propagation (EuCAP)* pp. 1-4, 2016.

[21] M. N. Hussein, J. Zhou, Y. Huang, M. Kod, and A. P. Sohrab, “A miniaturized low-Pprofile multilayer frequency-selective surface insensitive to surrounding dielectric materials,” *IEEE Transactions on Microwave Theory and Techniques*, 2017.

Chapter 9: Summary and Future Works

9.1 Summary

New techniques to design periodic structures for communications applications have been the main interest of this research. The new approaches have been well developed and applied to a number of problems concerning FSSs. As a result of these developments, the scanning and filtering performance can be significantly improved with FSSs of smaller size and lower profile. A summary of the developments in this area of research can be described as follows:

In Chapter 3, a new approach to miniaturise the size of the FSS array element has been proposed by interconnecting array elements in one direction in a two-layer FSS structure. The top layer acts as an enhanced inductor while the bottom layer acts as a capacitor. The interconnection between adjacent array elements changes the equivalent circuit and lowers the resonant frequency. The dimensions of the miniaturised FSS element are much smaller than the wavelength at the resonant frequency (periodicity << λ).

In Chapter 4, a novel multi-layer structure has been proposed to construct an FSS. The performance of the proposed structure is very stable when it is attached directly to a wide variety of dielectric materials of arbitrary thickness. Both single and dual polarised structures are displayed. The shape of the FSS element is designed by using stepped-impedance transmission lines. Novel methodology has been proposed to design the FSS by maximising the value of the capacitance between adjacent layers. Due to this strong capacitance, the proposed structure offers three distinctive advantages. Firstly, this strong cross-layer capacitance makes the FSS element very compact. The dimensions of the miniaturised element are as small as 0.012λ×0.012λ. Secondly, for the proposed structure, the lower the profile, the stronger the cross-layer capacitance, and the lower the resonant frequency. This is unique to the proposed structure since the resonant frequency is usually higher for a lower profile for traditional structures. Thirdly and most importantly, any external dielectric material attached to the FSS will not significantly affect the performance of the FSS due to this strong cross-layer capacitance. Through examples with a single polarised bandpass FSS at 1 GHz and a dual polarised bandpass FSS at 1.96 GHz, it is

demonstrated that a stable resonant frequency under various incident angles up to 75^o can be achieved. Measurement results confirm the stability of the performance of the proposed FSS structure.

New approaches to design multiband and high selectivity FSSs have been presented in Chapter 5. In these approaches, the stopband and passband frequencies can be easily controlled, as explained in the chapter. The structure is implemented and measured in microwave and millimeter wave.

In Chapter 6, miniaturised high order bandpass FSSs ($N \geq 1$) that can achieve high performance have been proposed. The FSS element is implemented by two miniaturised resonant surfaces coupled by a non-resonant inductive layer. The element size is $0.076\lambda \times 0.076\lambda$ for the proposed structure. This is significantly smaller than the element size of second-order FSSs designed using conventional approaches. The method could be particularly useful at lower frequencies with longer wavelengths. Thus, a further approach to design extreme low profile bandpass FSS has been introduced by using higher modes of the resonator. Unlike traditional ones, this structure has been built based on the third harmonics to achieve the desired response at a very thin dielectric substrate. The overall thickness of the proposed FSS was less than $\lambda/75$. FSSs operating at 3.8 GHz have been designed to verify the designs. The proposed structures are polarisation independent and suitable for both linear and circular polarization applications. The structure is also insensitive to incident angles.

In Chapter 7, new approaches to implement FSSs for THz band have been proposed. The structures exhibit a low insertion loss and high selectivity in the desired band. The high selectivity structure has been realised by combining bandstop and bandpass FSS structures on the same plane. By cascading more than one layer of surfaces separated by dielectric slabs, the response with the desired flat passband characteristics can be achieved. The structure is polarisation independent and exhibits high selectivity on the band (162.5-177.5 GHz). Another low loss FSS has been implemented by cascading two resonator surfaces separated by an air gap. The structure is also polarisation independent and exhibits low insertion loss at the passband around 166 GHz.

Chapter 8 focuses on the development of FSS for some applications such as HIS

and RFID. It proposes an extremely small size and low profile HIS array element. A trade-off between the miniaturised dimensions of the HIS element and the thickness of the grounded substrate is used to achieve an extremely low profile HIS. The structure is miniaturised based on a cross-layer capacitor. The overall thickness of the proposed HIS is extremely small, 0.627 mm, and the dimensions of the miniaturised element are much smaller than the wavelength at the resonant frequency. The two layers used in the proposed HIS are symmetrical to make it is applicable to circular polarisation applications. It demonstrates a stable resonant frequency under various incident angles (up to 75^{o}). In this chapter, a new FSS schematic has been developed for antenna applications to function efficiently when mounted on a wide variety of dielectric materials of arbitrary thicknesses. The new FSS structure exhibits a very stable frequency response when attached to different dielectric materials. An antenna can be loaded with the proposed FSS structure to avoid detuning due to nearby materials. In comparison with a high impedance surface (HIS), the proposed FSS exhibits a wider bandwidth with a smaller element size and lower profile. The proposed FSS array element size at the resonant frequency of the antenna, after coupling with the proposed FSS, is 0.0546λ × 0.0546λ with a thickness of 0.01456λ. The FSS structure and a planar dipole antenna were fabricated and tested. The experiment result proves that an antenna loaded with the proposed FSS will make the frequency response very stable against nearby dielectric media with medium to high permittivity and of varying thicknesses.

9.2 Future work

FSSs are well known in the literature for their filtering characteristics at microwave millimetre and submillimetre waves. Based on the summary above and considering the limitations of existing work, future research could be carried out in the following areas:

9.2.1 Lower frequency band

Chapter 2 proposed a design approach for an FSS structure for antennas to avoid detuning due to surrounding materials. This structure is applicable for antenna applications in frequency bands higher than 2 GHz. In the lower band (0.3-2 GHz), the size of the periodic structures is still an issue. More investigation to design a

compact structure to be applicable for lower frequency bands is required. In Chapter 2, a low profile HIS with a narrow band response has been introduced. Generally speaking, the bandwidth for an HIS is narrow and this can be an obstacle for using the HIS for a variety of applications. Designing one with a wider bandwidth will be very attractive for many applications.

9.2.2 A mobile phone

Wireless systems for the future 5G cellular system are increasingly proposing the utilisation of the mm-wave spectrum due to the growing requirement for wider bandwidths [1].

Moving to the mm-wave frequencies for 5G mobile terminals requires new techniques in the design of antennas for mobile-station (MS) and base-station (BS) systems. In order to achieve an efficient beam-steerable phased array antenna, which is one of the most important blocks for 5G cellular systems, smaller antennas arranged as an array can be employed [2, 3]. However, mutual coupling between the phased array antenna elements is relatively high and could be an obstacle to this technique. One way to resolve such an issue is to use FSS structures. These structures can improve the isolation between the adjacent array antenna elements. The FSS array element should be ultra-miniaturised to be applicable for such applications because of the limited dimensions of a mobile phone.

9.2.3 THz frequency band

Future work will aim to develop the fabrication process in order to investigate experimentally the FSS operation in the THz regime. A THz FSS that consists of a single metal-dielectric layer, which is relatively easy to fabricate, will be studied. A wideband THz FSS filter with low insertion-loss will be investigated. The THz filter will be proposed by using sub-wavelength elements to produce excellent filtering characteristics with an ability to improve frequency selectivity.

9.3 References

[1] P. Gupta, "Evolvement of mobile generations: 1G to 5G," *International Journal for Technological Research in Engineering,* vol. 1, pp. 152-157, 2013.

[2] W. Hong, K. Baek, Y. Lee, and Y. G. Kim, "Design and analysis of a low-profile 28 GHz beam steering antenna solution for future 5G cellular applications," in *Microwave Symposium (IMS), 2014 IEEE MTT-S International*, 2014, pp. 1-4.

[3] M. B. Gaucher, U. Pfeiffer, and J. Grzyb, "Advanced millimeter-wave technologies," ed: John Wiley & Sons, New Jersey, USA, 2009.